Synthesis and Evaluation of *M.tb* Glycosyltransferase (MshA) Inhibitors

Majimi James Sehata

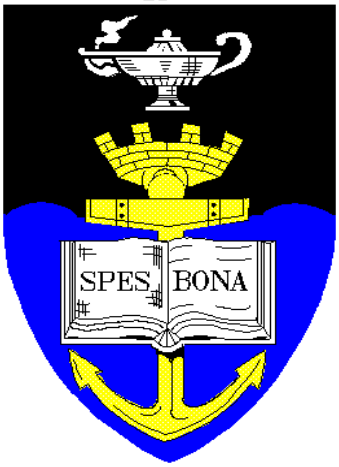

University of Cape Town, South Africa

October 2013

Synthesis and Evaluation of *M.tb* Glycosyltransferase (MshA) Inhibitors

By

Majimi James Sehata

A thesis submitted in fulfilment of the requirements for the degree of Doctor of Philosophy

Department of Chemistry

University of Cape Town, South Africa

Supervisor: Dr Anwar Jardine

October 2013

Declaration

I declare that **"Synthesis and Evaluation of *M.tb* Glycosyltransferase (MshA) Inhibitors"** is my own work and to the best of my knowledge has never been reported or submitted for any degree or examination in any university. All sources of information used herein are cited, acknowledged and completely referenced at the end of each chapter.

Signed by Candidate
Signature Removed

20-11-2014.....

Majimi James Sehata Date

Dedication

To my loving parents, Mosima Mmamoloko (*late*) and Mmona Simon Sehata.

Acknowledgements

First and foremost I would like to thank the almighty God for making everything possible for me in my studies, without him it would not have been possible.

I am also grateful to my supervisor Dr Anwar Jardine for the opportunity he granted me to join his research group and for all his assistance, guidance and patience throughout my PhD studies.

My special appreciation goes to the laboratories of Prof. Erick Strauss, Dr Benjameen Baker (Departments of Biochemistry and Biomedical Sciences, Stellenbosch University, RSA) and Dr Suhail Rafudeen (Department of Molecular and Cell Biology, University of Cape Town, RSA). They allocated me the space in their laboratories and also made their resources available to enable me to do the Biological work. Special thanks go to Prof. Kelly Chibale (Department of Chemistry, University of Cape Town, RSA) to allow me to use his facilities to do the computational studies.

To the former and current Jardine Research Group members, especially Dr Ebrahim Mohamed and Dr Yassir Younis, thank you very much for your advice and support. My gratitude also goes to others in the department that has given me their support and advice including Dr Setshaba David Khanye, Dr Banothile Charity Events Makhubela and Dr Grace Mugumbate for her assistance with computational work.

I am thankful to the National Research Foundation of South Africa (NRF), Department of Chemistry (UCT), Bill and Melinda Gates Foundation and Post Graduate Funding Office (PGFO UCT) for financial support.

Last but not least, in a classical move of “saving the best for last”, I thank my family and relatives for their love and undying support. This kind of achievement would have been impossible without the tremendous sacrifices you have made.

Abstract

The emergence of multiple drug resistant (MDR) and extremely drug resistant (XDR) strains of *Mycobacterium tuberculosis (M.tb)* against the known anti-tuberculosis drug regimens has prompted the need to search for new anti-tubercular drugs. In this study we report the design and synthesis of a series of thiazolidinethione derivatives and substrate mimics, aimed at targeting the mycothiol biosynthetic pathway which is specific to mycobacteria. The strategy involved design of molecules that are expected to compete for the UDP-GlcNAc binding site of the glycosyltransferase (MshA) of *M.tb*. The bioactivity of the designed molecules against *M.tb* in cell free and whole cell assays serves as a basis for further inhibitor optimisation. Amongst the thiazolidinethione derivatives screened, compounds (*Z*)-5-(2,4-dichlorobenzylidene)-2-thioxothiazolidin-4-one (**MJ3A**) and 2-((*Z*)-5-(4-hydroxy-3-methoxybenzylidene)-4-oxo-2-thioxothiazolidin-3-yl)acetic acid (**MJ7B**) were found to be the most potent compounds with a MIC_{50} of 10 μg/mL. In addition, substrate mimics were synthesized and screened for anti-tuberculosis activity. Substrate mimics displayed moderate activity, with exception of substrate mimic (**4-34**) which displayed the highest potency. Tunicamycin which is a known glycosyltransferase inhibitor displayed the highest potency against *M.tb* H37Rv whole cells by inhibiting cell growth with a MIC_{50} of 5 μg/mL. Tunicamycin inhibits the transfer of GlcNAc-1-P from UDP-GlcNAc to polyprenyl monophosphates in a variety of organisms including Gram positive bacteria.

Abbreviations

Å	Angstrom
AcOH	Acetic acid
AgOTf	Silver triflate
AIDS	Acquired Immunodeficiency Syndrome
ARG	Arginine
BnBr	Benzyl bromide
BnOH	Benzyl alcohol
BSH	Bacillithiol
B. anthracis	*Bacillus anthracis*
B. subtilis	*Bacillus subtilis*
Bu_2SnO	Dibutyltin oxide
^{13}C NMR	Carbon Nuclear Magnetic Resonance
CAZy	Carbohydrate-Active Enzyme database
$CDCl_3$	Deuterochloroform
CH_3CN/ACN	Acetonitrile
CO_2	Carbon dioxide
CoA	Coenzyme A
DBU	1,8-Diazabicyclo[5.4.0]undec-7-ene
δ	Chemical shift in ppm
D_2O	Deuterium oxide
d	Doublet
dd	Doublet of doublets
dt	Doublet of triplets
DCC	1,3-Dicyclohexylcarbodiimide

DCM	Dichloromethane
DMAP	*N,N*-Dimethylaminopyridine
DMF	Dimethylformamide
DMSO-d_6	Deuterodimethylsulfoxide
Dol-P	Dolichyl phosphate
ESH	Ergothioneine
et al	et alia
Et_3N	Triethylamine
EtOAc	Ethyl acetate
EtOH	Ethanol
eq.	Equivalent
FCS	Fetal calf serum
g	Grams
GA	Generic algorithm
GC	Guanine and Cytosine
GlcNAc	*N*-acetylglucosamine
GlcNAc-1-P	*N*-acetylglucosamine 1-phosphate
GLY	Glycine
GSH	Glutathione
^1H NMR	Proton Nuclear Magnetic Resonance
H_2	Hydrogen
HBC	High-TB burden countries
HIV	Human immunodeficiency virus
HCl	Hydrochloric acid
HPLC	High Performance Liquid Chromatography

hr	Hour
HRMS	High-resolution mass spectrometry
HTS	High-throughput screening
Hz	Hertz
INH	Isoniazid
INO1	1L-*myo*-inositol-1-phosphate synthase
IR	Infrared spectrometry
J	Coupling constant
KOH	Potassium hydroxide
1-L-Ins-1-P	1-L-*myo*-inositol-1-phosphate
LMT	Low Molecular Weight Thiols
LYS	Lysine
m	Meta
m	Multiplet
M^+	Molecular ion
M. smegmatis	*Mycobacterium smegmatis*
Mca	Mycothiol S-conjugate amidase
MDR	Multiple drug resistance
MeOH	Methanol
mg	Milligram(s)
$MgSO_4$	Magnesium sulphate
MHz	Mega hertz
mL	Millilitre(s)
mmol	Millimole(s)
MOI	Multiplicity of infection

mp	Melting point
MSH	Mycothiol
M.tb	*Mycobacterium tuberculosis*
m/z	Mass to charge ratio
NaCl	Sodium chloride
NaH	Sodium hydride
^{31}P	Phosphorous Nuclear magnetic resonance
P	Para
PDB	Protein data bank
Pd/C	Palladium-on-carbon
$PdCl_2$	Palladium(II) chloride
Pet ether	Petroleum ether
Ph	Phenyl
$(PhO)_2POCl$	Diphenyl phosphorochloridate
PMA	Phorbol myristic acetate
PPh_3	Triphenylphosphine
$(PPh_3)_4Pd$	Tetrakis(triphenylphosphine)palladium(0)
Psi	Pound-force per square inch
Rf	Retention factor
RMS	Root Mean Square
RPM	Revolution per minute
RPMI	Roswell Park Memorial Institute
rt	Room temperature
s	Singlet
SARs	Structure-activity relationships

t	Triplet
TB	Tuberculosis
TFA	Trifluoroacetic acid
THF	Tetrahydrofuran
TLC	Thin layer chromatography
TMSBr	Trimethylsilyl bromide
p-TsOH	*para*-Toluenesulfonic acid
q	Quartet
UDP	Uridine diphosphate
UDP-GlcNAc	Uridine 5'-diphospho-*N*-acetylglucosamine
UGM	UDP-galactopyranose mutase
UMP	Uridine monophosphate
US$	United States Dollar
UV	Ultra violet
v/v	Volume by volume
WHO	World Health Organization
w/v	Weight by volume
XDR	Extremely drug resistance

Table of Contents

CHAPTER 1

Introduction and Background

1.1 Tuberculosis

Tuberculosis (TB) is a bacterial infectious respiratory disease, caused by the bacillus *Mycobacterium tuberculosis* (*M.tb*) and characterized by the formation of tubercles and tissue necrosis as a result of host hypersensitivity and inflammation. TB may be caused under rare occasions, by other *Mycobacterium* species such as *M. bovis* and *M. africanum*.[1] Despite being known for more than a century, to date, TB still remains one of the leading and most deadly infectious diseases for humans globally.[2,3]

Each year, approximately nine million new cases of TB are reported and nearly three million of these cases result in death, thus making TB a major public health concern.[4] In 1993, the World Heath Organisation (WHO) declared TB as a global health emergency. The synergism between human immunodeficiency virus (HIV) and TB further amplifies the rapid spread of TB in developing countries, where fewer resources are available to ensure proper treatment and where HIV may be prevalent.[5] These pandemics (TB and HIV) are strongly interlinked and form a lethal combination, with each other speeding up the progress of one another. According to the WHO, at least one-third of the 33.2 million people living with HIV are co-infected with TB and around 80% of these patients live in Sub-Saharan Africa.[1]

1.1.1 Global distribution of tuberculosis

According to the 2009 WHO global control report the largest number of new TB cases occurred in the South-East Asia followed by the African region.[1] On average

Asian and African regions account for 55% and 31% of the global TB cases respectively and the other three regions account for a small fraction of global cases.[1] The WHO 2011[6] report, has shown a slight improvement on the African region with a drop of 5% from 31% in 2009 to 26% in 2010 whereas the Asian region saw an increase of 4% from 55% in 2009 to 59% in 2010.

1.1.2 Tuberculosis incidences in South Africa

South Africa has been identified as one of the 22 high-TB burden countries (HBC) in the world (WHO, 2011)[6] and it is ranked number three on the global stage (Fielding *et al.*).[7] Due to the high increase in the TB burden, the government adopted a global strategy for TB control called directly observed treatment, short course (DOTS) programme in 1996. This programme was launched by WHO in 1993 and its success rate was estimated to be 67%, which is relatively far lower than the WHO standard rate of 85% (Gandhi *et al.*).[8]

1.2 Drug resistant tuberculosis

The emergence of multiple drug resistance (MDR) and extremely drug resistant (XDR) forms of *M.tb* strains that are resistant to the combined action of the first and second line TB regiment necessitates the use of a new anti-tuberculosis regiment.[9] The current anti-tuberculosis drugs mainly target the biosynthesis of the cell wall.[2] The mycobacterial envelope distinguishes mycobacteria from other species with the aid of a complex, robust cell wall with the ability to withstand the hostile macrophage environment.[10]

These high rates of recurrence of tuberculosis and the emergence of drug resistant *M.tb* strains have led to increased interest and efforts in seeking a better understanding

of the molecular mechanisms of drug resistance and new knowledge which seeks to identify potential novel metabolic targets for chemotherapeutic intervention.[11]

1.3 The current tuberculosis therapy

The current TB therapy is prolonged and involves the use of the combination of first line drugs (rifampicin, isoniazid, pyrazinamide, ethambutol and streptomycin) and second line drugs (kanamycin, *P*-aminosalicyclic acid, ethionamide, cycloserine and fluoroquinolones) (Fig. 1-1).[12] The prolonged usage of multiple drugs leads to non-compliance by the patients and this paves the way for the drug resistance. The goals of TB therapy are to kill tubercle bacilli rapidly, prevent the emergence of drug resistance, eliminate persistent bacilli to prevent relapse, and minimize disease transmission. But these goals are not appropriately met with current TB therapy.

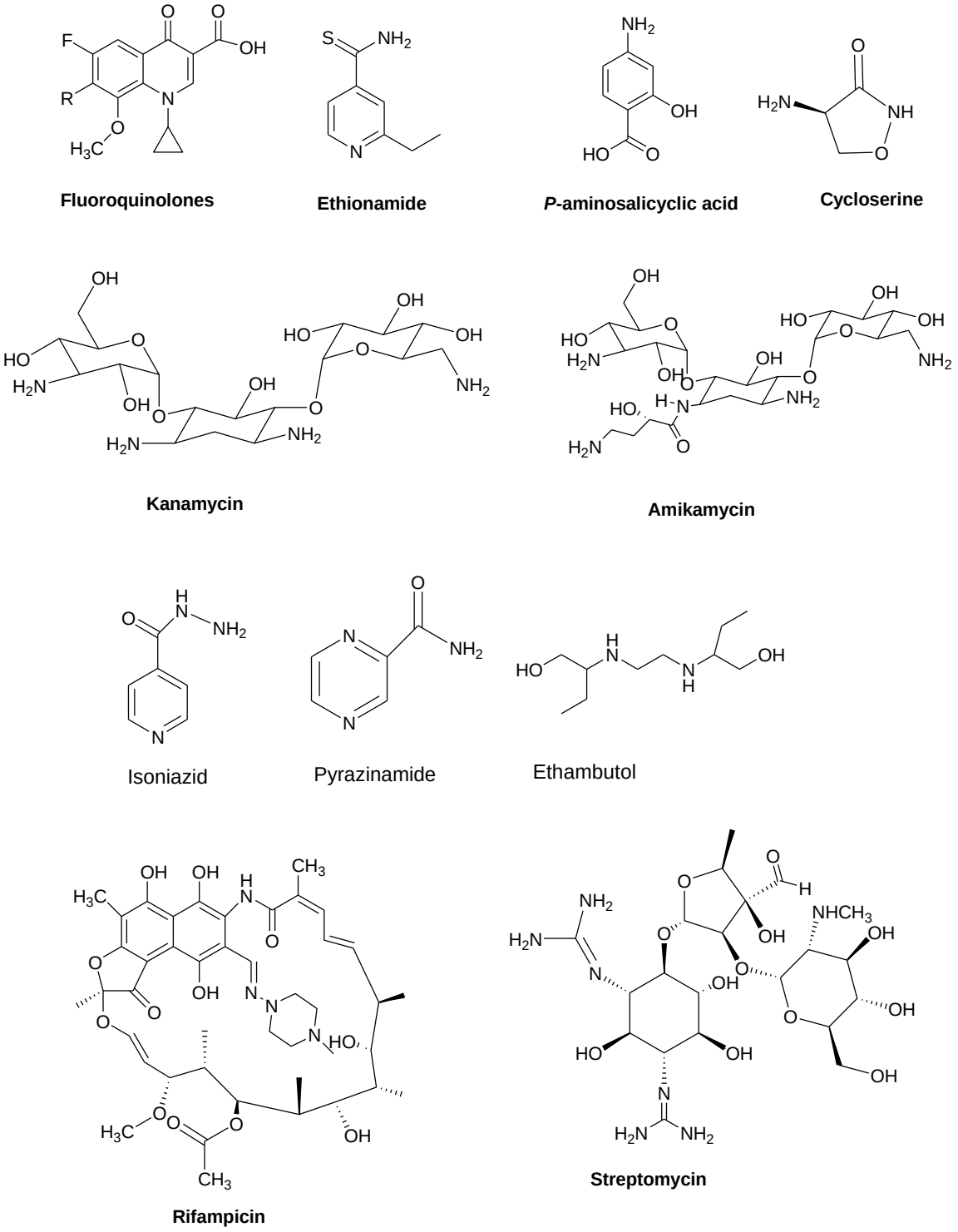

Figure 1-1: Structures of some commonly used anti-tuberculosis drugs.

1.4 The current anti-TB drug candidates in the drug discovery pipeline

Steady progress has been made towards the identification of the new drug targets, drug candidates, and active compounds and thus far very few promising new drugs have been identified (Fig. 1-2).[13,14] Moxifloxacin (MOXI) and gatifloxacin (GATI) are amongst the most promising active fluoroquinolones against *M. tuberculosis* and these drugs have entered the third phase of clinical trials.[15] The study by Nuermberger, *et al.*[16] showed that the use of the combination of drugs (MOXI, RIF and PZA) in mice shortens the treatment period by up to four months.

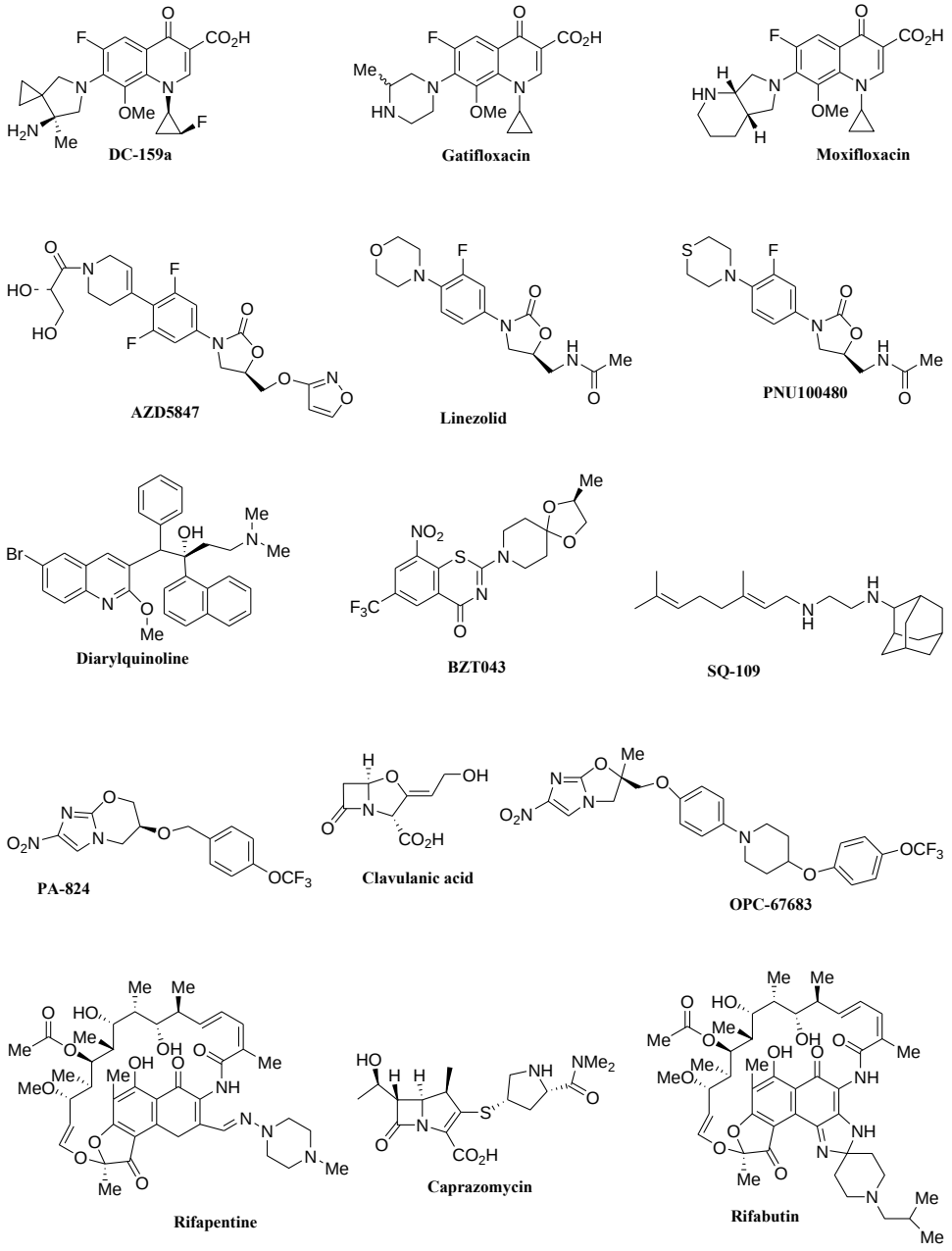

Figure 1-2: Structures of some TB drugs in the developmental stage.

1.5 Design and development of structure based glycosyltransferase inhibitors

In searching for new TB drugs, it is crucial to develop drugs that are active against MDR-TB and shorten the duration of treatment by targeting the recalcitrant and dormant bacilli. Needless to point out that it is important to identify new approaches to achieve these objectives. Developments of new drugs that inhibit novel targets are urgently needed.

Given the increasing need for the developments of new classes of anti-tuberculosis drugs, targeting the enzymes producing low molecular thiols (LMT) is of high interest considering the role the LMT play in the mycobacterial detoxification of xenobiotics. The current anti-TB drugs available function by inhibiting the synthesis of the bacterial cell wall and protein synthesis. The drug candidates under the development also target the inhibition of cell wall as well as DNA synthesis. Currently, there are no drug candidates that target the enzymes involved in the redox balance of the bacteria.

1.6 Low molecular thiol producing bacteria

Under normal circumstances, most bacterial species do not survive inside the macrophages of the host cells, due to the nature and abundance of the acidic phagocytic vacuoles and hydrolytic enzymes.[3] However, organisms have developed some mechanisms to defend themselves against these harsh conditions within various toxic environments of the activated macrophages by producing LMT to protect themselves.[4]

LMT play an important role in the maintenance of the cellular redox homeostasis, as well as for the protection of the cells against alkylating agents (*N*-ethylmaleimide, iodoacetamide) and electrophilic toxins (formaldehyde, methylglyoxal etc).[17] The LMT provides protection against an array of molecules by forming adducts that can be enzymatically converted into less harmful substances.[18] In most cells, the tripeptide glutathione (GSH) is the major LMT. However, many bacteria lack GSH and instead synthesize an alternative LMT such as bacillithiol, mycothiol and ergothioneine (Fig. 1-3).

In mycobacteria, mycothiol (MSH) is the major LMT[19] and studies have demonstrated that MSH has functions analogous to those of GSH in Gram-negative bacteria.[20,21]

These functions include the protection of *M.tb* from toxic oxidants and antibiotics.[22] Most eukaryotes and gram negative bacteria produce GSH as their major thiol instead of MSH.[23,24] Apart from MSH and GSH, filamentous fungi and some members of actinobacteria including mycobacteria produce ergothioneine (ESH) in addition to the major thiols (Ta *et al.*).[25] ESH is a naturally occurring amino acid and a 2-mercapto derivative of histidine.

However, in some low Guanine and Cytosine (GC) content Gram-positive bacteria, coenzyme A (CoA) has proven to be a major thiol. Interestingly, further studies on CoA related thiols in *Bacillus subtilis* and *Bacillus anthracis* lead to the discovery of a novel bacterial thiol, bacillithiol (BSH) as their LMT. Recently this thiol was also detected in *D. radiodurans* in sufficient abundance to permit isolation for structure determination.[26]

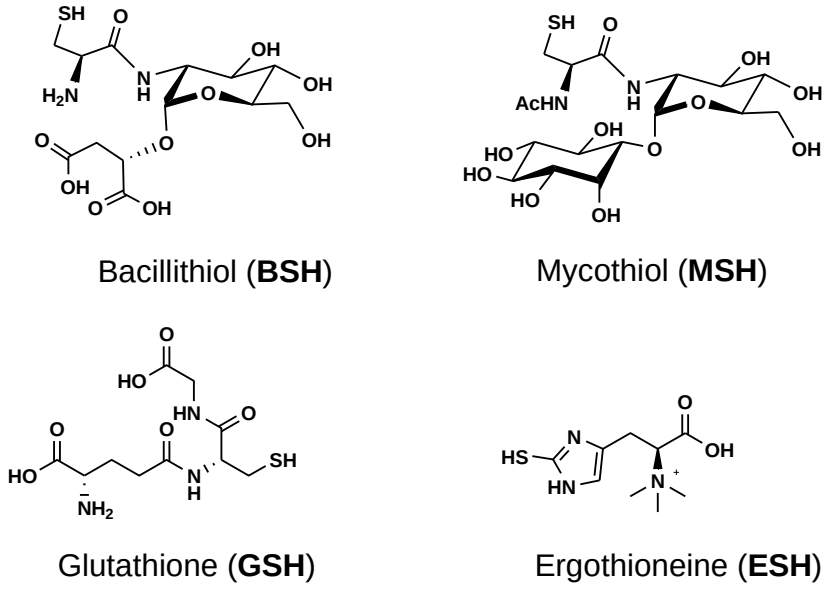

Figure 1-3: Structures of key low molecular major thiols.

1.7 Role of mycothiol (MSH) in cellular detoxification

Mycothiol (MSH) serves a key role in the detoxification of the alkylating agents, which was identified using the fluorescent alkylating agent monobromobimane

(mBBr) that can enter cells and react with LMT. Koledin *et al.*[23] and Newton *et al.*[24] have proposed a mechanism in which MSH detoxifies the harmful toxins entering bacterial cells (Fig. 1-4). According to this mechanism MSH reacts with the mBBr upon their entry into the cells to form a bimane-labelled MSH (MSmB) complex which is subsequently hydrolyzed by mycothiol-*S*-conjugate amidase (Mca) to form a mercapturic acid (AcCsymB) and GlcN-Ins. The mercapturic acid is excreted from the cells whereas GlcN-Ins is retained in the cells for the regeneration of the MSH from 1D-*myo*-inosityl 2-amino-2-deoxy-α-D-glucopyranoside.

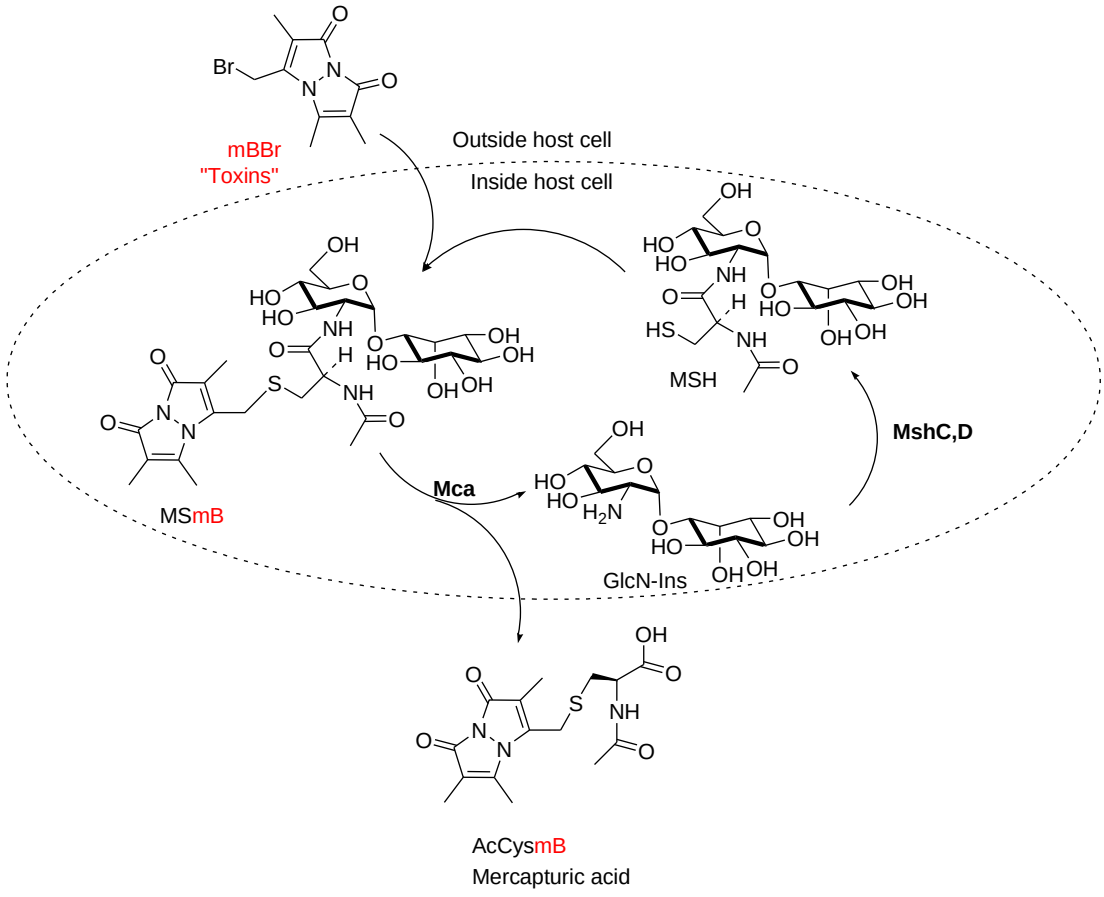

Figure 1-4: The detoxification of harmful thiol reactive agents from the cells.

1.8 The discovery of LMT

The term mycothiol (MSH), (1-*O*-[2-[[(2*R*)-2-(acetylamino)-3-mercapto-1-oxopropyl] amino]-2-deoxy-α-D-glucopyranosyl]-D-*myo*-inositol) was coined for the first time in

1994 and its trivial name was proposed by Spies and Steenkamp.[26] MSH was first isolated from *Streptomyces* strain AJ9463 as the disulfide (MSSM) by Sakuda *et al.*[27] and shortly there after it was reported by two independent studies of Newton *et al.*[28] and Spies *et al.*[26] whereby it was derived from *Mycobacterium bovis*. Sakuda *et al.*[27] eventually proposed the absolute structure of MSH based on NMR analysis and acid hydrolysis experiments. The structure was found to be comprised of three major components of MSH L-cysteine residue with an acetylated amino group and the carboxyl group linked *via* an amide group to D-glucosamine, which in turn forms an α-(1-1)-glycosidic bond with D-*myo*-inositol (Fig. 1-5). From the structure analysis it was noted that MSH was in actual fact discovered in the previous year by Newton and co-workers, labeled as U17, while working on the *Streptomycetes* cell extracts devoid of GSH.[28] Jardine *et al.*[29] first presented a detailed chemo-enzymatic synthesis of MSH. MSH and BSH share some structural similarities and this has facilitated the identification of the biosynthetic genes for BSH in the model organism *B. anthracis*.

BSH was first discovered in *B. anthracis* cell extracts[30] and also in *B. subtilis* as a mixed disulphide with OhrR.[31] Following its discovery, the structural analysis was achieved from the isolated metabolite from *D. Radiodurans*, indicating a compound with L-malate glycosidically linked to glucosamine, which is rare in natural products.[32] The structure of BSH resembles that of MSH with the difference being that the *myo*-inositol has been replaced by malic acid and the cysteine is not *N*-acetylated. The biosynthetic pathway of BSH has been established with the aid of the characterised biosynthetic pathway of MSH, which displayed strong similarities (Fig. 1-5).[31]

1.9 BSH biosynthesis

The partial biosynthetic pathway of BSH have been established[33] (Fig. 1-5) and three of the biosynthetic enzymes (BshA, BshB, BshC) in the pathway have been successfully identified and characterized thus far. The first step in the biosynthetic pathway involves the formation of GlcNAc-Mal using *L*-malate and UDP-*N*-acetyl glucosamine as substrates, catalyzed by BshA.[33,34,35] This is followed by the hydrolysis of the *N*-acetyl group from GlcNAc-Mal to generate GlcN-Mal.[33,34] The final step involves the ligation of cysteine by BshC to generate BSH (Cys-GlcN-Mal).

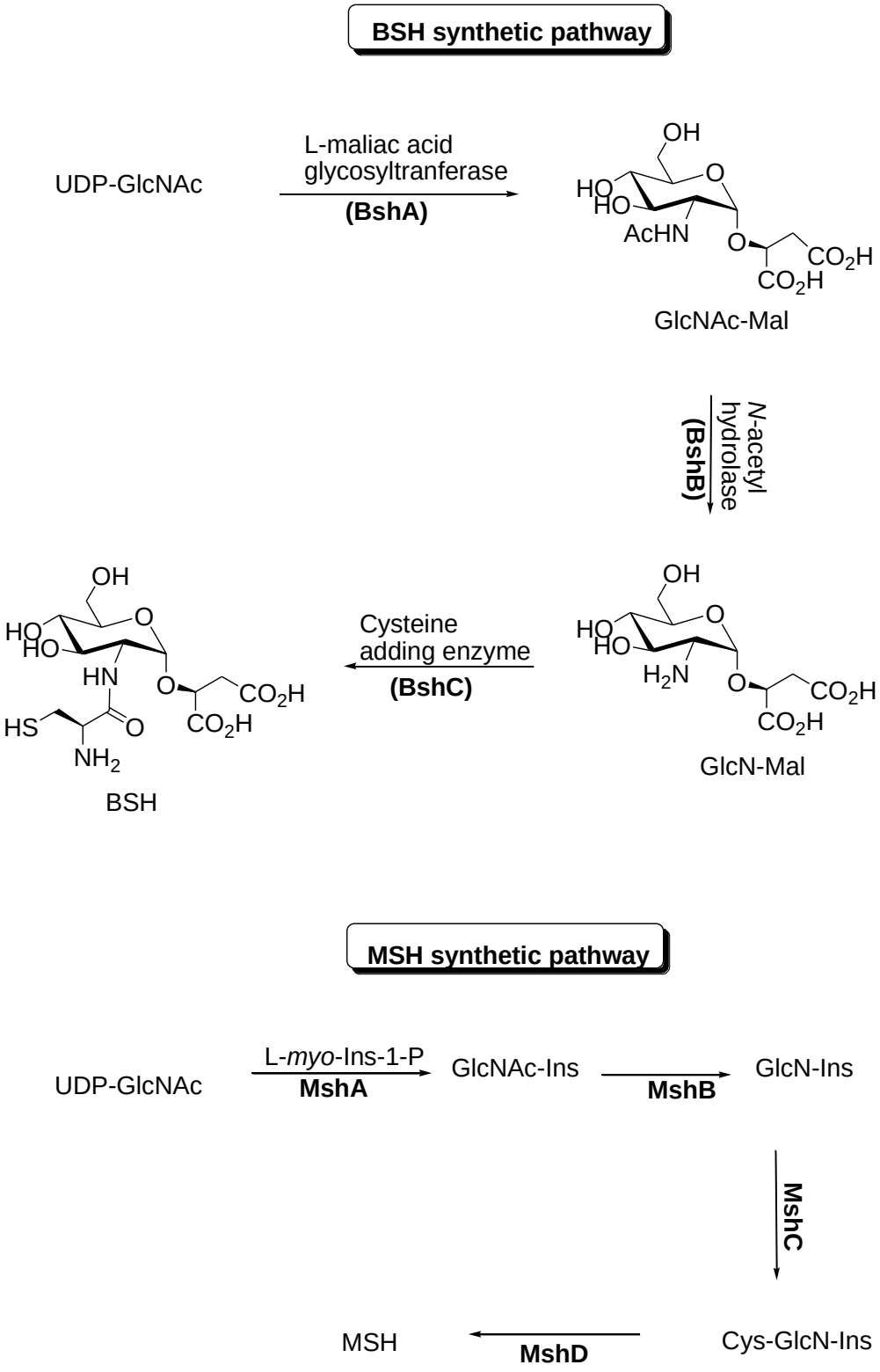

Figure 1-5: Comparison of the proposed BSH and MSH biosynthetic pathway.

1.10 MSH biosynthesis

The biosynthetic pathway of MSH have been established[36] (Fig. 1-6) and four of the five biosynthetic enzymes (MshA, MshB, MshC and MshD) in the pathway have been successfully identified and characterized thus far.[37] The enzymes involved in MSH biosynthesis have been found to be interesting as potential drug targets in the treatment of tuberculosis.

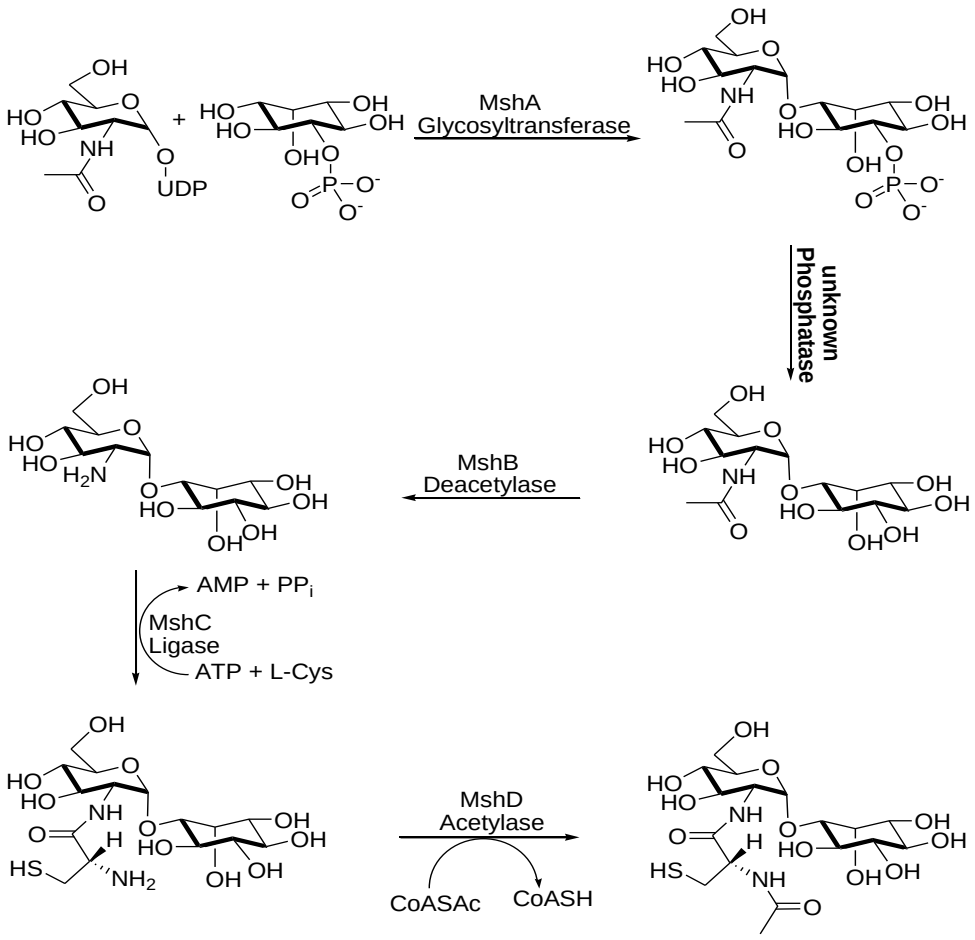

Figure 1-6: Biosynthetic pathway of mycothiol.

The first obligate step in the biosynthesis of MSH involves the glycosyltransferase (MshA). This enzyme catalyzes the formation of 3-phospho-1-D-*myo*-inosityl-2-acetamido-2-deoxy-α-D-glucopyranoside by transferring *N*-acetylglucosamine from

UDP-*N*-acetylglucosamine (UDP-GlcNAc) to 1-L-*myo*-inositol-1-phosphate (1-L-Ins-1-P) (Fig. 1-7), which is subsequently dephosphorylated by a yet to be identified phosphatase to generate GlcNAc-Ins.[38] Following the dephosphorylation of GlcNAc-Ins-3P, a zinc dependent *N*-acetyl hydrolase (MshB) catalyzes the hydrolysis of the *N*-acetyl group to give the free amino sugar $GlcNH_2$-Ins.[37] The resultant $GlcNH_2$-Ins is ligated with cysteine in a reaction catalyzed by MshC (ligase).[39] The final step in the MSH synthesis is carried out by MshD (mycothiol synthase) which transfers an acetyl group from acetyl-CoA to 1D-*myo*-inosityl 2-amido-2-deoxy-α-D-glucopyranoside.[23]

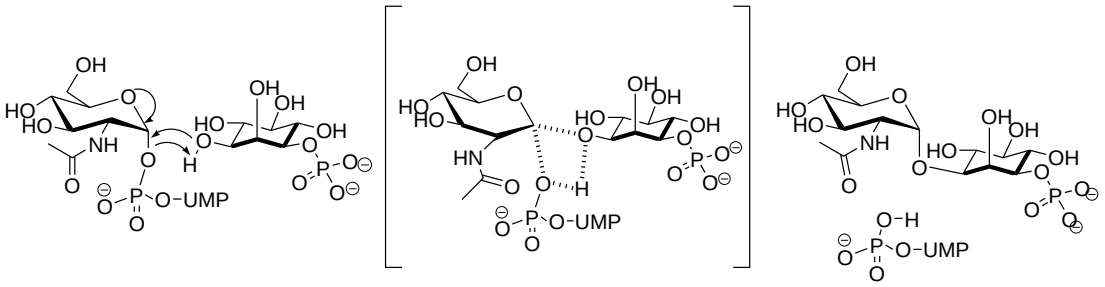

Figure 1-7: Summary of proposed catalytic mechanism for production of GlcNAc-Ins-P by MshA.

1.10.1 Glycosyltransferase (MshA)

The gene encoding MshA, Rv0486 (*mshA*) was discovered by Newton *et al.*[40] while working on *M. smegmatis* and demonstrated more than 75% sequence similarity with the corresponding gene in *M. tb* in a 446-residue overlap.[40] Based on the amino acid sequence homology and three-dimensional structure, MshA was grouped into the Carbohydrate-Active Enzyme database (CAZy) family GT-4, all of which have been found to be retaining glycosyltransferases and have a GT-B fold.[36,41]

The GT-4 is the second largest CAZy database family which comprises of 90 distinct families, which include several other key enzymes such as sucrose synthase, sucrose phosphate synthase, mannosyl transferase and GlcNAc transferase.[36,41] This group of

enzymes catalyze the transfer of a sugar residue from an activated nucleotide sugar donor to a specific acceptor molecule, resulting in the formation of a glycosidic bond. The transfer of sugar residue occurs with either retention or inversion of the configuration of the anomeric carbon (Fig. 1-8).[41,42]

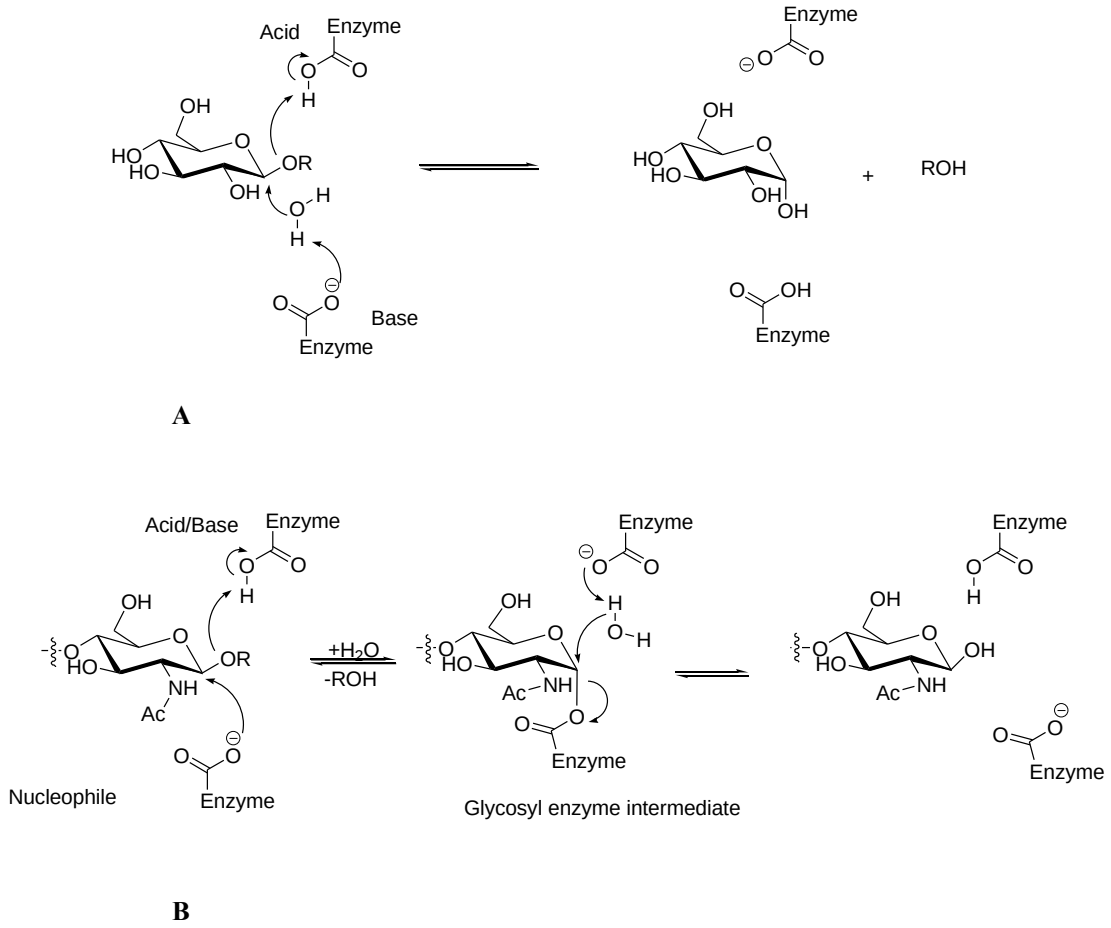

Figure 1-8: Illustration of enzyme mechanism (**A**: inversion and **B**: retention) of the anomeric carbon.

1.10.1.1 MshA as drug target

The mutated strains of *M. smegmatis* with modifications of genes encoding the MSH biosynthetic enzymes (MshA, MshB, MshC and MshD) have been investigated for MSH production and drug susceptibility.[23,39,40,43] Since most of the genes for mycothiol biosynthesis have been identified using the non-pathogenic *M. smegmatis*, similar strategies have been used to generate the corresponding mutants of *M.tb.* With the MSH pathway absent in the eukaryotes and other eubacteria, the enzymes

involved in the biosynthesis of MSH presents potential as specific chemotherapeutic targets against actinomycetes including mycobacteria species.[40,43]

Previous studies by Newton *et al.* have elucidated that the *mshA* gene was essential for the production of GlcNAc-Ins and therefore synthesis of MSH in *M. smegmatis*.[40] Further disruptions of the *mshA* gene in *M. tb Erdman* have indicated that the gene was essential for the growth of this pathogen.[44] Gene knockout studies of MshA-D and their effects on intracellular MSH levels in various MSH producing bacteria have been reported.[39,40,43] The most widely studied MshA-D gene knockouts effects have been done in *M. smegmatis*. A comparative analysis of *M. smegmatis* MshA-D mutants to antibiotics, pH, oxidative stress and osmotic stress have showed that mutants which are devoid of MSH show a greater increase in sensitivity to electrophiles, oxidants and a range of antibiotics. MshA mutants lead to no production of MSH and MSH biosynthetic intermidiates as compared to MshB-D mutants, which retain reduced levels of MSH and MSH biosynthetic intermidiates.

Two independent studies by Buchmeier *et al*[44] and Rawat *et al*[43] have demonstrated that the inactivation of the *mshB* gene does not completely block the biosynthesis of MSH in both the *M. smegmatis* and *M.tb.* These observations were attributable to the presence of a MshB orthologue, mycothiol amidase (Mca), which act as an alternative deacetylase in the absence of MshB, leading to modest production of GlcNAc-Ins in both species.[39,45]

Further studies on MSH by Newton *et al.* and Buchmeier *et al.* have respectively investigated and demonstrated that inactivation of the *mshD* gene in *M. smegmatis* and *M.tb* does not fully block the MSH production. Their findings were therefore attributed to the low levels of MSH being produced in both *mshD* mutants by the

chemical transacetylation reaction of acetyl-CoA with Cys-GlcN-Ins that accumulates at high levels in both *mshD* mutants.[45,46] Thus far, MshA is a key enzyme in the biosynthetic pathway of MSH and it would therefore be very interesting to find what are the implications of complete blockade of this enzyme.

1.10.1.2 The crystal structure of MshA

The crystal structure of MshA (Fig. 1-9) consists of two β/α/β Rossman-fold domains connected by a short hinge region.[41] According to Vetting *et al.*[36], the N-terminal domain consists of an eight-stranded β-sheet (β8, β7, β6, β5, β1, β2, β4, and β3) which is bounded by six-α-helices (α1-α5 and α14) whereas the C-terminal domain is made up of a six-stranded β-sheet (β11, β10, β9, β12, β13 and β14) which is bound to eight α-helices (α6–α13). The study further demonstrated that the active site was located between N- and C- terminal domains and it is > 30 Å from the dimer interface at its closest points.[36]

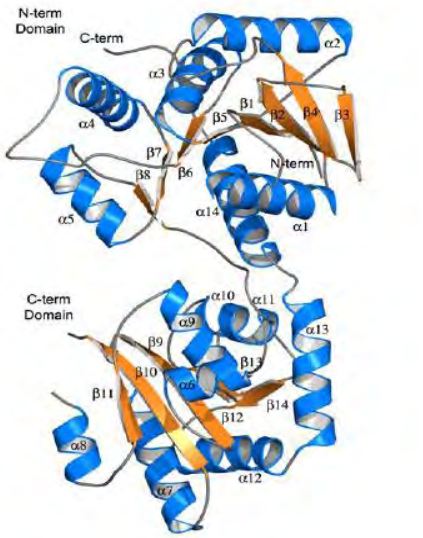

Figure 1-9: Shows a ribbon like crystal structure of cgMshA monomer (Helices: blue, strands: orange and coils: grey).

1.10.2 Deacetylase (MshB)

MshB is a metal-dependent hydrolase that catalyses the hydrolysis of the *N*-acetyl group to give the free amino sugar $GlcNH_2$-Ins, homologous to the mycothiol dependent detoxification enzyme mycothiol *S*-conjugate amidase (Mca).[47] Previous structural analysis of MshB has indicated Zn^{2+} as an active metal coordinator, however recent MshB structural analysis by Huang and Hernick[48] reported the high activity of iron coordinated by two histidine moieties (His13 and His147) and aspartame (Asp16) and two water molecules whereby one water molecule is displaced during the binding of MshB to the α-GlcN-Ins.

The catalytic mechanism for MshB was proposed by Maynes *et al.*[49] based on the crystal structure. According to this mechanism, Asp15 residue serves as a general base for the deprotonation of water molecule and the resulting hydroxyl group acts as a nucleophile to the amide carbonyl of the acetyl group. The developing negative charge on the carbonyl oxygen is stabilized by hydrogen bonding to the protonated His144. The last step of the deacetylation is accomplished by the proton transfer to the nitrogen of α-GlcN-Ins which is mediated through the acid function of Asp15. The mechanism for metal coordination by MshB is depicted in Figure 1-10.

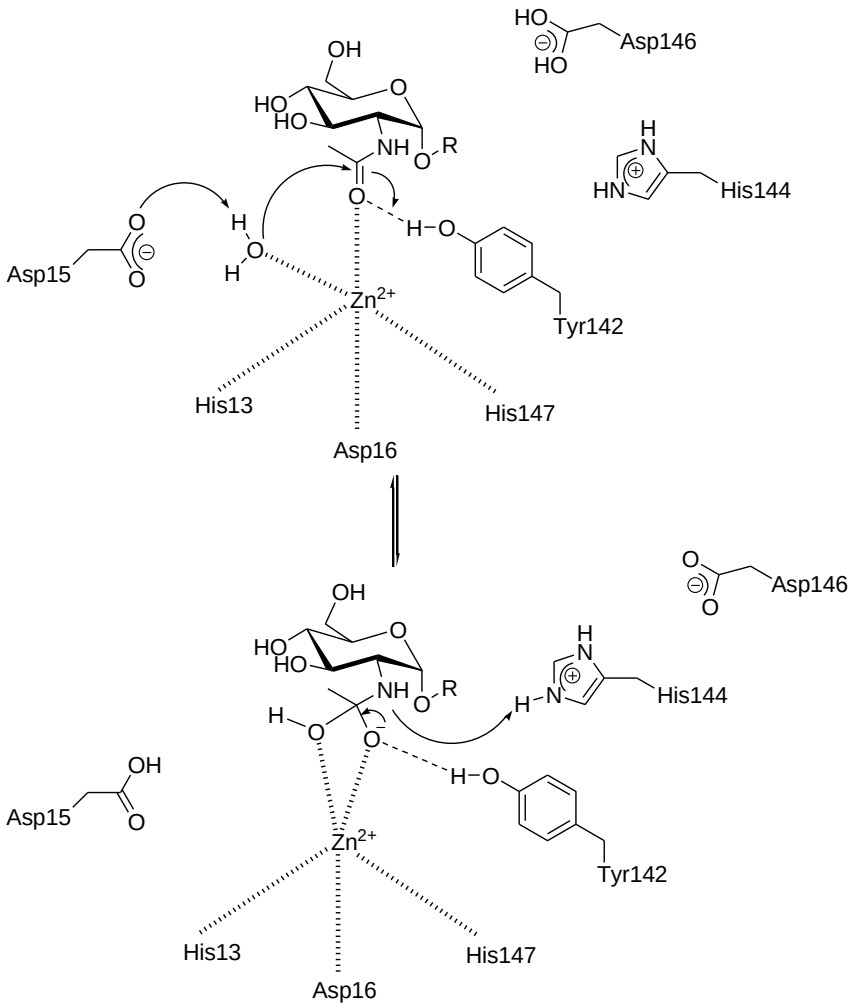

Figure 1-10: Proposed catalytic mechanism for MshB.

1.10.3 The ligase (MshC)

MshC is encoded for by the gene *Rv2130c* or *mshC* and it catalyses the ATP-dependent conjugation of cysteine with $GlcNH_2$-Ins. The mechanism show that ATP binds first followed by the coupling of the cysteine residue to give the Cys-AMP complex.[50,51] Subsequently, a pyrophosphate molecule is released after GlcN-Ins-amine complex formation followed by the release of CysGlcN-Ins and AMP (Fig. 1-11).

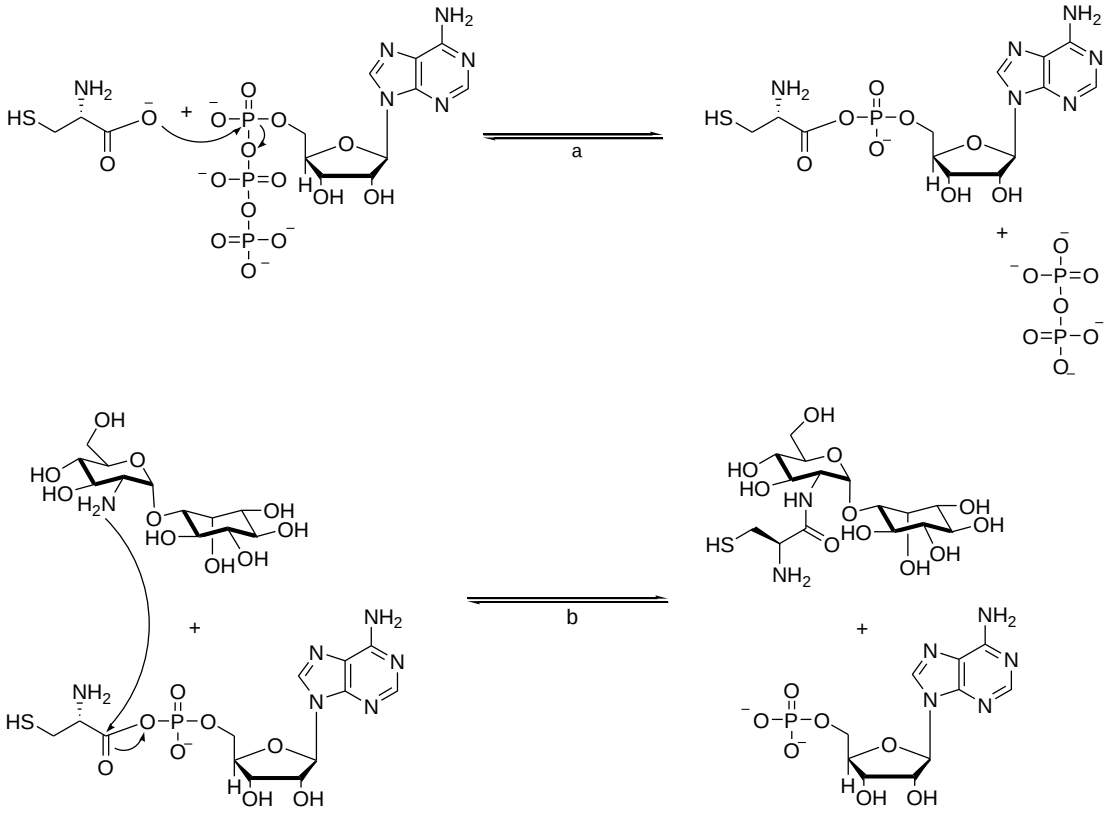

Figure 1-11: Catalytic mechanism for MshC. (**a**) ATP first binds to MshC followed by cysteine (Cys), forming an MshC-ATP-Cys complex. MshC releases a pyrophosphate molecule upon formation of the cysteine-adenylate compound which is still bound to the active site. (**b**) αGlcN-Ins bind to MshC and the amide bond between αGlcN-Ins and Cys is formed with the cleavage of the adenylate anhydride, resulting in Cys-αGlcN-Ins and AMP.

1.10.4 Mycothiol Synthase (MshD)

Mycothiol synthase (MshD) is the fifth and final enzyme in the MSH biosynthetic pathway. MshD belongs to the GCN5 related family of *N*-acetyltransferases (GNATS), which catalyses the transfer of an activated acetyl group from acetyl-CoA to the primary amine.[52] The presence of mycothiol synthase activity was first demonstrated in *M. smegmatis*[53] and the enzyme was later cloned and expressed in *Escherichia coli*.[54a] The sequence of MshD was found to be twice the length of the typical GNAT protein and also exhibited two distinct regions with homology to GNATs suggesting that MshD may be composed of two GNAT domains.[52] Blanchard

and co-workers reported the crystal structure of MshD derived from *M.tb*. Subsequently the catalytic mechanism of this enzyme (synthase) was proposed based on its crystal structure (Fig. 1-12).[54b] According to this mechanism the highly charged amino acid Glu234 acts as a base and therefore polarise a structured water molecule. The Leu238 and NH stabilize the negative charge developed during the transition state of the acetyl carbonyl residue. The Tyr294 protonates the complex to generate the thiolated CoA.

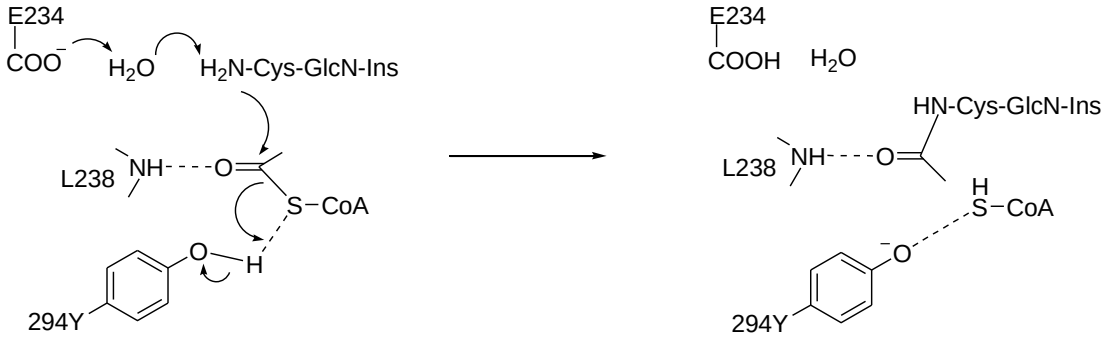

Figure 1-12: Catalytic mechanism for MshD.

1.11 Chemical synthesis of MSH

Since the discovery of MSH, enormous synthetic efforts were made in pursuit of chemically synthesized MSH. Previously the D-*myo*-inositol portion of the MSH was reported with the wrong stereochemical orientation and it was referred as L-*myo*-inositol.[26,55] The ambiguity surrounding the stereochemistry of the MSH structure was resolved by the chemical synthesis of bimane-labelled MSH (MSmB) whose optical rotation, circular dichroism and Mca substrate properties were reported to be the same as that of the MSmB prepared from the cell extracts.[56]

Several possible methods for the synthesis of MSH have been reported in the literature. The classical methods for the synthesis of MSH start with the ketalization

of *myo*-inositol which is cheap and readily available. Vacca *et al.*[57] reported the ketalization of *myo*-inositol by employing 1-ethoxycyclohexene in the presence of catalytic amount of *p*-toluenesulphonic acid monohydrate to yield biscyclohexylidine ketals in quantitative yields (Scheme 1-1).

Selective benzylation of 1,2:4,5-dicyclohexylidene-*myo*-inositol (**1-3**) gave the 3-benzyl-1,2:4,5-dicyclohexylidene-*myo*-inositol (**1-4**).[29] Subsequently, the 3-benzyl-1,2:4,5-dicyclohexylidene-*myo*-inositol (**1-4**) products were resolved as the camphanate esters, using known literature procedures to give (**D**) and (**L**), respectively (Scheme 1-1).[57,58]

Basic hydrolysis of the camphanate ester and ketal cleavage of desired D enantiomer in acetic acid ensured the monobenzylated *myo*-inositol which was subsequently acetylated to give D-1-*O*-benzyl-2,3,4,5,6-penta-*O*-actetyl-*myo*-inositol (Scheme 1-1).[59]

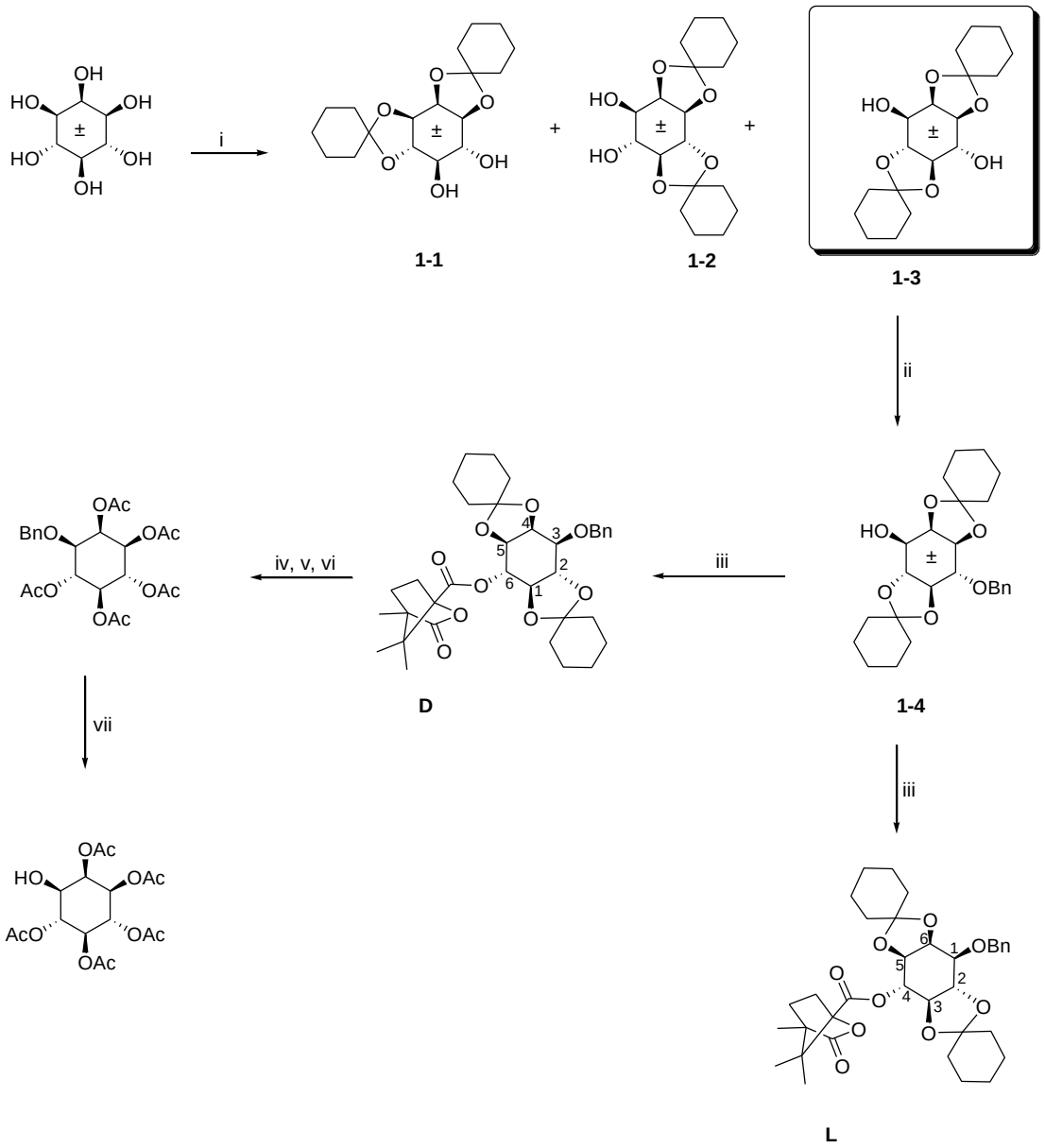

Scheme 1-1: Reaction conditions: (i) 1-ethoxycyclohexane, *P*-TsOH and DMF; (ii) NaH, BnBr and toluene; (iii) camphanic acid chloride; Et_3N and DCM; (iv) (a) KOH and ethanol; (b) 80 % acetic acid (v/v); (v) acetic anhydride and pyridine; (vi) H_2 and Pd/C.

Jardine *et al*. reported the Koenigs-Knorr mediated coupling of (-)-2,3,4,5,6-penta-*O*-actetyl-*myo*-inositol and 3,4,6-tri-O-accetyl-2-deoxy-2-(2,4-dinitrophenylamino)-α-D-glucopyranosyl bromide to obtain a (1:1) mixture of α/β pseudo-disaccharide in 60% yield (Scheme 1-2). Similar glycosylation studies were reported by Nicholas *et al*. by directly coupling 2,3:4,5 cyclohexylidene with 3,4,6-tri-O-acetyl-2-deoxy-2-azido-2-

deoxy-α-D-glucopyranosyl chloride prior to deprotection of the sugar moiety in the presence of silver triflate (AgOTf) and 2,6-diisopropyl-4-methylpyridine to obtain a mixture of anomers α/β in 2:1 ratio in 70% yield. Treatment of the protected pseudo-disaccharides using an anion exchange resin (IR400-OH) was reported and followed by the enzymatic coupling of the cysteine to the pseudo-disaccharide in the final synthesis of the mycothiol.

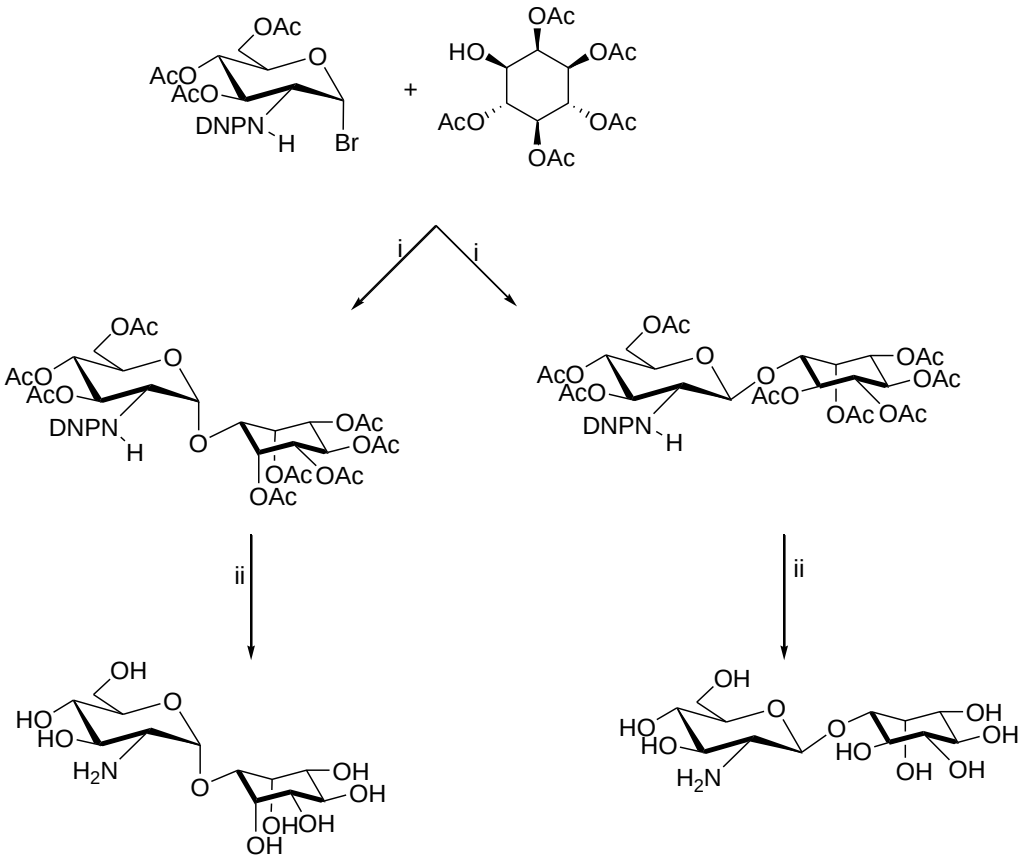

Scheme 1-2: Reaction conditions: (i) AgOTf, 2,6-*tert*-dibutylpyridine and DCM; (ii) Amberlite IR400 (OH).

1.12 Concluding remarks

The enzymes in the MSH pathway has been identified as a potential drug targets for drug discovery considering the role MSH is playing in the detoxification of xenobiotics and as redox buffer. The enzymes involved in the biosynthetic pathway of

MSH are essential for the production of MSH and could serve as potential drug targets for tuberculosis co-therapy. This is based on the fact that the previous studies have demonstrated that inhibition of MSH genes responsible for the production of these enzymes has significantly reduced the survival of *M.tb* and *M. smegmatis* mutants. Moreover, the successful inhibition of MSH biosynthetic enzymes will lead to the disruption of the MSH-dependent detoxification pathway at two levels: biosynthesis and detoxification.

1.13 Scope and objectives of the study

(i) The primary objective of this work is to design and synthesize selective inhibitors targeting the glycosyltransferase MshA, the first committed step in the biosynthesis of MSH. These inhibitors incorporate the UDP and sugar components of the natural substrate, while altering the pyrophosphate moiety to abolish turnover or enhance the binding. Substitution of the anomeric oxygen in oligosaccharides and other glycoconjugates with a sulfur atom will present a very interesting class of compounds in the form of thioglycosides.[60] Furthermore, the thioglycosylated saccharides resists glycosidase mediated degradation, thus making them more favorable targeted compounds with greater likelihood of reaching their intended target Xhu *et al*.[61] In addition to their wide range of applications the *S*-glycosidic compounds can also be used as glycosyl donors, enzyme inhibitors, enzyme resistant scaffolds and enzyme mimetic.

(ii) Perform enzyme assays and screen whole cells in order to assess and evaluate the effectiveness of the inhibitors synthesized towards the selectivity of MshA.

(iii) In order to achieve these objectives, 1-L-*myo*-inositol-1-phosphate (1-L-Ins-1-P) had to be synthesized. 1-L-Ins-1-P is an important co-substrate required by MshA and

it is currently isolated from the yeast cells. This product is isolated in low yields and it is too expensive (400$/mg). It was decided to synthesize this substrate as large quantity was required for the planned enzyme assays.

1.14 References:

1. **WHO, 2009.** Fact Sheet. http://www.who.int/tb/challenges/hiv/factsheet_hivtb_2009.pdf. Accessed June 2009.

2. **Mdluli, K. and Spigelman, M. 2006.** Novel targets for tuberculosis drug discovery. *Current opinion in Pharmacology*. **6**: 459-467.

3. **Fenton, M. J. and Vermeulen, M. W. 1996.** Immunopathology of tuberculosis. Roles of macrophages and monocytes. *Infection and immunity*: **64**(3): 683-690.

4. **Ung, K. S. E. and Av-Gay, Y. 2006.** Mycothiol-dependent mycobacterial response to oxidative stress. *FEBS letters*. **580**: 2712-2716.

5. **de Azevedo Jr, W. F., Canduri, F., de Oliveria, J. S., Basso, L. A., Palma, M. S., Pereira, J. H. and Santos, D. S. 2002.** Molecular model of shikimate kinase from *Mycobacterium tuberculosis*. *Biochemical and Biophysical research communications*. **295**: 142-148.

6. **WHO, 2011.** Global tuberculosis control. http://www.who.int/tb/publications/global_report/en/. Accessed 07 March 2012.

7. **Fielding, K. L., Grant, A. D., Hayes, R. J., Chaisson, R. E., Corbett, E. L. and Churchyard, G. J. 2011.** Thibela TB: Design and methods of a cluster randomized trial of the effect of community-wide isoniazid preventive therapy on tuberculosis amongst gold miners in South Africa. *Contemporary clinical trials*. **32**: 382-392.

8. **Gandhi, N. R., Moll, A., Sturm, A. W., Pawinski, R., Govender, T., Lalloo, U., Zeller, K., Andrews, J. and Friedland, G. 2006.** Extensive drug resistant tuberculosis as a cause of death in patients co-infected with tuberculosis and HIV in a rural area of South Africa. *Lancet*. **368**: 1575-1580.

9. **Zhang, Y., Post-Martens, K. and Denkin, S. 2006.** New drug discovery candidates and therapeutic targets for tuberculosis therapy. *Drug discovery today*. **11**: 21–27.

10. **Rusch-Gerdes, S., Domehl, C., Nardi, G., Gismondo, M. R., Welscher, H. and Pfyffer, G. E. 1999.** Multicenter evaluation of the mycobateria growth inhibitor tube for testing susceptibility of *Mycobacterium tuberculosis* to first line drugs. *Journal of clinical Microbiology*. **37**(1): 45-48.

11. **Patel, M. P. and Blanchard, J. S. 1999.** Expression, purification and characterization of *Mycobacterium tuberculosis* mycothione reductase. *Biochemistry*. **38**: 11827-11833.

12. **Zhang, Y., Post-Martens, K. and Denkin, S. 2006.** New drug discovery candidates and therapeutic targets for tuberculosis therapy. *Drug discovery today*. **11**: 21-27.

13. **Zhang, Y. 2007.** Advances in the treatment of tuberculosis. *Clinical Pharmacology and Therapeutics*. **82**(5): 595–600.

14. **Kanelo, T., Cooper, C. and Mdluli, K. 2011.** Challenges and opportunities in developing novel drugs for TB. *Future Medicinal Chemistry*. **3**(11): 1373-1400.

15. **Ginsberg, A. M. and Spigelman, M. 2007.** Challenges in tuberculosis drug research and development. *Nature Medicine*. **13**(3): 290-294.

16. **Nuermberger, E., Yoshimatsu, T., Tyagi, S., O'Brien, R. J., Vernon, A. N., Chaisson, R. E., Bishai, W. R. and Grosset, J. H. 2004.** Moxifloxacin-containing regimen greatly reduces time to culture conversion in murine tuberculosis. *American Journal Respiratory and Critical Care Medicine.* **169**: 421–426.

17. **den Hengst, C. D. and Buttner, M. J. 2008.** Redox control in actinobacteria. *Biochimia et Biophysica Acta*. **1780**: 1201-1216.

18. **Antelmann, H., Hecker, M., Zuber, P. 2008.** Proteomic signatures uncover thiol-specific electrophile resistance mechanisms in *Bacillus subtilis*. *Expert Review of Proteomics*. **5**: 77–90.

19. **Newton, G. L., Arnold, K., Price, M. S., Sherrill, C., delCardayré, S. B., Aharonowitz, Y., Cohen, G., Davies, J., Fahey, R. C., and Davis, C. 1996.** Distribution of thiols in microorganisms: Mycothiol is a major thiol in most actinomycetes. *Journal of Bacteriology*. **178**: 1990−1995.

20. **Newton, G. L., Buchmeier, N., and Fahey, R. C. 2008**. Biosynthesis and functions of mycothiol, the unique protective thiol of Actinobacteria. *Microbiology and Molecular Biology Reviews*. **72**: 471−494.

21. **Rawat, M. and Av-Gay, Y. 2007.** Mycothiol-dependent proteins in actinomycetes. *FEMS Microbiology Reviews*. **31**: 278−292.

22. **Dipti, S., Newton, G. L., Fahey, R. C. and Buchmeier, N. A. 2003.** Mycothiol is essential for growth of mycothiol tuberculosis Erdman. *Journal of Bacteriology*. **185**(22): 6736-6740.

23. **Koledin, T., Newton, G. L. and Fahey, R. C. 2002**. Identification of the mycothiol synthase gene (mshD) encoding the acetyltranseferase producing mycothiol in actinomycetes. *Archives of Microbiology*. **178**: 331-337.

24. **Newton, G. L., Av-Gay, Y. and Fahey, R. C. 2000.** A novel mycothiol-dependent detoxification pathway in mycobacteria involving mycothiol S-conjugate amidase. *Biochemistry*. **39**: 10739-10746.

25. **Ta, P., Buchmeier, N., Newton, G. L., Rawat, M. and Fahey, R. C. 2011.** Organic hydroperoxide resistance protein and ergothioneine compensate for loss of mycothiol in *Mycobacterium smegmatis* mutants. *Journal of Bacteriology*. **193**(8): 1981-1990.

26. **Spies, H. S. C. and Steenkamp, D. J. 1994.** Thiols of intracellular pathogens identification of ovothiol A in *Leishmania donovani* and structural analysis of a novel thiol from *Mycobacterium bovis*. *European Journal of Biochemistry*. **224**: 203–213.

27. **Sakuda, S. Z., Zhou, Y. and Yamada, Y. 1994.** Structure of a novel disulfide of 2-(*N*-acetylcysteinyl)amido-2-deoxy-α-D-glucopyranosyl-*myo*-inositol produced by *Streptomyces* sp. *Bioscience, Biotechnology and Biochemistry*. **58**: 1347–1348.

28. **Newton, G. L., Bewley, C. A., Dwyer, T. J., Horn, R., Aharonowitz, Y., Cohen, G., Davies, J., Faulkner, D. J. and Fahey, R. C. 1995**. The structure of U17 isolated from *Streptomyces clavuligerus* and its properties as an antioxidant thiol. *European Journal of Biochemistry*. **230**: 821–825.

29. **Jardine, M. A., Spies, H. S. C., Nkambule, C. M., Gammon, D. W. and Steenkamp, D. J. 2002**. Synthesis of mycothiol, 1D-1-O-(2-[*N*-acetyl-L-cysteinyl]amino-2-deoxy-α-D-glucopyranosyl)-*myo*-inositol, principal low molecular mass thiol in the actinomycetes. *Bioorganic and Medicinal Chemistry*. **10**(4): 875–881.

30. **Soonsanga, S., Lee, J. W. and Helmann, J. D. 2008.** Oxidant-dependent switching between reversible and sacrificial oxidation pathways for *Bacillus subtilis* OhrR. *Molecular Microbiology*. **68**(4): 978–986.

31. **Helmann, J. D. 2011.** Bacillithiol, a new player in bacterial redox homeostasis. *Antioxidants and Redox signalling*. **15**(1): 123-133.

32. **Newton, G. L., Rawat, M., La Clair, J. J., Jothivasan, V. K., Budiarto, T., Hamilton, C. J., Clairborne, A., Helmann, J. D. and Fahey, R. C. 2009.** Bacillithiol is an antioxidant thiol produced in bacilli. *Nature Chemical Biology*. **5**(9): 625–627.

33. **Gaballa, A., Newton, G. L., Antelmann, H., Parsonage, D., Upton, H., Rawat, M., Claiborne, A., Fahey, R. C. and Helmann, J. D. 2010.** Biosynthesis and functions of bacillithiol, a major low-molecular-weight thiol in bacilli. *PNAS*. **107**(14): 6482-6486.

34. **Parsonage, D., Newton, G. L., Holder, R. C., Wallace, B. D., Paige, C., Hamilton, C. J., Dos Santos, P. C., Redinbo, M. R., Reid, S. D. and Claiborne, A. 2010.** Characterization of the *N*-acetyl-α-D-glucosaminyl l-malate synthase and deacetylase functions for bacillithiol biosynthesis in *Bacillus anthracis*. *Biochemistry*. **49**: 8398-8414.

35. **Upton, H., Newton, G. L., Gushiken, M., Lo, K., Holden, D., Fahey, R. C. and Rawat, M. 2012.** Characterization of BshA, bacillithiol glycosyltransferase from *Staphylococcus aureus* and *Bacillus subtilis*. *FEBS letter*. **586**: 1004–1008.

36. **Vetting, M. W., Frantom, P. A. and Blanchard, J. S. 2008.** Structural and enzymatic analyses of MshA from *Corynebacterium glutamicum*: Substrate-assisted catalysis. *Journal of Biochemistry and Molecular Biology*. **283**(23): 15834-15844.

37. **Jothivasan, V. K. and Hamilton, C. J. 2008.** Mycothiol: synthesis, biosynthesis and biological functions of the major low molecular weight thiol in actinomycetes. *Natural Products Report*. **25**: 1091-1117.

38. **Buchmeier, N. and Farey, R. C. 2006.** The MshA gene encoding the glycosyltranferase of mycothiol biosynthesis is essential in *Mycobacterium tuberculosis* Erdman. *FEMS Microbiology letter*. **264**: 74-79.

39. **Rawat, M., Kovacevic, S., Billman-Jacobe, H. and Av-Gay, Y. 2003**. Inactivation of mshB, a key gene in the mycothiol biosynthesis pathway in *Mycobacterium smegmatis*. *Microbiology*. **149**: 1341-1349.

40. **Newton, G. L., Koledin, T., Gorovitz, B., Rawat, M., Fahey, R. C. and Av-Gay, Y. 2003.** The glycosyltransferase gene encoding the enzyme catalyzing the first step of mycothiol biosynthesis (*mshA*). *Journal of Bacteriology*. **185**: 3476-3479.

41. **Fan, F., Vetting, M. W., Frantom, P. A. and Blanchard, J. S. 2009.** Structures and mechanisms of the mycothiol biosynthetic enzymes. *Current opinion in Chemical Biology*. **13**: 444-452.

42. **Newton, G. L., Ta, P., Bzymek, K. P. and Fahey, R. C. 2006.** Biochemistry of the initial steps of mycothiol biosynthesis. *Journal of Biological Chemistry*. **201**(45): 33910-33920.

43. **Rawat, M., Newton, G. L., Ko, M., Martinez, G. J., Fahey, R. C. and Av-Gay, Y. 2002.** Mycothiol deficient *Mycobacterium smegmatis* mutants are hypersensitive to alkylating agents, free radicals and antibiotics. *Antimicrobial Agents and Chemother*. **46**: 3348-3355.

44. **Buchmeier, N. A., Newton, G. L. and Fahey, R. C. 2006.** A mycothiol synthase mutant of *Mycobacterium tuberculosis* has an altered thiol-disulfide content and limited tolerance to stress. *Journal of Bacteriology*. **188**(17): 6425-6252.

45. **Buchmeier, N. A., Newton, G. L., Koledin, T. and Fahey, R. C. 2003.** Association of mycothiol with protection of *Mycobacterium tuberculosis* from toxic oxidants and antibiotics. *Molecular Microbiology*. **47**(6): 1723-1732.

46. **Newton, G. L., Ta, P. and Fahey, R. C. 2005.** A mycothiol synthase mutant of *Mycobacterium smegmatis* produces novel thiols and has an altered thiol redox status. *Journal of Bacteriology*. **187**(21): 7309-7316.

47. **McCarthy, A. A., Peterson, N. A., Knijff, R. and Baker, E. N. 2004.** Crystal structure of MshB from *Mycobacterium tuberculosis* a deacetylase involved in mycothiol biosynthesis. *Journal of Molecular Biology*. **335**: 1131-1141.

48. **Huang, X. and Hernick, M. 2012.** Examination of mechanism of *N*-acetyl-1-D-*myo*-inosityl-2-amino-2-deoxy-α-D-glucopyranoside deacetylase (MshB) reveals unexpected role for dynamic tyrosine. *The Journal of Biological Chemistry*. **287**(13): 10424–10434.

49. **Maynes, J. T., Garen, C., Cherney, M. M., Newton, G. L., Arad, D., Av-Gay, Y., Fahey, R. C. and James, M. N. 2003.** The crystal structure of 1-D-*myo*-inosityl 2-acetamido-2-deoxy-alpha-D-glucopyranoside deacetylase (MshB) from *Mycobacterium tuberculosis* reveals a zinc hydrolase with a lactate dehydrogenase fold. *Journal of Biological Chemistry*. **278**: 47166–47170.

50. **Fan, F., Luxenburger, A., Painter, G. F. and Blanchard, J. S. 2007**. Steady-state and pre-steady-state kinetic analysis of *Mycobacterium smegmatis* cysteine ligase (MshC). *Biochemistry*. **46**: 11421–11429.

51. **Williams, L., Fan, F., Blanchard, J. S. and Raushel, F. M. 2008**. Positional isotope exchange analysis of the *Mycobacterium smegmatis* cysteine ligase (MshC). *Biochemistry*. **47**(16): 4843–4850.

52. **Vetting, M. W., Roderick, S. L, YU, M. and Blanchard, J. S. 2003.** Crystal structure of mycothiol synthase (Rv0819) from *Mycobacterium tuberculosis* shows structural homology to the GNAT family of *N*-acetyltransferases. *Protein Science*. **12**: 1954–1959.

53. **Bornemann, C., Jardine, M. A., Spies, H. S. and Steenkamp, D. J. 1997.** Synthesis of mycothiol: Elucidation of the sequence of the steps in *Mycobacterium smegmatis*. *Biochemical Journal*. **325**: 623-629.

54. (a) **Koledin, T., Newton, G. L. and Fahey, R. C. 2002**. Identification of the mycothiol synthase gene (mshD) encoding the acetyltransferase producing mycothiol in actinomycetes. *Archives of Microbiology*. **178**: 331-337. (b). **Vetting, M. W., Yu,**

M., Rendle, P. M. and Blanchard, J. S. 2006. The substrate-induced conformational change of *Mycobacterium tuberculosis* mycothiol synthase. *Journal of Biological Chemistry*. **281:**2795–2802.

55. **Fahey, R. C. 2001.** Novel thiols of prokaryotes. *Annual Review of Microbiology*. **55**: 333–356.

56. **Nicholas, G. M., Kovac, P. and Bewley, C. A. 2002.** Total synthesis and proof of structure of mycothiol bimane. *Journal American Chemical Society*. **124**: 3492–3493.

57. **Vacca, J. P. deSolms, S. J., Huff, J. R., Billington, D. C., Baker, R., Kulagowski, J. J. and Mawer, I. M. 1989.** The total synthesis of *myo*-inositol polyphosphates. *Tetrahedron*. **45**(17): 5679-5702.

58. **Billington, D. C., Baker, R., Kulagowski, J. J. and Mawer, I. M. 1989.** Synthesis of *myo*-inositol 1-phosphate and 4-phosphate, and of their individual enantiomers. *Journal of the Chemical Society, Chemical communication*. 314-316.

59. **Lee, S. and Rossaza, J. P. N. 2004.** First total synthesis of mycothiol and mycothiol disulfide. *Organic letters*. **6**(30): 365-368.

60. **Knapp, S. and Myers, D. S. 2002.** Synthesis of α -GalNAc thioconjugates from an α-GalNAc mercaptan. *The Journal of Organic Chemistry*. **67**: 2995–2999.

61. **Zhu, X., Stolz, F. and Schmidt, R. R. 2004.** Synthesis of thioglycoside-based UDP-sugar analogues. *The Journal of Organic Chemistry*. **69**: 7367–7370.

CHAPTER 2

Synthesis of 1L-*myo*-inositol-1-phosphate

2.1 Introduction

The synthesis of *myo*-inositol phosphate derivatives has received widespread attention in recent years due to its crucial roles in biological processes such as cellular signal transduction, homeostasis and regulation of many other important cellular processes in living organisms.[1-4] The potential therapeutic uses of *myo*-inositol derivatives and their use as the precursor for the synthesis of other natural products have also been reported.[5] *myo*-Inositol belongs to a large family of naturally occurring compounds known as the cyclitols and it is by far the most abundant amongst all possible nine inositol stereoisomers.[6]

The nomenclature of inositols has been a subject of debate for many years. In order to clear the ongoing confusion about the numbering of cyclitols and also to ensure that the cyclitol ring is numbered consistently on the side containing the axial hydroxyl group, Agranoff[7a] has created a mnemonic in the form of turtle with the head erected at C-2 and the tail at C-5 (Fig. 2-1).

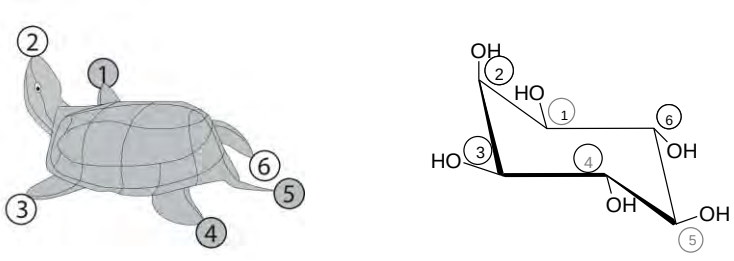

A B

Figure 2-1: (a). Agranoff's turtle. (b). *myo*-Inositol.[7b] The most stable chair conformation with 1-axial and 5-equatorial hydroxyl groups, *myo*-inositol has been said to resemble a turtle (Agranoff, 1978). The axial hydroxyl is represented by the turtle's head (position 2) and the equatorial hydroxyls by the limbs and tail.

Loewus and Murthy[8] indicated that *myo*-inositol is a *meso* compound with a plane of symmetry that rotates the structure about C-2 and C-5 at fixed positions (Fig. 2-2). Therefore the other four carbon atoms consist of two prochiral pairs, C-1: C-3 and C-4: C-6. If the carbon ring is numbered clockwise, assignment of a single substituent on carbon 1 is 1L (Fig. 2-2). On the other hand, if the carbon ring is numbered anti-clockwise, the orientation is 1D (Fig. 2-2).

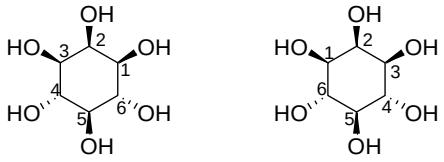

Figure 2-2: D/L-nomenclature and numbering for *myo*-inositol.

1-L-*myo*-Inositol-1P (1-L-Ins-1-P) is a product of 1L-*myo*-inositol-1-phosphate synthase (INO1) and it is synthesized enzymatically from glucose 6-phosphate.[9,10] The Rv0046c gene was first identified in *M.tb* as *ino1* encoding an inositol phosphate synthase based on the sequence similarity with yeast INO1. This was later confirmed genetically by Bachhawat and Mande by showing that the mycobacterial gene complemented a *Saccharomyces cerevisiae ino1* mutant.[11] In *M.tb,* inositol is supplied in the form of 1-L-Ins-1-P from glucose 6-phosphate by means of 1L-*myo*-inositol-1-phosphate synthase. *M.tb* strains carrying the *ino1* gene mutation are inositol auxotrophs and lack inositol-1-phosphate synthase activity. Although these mutants have normal levels of phosphatidyl-inositol mannosides, lipomannan and lipoarabinomannan, the mutants produce low levels of MSH and this could be attributed to the presence of *myo*-inositol kinases which generates 1-L-Ins-1-P which is required for the synthesis of MSH. Two independent studies of Loewus *et al.* and Stephens *et al.* have demonstrated that the inositol kinases activity produce 1-L-Ins-1-

P in wheat germ and *Dictyostelium discoideum* respectively.[12,13] In yeast (*Saccharomyces cerevisiae),* biosynthesis of 1-L-Ins-1-P is a tightly regulated processes.[14]

The history of *myo*-inositol-1-phosphate in the literature dates back to 1959.[15] Ballou and Pizer reported the synthesis of *myo*-inositol-1-phosphate from the base hydrolysis of phosphoinositide isolated from soybean.[15] Subsequently absolute configuration and the optical rotation between the synthetic and naturally occurring *myo*-inositol-1-phosphate was established. Ballou and Pizer synthesized an asymmetric *myo*-inositol-1-phosphate using galactinol as a starting material and compared it with the naturally occurring soybean *myo*-inositol-1-phosphate. The synthetic compound was found to have assumed the absolute configuration of galactinol whereas the soybean *myo*-inositol-1-phosphate was found to be its mirror image (Fig. 2-3).[16] Lardy[17] proposed that the synthetic compound be called D-*myo*-inositol-1-phosphate whereas the soybean isolate would be referred to as L-*myo*-inositol-1-phosphate (Fig. 2-3). The previous study by Sculimbrene *et al*.[18] also reported the synthesis of optically pure enantiomers of D-*myo*-inositol-1-phosphate and D-*myo*-inositol-3-phosphate by using an enantioselective pentapeptide catalyst. The first comprehensive linear synthesis of optically pure 1-L-Ins-1-P enantiomer was reported by Billington and co-workers.[19] Although the product was reported without any synthetic details.

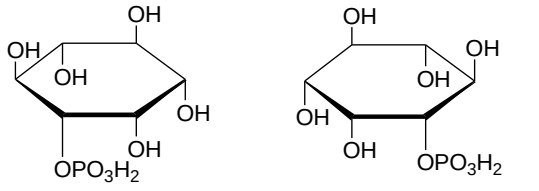

Synthetic compound Soybean compound

Figure 2-3: Mirror images of *myo*-inositol phosphate.

A key objective in this research effort is to synthesize 1-L-Ins-1-P (Fig 2-4) which is the required co-substrate for the enzyme, MshA, in the first step of mycothiol biosynthesis. In this chapter, a detailed synthesis of 1-L-Ins-1-P is described.

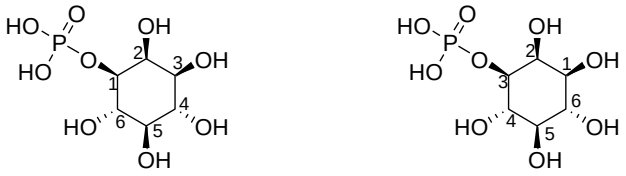

Figure 2-4: The structures of 1-L-Ins-1-P (clockwise) or 1-D-Ins-3-P (anti-clockwise).

2.2 Rationale for synthesizing 1-L-Ins-1-P

In order to discover inhibitors of glycosyltransferase (MshA) activity, an adequate supply of 1-L-Ins-1-P was necessary. Although 1-L-Ins-1-P is commercially available in small quantities, it was prudent to synthesize it in our laboratory as large quantities were needed to conduct several assay experiments. Also, the commercially available substrate is primarily isolated from yeasts cells, it took many months for delivery, is costly and unsustainable at 400 $/mg. It is for this reason that considerable effort has been devoted towards the synthesis of 1-L-Ins-1-P. To the best of our knowledge there is no known report that has presented the full synthetic details of 1-L-Ins-1-P other than that of Spiers *et al.*[20a] It was for this reason that the synthesis of 1-L-Ins-1-P was pursued. Furthermore, the synthesis of 1-L-Ins-1-P also produces the inositol part required for MSH synthesis. While MSH synthesis was not part of the objectives of this project, it was required by another project in our lab.

2.3 Retrosynthetic approach of 1-L-Ins-1-P

In order to synthesize the target molecule (1-L-Ins-1-P), a selectively protected L-*myo*-inositol derivative is required. To resolve this problem, a retrosynthetic approach was envisaged as outlined in Fig. 2-5. A selectively protected L-*myo*-inositol

derivative (**I**) could be obtained indirectly from commercially available *myo*-inositol. However, the intermediate stage would involve selective protection and chiral resolution.

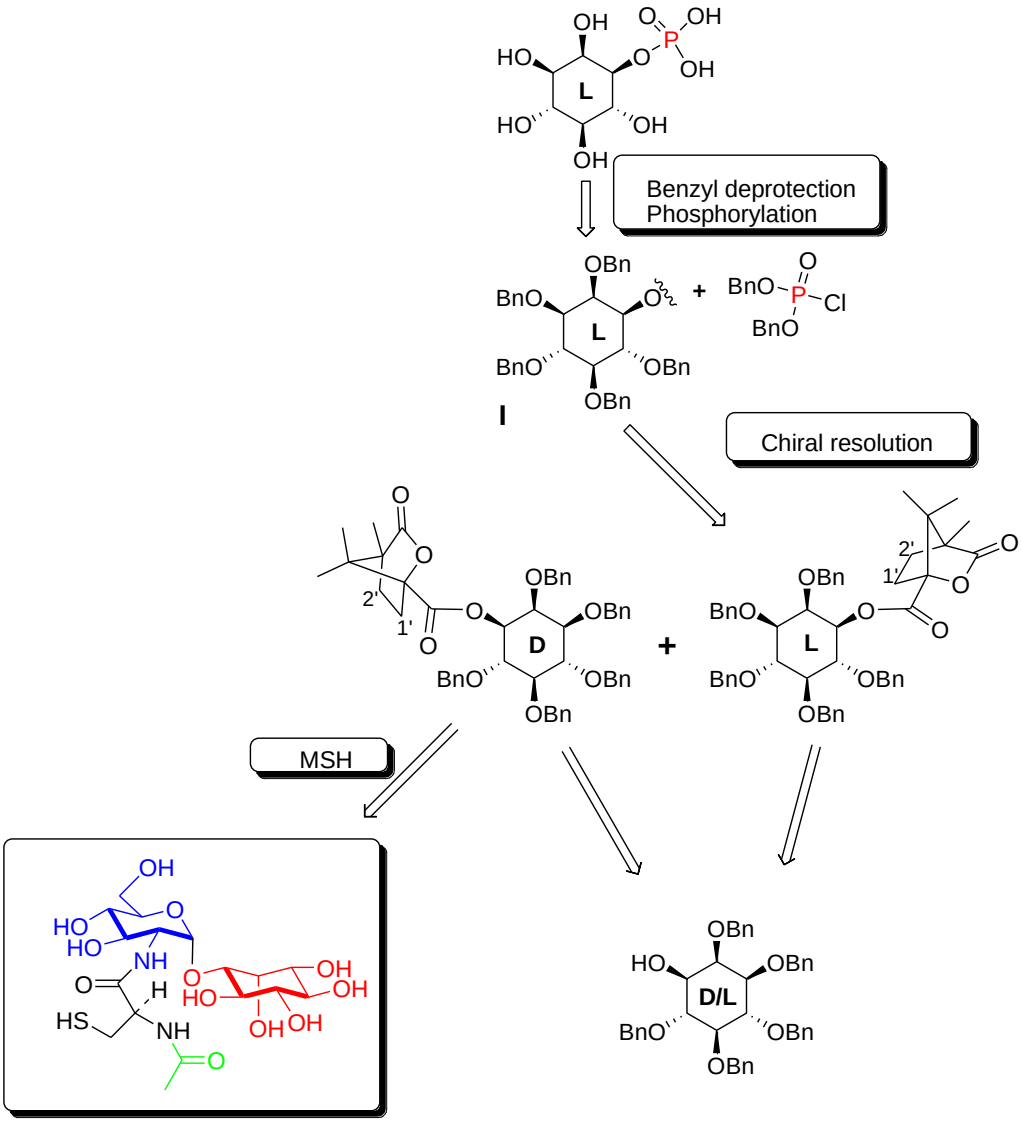

Figure 2-5: Retrosynthetic analysis of 1-L-Ins-1-P. L-*myo*-Inositol leads to the synthesis of 1-L-Ins-1-P whereas D-*myo*-inositol is crucial for the synthesis of MSH. D-*myo*-inositol is highlighted in red color in the structure of MSH.

2.4 Synthetic approach toward the 1-L-Ins-1-P

2.4.1 Ketal protecting groups of *myo*-inositol

The synthesis of our target molecule 1-L-Ins-1-P (Fig. 2-4) started with ketalization of *myo*-inositol, which is a cheap and readily available starting material. The ketalization of *myo*-inositol was carried out using 1-ethoxycyclohexene which was synthesized *in situ* using a mixture of cyclohexanone dimethyl ketal and *p*-toluenesulphonic acid monohydrate following the procedure reported by Vacca *et al*.[21] The reaction resulted in the formation of three bis-cyclohexylidene ketals of *myo*-inositol (**2-1**), (**2-2**) and (**2-3**) (Scheme 2-1) in good yield. Partial hydrolysis of the *trans*-ketal diastereoisomers (**2-1**), (**2-2**) and (**2-3**) in the presence of a catalytic amount of *p*-toluenesulphonic acid gave mono-ketal, (**2-4**) as the major product. The product was characterized by NMR which confirmed the mono-ketal structure.

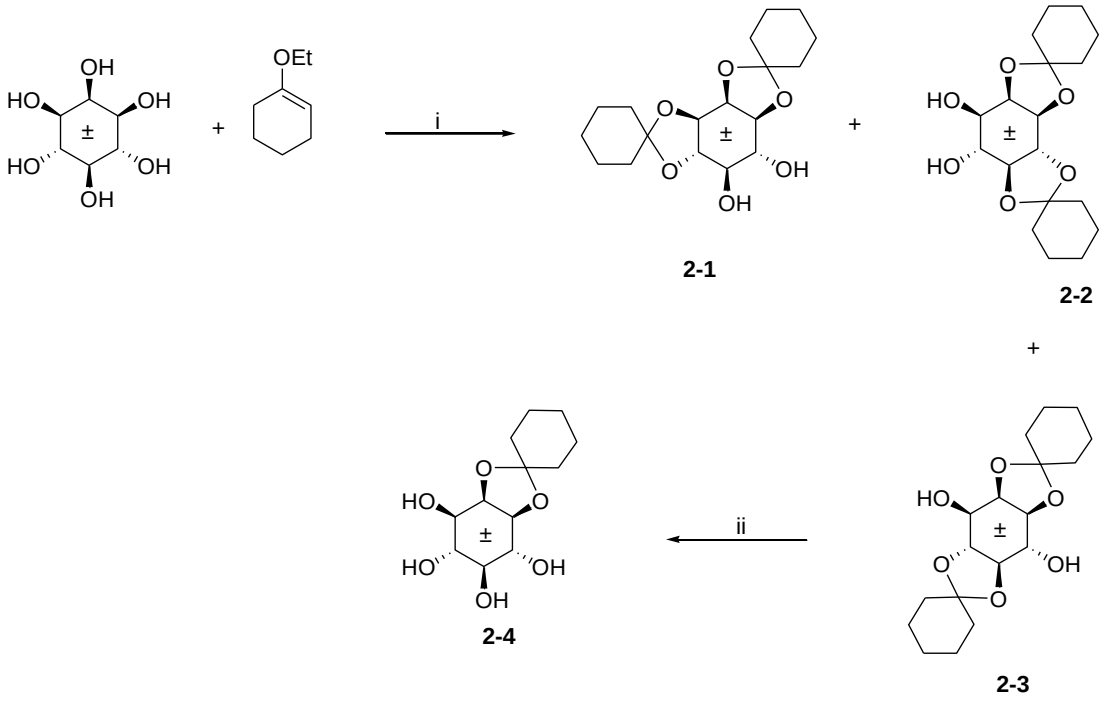

Scheme 2-1 Reaction conditions: (i) 1-ethoxycyclohexene, *P*-TsOH, DMF 100 °C, 2hr; (ii) *P*-TsOH, DCM: 76%.

2.4.2 Synthesis of 3,4,5,6-*tetra*-*O*-benzyl-1,2-*O*-cyclohexylidene-D/L-*myo*-inositol

The global benzylation of 1,2-*O*-cyclohexylidene-*myo*-inositol (**2-4**) with excess benzyl bromide in the presence of NaH afforded 3,4,5,6-*tetra*-*O*-benzyl-1,2-*O*-cyclohexylidine-D/L-*myo*-inositol (**2-5**) (Scheme 2-2) as a racemic mixture in 68%.

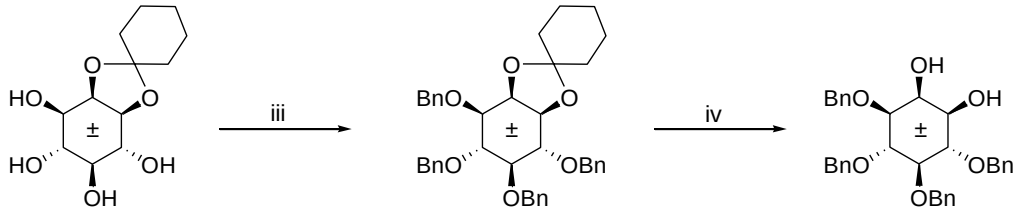

2-4 **2-5** **2-6**

Scheme 2-2 Reaction conditions: (iii) BnBr, NaH, DMF, 0 °C - 80 °C; 85% (iv) 80% aq. AcOH; 79%.

The structure of compound (**2-5**) was confirmed by ^{1}H NMR with the appearance of signals resonating at δ_H 7.45 – 7.17 ppm (m, 20H). Thus, confirming the presence of the benzyl aromatic protons. The other diagnostic feature was the presence of signals at δ 1.84 – 1.30 ppm (m, 10H), which confirmed the presence of cyclohexyl methylene protons. Also evidence of benzylation was the presence of benzyl methylene protons integrating for eight protons resonating between δ_H 4.90 and δ_H 4.72 ppm as a multiplet. ^{13}C NMR spectroscopy further confirmed the structure by indicating the presence of key benzyl signals resonating at δ_C 138.71 - 127.45 ppm.

Hydrolysis of 3,4,5,6-tetra-*O*-benzyl-1,2-*O*-cyclohexylidene-DL-*myo*-inositol (**2-5**) in aqueous acetic acid gave a racemic mixture of 3,4,5,6-tetra-*O*-benzyl-*myo*-inositol (**2-6**) (Scheme 2-2). The structure of 3,4,5,6-tetra-*O*-benzyl-*myo*-inositol (**2-6**) was confirmed by the ^{1}H NMR spectrum and by comparison with a spectrum reported in literature.[22] The key diagnostic being the disappearance of the signals associated with the cyclohexylidene protons and the appearance of a broad singlet peak at δ_H 2.5 ppm integrating for two protons corresponded to the two hydroxyl groups of the diol. In

addition, the IR spectrum of 3,4,5,6-tetra-*O*-benzyl-*myo*-inositol (**2-6**) showed absorption at ν_{max}/cm^{-1} 3400, confirming the presence of a hydroxyl group.

2.4.3 Regioselective allylation of the 1,2-diol (2-7)

The 3,4,5,6-tetra-*O*-benzyl-*myo*-inositol (**2-6**) derivative of *myo*-inositol comprises of an equatorial hydroxyl group at the C-1 position and the axial hydroxyl group at C-2 position, thus selection of the desired hydroxyl remains a challenge. However, this problem has been overcome by selective temporary allyl protection of the hydroxyl group at C-1, followed by the benzyl protection of the remaining hydroxyl groups and finally removing the C-1 protecting group using a deallylation procedure. Thus, the regioselective allylation[23] of 3,4,5,6-tetra-*O*-benzyl-*myo*-inositol (**2-6**) was achieved by sequential treatment of 3,4,5,6-tetra-*O*-benzyl-*myo*-inositol (**2-6**) with Bu_2SnO followed by allyl bromide to give 1-*O*-allyl-3,4,5,6-tetra-*O*-benzyl-DL-*myo*-inositol (2-**7**) in 63% yield (Scheme 2-3).[24]

The allylation mechanism involves the formation of dibutylstannylidene acetals. Xue and Guo[25] proposed that the regioselective allylation of the diol occurs as a result of steric hindrance at 1-position of the tin complex (Fig. 2-6) which is more sterically hindered than the 6-position. It can be suggested that the selective allylation of an equatorial hydroxyl group of 3,4,5,6-tetra-*O*-benzyl-DL-*myo*-inositol (**2-6**) is favoured because it is less hindered as compared to an axial hydroxyl group because of the steric hindrance of the benzyl ether groups.[26-28]

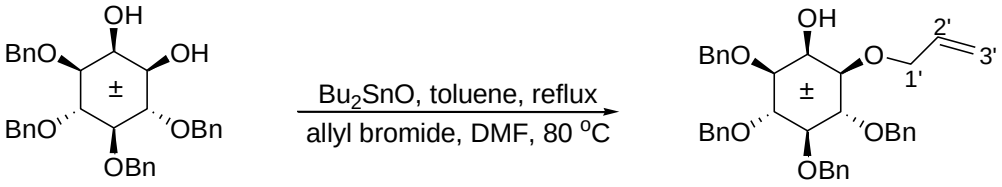

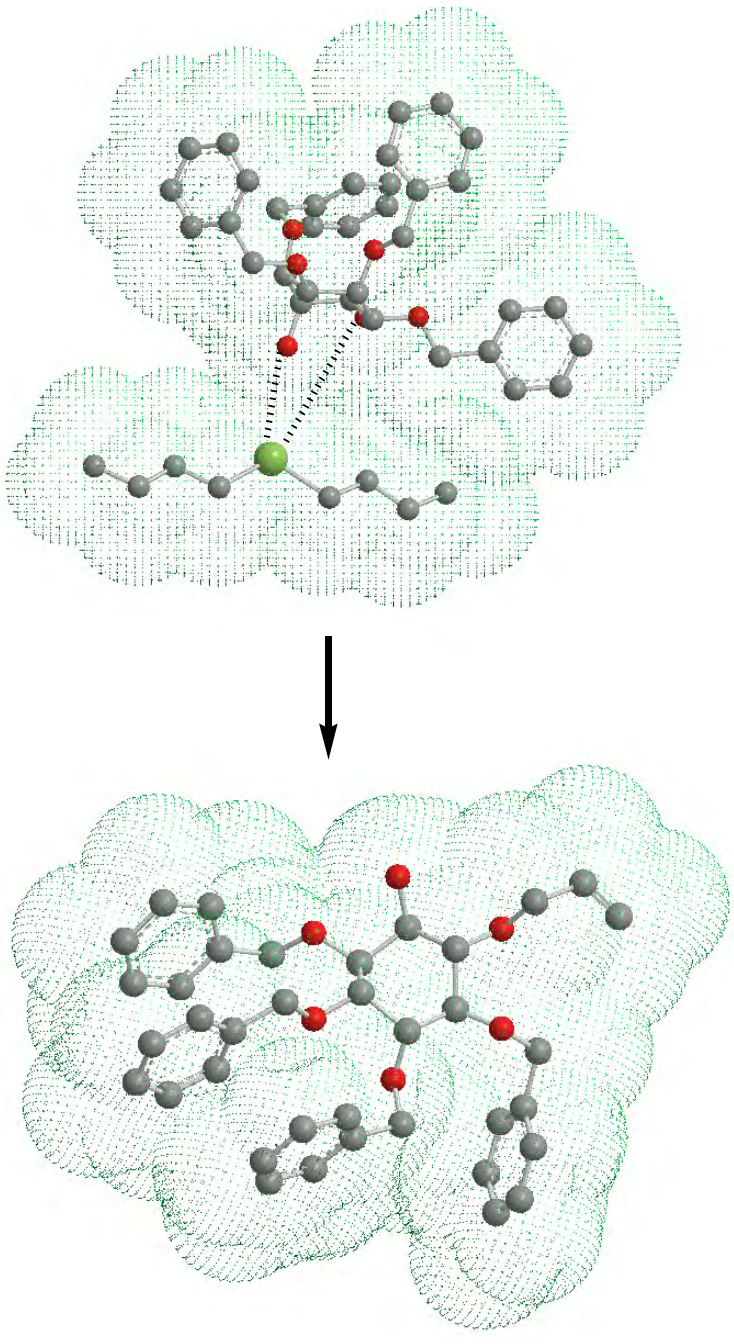

Figure 2-6: 3D possible conformation of selective allylation of diol (**2-7**) (Chem3D Ultra, minimized energy).

The structure of 1-*O*-allyl-3,4,5,6-tetra-*O*-benzyl-DL-myo-inositol (**2-7**) was confirmed by ^{1}H NMR analysis, which indicated the presence of the allyl moiety as well as the inositol ring protons, H-1 and H-2 with a small coupling of J = 2.8 Hz and larger coupling of J = 9.5 Hz between H-1 and H-6 and thus confirming the axial orientation of the H-1 proton. Furthermore, there was a presence of a multiplet around δ_H 5.93 ppm for H-2' and a doublet of doublets which resonated at δ_H 5.28 and δ_H 5.18 ppm for H-3'a and H-3'b, respectively. In addition, there was two upfield signals for H-1'a and H-1'b resonating at 4.23-4.21 ppm.

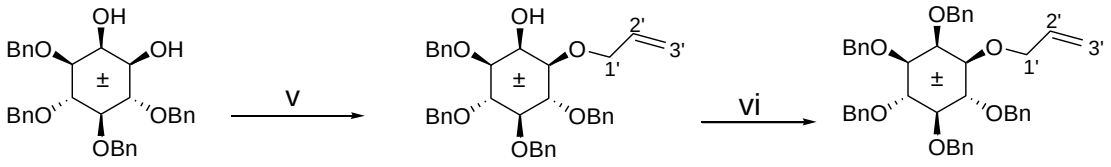

2-6 **2-7** **2-8**

Scheme 2-3 Reaction conditions: (v) (a) Bu_2SnO, toluene, reflux; (b) allyl bromide, DMF, 80 °C, 4hr; 83% (vi) BnBr, NaH, DMF; 90%.

In addition, the IR spectrum of 1-*O*-allyl -3,4,5,6-tetra-*O*-benzyl-DL-myo-inositol (**2-7**) showed an absorption ν_{max}/cm^{-1} 3400, confirming the presence of a hydroxyl group. The mono-benzylation of an axial hydroxyl group ensured a fully protected 1-*O*-allyl -2,3,4,5,6-penta-*O*-benzyl-DL-myo-inositol (**2-8**) in 90% yield (Scheme 2-4). The structure was confirmed by its ^{1}H and ^{13}C NMR spectra.

A diagnostic feature was the disappearance of the hydroxyl protons of 1-*O*-allyl-3,4,5,6-tetra-*O*-benzyl-DL-*myo*-inositol (**2-7**) and the increase in the ratio of benzylic protons of 1-*O*-allyl-2,3,4,5,6-penta-*O*-benzyl-DL-*myo*-inositol (**2-8**). Allylic and *myo*-inositol ring proton signals remained similar in pattern indicating that no other transformation had taken place.

Several possible mechanisms for the deallylation of allyl ethers with a palladium catalyst exist. Elliott *et al*.[29,30,31] suggested that $PdCl_2$ undergoes an anti-Markovnikov methoxy-palladation followed by β-alkoxy cleavage resulting in the formation of the desired deprotected hydroxyl group. It was further postulated that the $PdCl_2$ isomerises the allyl group to the corresponding enol ether and that a low concentration of HCl is generated, which catalyses methanolysis of the enol ether.[29]

Deallylation[32] of 1-*O*-allyl -2,3,4,5,6-penta-*O*-benzyl-DL-*myo*-inositol (**2-8**) (Scheme 2-4) with $PdCl_2$ in a mixture of methanol/ethanol gave the racemic mixture of 2,3,4,5,6-penta-*O*-benzyl-DL-*myo*-inositol (**2-9**) in good yield (83%). The spectroscopic data indicated the disappearance of signals associated with the allyl moiety. In addition, the IR spectra showed the absorption at ν_{max}/cm^{-1} 3450 which confirmed the presence of the hydroxyl group.

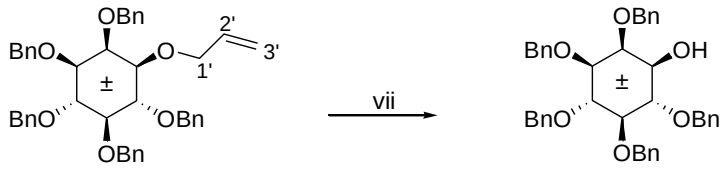

2-8 **2-9**

Scheme 2-4 Reaction conditions: (vii) $PdCl_2$, EtOH-MeOH; 79%.

2.4.4 Resolution of racemic D/L-*myo*-inositol

Having successfully synthesized the appropriately protected racemic, 2,3,4,5,6-penta-*O*-benzyl-DL-*myo*-inositol (**2-9**) with the free hydroxyl group at the C-1 position, the next step was to perform a chiral resolution of the racemic 2,3,4,5,6-penta-*O*-benzyl-DL-*myo*-inositol (**2-9**). The separation was achieved by chiral resolution utilizing the camphanate ester of (**2-9**). Thus, the esterification of the racemic alcohol with (R)(-)-camphanic acid chloride in the presence of Et_3N and catalytic amount of DMAP in

chloroform gave a mixture of the diastereoisomeric camphanic esters (**2-10**) and (**2-11**) in quantitative yield (Scheme 2-5).[19]

The esters were separated by multiple rounds of silica-gel column chromatography to effect complete separation in order to obtain diastereoisomerically pure material. Furthermore, the correct stereochemistry of the desired stereoisomer 2,3,4,5,6-penta–*O*-benzyl-1-*O*-[(1S-(-)-camphanoyl]-L-*myo*-inositol (**2-10**) was confirmed through association of its previously reported optical rotation. $[[\alpha]^{20}_D = -18°$ (c = 1, $CHCl_3$, for D-1-*O*-[(1S)-(-)-camphanoyl]-2,3,4,5,6-penta-*O*-benzyl-*myo*-inositol (**2-11**) and L-diastereoisomer, L-1-*O*-[(1S)-(-)-camphanoyl]-2,3,4,5,6-penta-*O*-benzyl-*myo*-inositol (**2-10**), $[\alpha]^{20}_D = +11.8°$ (c = 1, $CHCl_3$)].[24] The discrepancy in optical rotation could be due to the presence of a small amount of the D-diastereoisomer or simply the error in measurement of this relatively low optical rotation value.

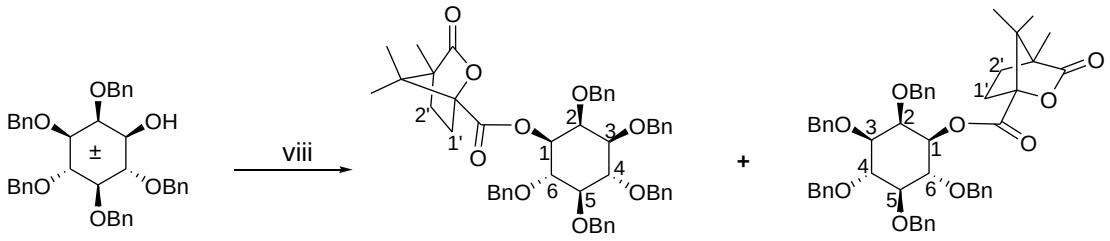

2-9 **2-10** **2-11**

Scheme 2-5 Reaction conditions: (viii) Camphanic acid chloride, Et_3N, DMAP, DCM, RT; 48%.

Basic hydrolysis of the desired L-enantiomer (**2-10**) (Scheme 2-6) with KOH in ethanol under gentle reflux gave the desired alcohol (**2-12**) in low yield (39%) following the work-up and column chromatography. The spectroscopic data confirmed the disappearance of the protons associated with the camphonate esters.

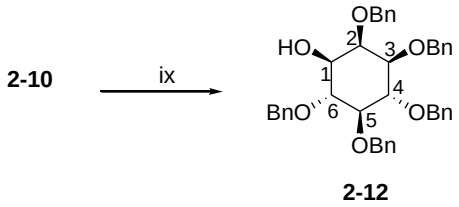

2-12

Scheme 2-6 Reaction conditions: (ix) KOH, EtOH, reflux, 2hr; 85%.

2.4.5 Attempted phosphorylation of 2,3,4,5,6- pentabenzyl *myo*-inositol

The final stage of the synthetic plan (Scheme 2-7) involves phophorylation of penta-*O*-benzylated inositol derivative (**2-12**) followed by deprotection to give the pure enantiomer of 1-L-Ins-1-P. The latter strategy worked well for Billington *et al*.[19], who reported the synthesis of racemic 1-D/L-*myo*-inositol-1-P as the crystalline bis-cyclohexylammonium salt in 95% yield. Although this product was reported without spectroscopic data.

Efforts to convert 2,3,4,5,6- pentabenzyl *myo*-inositol (**2-12**) to the phosphate ester (**2-13**) were attempted, using $(PhO)_2POCl$ as phosphorylating agent (Scheme 2-7). Thus, $(PhO)_2POCl$ in the presence of a catalytic amount of DMAP and Et_3N proved to be unsuccessful. This is despite varying all reaction parameters as previously reported for a similar reaction by Billington *et al*.[19]

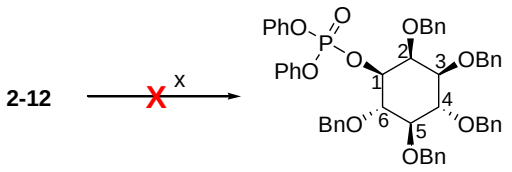

2-13

Scheme 2-7 Proposed reaction condition: (x) $(PhO)_2POCl$, DCM, Et_3N, DMAP, 25 °C.

It was reasoned that the phosphorylation of mono-hydroxy pentabenzyl *myo*-inositol (**2-12**) could not occur due to steric hindrance. This could be attributed to the fact that diphenylphosphoryl chloride is a relatively bulky molecule with relatively large

vicinal benzyl groups. Figure 2-7 below shows the 3D view of this steric demand of this

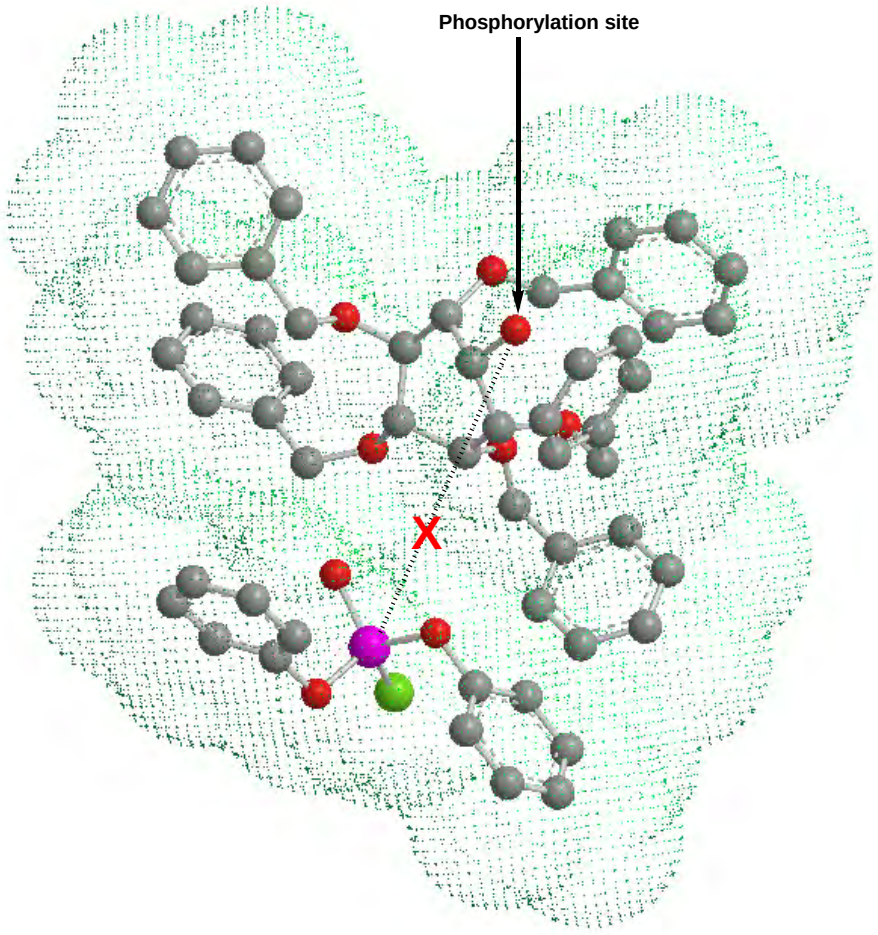

Figure 2-7: 3D possible conformation of (**2-13**) showing steric demand (Chem3D Ultra, minimized energy).

Other phosphorylating agents such as dibenzylphosphoryl chloride have been tried but it also did not result in the target phosphate ester. In addition, several attempts were made to synthesize small phosphorylating agents in the laboratory with no success. As a result we could not proceed with subsequent phosphorylation and deprotection steps for the synthesis of 1-L-Ins-1-P using this synthetic approach (Scheme 2-8).

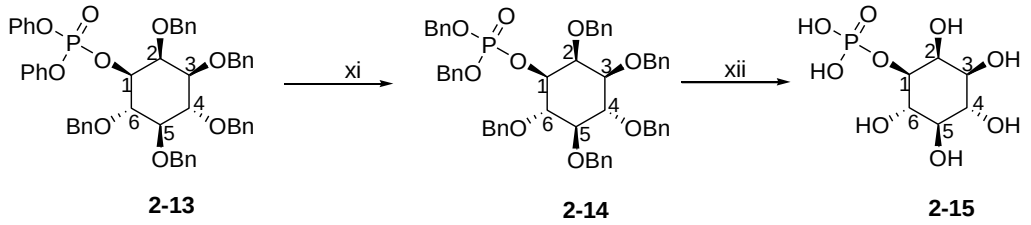

2-13 **2-14** **2-15**

Scheme 2-8 Proposed reaction condition: (xi) BnBr, NaH, DMF, (xii) Pd/C, H_2, EtOH-H_2O.

2.5 Alternative synthetic route to 1-L-Ins-1-P

Due to the lack of successful synthesis of 1-L-Ins-1-P using the synthetic route involving benzyl protection (Section 2.4, scheme 2-7), an alternative route was sought (Fig 2-8).

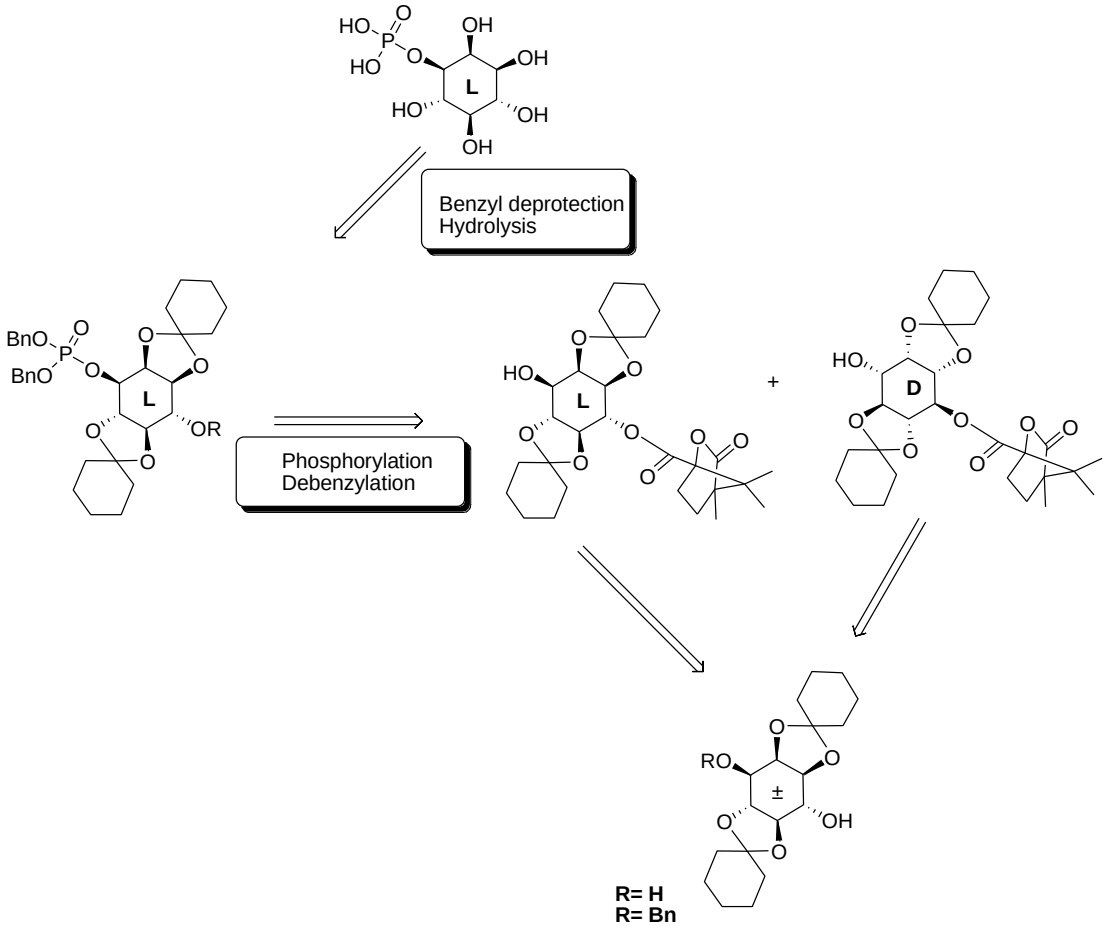

Figure 2-8: Retrosynthetic analysis of 1-L-Ins-1-P (Second approach).

As indicated by our retrosynthetic analysis (Fig. 2-8), the total synthesis of 1-L-Ins-1-P, requires a coupling of the phosphorylating agent to a suitably protected L-*myo*-

inositol enantiomer. The selectively protected enantiomer can be achieved through the hydrogenolysis of the benzyl protecting group, followed by the hydrolysis of cyclohexylidene and camphor respectively. Finally selectively protected 1L-*myo*-inositol can be achieved *via* the transesterification of the diphenylphosphate groups with the dibenzylphosphate group, followed by phosphorylation and chiral resolution of the racemic mixture.

Accordingly, the selective protection of *myo*-inositol using the cyclohexylidene to give 2,3:5,6-dicyclohexylidene *myo*-inositol (**2-3**), followed by selective mono-benzylation of *myo*-inositol at C-1 to give the desired alcohol (**2-16**) as a racemic mixture, which was subsequently separated by chiral resolution of the camphanate ester (Scheme 2-9). Hydrogenolysis of the benzyl groups of desired L-enantiomer (**2-17**) resulted in the formation of 4-*O*-camphanoyl-2,3,5,6-di-*O*-cyclohexylidene-L-*myo*-inositol (**2-18**).

Thus, 4-*O*-camphanoyl-2,3,5,6-di-*O*-cyclohexylidene-1-*O*-benzyl-L-*myo*-inositol (**2-17**) was prepared in two steps from commercially available *myo*-inositol by the method of Billington.[19] The benzyl group of (**2-17**) was removed by hydrogenolysis using 10% palladium on carbon in aqueous ethanol to afford 4-*O*-camphanoyl-2,3,5,6-di-*O*-cyclohexylidene-L-*myo*-inositol (**2-18**) as a white solid in quantitative yield (Scheme 2-9).

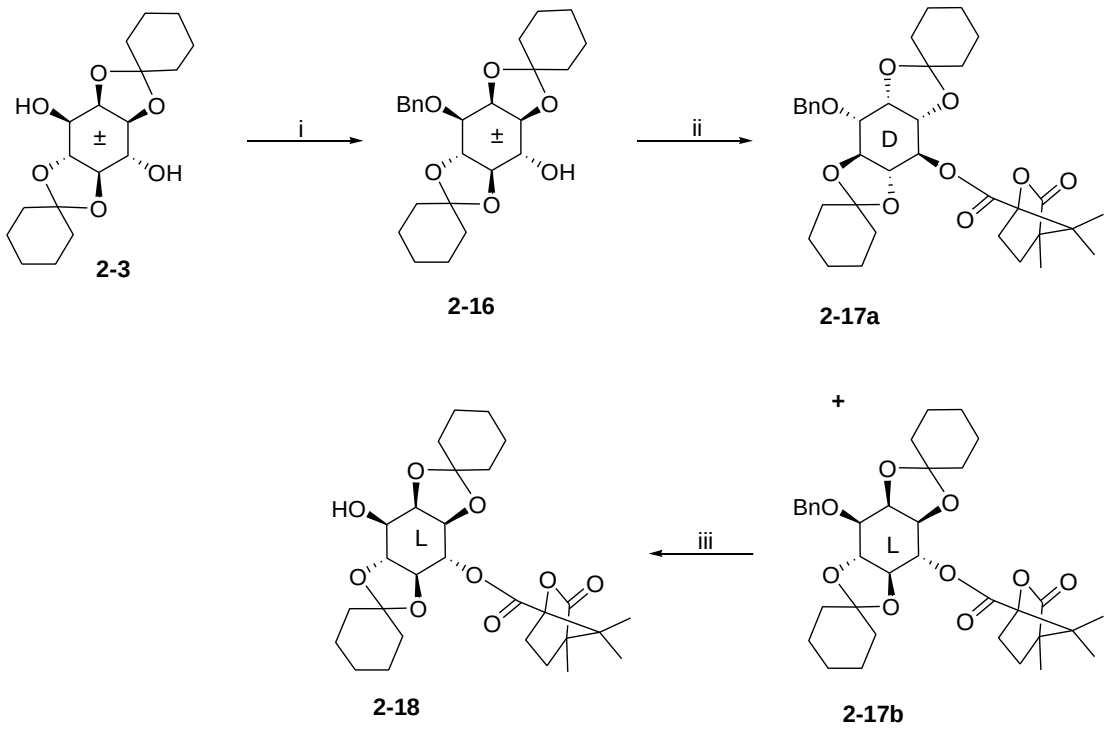

2-3 **2-16** **2-17a** **2-18** **2-17b**

Scheme 2-9 Reaction condition: (i) BnBr, NaH, DMF; (ii) Camphanic acid chloride, Et_3N, DMAP, DCM, RT; (iii) Pd/C, H_2, 50 psi, RT; 91%.

4-*O*-camphanoyl-2,3,5,6-di-*O*-cyclohexylidene-L-*myo*-inositol (**2-18**) was used in the subsequent step without any further purification. The ^{1}H NMR spectrum of the crude product showed complete disappearance of the benzylic protons. The IR spectrum was also used to confirm the presence of the alcohol in 4-*O*-camphanoyl-2,3,5,6-di-*O*-cyclohexylidene-L-*myo*-inositol (**2-18**) which indeed confirmed the presence of a hydroxyl group with absorption band resonating at ν_{max}/cm^{-1} 3455.

Following the successful synthesis of 4-*O*-camphanoyl-2,3,5,6-di-*O*-cyclohexylidene-L-*myo*-inositol (**2-18**), the 4-*O*-camphanoyl-2,3,5,6-di-*O*-cyclohexylidene-1-*O*-diphenylphosphoryl-L-*myo*-inositol (**2-19**) could be synthesised following the phosphorylation of (**2-18**) using the diphenylphosphoryl chloride in the presence of catalytic amount of DMAP and Et_3N in DCM (Scheme 2-10). Analysis of the ^{1}H NMR spectrum revealed the presence of phenyl protons resonating between δ_H 7.18

and 7.23 ppm (m, 10H). The presence of the phosphate group was further confirmed by the ^{31}P NMR spectrum, which indicated the presence a strong phosphate resonance at -12.45 ppm. This value is consistent with literature value of similar compounds.[20a]

Transesterification of (**2-19**) in the presence of benzyl alcohol and strong base (NaH) in THF gave 4-*O*-camphanoyl-2,3,5,6-di-*O*-cyclohexylidene-1-*O*-dibenzylphosphoryl-L-*myo*-inositol (**2-20**) (Scheme 2-10). The transesterification of the phosphate protecting groups between the phenyl and the benzyl groups deemed necessary because benzyl protecting groups are better leaving groups and will therefore facilitate the final deprotection of the product in a single step. In addition, the transesterification step deemed necessary because it would prevent the possible migration of phosphate group from position one to position two of the *myo*-inositol. Analysis of ^{1}H NMR spectroscopic data of 4-*O*-camphanoyl-2,3,5,6-di-*O*-cyclohexylidene-1-*O*-dibenzylphosphoryl-L-*myo*-inositol (**2-20**) indicated the presence of methylene protons that resonated between δ_H 5.12 and 5.25 ppm (m, 4H) and an integral that was consistent with 10 aromatic protons and four benzylic protons.

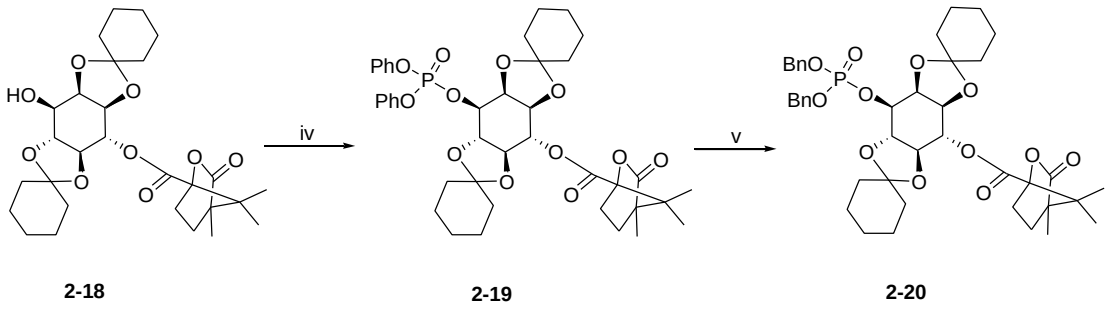

2-18 **2-19** **2-20**

Scheme 2-10 Reaction conditions: (iv) Et_3N, DMAP, $(PhO)_2POCl$, DCM; 100% (v) NaH, BnOH, RT; 63%.

Basic hydrolysis of 4-*O*-camphanoyl-2,3,5,6-di-*O*-cyclohexylidene-1-*O*-dibenzylphosphoryl-L-*myo*-inositol (**2-20**) with KOH under the gentle reflux gave the 2,3,5,6-di-*O*-cyclohexylidene-1-*O*-dibenzylphosphoryl-L-*myo*-inositol (**2-21**) in low yield (Scheme 2-11). The crude ^{1}H NMR spectroscopic data confirmed the presence of the benzyl aromatic protons (resonating at δ_H 7.41 – 7.19 ppm) and benzyl methylene protons (resonating at δ_H 4.89 – 4.70 ppm). The other diagnostic feature was the presence of cyclohexylmethylene protons resonating δ_H 1.80 – 1.28 ppm. Most importantly, the crude ^{1}H NMR spectroscopic data confirmed the disappearance of the protons associated with the camphonate esters. In addition, crude ^{31}P NMR spectroscopic data confirmed the presence of phosphate moiety by showing a strong resonance at -13.05 ppm. This product was used in the next step without further purification.

Acidic hydrolysis of cyclohexylidene groups of compound (**2-21**) in aqueous acetic acid gave the 1-*O*-dibenzylphosphoryl-L-*myo*-inositol (**2-22**) (Scheme 2-11). The structure of (**2-22**) was confirmed by the analysis of the ^{1}H NMR spectrum and the key diagnostic signal was the disappearance of the cyclohexylidene methylene protons. The benzylic protons remained intact emphasizing that no transformation had taken place on them.

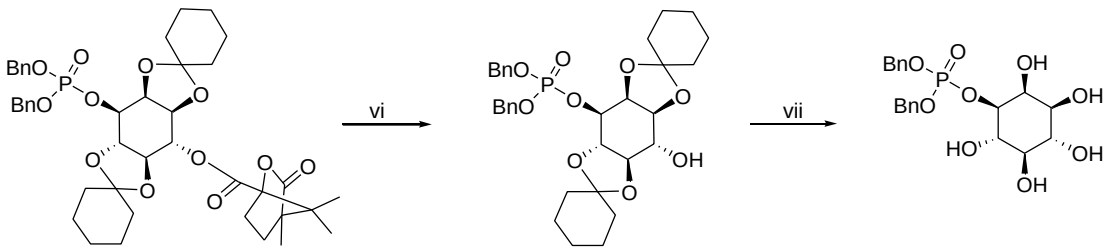

Scheme 2-11 Reaction condition: (vi) KOH, EtOH, reflux, 2 h; 65% (vii) 80% aq. AcOH, reflux, 2 hr; 42%.

Finally, the removal of the remaining two benzyl protecting groups on the phosphate moiety *via* hydrogenation of (**2-22**) gave 1-L-Ins-1-P (**2-15**, (Scheme 2-12)) which was isolated as a water soluble cream white powder following lyophilization. The ^{31}P, ^{13}C and ^{1}H NMR spectroscopic data were used to confirm the structure of the target compound 1-L-Ins-1-P (**2-15**).

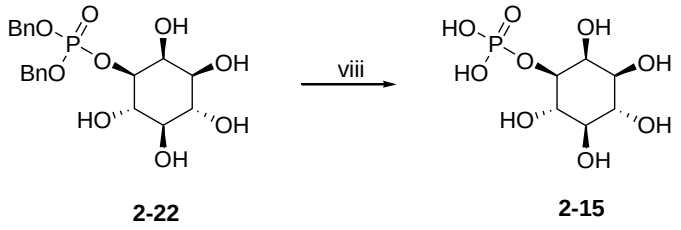

2-22 **2-15**

Scheme 2-12 Reaction condition: (viii) Pd/C, H_2, 50 psi, RT; 71%.

The ^{1}H NMR spectrum data of 1-L-Ins-1-P (**2-15**) showed the disappearance of key signals associated with the benzyl protons which were indicative that the molecule was successfully deprotected. Furthermore, the resonance of the H-1 shifted furthest downfield to approximately 4.71 ppm and this deshielding could be attributed to the phosphorylation on C-1. However, H-1 protons could not be properly integrated in this region 4.71 ppm due to the hygroscopic nature of the compound and as such some of the signals were suppressed by a huge water peak. The pair of enantiotopic protons (H-2 and H-6; H-3 and H-5) resonated at approximately 4.10 and 3.93 ppm respectively. This pair of enantiotopic protons was followed by H-4, which resonated at 3.81 ppm which was in agreement with that reported in literature.[20a,33,34]

Furthermore the ^{13}C NMR spectroscopic data corroborated by the ^{1}H NMR spectrum showed the appearance of key signals. The ^{13}C NMR gave four resonances of different intensities resonating between δ_C 66.80 and 60.45 ppm and thus confirming the symmetry of the molecule (Fig. 2-9).

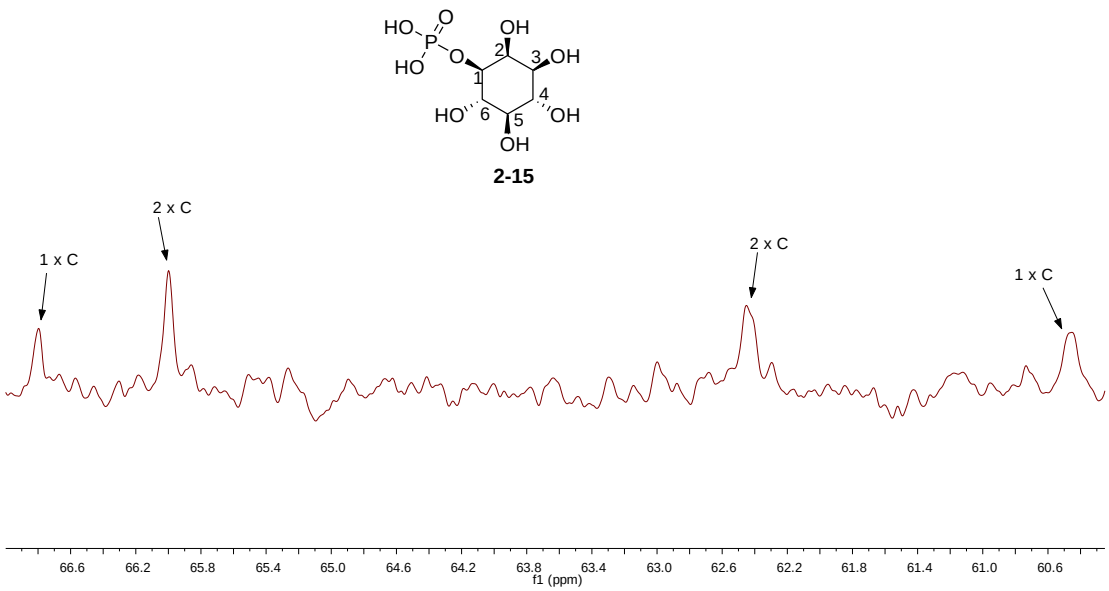

Figure 2-9: ^{13}C NMR spectrum of 1-L-Ins-1-P (2-**15**) in D2O.

In addition, the ^{1}H-decoupled ^{31}P NMR spectroscopic data was used to confirm the presence of phosphate moiety by showing a strong resonance at 5.23 ppm which was in agreement with that reported in the literature.[20a]

However, in order to confirm that the phosphorus moiety is attached to the inositol ring, the ^{1}H-coupled ^{31}P NMR spectrum of 1-L-Ins-1-P was obtained. The key feature of this spectrum was the appearance of doublet, caused by H-C-O-P splitting resonating at 5.14 ppm. Thus, providing an additional proof that phosphorus moiety is attached to the inositol ring. The observed coupling constant between H-1 and phosphorus is 9.0 Hz, a value in good agreement with the observation made considering the coupling is long range. The present ^{1}H-coupled ^{31}P NMR spectral evidence for the formation of 1-L-Ins-1-P (**2-15**) is in agreement with the work of Spiers *et al*[20a] who reported 1-L-Ins-1-P as the biscyclohexylammonium salt. The ^{1}H-coupled ^{31}P NMR spectrum further corroborated with the study of Chen *et al*.[20b]

which reported ^{1}H-coupled ^{31}P NMR spectrum of 1-L-Ins-1-P isolated from cell extracts as a doublet with the a large coupling constant (J_{HP} 8.5).

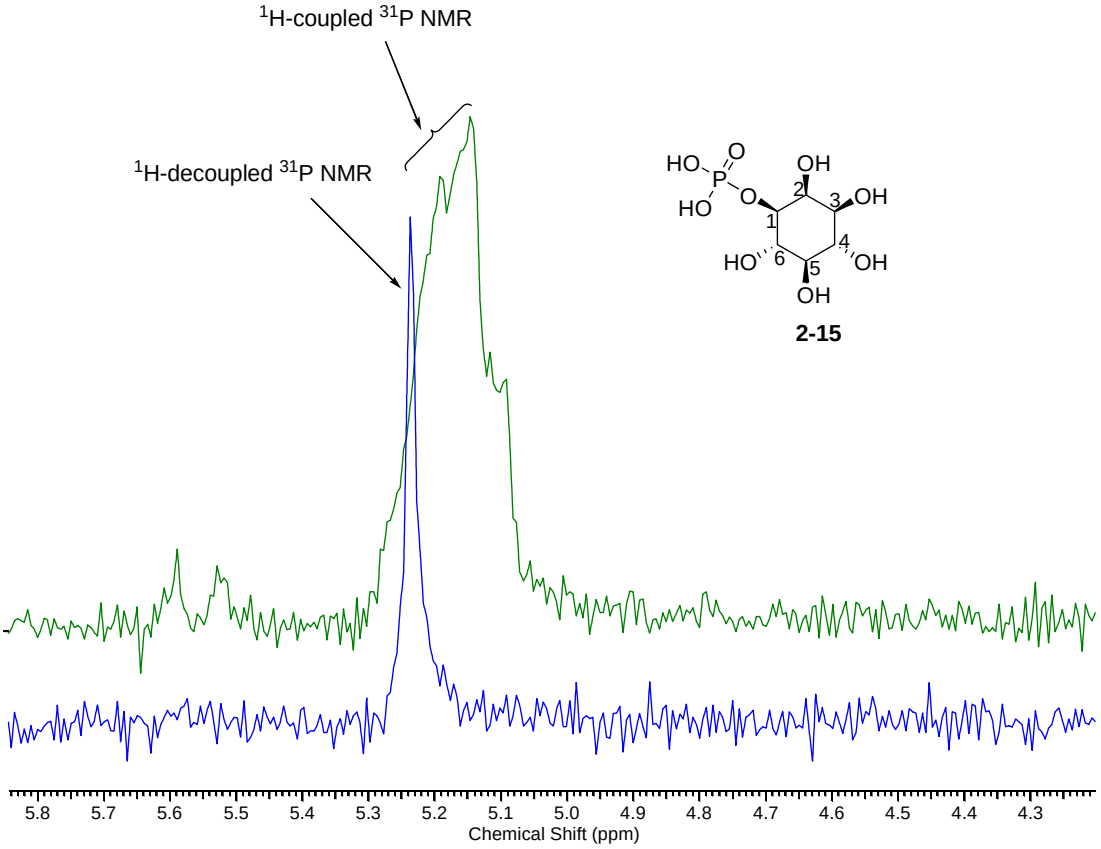

Figure 2-10: Superimposed ^{31}P NMR spectra of 1-L-Ins-1-P (**2-15**) in D2O. ^{1}H-decoupled ^{31}P NMR shows a strong singlet peak (Blue). ^{1}H-coupled ^{31}P NMR appears as a doublet due a splitting caused by H-C-O-P (Green).

Finally, a HRMS evaluation gave an *m/z* 262.0358 $[M]^{+}$, $C_6H_{13}O_9P$ which requires *m/z* 262.0340 $[M]^{+}$, thus supporting the proposed structure of compound (**2-15**) (Fig. 2-11). In addition, a base peak fragment of *m/z* 244.1900 $[M]^{+}$, corresponding to a possible loss of one oxgen molecule in $C_6H_{13}O_9P$ was observed.

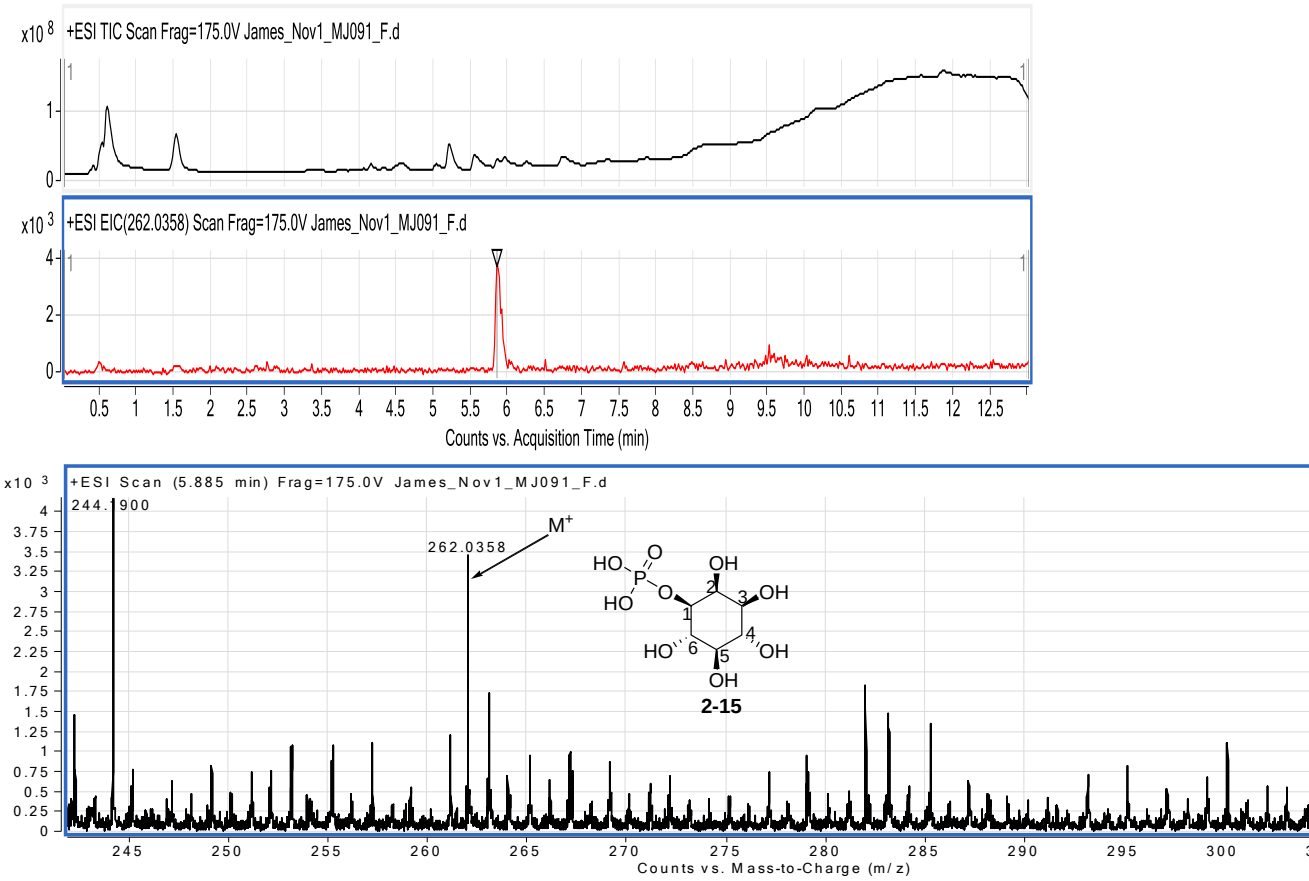

Figure 2-11: TIC extracted (top) and ESI HRMS spectrum (bottom) of 1-L-Ins-1-P (**2-15**)

2.6 Conclusion

In conclusion, the substrate (1-L-Ins-1-P) (**2-15**) was successfully synthesized in total of 9 steps from *myo*-inositol. Furthermore no steric hindrance at the phosphorylation step was experienced with the latter procedure in comparison with the former procedure. The spectroscopic techniques employed unambiguously supported the target molecule structure. Thus, through this synthetic effort 1-L-Ins-1-P was available for enzyme assays using *Corynebacterium glutamicum* MshA. Although, in the end commercially obtained substrates (1-L-Ins-1-P and UDP-GlcNAc) sufficed for the enzyme assays performed here. However, larger sized libraries screening will require more substrate. The details of the enzyme assays will be discussed in Chapter 5.

2.7 Experimental

All the dry solvents used in all the reactions were purchased from commercial suppliers. ^{1}H NMR spectra were performed in deuterated solvents [chloroform ($CDCl_3$), dimethyl sulfoxide (DMSO), methanol (CD_3OD) and D_2O] on either a Varian unity spectrometer 400 MHz (100 MHz for ^{13}C) or Varian mercury spectrometer 300 MHz (75 MHz for ^{13}C) using TMS as an internal standard and H_3PO_4 for ^{31}P NMR. The chemical shift (δ) is given in ppm relative to TMS (δ 0.00) or Na_2HPO_4. The coupling constant *J* is given in Hz. The melting points were determined using the Reichert Jung Thermovar hot stage microscope and are uncorrected. The reactions were monitored by thin layer chromatography (TLC) using Merck aluminium silica gel F_{254} plates. All the fluorescent compounds were visualized under ultra violet (UV) light at the wavelength of 254 nm and all the non-fluorescent compounds were visualized by spraying the TLC plate with anisaldehyde, ninhydrin or ceric ammonium sulfate spray respectively followed by heating the plate until the colour develops.

2.7.1 Synthesis of 1,2-*O*-cyclohexylidine-DL-*myo*-inositol (2-4)[35]

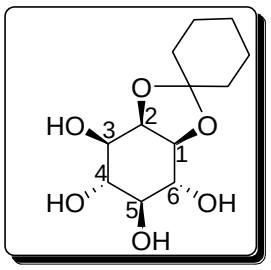

A mixture of *myo*-inositol, 1-ethoxycyclohexene and *p*-toluenesulphonic acid monohydrate in dry DMF was heated at 100 °C for 4 hr. The solution was allowed to cool down to room temperature before being diluted with DCM and washed sequentially with 5% aqueous $NaHCO_3$, water and saturated NaCl. The organic phase was dried and evaporated to give an oil. Subsequently the oil was dissolved in the minimum amount of acetone into which petroleum ether was added. The product crystallized out as a white solid. After re-acidification (0.2 g TsOH), the filtrate yielded two similar crops. The combined crystals were re-crystallized from ethanol

and washed several times with pet ether to afford 1,2-*O*-cyclohexylidine-DL-*myo*-inositol (**2-4**) as a white solid (11.0 g, 76%). M.p (179-181 °C) (lit. 179-180).[35]

2.7.2 Synthesis of 3,4,5,6-tetra-*O*-benzyl-1,2-*O*-cyclohexylidine-DL-*myo*-inositol (2-5)[36a]

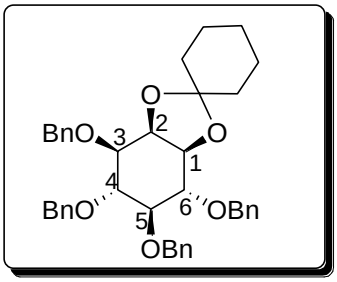

Anhydrous 1,2-*O*-cyclohexylidine-DL-*myo*-inositol (0.60 g, 2.31 mmol) in THF (10 mL) was cooled to 0 °C, followed by the addition of NaH (60%, 1.06 g, 15.9 mmol) portion-wise whilst stirring. After 30 min, benzyl bromide (1.4 mL) was added slowly, followed by the removal of the ice bath and the heterogeneous mixture were heated at reflux overnight. The resulting clear solution was quenched with methanol (10 mL), which was allowed to stir for 5 minutes, followed by the addition of water (10 mL). The organic solvent was removed under reduced pressure and the aqueous mixture was extracted with ethyl acetate (100 mL x 2). The pooled organic layers were then dried over $MgSO_4$ after which it was concentrated under reduced pressure. Purification by chromatography using silica-gel column (60 g; EtOAc/Pet ether, 3:7) gave 3,4,5,6-tetra-*O*-benzyl-1,2-*O*-cyclohexylidene-D,L-*myo*-inositol as an oil (1.22 g, 85%). ^{1}H NMR (400 MHz, $CDCl_3$) δ 7.45 – 7.17 (m, 20H, 4 x Ph), 4.94 – 4.67 (m, 8H, 4 x PhC*H*2), 4.29 (dd, *J* = 5.7, 3.8 Hz, 1H, H-2), 4.11 (dd, *J* = 7.2, 6.3 Hz, 1H, H-6), 3.91 (t, *J* = 8.2 Hz, 1H, H-3), 3.82 (dd, *J* = 9.6, 7.0 Hz, 1H, H-4), 3.69 (dd, *J* = 8.3, 3.8 Hz, 1H, H-1), 3.41 (dd, *J* = 9.6, 8.2 Hz, 1H, H-5), 1.84 – 1.30 (m, 10H, $C(CH_2)_5$,-cyclohexylidene). ^{13}C NMR (75 MHz, $CDCl_3$): δ 138.71, 138.66, 138.62, 137.34, 138.33, 128.34, 128.32, 128.26, 128.23, 127.96, 127.94, 127.91, 127.73, 127.58, 127.50, 127.45, 110.44 (quaternary C, cyclohexylidene), 82.89, 82.18, 80.95, 78.79, 77.28, 75.17, 75.00 (2 x PhCH_2),

74.03, 73.93, 73.11(2 x PhC*H*$_2$), 37.38, 35.04, 25.08, 23.94, 23.68 (5 x CH_2, cyclohexylidene).

2.7.3 Synthesis of 3,4,5,6-tetra-*O*-benzyl-*myo*-inositol (2-6)[36b,c]

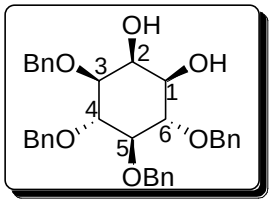

3,4,5,6-Tetra-*O*-benzyl-1,2-*O*-cyclohexylidine-DL-*myo*-inositol (1 g, 1.61 mmol) was suspended in aqueous acetic acid (80%, 25 mL) and the reaction mixture was heated to reflux at 100 °C for 2 hr. Upon completion, the solvent was removed under reduced pressure. The residue was dissolved in petroleum ether upon which a white solid crystallized (0.69 g, 79%). M.p (127 - 129 °C) (lit.[36b] 127 - 128 °C, lit.[36c] 127 °C) ^{1}H NMR (400 MHz, $CDCl_3$): δ 7.45 – 7.14 (m, 20H, 4 x Ph), 4.99 – 4.58 (m, 8H, 4 x $PhCH_2$), 4.18 (t, *J* = 2.9 Hz, 1H, H-2), 3.97 (t, *J* = 9.5 Hz, 1H, H-4), 3.88 (t, *J* = 9.5 Hz,1H, H-6), 3.49 (t, *J* = 9.5 Hz, 1H, H-5), 3.47 (m, 1H, H-1), 3.46 (t, *J* = 9.5 Hz,1H, H-3), 2.50 (s, 2H, -O*H*). ^{13}C NMR (100 MHz, $CDCl_3$): δ 138.78, 138.68, 138.65, 137.82, 128.72, 128.63, 128.56, 128.44, 128.41, 127.93, 127.91, 127.76, 127.68, 127.67, 127.63, 127.61, 83.34, 81.73, 81.42, 80.15, 75.94, 75.75, 75.63, 72.81, 71.77, 69.24.

2.7.4 Synthesis of 1-*O*-allyl-3,4,5,6-*tetra*-*O*-benzyl-DL-*myo*-inositol (2-7)

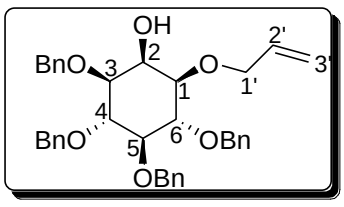

A mixture of 3,4,5,6-tetra-*O*-benzyl-*myo*-inositol (**2-6**) (0.5 g, 0.925 mmol) and Bu_2SnO (0.025 g, 0.100 mmol) was dissolved in toluene (20 mL) and the reaction mixture was heated to reflux (111 °C) for 4 hr. The reaction mixture was then cooled to room temperature and the solvent was removed under reduced pressure. The residue was dissolved in DMF (5 mL) followed by the addition of allyl bromide (10 μL). The reaction mixture was cooled down to 0 °C before the addition of cesium

fluoride (0.04 g, 0.263 mmol). Subsequently, the reaction mixture was allowed to equilibrate to room temperature whilst stirring overnight. Upon completion, the reaction mixture was extracted with EtOAc (100 mL) and washed with water (100 mL). The organic layer was concentrated under the reduced pressure. Purification by chromatography using a silica-gel column (50 g, EtOAc/Pet ether, 3: 7, R_f 0.1) gave 1-*O*-allyl -3,4,5,6-tetra-*O*-benzyl-DL-*myo*-inositol (**2-7**) as an oil (0.45 g, 83%). ^{1}H NMR (400 MHz, $CDCl_3$): δ 7.38 – 7.21 (m, 20H, 4 x Ph), 5.93 (m, 1H, H-2'), 5.28 (dd, J = 17.2, 1.4 Hz, 1H, H-3'$_a$), 5.18 (dd, J = 10.4, 1.4 Hz, 1H, H-3'$_b$) 4.91 – 4.70 (m, 8H, 4 x PhCH_2), 4.22 (t, J = 2.8 Hz, 1H, H-2), 4.20 – 4.15 (m, 2H, H-1'$_a$, H-1'$_b$), 4.22 (t, J = 9.5 Hz, 1H, H-6), 3.47 – 3.39 (m, 1H, H-4), 3.97 (t, J = 9.6 Hz, 1H, H-5), 3.42 (dd, J = 9.6, 2.8 Hz, 1H, H-3), 3.29 (dd, J = 9.6, 2.8 Hz, 1H, H-1).^{13}C NMR (101 MHz, $CDCl_3$): δ 138.78, 138.68, 138.65, 138.27, 128.48, 128.42, 128.36, 128.34, 128.01, 127.83, 127.79, 127.76, 127.68, 127.63, 127.60, 127.54, 83.63, 82.19, 81.92, 81.15, 77.34, 75.85, 75.73, 75.50, 74.77, 73.01, 72.45.

2.7.5 Synthesis of 1-*O*-allyl -2,3,4,5,6-penta-*O*-benzyl-DL-*myo*-inositol (2-8)

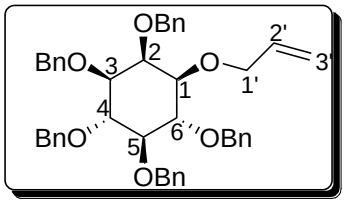

To a solution of 1-*O*-allyl -3, 4, 5, 6-tetra-*O*-benzyl-L-*myo*-inositol (**2-7**) (0.20 g, 0.344 mmol) in THF (2 mL) was added portion-wise NaH (60 %, 0.0840 g, 3.50 mmol) at 0 °C. The reaction mixture was allowed to stir for 30 min at 0 °C, followed by the addition of benzyl bromide (0.06 mL, 0.504 mmol). The reaction mixture was heated to reflux (66 °C) for 3 hr. The reaction mixture was quenched with MeOH (5 mL) and allowed to stir for 30 minutes, followed by the addition of water (5 mL). The MeOH was removed under reduced pressure and the aqueous phase extracted with EtOAc (100 mL x 2). The organic solvent was washed twice with saturated NaCl (100 mL) after which it was dried over $MgSO_4$ followed by filtration. The filtrate was

concentrated under reduced pressure. Purification by chromatography using a silica-gel column (20 g, EtOAc/Pet ether, 1: 19) gave 1-*O*-allyl -3,4,5,6-tetra-*O*-benzyl-L-*myo*-inositol (**2-8**) as an oil (0.180 g, 90%). ^{1}H NMR (300 MHz, $CDCl_3$): δ 7.37 – 7.19 (m, 25H, 5 x Ph), 5.97 – 5.84 (m, 1H, H-2'), 5.30 (dd, *J* 17.2 Hz, 1.7 Hz, 1H, H-3' $_a$), 5.17 (dd, *J* 10.4 Hz, 1.6 Hz, 1H, H-3' $_b$) 4.96 – 4.73 (m, 10H, 5 x PhC*H*$_2$), 4.13 – 3.96 (m, 5H, H-2, H-4, H-6, H-1' $_a$, H-1' $_b$), 3.46 (t, *J* = 9.2 Hz, 1H, H-5), 3.37 (dd, *J* = 9.9, 2.3 Hz, 1H, H-3), 3.26 (dd, *J* = 9.8, 2.3 Hz, 1H, H-1). ^{13}C NMR (101 MHz, $CDCl_3$): δ 139.05, 138.97, 138.95, 138.93, 138.91, 138.43, 128.54, 128.35, 128.17, 128.14, 128.08, 127.82, 127.77, 127.68, 127.56, 127.54, 127.45, 127.42, 127.39, 116.64, 83.77, 81.74, 81.71, 80.94, 80.78, 77.02, 76.69, 75.83, 74.42, 74.14, 72.86, 71.63.

2.7.6 Synthesis of 2,3,4,5,6-penta-*O*-benzyl-DL-*myo*-inositol (2-9)

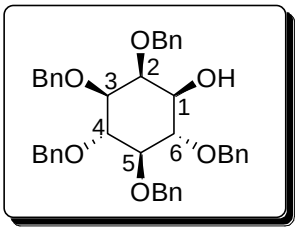

To a solution of 1-*O*-allyl -3,4,5,6-tetra-*O*-benzyl-D-*myo*-inositol (**2-8**) (0.70 g, 1.04 mmol) in EtOH/MeOH (1:1, 8 mL) was added $PdCl_2$ (0.034 g, 0.192 mmol). The mixture was allowed to stir at room temperature for 5 hr. Upon completion the $PdCl_2$ solids were filtered through celite and the filtrate was concentrated under reduced pressure. Purification by chromatography using a silica-gel column (70 g, EtOAc/Pet ether, 3:7, R_f 0.2) gave 2,3,4,5,6-penta-*O*-benzyl-DL-*myo*-inositol (**2-9**) as an oil (0.52 g, 79%). ^{1}H NMR (300 MHz, $CDCl_3$): δ 7.40 – 7.22 (m, 25H, 5 x Ph), 5.01 – 4.67 (m, 10H, 5 x PhC*H*$_2$), 4.09 (d, *J* = 9.6 Hz, 1H, H-4), 4.04 (t, *J* = 2.0 Hz, 1H, H-2), 3.86 – 3.78 (m, 1H, H-6), 3.52 (d, *J* = 4.3 Hz, 1H, H-3), 3.51 – 3.47 (m, 1H, H-5), 3.47 – 3.44 (m, 1H, H-1), 2.23 (d, *J* = 6.4 Hz, 1H, O*H*). ^{13}C NMR (101 MHz, $CDCl_3$): δ 138.74, 138.66, 138.61, 138.25, 128.46, 128.41, 128.35,

128.31, 128.00, 127.82, 127.77, 127.75, 127.67, 127.61, 127.58, 127.54, 83.63, 82.20, 81.92, 81.20, 76.70, 75.85, 75.73, 75.50, 74.77, 73.01, 72.44.

2.7.7 Synthesis of 2,3,4,5,6-penta–*O*-benzyl-1-*O*-[(1*S*-(-)-camphanoyl]-L-*myo*-inositol (2-10)

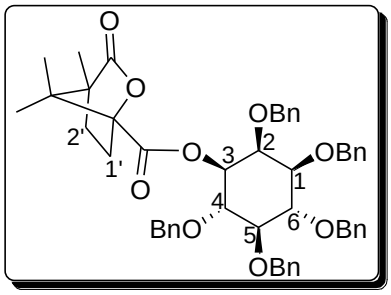

To a solution of 2,3,4,5,6-penta-*O*-benzyl-D/L-*myo*-inositol (**2-9**) (1.56 g, 2.48 mmol) in DCM (20 mL) was added camphanic acid chloride (0.695 g, 3.21 mmol), Et_3N (1.35 mL, 9.85 mmol) and DMAP (0.06 g, 0.49 mmol). The reaction was allowed to stir at room temperature overnight. 2,3,4,5,6-Penta–*O*-benzyl-1-*O*-[(1S-(-)-camphanoyl]-L-*myo*-inositol (**2-10**) was obtained as an amorphous solid. Purification by chromatography using a silica-gel column (*n*-hexane/diethyl ether, 1: 1, R_f = 2.5) gave 2,3,4,5,6-penta–*O*-benzyl-1-*O*-[(1*S*-(-)-camphanoyl]-L-*myo*-inositol (**2-10**) as a white solid (0.963 g, 48%) M.p (116-118 °C), $[\alpha]^{20}_D$ = -18° (c = 1, $CHCl_3$ ^{1}H NMR (400 MHz, $CDCl_3$): δ 7.39 – 7.19 (m, 25H, 5 x Ph), 5.02 – 4.68 (m, 10H, 5 x PhC*H*$_2$), 4.62 (dd, *J* = 10.2, 2.2 Hz, 1H, H-1), 4.22 (t, *J* = 2.0 Hz, 1H, H-6), 418 (1H, dd, *J* = 10.2, 9.5 Hz, H-2), 4.12 (t, *J* = 9.5 Hz, 1H, H-4), 3.58 (t, *J* = 9.5 Hz, 1H, H-3), 3.55 (1H, dd, *J* = 9.5, 2.3 Hz, H-5), 2.29 – 2.22 (m,1H, H-1'$_a$). 1.92 – 1.78 (m, 2H, H-1'$_b$, H-2'$_b$) 1.70 – 1.59 (m, 1H, H-2'$_a$) 1.06, (s, 3H, CH_3, camphonyl), 1.05, (s, 6H, CH_3, camphonyl). ^{13}C NMR (101 MHz, $CDCl_3$): δ 177.89, 166.46 (2 x C=O), 138.61, 138.41, 138.35, 138.28, 138.03, 128.46, 128.41, 128.35, 128.32, 128.31, 128.26, 128.00, 127.97, 127.79, 127.75, 127.69, 127.61, 127.58, 127.40, 127.23, 83.56, 81.42, 80.98, 78.94, 75.89, 75.27, 75.26, 75.25, 74.70, 73.09, 54.77, 54.07, 30.92, 28.93 (2C), 16.63, 16.56, 9.61 (3 x C*H*$_3$).

2.7.8 Synthesis of 2,3,4,5,6-penta-*O*-benzyl-L-*myo*-inositol (2-12)[29]

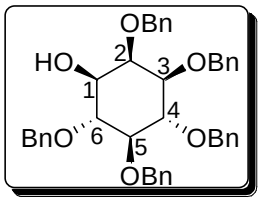

A mixture of 2,3,4,5,6-penta-O-benzyl-D-*myo*-inositol (**2-10**) (0.093 g, 0.115 mmol) and potassium hydroxide (0.065 g, 1.16 mmol) in absolute ethanol (20 mL) was gently refluxed for 2 hr. Upon completion of the reaction, the solvent was removed under reduced pressure followed by the addition of water (10 mL) to the residue, and thereafter the mixture was extracted with DCM (50 mL x 2). The organic layers were collected and dried over $MgSO_4$. The solvent was removed under reduced pressure. Purification by chromatography using a silica-gel column (EtOAc/Pet ether, 3:7) gave 2,3,4,5,6-penta-*O*-benzyl-L-*myo*-inositol (**2-12**) as an oil (0.0616 g, 85%). ^{1}H NMR (300 MHz, $CDCl_3$): δ 7.40 – 7.22 (m, 25H, 5 x Ph), 5.01 – 4.67 (m, 10H, 5 x PhC*H*$_2$), 4.09 (d, *J* = 9.6 Hz, 1H, H-4), 4.04 (t, *J* = 2.0 Hz, 1H, H-2), 3.86 – 3.78 (m, 1H, H-6), 3.52 (d, *J* = 4.3 Hz, 1H, H-3), 3.51 – 3.47 (m, 1H, H-5), 3.47 – 3.44 (m, 1H, H-1), 2.23 (d, *J* = 6.4 Hz, 1H, O*H*). ^{13}C NMR (101 MHz, $CDCl_3$): δ 138.74, 138.66, 138.61, 138.25, 128.46, 128.41, 128.35, 128.31, 128.00, 127.82, 127.77, 127.75, 127.67, 127.61, 127.58, 127.54, 83.65, 82.23, 81.97, 81.23, 77.44, 75.86, 75.78, 75.54, 74.77, 73.03, 72.41.

2.7.9 Synthesis of 4-*O*-camphanoyl-2,3,5,6-di-*O*-cyclohexylidene-L-*myo*-inositol (2-18)

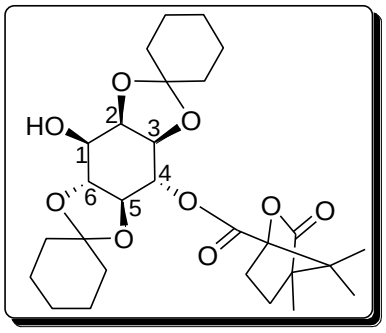

To a solution of 4-*O*-camphanoyl-2,3,5,6-di-*O*-cyclohexylidene-1-*O*-benzyl-L-*myo*-inositol (**2-17**) (0.5 g, 0.819 mmol) in ethanol/THF (50:50) was added 10% Pd/C (0.25 g, 2.35 mmol) followed by hydrogenation at 50 psi at room temperature for 24 hr. Upon the completion of the reaction, Pd/C was filtered through a celite pad. The filtrate was concentrated under reduced pressure to give 4-*O*-camphanoyl-2,3,5,6-di-

O-cyclohexylidene-L-*myo*-inositol (**2-18**) as a white solid (0.470 mg, 91%). The product was used in the next step without further purification. M.p (220-222 °C).

2.7.10 Synthesis of 4-*O*-camphanoyl-2,3,5,6-di-*O*-cyclohexylidene-1-*O*-diphenylphosphoryl-L-*myo*-inositol (2-19)

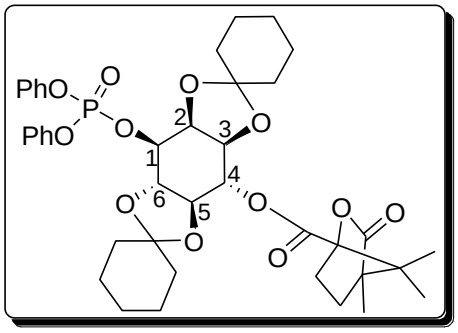

To a solution of 4-*O*-camphanoyl-2,3,5,6-di-*O*-cyclohexylidene-L-*myo*-inositol (**2-18**) (0.2 g, 0.384 mmol) in DCM (10 mL) was added Et_3N (0.111 mL), catalytic amount of DMAP and $(PhO)_2POCl$ (0.276 mL). The reaction mixture was allowed to stir overnight at room temperature. Upon the completion, the solvent was removed under reduced pressure. Purification by chromatography using a silica-gel column (20 g, EtOH/Pet ether, 1: 1) gave 4-*O*-camphanoyl-2,3,5,6-di-*O*-cyclohexylidene-1-*O*-diphenylphosphoryl-L-*myo*-inositol (**2-19**) as a white solid (0.289 g, 100%). M.p (183-186 °C). ^{31}P NMR (162 MHz, $CDCl_3$) δ -12.45; ^{1}H NMR (400 MHz, $CDCl_3$): δ 7.36- 7.13 (m, 10H, 5 x Ph), 4.92 – 475 (m, 1H, H-4), 4.65 – 4.19 (m, 1H, H-1), 3.65-362 (m, 2H, H-3, H-5), 3.47 - 3.42 (m, 2H, H-2, H-6), 2.51 – 2.38 (m,1H, H-1'$_a$), 2.09 – 1.98 (m, 1H, H-1'$_b$), 1.94 – 1.87 (m, 1H, H-2'$_b$) 1.80 – 1.75 (m, 1H, H-2'a) 1.63 – 1.28 (m, 20H, C(CH_2)10, cyclohexylidene) 1.10, (s, 3H, CH_3, camphonyl), 1.05, (s, 3H, CH_3, camphonyl), 0.96, (s, 3H, CH_3, camphonyl). ^{13}C NMR (75 MHz, $CDCl_3$): δ 167.35, 166.32, 150.44, 129.66, 125.52, 120.15, 114.00, 111.52, 71.06. 68.23, 64.45, 54.78, 54.20, 37.45, 36.27, 31.71, 29.69, 29.00, 24.81. 23.62. 16.60. HRMS (ESI) calculated for $C_{42}H_{53}O_{12}P$: [M + H] 752.2962; found: 752.2958.

2.7.11 Synthesis of 4-*O*-camphanoyl-2,3,5,6-di-*O*-cyclohexylidene-1-*O*-dibenzylphosphoryl-L-*myo*-inositol (2-20)

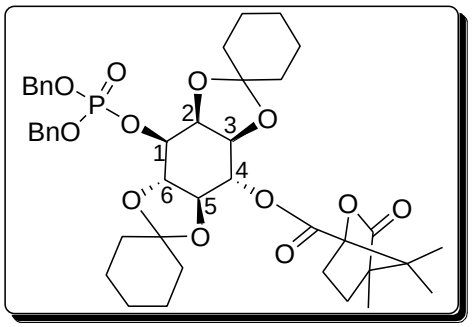

To a solution of 4-*O*-camphanoyl-2,3,5,6-di-*O*-cyclohexylidene-1-*O*-diphenylphosphoryl-L-*myo*-inositol (**2-19**) (0.882 g, 1.17 mmol) in THF (8 mL) at 0 °C was added NaH (0.0452 g, 1.13 mmol). The reaction mixture was allowed to stir for 30 mins before BnOH (0.293 mL) was added. The reaction mixture was allowed to equilibrate to room temperature whilst stirring overnight. The reaction was judged as complete by TLC (EtOAc/Pet ether, 3: 7, R_f 0.1). The solvent was concentrated under reduced pressure and 4-*O*-camphanoyl-2,3,5,6-di-*O*-cyclohexylidene-1-*O*-dibenzylphosphoryl-L-*myo*-inositol (**2-20**) was obtained as a semi-solid material (0.576 g, 63%). ^{1}H NMR (400 MHz, $CDCl_3$): δ 7.41 – 7.19 (m, 10H, 2 x Ph), 5.13 – 503 (m, 4H, C*H*$_2$Ph), 4.75 – 4.66 (m, 1H, H-4), 4.56 – 4.50 (m, 1H, H-1), 4.06-3.91 (m, 2H, H-3, H-5), 3.86 - 3.80 (m, 1H, H-6), 3.34-3.26 (m, 1H, H-2), 2.29 – 2.22 (m, 1H, H-1'$_a$), 1.92 – 1.78 (m, 2H, H-1'$_b$, H-2'$_b$), 1.70 – 1.59 (m, 1H, H-2'$_a$), 1.64 – 1.27 (m, 20H, C(C*H*$_2$)10, cyclohexylidene), 1.06 (s, 3H, CH_3, camphonyl), 1.05 (s, 6H, CH_3, camphonyl). HRMS (ESI) calculated for $C_{42}H_{53}O_{12}P$: [M + H] 780.3275; found: 780.3269.

2.7.12 Synthesis of 2,3,5,6-di-*O*-cyclohexylidene-1-*O*-dibenzylphosphoryl-L-*myo*-inositol (2-21)

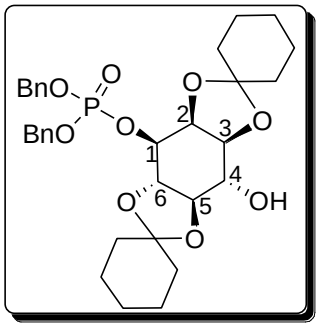

To a solution of 4-*O*-camphanoyl-2,3,5,6-di-*O*-cyclohexylidene-1-*O*-diphenylphosphoryl-L-*myo*-inositol (**2-20**) (0.55 g, 0.705 mmol) in absolute ethanol (10 mL) was added powdered KOH (0.39 mg, 0.007 mmol). The reaction was heated to a reflux and followed on TLC (50 g, MeOH/EtOAc, 0.2: 9.8, R_f 0.2) and was judged as complete after 2 hr. The solvent was removed under reduced pressure to give 2,3,5,6-di-*O*-cyclohexylidene-1-*O*-dibenzylphosphoryl-L-*myo*-inositol (**2-21**) as a colourless film (0.275 g, 65%). The product was used in the next step without any further purification.

2.7.13 Synthesis of 1-*O*-dibenzylphosphoryl-L-*myo*-inositol (2-22)

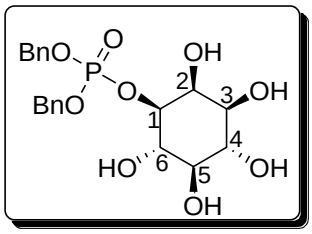

2,3,5,6-di-*O*-Cyclohexylidene-1-*O*-dibenzylphosphoryl-L-*myo*-inositol (**2-21**) (0.2 g, 0.333 mmol) was suspended in aqueous acetic acid (80%, 5 mL) and the suspension was heated to reflux at 100 °C for 2 hr. Upon the completion, the solvent was evaporated under reduced pressure and the residue was dissolved in petroleum ether upon which 1-*O*-dibenzylphosphoryl-L-*myo*-inositol (**2-22**) crystallized as a white solid (0.0616 g, 42%). ^{1}H NMR (400 MHz, D_2O): δ 7.41 – 7.32 (m, 10H, 5 x Ph), 5.17 – 5.03 (m, 4H, 2 x PhC*H*$_2$), 3.92-3.80 (m, 3H, H-6, H-2, H-1), 3.69 – 3.58 (m, 2H, H-3, H-5), 3.52 – 3.38 (m, 1H, H-4). HRMS (ESI) calculated for $C_{20}H_{25}O_9P$: [M^+] 440.1236; found: 440.1229.

2.7.14 Synthesis of 1-L-Ins-1-P (2-15)

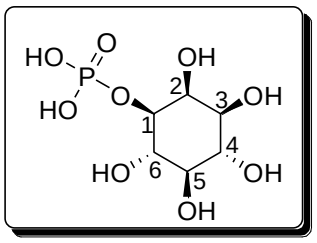

To a solution of 1-*O*-dibenzylphosphoryl-L-*myo*-inositol (**2-22**) (30 mg, 0.0682 mmol) in ethanol/water (50 mL, 80:20) was added 10% Pd/C (35 mg, 0.329 mmol), followed by hydrogenation at 50 psi at room temperature for 24 hr. Upon the completion of the reaction, Pd/C was filtered through celite and the filtrate was concentrated under reduced pressure. The resulting aqueous solution was passed through C18 and eluted with Milli-Q water, after which it was lyophilized to give 1-L-Ins-1-P (**2-15**) as a white solid (25 mg, 71%). M.p (105 – 108 °C). ^{1}H NMR (400 MHz, D_2O) δ 4.65 (1H, H-1), 4.10 (m, 2H, H-6, H-2,), 3.98 – 3.88 (m, 2H, H-3, H-5), 3.86 – 3.75 (m, 1H, H-4). ^{13}C NMR (101 MHz, D_2O) δ 66.80, 66.00 (2 x C), 62.45 (2 x C), 60.45. ^{31}P NMR (^{1}H NMR decoupled) (162 MHz, D_2O): δ 5.23 (s); ^{31}P NMR (^{1}H NMR coupled) (121.5 MHz, D_2O): δ 5.14 (J_{PH} = 9.0 Hz). HRMS (ESI) calculated for $C_6H_{13}O_9P$: [M^+] 262.0340; found: 262.0358.

2.8 References:

1. **Migaud, M. E. and Frost, J. W. 1996.** Elaboration of a general strategy for inhibition of *myo*-inositol 1-phosphate synthase: Active site interactions of analogues possessing oxidized reaction centers. *Journal of the American Chemical Society.* **118**: 495-501.
2. **Irvine, R. F. and Schell, M. J. 2001.** Back in the water: the return of inositol phosphates. *Nature Review Molecular Cell Biology*. **2**: 327–338.
3. **Berridge, M. J. and Irvine, R. F. 1989.** Inositol phosphates and cell signaling. *Nature*. **341**: 197–205.
4. **Billington, D. C. 1993**. The inositol phosphates: chemical synthesis and biological significance. *Cell Biochemistry and Function*. **12**(1): 77-78.
5. **Sureshan, K. M., Kiyosawa, Y., Han, F., Hyodo, S., Uno, Y. and Watanabe, Y. 2005.** Resolution of synthetically useful *myo*-inositol derivatives using the chiral auxiliary *O*-acetylmandelic acid. *Tetrahedron: Asymmetry*. **16**(1): 231-241.
6. **Shaldubina, A., Ju, S., Vaden, D. L., Ding, D., Belmaker, R. H. and Greenberg, M. L. 2002.** *epi*-Inositol regulates expression of the yeast *INO1* gene encoding inositol-1-P synthase. *Nature Publishing Group*. **7**: 174-180.
7. (a) **Agranoff, B. W. 1978.** Cyclitols confusion. *Trends in Biochemical Sciences.* **3**: 283-285. (b) **Shears, S. B. 2004.** How versatile are inositol phosphate kinases? *Biochemical Journal.* **377**: 265–280.
8. **Loewus, F. A. and Murthy, P. P. N. 2000.** *myo*-Inositol metabolism in plants. *Plant Science*. **150**: 1-19.
9. **Azevedo, C. and Saiardi, A. 2006.** Extraction and analysis of soluble inositol polyphosphates from yeast. *Nature Protocols*. **1**(5): 2416-2422.

10. **Chen, L., Zhou, C., Yang, H. and Roberts, M. F. 2000.** Inositol-1-phosphate synthase from *Archaeoglobus fulgidus* is a class II aldolase. *Biochemistry*. **39**: 12415-12423.
11. **Bachhawat, N. and Mande, S. C. 1999.** Identification of the INO1 gene of *Mycobacterium tuberculosis* H37Rv reveals a novel class of inositol-1-phosphate synthase enzyme. *Journal of Molecular Biology.* **291**: 53-536.
12. **Loewus, M. W., Sasaki, K., Leavitt, A. L., Munsell, L., Sherman, W. R. and Loewus, F. A. 1982.** The enantiomeric form of *myo*-inositol-1-phosphate produced by *myo*-inositol-1-phosphate synthase and *myo*-inositol kinase in higher plants. *Plant Physiology.* **70**: 1661–1663.
13. **Stephens, L. R., Kay, R. R. and Irvine, R. F. 1990.** A *myo*-inositol D-3 hydroxykinase activity in *Dictyostelium*. *Biochemical Journal.* **272**: 201–210.
14. **Dean-Johnson, M. and Henry, S. A. 1989.** Biosynthesis of inositol in yeast. *The Journal of Biological Chemistry.* **264**(2): 1274-1283.
15. **Ballou, C. E. and Pizer, L. I. 1959.** Synthesis of an optically active *myo*-inositol 1-phosphate. *Journal of the American Chemical Society*. **81**: 4745-4745.
16. **Ballou, C. E. and Pizer, L. I. 1960.** The absolute configuration of the *myo*-inositol 1-phosphate and confirmation of bornesitol configuration. *Journal of the American Chemical Society*. **82**: 3333-3335.
17. **Lardy, H. A. 1954.** The Vitamins. *New York Academic Press*. **11**: 325.
18. **Sculimbrene, B. R., Morgan, A. J. and Miller, S. J. 2002.** Enantiodivergence in small-molecule catalysis of asymmetric phosphorylation: Concise total syntheses of the enantiomeric D-*myo*-Inositol-

1-phosphate and D-*myo*-Inositol-3-phosphate. *Journal of the American Chemical Society.* **124**, 11653-11656.

19. **Billington, D. C., Baker, R., Kulagowski, J. J. and Mawer, I. M. 1987.** Synthesis of *myo*-inositol 1-phosphate and 4-phosphate, and of their individual enantiomers. *Journal of the Chemical Society, Chemical Communications*. **4**: 314-316.
20. (a) **Spiers, I. D., Schwalbe, C. H., Blake, A. J., Solomons, K. R. H. and Freeman, S. 1997.** Structure of (±)-1,2;4,5-di-O-cyclohexylidene *myo*-inositol and synthesis of *myo*-inositol 3-phosphate *via* its phosphorylation with (2*R*,4*S*,5*R*)-2-chloro-3,4-dimethyl-5-phenyl-1,3,2-oxazaphopholidin-2-one. *Carbohydrate Research*. **302**: 43-51. (b) **Chen, L., Spiliotis, E. T. and Roberts, M. F. 1998.** Biosynthesis of di-*myo*-inositol-1,1'-phosphate, a novel osmolyte in hyperthermophilic archaea. *Journal of Bacteriology*. **180** (15): 3785–3792.
21. **Vacca, J. P. deSolms, S. J., Huff, J. R., Billington, D. C., Baker, R., Kulagowski, J. J. and Mawer, I. M. 1989.** The total synthesis of *myo*-inositol polyphosphates. *Tetrahedron*. **45**(17): 5679-5702.
22. **Bruzik, K. S. and Salamonczyk, G. M. 1989.** Synthesis of the enantiomeric 1,4,5,6-tetra-*O*-benzyl-*myo*-inositols. *Carbohydrate Research*. **195**(1): 67-73.
23. **Gigg, J., Gigg, R. and Martin-Zamora, E. 1993.** The alkylation of dibutylstannylene derivatives of 1,2-O-isopropylidene-*myo*-inositol. *Tetrahedron Letters*. **34**(17): 2827-2830.
24. **Vishwakarma, R. A., Vehring, S., Mehta, A., Sinha, A., Pomorski, T., Herrmann, A. and Menon, A. K. 2005.** New fluorescent probes reveal that flippase-mediated flip-flop of phosphatidylinositol across the endoplasmic

reticulum membrane does not depend on the stereochemistry of the lipid. *Organic and Biomolecular Chemistry*. **3**: 1275-1283.

25. **Xue, J. and Guo, Z. 2002.** Convergent synthesis of an inner core GPI of sperm CD52. *Bioorganic and Medicinal Chemistry Letters*. **12**: 2015–2018.
26. **Damager, I., Engelsen, S. B., Blennow, A., Moller, B. L. and Motawia, M. S. 2010.** First principles insight into the α-glucan structures of starch: Their synthesis, conformation, and hydration. *Chemical Reviews*. **110**: 2049–2080.
27. **Keinan, E., Sahai, M. and Roth, Z. 1985.** Palladium-catalyzed allylic etherification with tin alkoxides. *The Journal of Organic Chemistry*. **50**: 3558-3566.
28. **Zhang, Z. and Wong, C. H. 2002.** Regioselective benzoylation of sugars mediated by excessive Bu_2SnO: Observation of temperature promoted migration. *Tetrahedron*. **58**: 6513-6519.
29. **Elliott, T. S., Nemeth, J., Swain, S. A. and Conway, S. J. 2009.** A synthesis of dioctanoyl phosphatidylinositol. *Tetrahedron: Asymmetry*. **20**: 2809-2813.
30. **Guibe, F. 1997.** Allylic protecting groups and their use in a complex environment part I: Allylic protection of alcohols. *Tetrahedron*. **53**(40): 1350-13556.
31. **Yamamoto, Y. and Radhakrishnan, U. 1999.** Palladium catalyzed pronucleophile addition to unactivated carbon–carbon multiple bonds. *Chemical Society Reviews*. **28**: 199–207.
32. **Desai, T.**, **Gigg, J. and Martin-Zamora, E. 1994.** The preparation of intermediates for the synthesis of 1D-*myo*-inositol 1,4,5-and 2,4,5-triphosphates, 1,4-bisphosphate 5-phosphorothioate, and 4,5-bisphosphate 1-

phosphorothiate from 1D-3,6-di-*O*-benzyl-1,2-*O*-isopropylidene-*myo*-inositol. *Carbohydrates Research*. **262**(1): 59-77.

33. **Quan, C., Fan, S. and Ohta, Y. 2003.** Pathway of dephosphorylation of *myo*-inositol hexakisphosphate by a novel phytase from *Candida krusei* WZ-001. *Journal of Biosciences and Bioengineering*. **95**(5): 530-533.
34. **Johansson, C.**, **Koedel, J. and Drakenberg, T. 1990.** Analysis of *myo*-inositol phosphates by 2D 1H NMR spectroscopy. *Carbohydrate Research*. **207**: 177-183.
35. **Jiang, C. and Baker, D. C. J. 1986.** Improved preparation of cyclohexylidene derivatives of *myo*-inositol. *Journal of Carbohydrate Chemistry*. **5**(4): 615-620.
36. (a) **Nkambule, C. M., Kwezi, N. W., Kinfe, H. H., Nokwequ, M. G., Gammon, D. W., Oscarson, S. and Karlsson, E. 2011.** Efficient regioselective protection of *myo*-inositol *via* facile protecting group migration. *Tetrahedron*. **67**: 618-623. (b). **Shvets, V. I., Klyashchitskii, B. A., Stepanov, A. E. and Evstigneeva, R. P. 1973.** Resolution of asymmetrically substituted *myo*inositols into optical antipodes. *Tetrahedron*. **29**(2): 331-340. (c). **Angyal, S. J. and Tate, M. E. 1965.** Cyclitols. Part XXI. Benzyl ethers of *myo*-inositol. Aromatisation of a tosyl derivative of *myo*-inositol. *Journal of the Chemical Society*. 6949-6955.

CHAPTER 3

Design and synthesis of potential inhibitors against MshA

3.1 Introduction

In this chapter the design of potential inhibitors of MshA using computational modeling and simulation studies is reported. Computational modeling and simulation studies play a significant role in modern day drug discovery and have become an essential tool in rational drug design.[1]

In medicinal chemistry, computational modeling and simulation has been used as a tool not only for *in silico* hit identification and lead optimization but also to predict the binding and interaction between the ligand and the target.[2,3] In addition, computational modeling are often used to predict the pharmacokinetics and pharmacological analysis of ADMET (Absorption, distribution, metabolism, excretion and toxicity) properties of drug molecules.[2-4]

In order to improve on the traditional methods of drug discovery, computational scientists have developed modern drug discovery approaches through the development of improved simulation algorithms. The advantage of computational methods is that it enables one to tailor drugs with desired drug-like properties before starting with actual synthesis of target compounds. The concept of drug design begins with a hypothesis that modulate the interaction between a drug and biological drug target that may be considered to be of high therapeutic significance.[5] While computational approaches have already provided significant benefits, they hold a great promise for future in drug discovery and development. However, the computer assisted drug discovery and development is an emerging technology and has a number

of limitation such as generation of undesirable chemical structures which may be chemically unstable, synthetically unfeasible or have high toxicity.

The progress in molecular modeling studies of glycosyltransferases has been very slow owing to the limited number of available crystal structures. Helm *et al.*[6] proposed that the crystal structures of existing glycosyltransferases could serve as starting points for the design of substrate analogues for other related glycosyltransferases mainly because of their structural similarities. Fortunately in this study, the availability of a MshA crystal structure from *Corynebacterium glutamicum* (cgMshA) made it possible to search for potential selective inhibitors of glycosyltransferase MshA.[7a]

Comparison of the MshA structures of *M. tuberculosis*, *Corynebacterium glutamicum* and *M. smegmatis* were reported to have a high sequence homology. According to the literature reports, the monomeric homology model of *M. tuberculosis* MshA was created using CPH-models 2.0 with the UDP-complexed cgMshA (PDB: 3C4Q) as template. Superimposition of the model of *M. tuberculosis* MshA (consisting of Arg46–Ile445) and the chain B from UDP/inositol-phosphate bound cgMshA (PDB: 3C4V) yields an root mean square deviation (RMSD) of 0.65 Å, indicating a high homology between MshA.[7b] Prior to that Newton and co-workers also reported a high sequence homology between MshA structures of *M. tuberculosis* and *M. smegmatis*.[7c] Thus, it can be conluded that there is high sequence homology between MshA structures of the isolates.

Walker and co-workers have developed a high throughput assay (HTS) for *E. coli* glycosyltransferase MurG and used it to screen a library of over 50 000 compounds to identify selective glycosyltransferase MurG inhibitors.[8] The HTS identified several

compounds with heterocyclic cores including rhodanine and its analogues 2-iminothiazolidin-4-one. Interestingly, the inhibitors **3-1** (IC_{50} = 1.4 μM), **3-2** (IC_{50} = 27 μM) and **3-3** (IC_{50} = 27 μM) (Fig 3-1) were selective of glycosyltransferase, MurG over another closely related enzyme, MurA, having strong structural and mechanistic similarities. Furthermore, compound **3-1** was found to be a competitive inhibitor of the substrate UDP-GlcNAc for the binding of the active site of MurG.

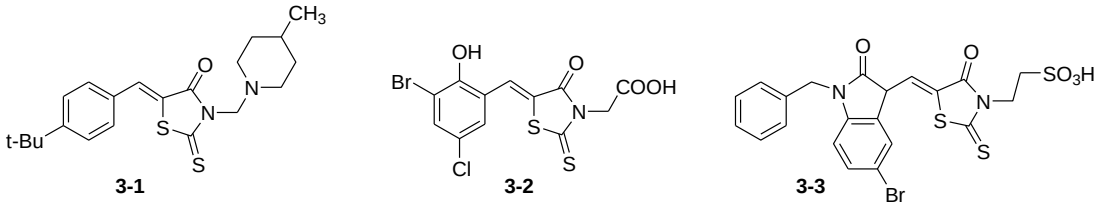

Figure 3-1: Inhibitors of glycosyltransferase MurG.[8]

The previous studies by Carlson *et al*.[9] and Soltero-Higgin *et al.*[10] identified the inhibitors for UDP-galactopyranose mutase (UGM) enzyme, which also uses a UDP coupled sugar as a substrate. Furthermore, the UGM inhibitors demonstrated the ability to be selective, when its ability to block galactosyltransferase activity was tested. The concept of selectivity of the inhibitors towards specific enzyme presented an exciting opportunity for design and development of novel enzyme-selective inhibitors for glycosyltransferase.

Amongst the compounds screened, the most potent compounds contained a heterocyclic ring and they appeared to have high binding affinity in the active site of glycosyltransferase MurG and galactosyltransferase respectively. It was against this background that the molecular docking of the thiazolidinethione (rhodanine/ rhodanine-3 acetic acid) scaffold (Fig. 3-2) in the active site of glycosyltransferase MshA was conceptualized.

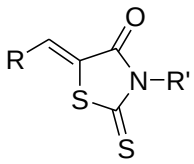

Figure 3-2: General structure of thiazolidinethione (rhodanine).

Thiazolidinethione derivatives were our preferred choice because of their structural similarities with the classes of the compounds assessed on glycosyltransferase MurG.[8] Furthermore there is overwhelming literature support that thiazolidinethione derivatives possess broad-spectrum of biological activities.[11-13] In order to investigate the binding mode of thiazolidinethione derivatives, selected classes of thiazolidinethione derivatives were docked into the active site of MshA.

3.2 Molecular docking studies

Following a computational simulation procedure described (software Autodock 4.2), molecular docking simulations were performed on selected thiazolidinethiones. With the availability of crystal structure coordinates of MshA, a model was created using a complex of MshA (PDB: 3C4Q) with bound ID (identification number) ligands. To provide enough space for free movements of the ligands the grid box was constructed to cover the whole uridine diphosphate (UDP) active site using Autodock tools and it was defined using AutoGrid4. The grid points were set to 50, 40 and 42 (xyz dimension), at a grid centre of (xyz) 79.66, 46.78 and 13.02 with spacing of 0.375 Å. In these calculations a maximum possible torsional degree of freedom for each molecule was utilized. For a population of 150 individuals, 5 x 10^6 maximum energy evaluations and operations were applied. All other parameters were set to Autodock 4.2 default values including the rate of gene mutation (0.02) and rate of crossover (0.8). A total of 50 generic algorithm (GA) trials were executed for each ligand. The generated 50 docked conformations were clustered at a tolerance of 2.0 Å and ranked

based on their binding energies. Autodock tools were used to view and analyze the best docked conformations.

3.2.1 Docking of thiazolidinethione compounds in the active site of MshA

Prompted by the previous studies on glycosyltransferase MurG.[8] A library of twelve 2-thioxo-thiazolidin-4-one derivatives have been designed *in silico* and analyzed by molecular docking simulation to identify the thiazolidinethione derivatives that occupy the active binding pocket of MshA, without wobbling into other important parts of the binding pocket. Docking of these thiazolidinethiones into the UDP-GlcNAc binding pocket of MshA gave some indication that these molecules may occupy the same binding site as UDP-GlcNAc (Fig. 3-3).

The docking studies further revealed that the thiazolidinethiones were best accommodated in the binding site when the thiazolidinethione ring is located in the vicinity of the diphosphate binding site, facing toward the GlcNAc binding site, whereas the benzene ring is orientated towards the uridine binding site. The position and the orientation of the representative thiazolidinethione derivative and superimposed substrate (UDP) inside the binding pocket of MshA are illustrated in Fig. 3-3.

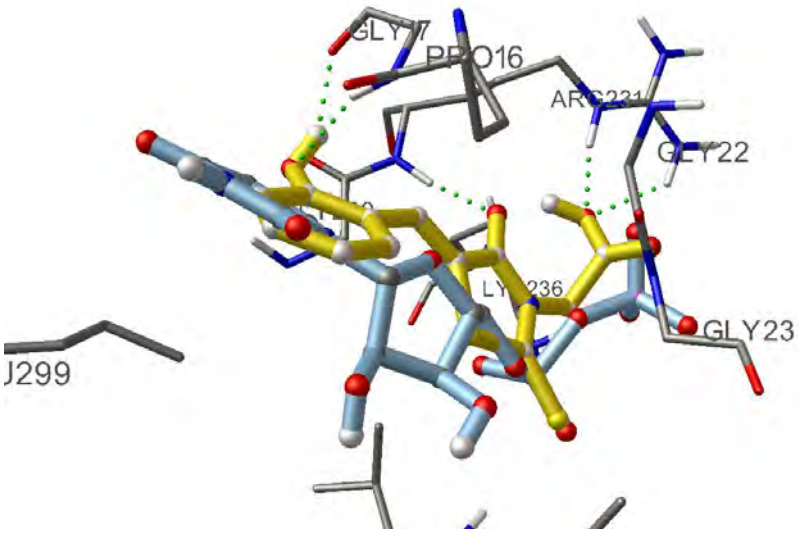

Figure 3-3: Crystal structure of MshA with UDP-GlcNAc substrate (light blue) and thiazolidinethione (yellow). Newly formed hydrogen bonds are indicated by green lines.

In addition, it has been observed that the thiazolidinethione interacts with essential vicinal amino acid residues (GLY17, ARG231, GLY22, LYS236 and GLY23) in the binding pocket, thus, forming six new hydrogen bonds (Fig. 3-3). Furthermore, it has been observed that amino acid residues (ARG231, GLY23, and LYS236) could be essential for both interaction of substrate and potential inhibitor respectively. In the absence of the inhibitor, these amino acid residues interact with substrate (UDP-GlcNAc) (Fig. 3-4). This observation suggest that it could be possible that the thiazolidinethione fit better than the substrate in the binding pocket and subsequently compete with the substrate for interacting with the active site amino acids residues (Fig. 3-4).

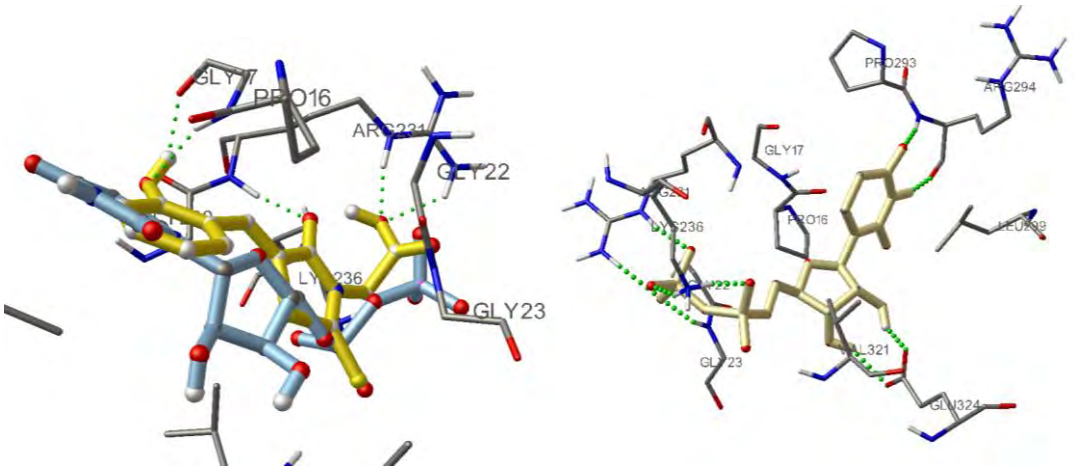

A **B**

Figure 3-4: Comparison between the crystal structures of MshA with/without inhibitors. **A**: Shows an inhibitor-substrate complex inside the binding pocket of MshA. **B**: Substrate inside the binding pocket.

The docking accuracy was validated by comparing difference between the crystal structure and the regenerated structure which was found to be 0.56 Å RMS (Root Mean Square). All the thiazolidinethione derivatives docked in the binding site shown some similar trend in their binding energies and inhibition constants owing to their structural similarities. The binding energies and inhibition constants for the docked thiazolidinethione derivatives range between -7.11 and -9.24 kcal/mol and 6.1 and 0.17 μM respectively. The orientation of the inhibitor in the binding pocket was in agreement with previous studies.[8] The study by Walker and co-workers demonstrated that the thiazolidinethione ring in the crystal structure of MurG is located near the phosphate bridge with the nitrogen orientated towards the GlcNAc binding pocket (Fig. 3-5). This phenomenon was further supported by previous studies by Sim *et al.*[14] and Andres *et al.*[15], whereby they suggested that the thiazolidinethione ring acts as a possible mimic for the diphosphate.

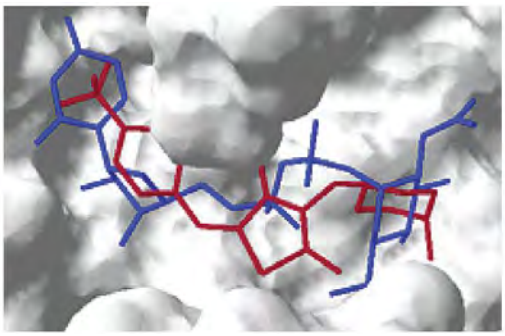

Figure 3-5: Crystal structure of MurG with UDP-GlcNAc substrate (blue) and competitive thiazolidinethione inhibitor (red).[8]

Based on the crystal structure of MshA and the orientation of the thiazolidinethione ring, the ring nitrogen allows possible extension of the thiazolidinethione moiety towards the GlcNAc binding pocket of the substrate. Subsequent modifications on this nitrogen with a propargyl moiety, lead to a significant improvement of the binding energy (-9.24 kcal/mol) and inhibition constant (K_i 0.17 μM) of the representative molecule (Fig. 3-6). The results suggest that propargylated thiazolidinethione derivatives could be potential inhibitors as evident with the lower binding energy, lower inhibition constant (K_i) and involves three hydrogen bonds interactions with amino acid residues (GLY17 and ARG231) of the active site. Other modifications such as *N*-CH_2CO_2H, *N*-$(CH_2)_3SO_3H$ were also performed on the *N*-terminal of the thiazolidinethione derivatives, in an effort to probe for an improved binding in the UDP-GlcNAc binding pocket. The simulation results (Table 3-1), summarily suggest that thiazolidinethione derivatives could be potential inhibitors of MshA. As a result, the next section (Section 3.3.1) has been dedicated to the description of synthesis of the potential thiazolidinethione based inhibitors of MshA.

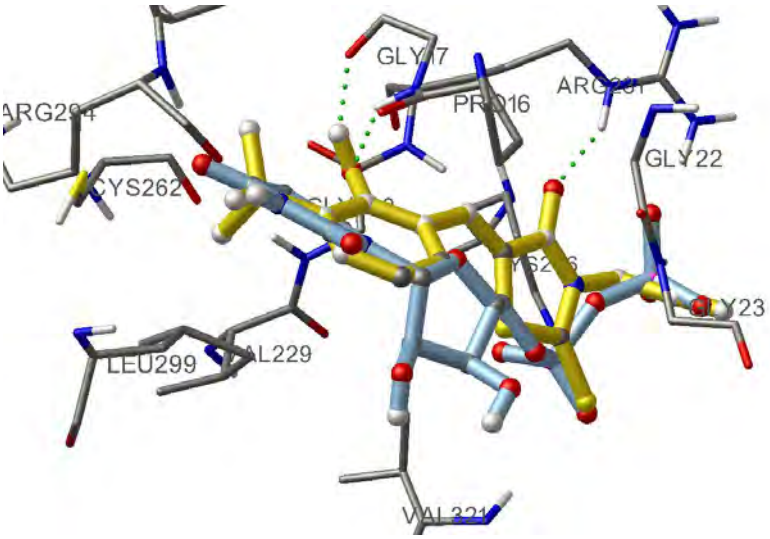

Figure 3-6: Crystal structure of MshA with UDP-GlcNAc substrate (light blue) and propargylated thiazolidinethione (yellow).

Table 3-1: Summary of the thiazolidinethione derivatives docked in MshA binding pocket

Entry	Code	Binding energy (Kcal/mol)	Inhibition constant (µM)
1	**MJ3A**	-7.61	6.1
2	**MJ2B**	-8.53	5.2
3	**MJ7B**	-8.76	3.7
4	**MJ12B**	-8.92	4.9
5	**MJ029-1**	-8.61	1.1
6	**MJ029-2**	-9.11	0.28
7	**MJ029-3**	-9.17	0.21
8	**MJ029-5**	-9.19	0.19
9	**MJ029-9**	-9.24	0.17
10	**MJ029-11**	-9.03	0.19

3.3 Synthesis of thiazolidinethione derivatives

Rhodanine represents a very important privileged scaffold in drug discovery and the importance of its derivatives such as thiazolidinethione-based compounds in pharmacological activities has been well documented.[16,17] Because of their biological importance in the development of new drug candidates, several possible methods for the synthesis thiazolidinethione derivatives have since been reported in the literature.[18]

Established methods for the preparation of thiazolidinethione derivatives require few steps and generally involve preparation of the rhodanine moiety followed by Knoevenagel condensation with aldehydes.[19] Eltsov *et al.*[20] reported a convenient one-pot cyclization reaction protocol which involved the reaction of ethyl 5-phenyl-thioureido-3*H*-imidazole-4-carboxylate with bromoacetic acid to obtain the desired thiazolidinethione derivative.

Pratap *et al*. recently reported the synthesis of 2,3-diaryl-4-thiazolidinones by utilizing the lipase from baker's yeast (*Saccharomyces cerevisiae*) as a catalyst.[21] Microwave assisted reactions between benzylidene-anilines and mercaptoacetic acid were reported recently by Bolognese *et al*.[22] These reactions were performed in the presence of benzene at room temperature and excellent yields between 65-90% were isolated after purification by silica gel column chromatography.

3.3.1 Synthesis of thiazolidinethione derivatives (MJ1A – MJ12A) *via* the Knoevenagel condensation

Herein we report the synthesis of the thiazolidinethione derivatives (Table 3-2) following a modified procedure (Scheme 3-1) reported by Gouveia *et al.*[23] using the

Knoevenagel condensation between aldehydes and rhodanine in refluxing glacial acetic acid for overnight.

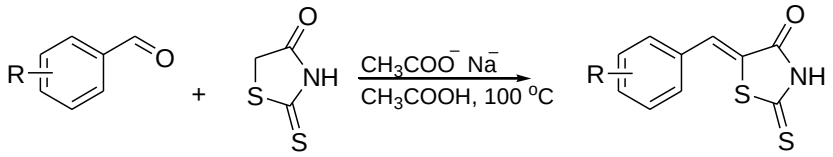

Scheme 3-1: Synthesis of thiazolidinethione derivatives (**MJ1A - MJ12A**).

This procedure resulted in the formation of several key corresponding 2-thioxothiazolidin-4-one derivatives. The compounds were crystallized from the reaction mixture as bright yellow solids with high purity and isolated in high yields (Table 3-2). The thiazolidinethione derivatives were washed with petroleum ether followed by ice cold water and samples were subsequently lyophilized to give desired compounds as solids. Compounds were then tested in an enzyme assay as described in Chapter 5.

Table 3-2: 2-Thiazolidinethione derivatives (**MJ1A–MJ12A**)

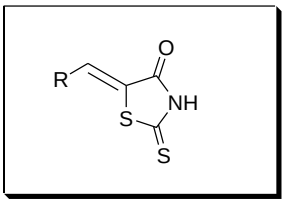

Entry	Code	R	Yield %	MP	Mw	M^+
1	**MJ1A**		93	202-203 (205-206)[24]	220.9969	220.9961
2	**MJ2A**	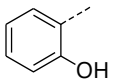	96	187-189	236.9918	236.9910
3	**MJ3A**	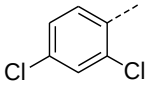	94	181-183	288.9190	288.9190
4	**MJ4A**	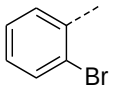	92	213-215	298.9074	298.9069
5	**MJ5A**	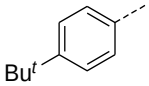	93	149-152	277.0595	278.0673
6	**MJ6A**	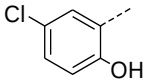	97	220-223	270.9528	270.9521
7	**MJ7A**	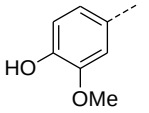	92	223-224 (230-231)	267.0024	268.0108
8	**MJ8A**	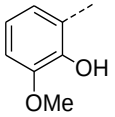	90	249-251	267.0024	268.0102
9	**MJ9A**	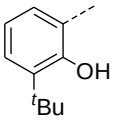	90	148-150	293.0544	293.0548
10	**MJ10A**	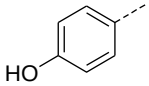	93	292-294 (294-295)[25]	236.9918	236.9910
11	**MJ11A**	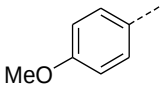	91	254-255 (260-261)[25]	251.0075	252.0134
12	**MJ12A**	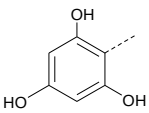	96	159-161	268.9816	268.9809

3.3.2 Characterization of thiazolidinethione derivatives (MJ1A – MJ12A)

The structures of the prepared thiazolidinethione derivatives were characterized and confirmed using ^{1}H, ^{13}C NMR and IR spectroscopic techniques. Melting points and HPLC were employed to assess the purity of prepared compounds. The HPLC results have indicated a high purity which exceeded 95%.

The ^{1}H NMR spectra of compounds (**MJ1A – MJ12A**) showed one common singlet proton which resonated at the region δ_H 7.51-7.79 ppm, corresponding to the methylidene proton. These protons appeared at high chemical shifts due to the deshielding effect of the adjacent phenyl rings. The signals were a clear indication that the coupling of the two molecules has taken place. The ^{13}C NMR spectral data of this series of compounds showed that only one geometrical isomer (*Z*) is present and no traces of the isomer (*E*) could be detected which was in agreement with the literature.[23,25] Mass spectrometry was used to confirm the required accurate mass of each compound. The IR spectroscopy of all the compounds showed the diagnostic bands in the regions 3014 – 3348, 3054 – 3076, 2848 - 2953 and 3087 – 3348 cm^{-1} which were assigned to N*H*, CH, C=C and O*H* stretches respectively.

3.3.3 Synthesis of thiazolidinethione derivatives (MJ1B – MJ12B)

A second series of thiazolidinethione derivatives (**MJ1B – MJ12B**) was deemed necessary as part of extension into the GlcNAc binding pocket. This series of compounds was also synthesized in the same manner as described in section **3.3.1.** Knoevenagel condensation was achieved through the coupling of different aldehydes with rhodanine-3 acetic acid in refluxing glacial acetic acid (Scheme 3-2). This series of compounds shared similar properties with the thiazolidinethione derivatives (**MJ-1A – MJ12A**); the compounds precipitate out of the reaction mixture as bright yellow

crystals without requiring further purification. The compound properties are summarized in Table 3-3.

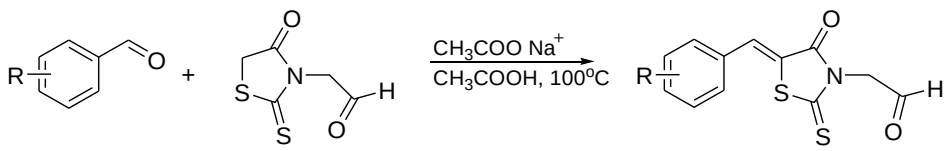

Scheme 3-2: Synthesis of thiazolidinethione derivatives (**MJ1B – MJ12B)**.

Table 3-3: Thiazolidinethione derivatives (**MJ1B – MJ12B**)

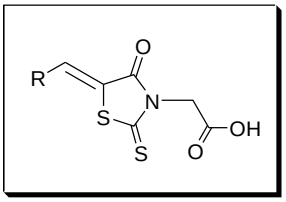

Entry	Code	R	Yields (%)	MP	Mw	M^+
1	**MJ1B**		95	118–120 (247-248)[26]	279.0024	279.0024
2	**MJ2B**		94	221-224	294.9973	294.9969
3	**MJ3B**	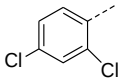	97	209-213	346.9244	346.9238
4	**MJ4B**		93	244-247	356.9129	356.9122
5	**MJ5B**	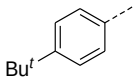	95	149–152	335.0650	336.0744
6	**MJ6B**	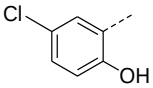	98	252-254	328.9583	328.9583
7	**MJ7B**	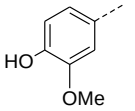	96	255–256	325.0079	326.0184
8	**MJ8B**	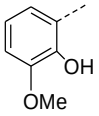	98	249–251	325.0079	326.0193
9	**MJ9B**	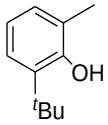	94	231-236	351.0599	351.0589
10	**MJ10B**	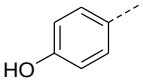	93	>300	294.9973	294.9973
11	**MJ11B**	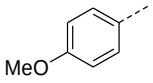	97	136–138	309.0129	310.0201
12	**MJ12B**	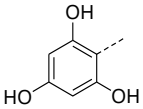	95	228-231	326.9871	326.9862

3.3.4 Characterization of thiazolidinethiones (MJ1B – MJ12B) structures

Similarly, the ^{1}H, ^{13}C NMR and IR spectroscopic techniques were employed to confirm the structures of synthesized compounds. Melting points and HPLC were employed to assess the purity of the compounds. The HPLC results have indicated a high purity which exceeded 95%.

Besides the methylidene proton resonating between δ_H 7.60 and 8.07 ppm, ^{1}H NMR spectroscopic data further showed the -C*H*$_2$-CO$_2$H as a key diagnostic signal. The other noticeable signal was the presence of the more deshielded broad singlet peak corresponding to the COO*H*.

The IR spectroscopy of all the compounds revealed new absorption bands in the regions 1600 – 1700 cm^{-1} for COO*H* apart from similar patterns of signals noted in the previous series of compounds. As expected no amine (N*H*) stretches were present.

3.4 Synthesis of propargylated thiazolidinethione derivatives (MJ029 series)

Propargylated thiazolidinethione derivatives (**MJ029-1 – MJ029-12**) were prepared in low yields ranging from 23-38% by *N*-alkylation of the corresponding 2-thioxothiazolidin-4-one with propargyl bromide (Scheme 3-3). In each reaction, 1 mol equivalent of each compound (**MJ1A – MJ12A**) was dissolved in dry DMF followed by addition of 1.5 mol equivalents of K_2CO_3. After 30 min of the reaction time, 1.5 mol equivalents of propargyl bromide were added at ambient temperature. The reaction was allowed to stir at room temperature for 24 h. The reaction progress was monitored by thin layer chromatography (TLC), which showed full conversion to form products. The DMF was co-evaporated several times with toluene to give brown-yellowish residues. The products were isolated in poor yields as bright yellow solids after purification with silica-gel chromatography. However, the reaction

condition was not optimized since enough material was obtained for subsequent experiments. The compound properties are summarized in Table 3-4.

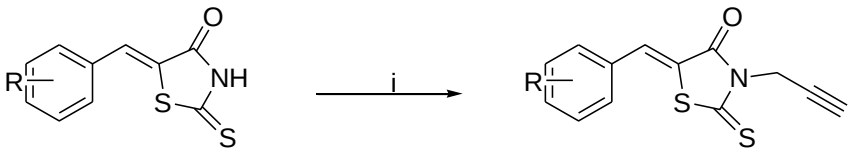

Scheme 3-3: K_2CO_3, C_3H_3Br, DMF, RT.

Table 3-4: Propargylated thiazolidinethione derivatives (**MJ029** series)

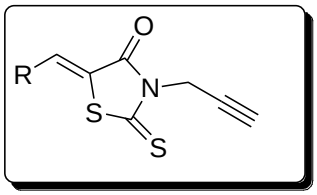

Entry	Code	R	Yields (%)	MP
1	**MJ029-1**		23	115-117
2	**MJ029-2**		25	133-134
3	**MJ029-3**	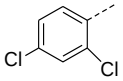	38	86-87
4	**MJ029-5**	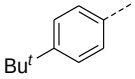	33	105-107
5	**MJ029-11**	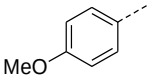	29	130-132

3.4.1 Characterization of propargylated thiazolidinethione derivatives (MJ029 series)

The prepared series of compounds was characterized using ^{1}H, ^{13}C NMR and IR spectroscopic techniques. HPLC traces and melting points were employed to assess the purity of target compounds. The ^{1}H NMR spectra of (**MJ029-1 – MJ029-12**) showed a triplet signal that resonated between δ_H 2.52 and 2.54 ppm, corresponding to alkyne proton (C≡C*H*). The other diagnostic signal was the appearance of

methylene protons ranging between δ 3.95 and 4.78 ppm. Furthermore, the absence of a N*H* associated peak from the 2-thioxothiazolidin-4-one provided additional proof that *N*-alkylation had taken place. The chemical shifts of the propargyl moiety were in agreement with those reported in literature.[27] The methylene protons appear as singlets downfield due to the deshielding effects of the adjacent nitrogen. The ^{13}C NMR spectrum was employed to confirm the structure and the assignment of the carbon atoms and that it was consistent with the literature.[28] In addition, the propargyl carbon atom bonded to nitrogen (N-C) appeared slightly deshielded because of the strong electronegativity conferred by nitrogen, thus confirming that the molecule is *N*-alkylated.

3.5 Synthesis of sulfonated thiazolidinethione derivatives (MJ081 series)

The synthesis of the sulfonated thiazolidinethione derivatives (**MJ081** series) was accomplished by *N*-alkylating the 2-thioxothiazolidin-4-one ring in the presence of NaH and 1,3-propanesultone in DMF (Scheme 3-4) at 0 °C. The compound properties are summarized in Table 3-5.

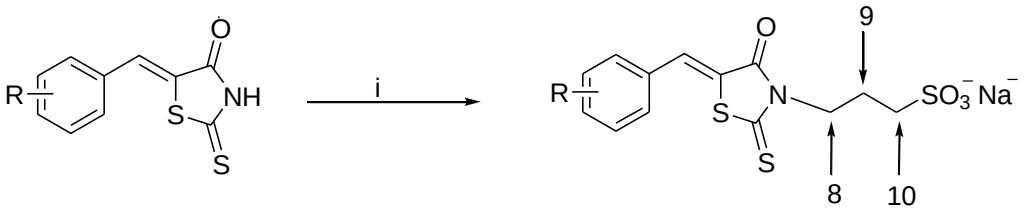

Scheme 3-4: Reaction conditions: NaH, 1,3-propanesultone and DMF at 0 °C.

Table 3-5: Sulfonated thiazolidinethione derivatives **(MJ081-1 – MJ081-12)**

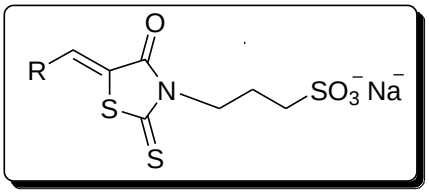

Entry	Code	R	Yields (%)	MP
1	**MJ081-1**		80	158-161
2	**MJ081-5**	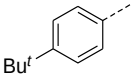	81	114-118
3	**MJ081-8**	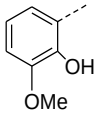	83	269–272
4	**MJ081-11**	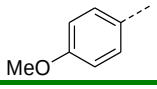	85	324-327

This series of compounds was characterized by ^{1}H and ^{13}C NMR spectroscopic techniques. The melting points were employed to check the purity of the compounds. The ^{1}H NMR spectra showed some distinct signal peaks resonating at δ_H 4.14 - 4.05 ppm (triplet, H-10), δ_H 2.55 – 2.45 ppm (triplet, H-8) and δ_H 2.04 – 1.94 ppm (quintet, H-9), which were assigned to alkyl protons of the propanesulfonate moiety. Likewise, the ^{13}C NMR spectrum was employed to confirm that alkylation occurred on the nitrogen of the rhodanine moiety. Again, the carbon bonded to nitrogen (*N*-C) appeared downfield due to the deshielding nature of the adjacent nitrogen, thus the confirming that the molecule is *N*-alkylated. The 2-thioxothiazolidin-4-one derivatives prepared here were subjected to a screen for anti-mycobacterial activity in an *in vitro* assay against *M.tb*. The results of the enzyme assays and whole cell inhibition will be discussed in Chapter 5 and Chapter 6 respectively.

3.6 Conclusion

In summary, a series of thiazolidinethione-based compounds have been successfully prepared as directed by molecular docking studies. The molecular docking studies were performed in the UDP-GlcNAc active binding site to aid with drug design. Furthermore the prepared thiazolidinethione-based libraries of compounds were fully characterized using spectroscopic and analytical techniques including: IR, ^{1}H and ^{13}C NMR spectroscopy. LC-MS was employed to determine the accurate masses of the novel compounds. The inhibition studies of the thiazolidinethione-based derivatives are reported in chapter 5 and chapter 6 respectively.

3.7 Experimental

3.7.1 General procedure for the synthesis of thiazolidinethione derivatives (MJ1A - MJ12A and MJ1B - MJ12B)

To a solution of either rhodanine or rhodanine-3-acetic acid and anhydrous sodium acetate (4 equiv.) in glacial acetic acid was added to the respective aldehydes (4 equiv.) (2,4- dichlorobenzaldehyde, 2-bromobenzaldehyde, 4-*tert*-butylbenzaldehyde, 5-chlorosalicylaldehyde, vanillin, *O*-vanillin, 3-*tert*-butyl-2-hydrobenzaldehyde, 4-hydrobenzaldehyde, 4-methoxybenzaldehyde, 2,4,6-trihydroxybenzaldehyde, benzaldehyde and salicaldehyde). The mixture was heated at 100 °C and allowed to stir under reflux overnight. Immediately after cooling, the solution was added to ice-cold water and the resulting precipitate was filtered, washed with water, followed by *n*-hexane, dried and purified by column chromatography.

3.7.1.1 (Z)-5-benzylidene-2-thioxothiazolidin-4-one (MJ1A)[24,25]

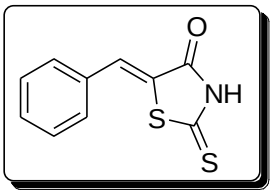

Bright yellow crystal (1.22 g, 92%); R_f 0.4 (EtOAc/Pet ether, 3: 7). M.p. 202 – 203 °C (lit. 205 – 206 °C[16a]); υ_{max} (KBr)/cm^{-1} 3159s υ (NH), 3057s υ (CH), 2848s υ (C=C), 1707s υ (C=O), 1193s υ (C=S) ^{1}H NMR (400 MHz, DMSO-d_6): δ 7.64 (s, 1H, H-7), 7.55 (m, 5H, Ph).^{13}C NMR (101 MHz, DMSO-d_6): δ 196.16, 169.82, 133.45, 132.08, 131.18, 130.91 (2 x C), 129.90 (2 x C), 126.04. EI-MS: $C_{10}H_7NOS_2$ found: *m/z* 220.9961[M-H]$^+$, calculated 220.9969.

3.7.1.2 2-((Z)-5-Benzylidene-4-oxo-2-thioxothiazolidin-3-yl) acetic acid (MJ1B)

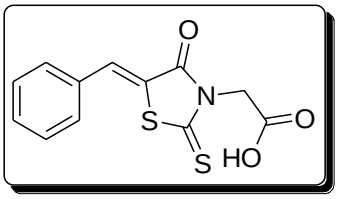

Bright yellow crystal (1.11 g, 95%) R_f 0.4 (EtOAc/Pet ether, 3: 7). M.p 118 – 120 °C (lit. 254 – 256 °C), υ_{max} (KBr)/cm^{-1} 1739s υ (C=O), 1730s υ (C=O), 1190s υ

(C=S) ^{1}H NMR (400 MHz, DMSO-d$_6$): δ 13.17 (s, 1H, OH), 7.64 (s, 1H, H-7), 7.55 (m, 5H, Ph), 4.57 (s, 2H, C*H*$_2$).^{13}C NMR (101 MHz, DMSO-d$_6$): δ 203.27, 174.19, 167.74, 134.43, 133.28, 131.21, 130.02, 129.71 (2C), 129.00 (2C), 45.39. HRMS (ESI): *m/z* $C_{12}H_9NO_3S_2$ found: 279.0024 $[M-H]^+$, calculated 279.0024.

3.7.1.3 (Z)-5-(2-hydroxybenzylidene)-2-thioxothiazolidin-4-one (MJ2A)

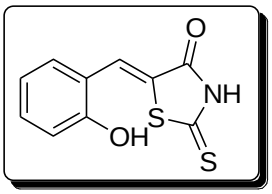

Bright yellow crystal (1.10 g, 95%) R$_f$ 0.4 (EtOAc/Pet ether, 3: 7). M.p (221-224 °C) ^{1}H NMR (400 MHz, DMSO) δ 7.88 (s, 1H, H-7), 7.78 (dd, *J* = 7.7, 0.8 Hz, 1H), 7.58 – 7.51 (m, 2H), 7.46 – 7.36 (m, 1H). ^{13}C NMR (101 MHz, DMSO) δ 193.57, 167.61, 166.46, 134.26, 133.02, 131.73, 130.13, 129.35, 125.97, 45.60. HRMS (ESI): *m/z* $C_{10}H_7NO_2S_2$ found: 236.9910 $[M-H]^+$, calculated 236.9918.

3.7.1.4 2-((Z)-5-(2-hydroxybenzylidine)-4-oxo-2-thioxothiazolidin-3-yl)acetic acid (MJ2B)

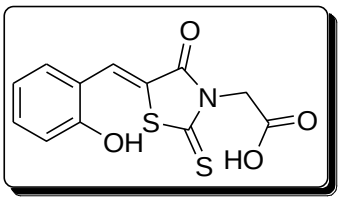

Bright yellow crystal (1.34 g, 95%); R$_f$ 0.4 (EtOAc/Pet ether, 3: 7). M.p (221-224 °C) ^{1}H NMR (400 MHz, DMSO) δ 7.88 (s, 1H, H-7), 7.78 (dd, *J* = 7.7, 0.8 Hz, 1H), 7.58 – 7.51 (m, 2H), 7.46 – 7.36 (m, 1H), 4.69 (s, 2H, CH$_2$). ^{13}C NMR (101 MHz, DMSO) δ 193.57, 167.61, 166.46, 134.26, 133.02, 131.73, 130.13, 129.35, 125.97, 45.60. HRMS (ESI): *m/z* $C_{12}H_9NO_4S_2$ found: 294.9969 $[M]^+$, calculated 294.9973.

3.7.1.5 (Z)-5-(2,4-dichlorobenzylidene)-2-thioxothiazolidin-4-one (MJ3A)

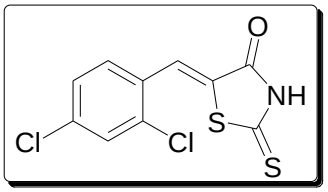

Bright yellow crystal (1.40 g, 94%); R$_f$ 0.4 (EtOAc/Pet ether, 3: 7). M.p. 181 – 183 °C. ^{1}H NMR (400 MHz,

DMSO-d_6): δ 7.70 (s, 1H, H-7), 7.11 – 7.26 (m, 3H, H-3, H-5, H-6). ^{13}C NMR (101 MHz, DMSO-d_6): δ 194.59, 172.03, 138.03, 136.99, 133.74, 133.42, 132.69, 131.61, 131.39, 129.70. HRMS (ESI): *m/z* $C_{10}H_5Cl_2NOS_2$ found: 288.9190 $[M+H]^+$, calculated 288.9190 $[M+H]^+$.

3.7.1.6 2-((Z)-5-(2,4-dichlorobenzylidene)-4-oxo-2-thioxothiazolidin-3-yl)acetic acid (MJ3B)

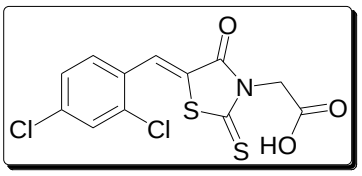

Bright yellow crystal (1.50 g, 90%); R_f 0.4 (EtOAc/Pet ether, 3: 7). M.p (209-213 °C) ^{1}H NMR (400 MHz, DMSO-d_6): δ 7.74 (s, 1H, H-7), 7.23 - 6.91 (m, 3H, Ph), 4.37 (s, 2H, CH_2). ^{13}C NMR (101 MHz, DMSO-d_6) δ 192.98, 166.91, 166.19, 154.22, 133.52, 130.52, 130.36, 126.24, 120.77, 45.01. HRMS (ESI): *m/z* $C_{12}H_7Cl_2NO_3S_2$ found: 346.9238 $[M]^+$, calculated 346.9244.

3.7.1.7 (Z)-5-(2-bromobenzylidene)-2-thioxothiazolidin-4-one (MJ4A)

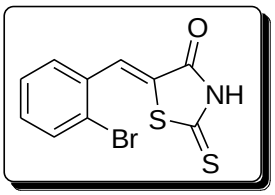

Bright yellow crystal (1.63 g, 92%); R_f 0.4 (EtOAc/Pet ether, 3: 7). M.p. 213 – 215 °C, ^{1}H NMR (400 MHz, DMSO-d_6): δ 7.70 (s, 1H, H-7), 7.40 (m, 1H, H-3), 7.18 – 7.14 (m, 2H, H-5, H-6), 7.01 (m, 1H, H-4). ^{13}C NMR (101 MHz, DMSO-d_6): δ 193.44, 169.28, 142.33, 132.69, 132.41, 129.59, 129.34, 129.09, 129.01, 125.88. HRMS (ESI): *m/z* $C_{10}H_6BrNOS_2$ found: 298.9069 $[M+H]^+$, calculated 298.9074 $[M+H]^+$.

3.7.1.8 2-((Z)-5-(2-bromobenzylidene)-4-oxo-2-thioxothiazolidin-3-yl)acetic acid (MJ4B)

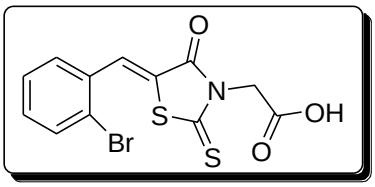

Bright yellow crystal (1.63 g, 93%); R_f 0.4 (EtOAc/Pet ether, 3: 7). M.p. 244 – 247 °C, ^{1}H NMR

(400 MHz, DMSO-d_6): δ 7.74 (s, 1H, H-7), 7.40 (m, 1H, H-3), 7.18 – 7.14 (m, 2H, H-5, H-6), 6.95-6.88 (m, 1H, H-4), 4.37 (s, 2H, C*H*$_2$). ^{13}C NMR (101 MHz, DMSO-d_6): δ 193.90, 167.25, 158.43, 132.49, 132.41, 129.59, 129.34, 129.09, 129.01, 128.80, 125.88, 48.08. HRMS (ESI): *m/z* $C_{12}H_8BrNO_3S_2$ found: 356.9122 $[M+H]^+$, calculated 356.9129 $[M+H]^+$.

3.7.1.9 (Z)-5-(4-*tert*-Butylbenzylidene)-2-thioxothiazolidin-4-one (MJ5A)

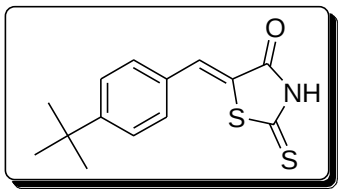

Bright yellow crystal (1.60 g, 93%); R_f 0.4 (EtOAc/Pet ether, 3: 7); m.p. 149 – 152 °C; υ_{max} (KBr)/cm^{-1} 3170s υ (NH), 3076s υ (CH), 2953s υ (C=C), 1701s υ (C=O), 1223s υ (C=S) ^{1}H NMR (300 MHz, DMSO-d_6): δ 7.60 (s, 1H, H-7), 7.56 (m, 2H, H-2, H-6), 7.52 (m, 2H, H-3, H-5), 1.30 (s, 9H, (C*H*$_3$)3. ^{13}C NMR (75 MHz, DMSO-d_6): δ 195.44, 176.32, 169.20, 153.78, 131.38, 130.15 (2C), 126.11 (2C), 124.35, 34.52, 30.60. HRMS (ESI): *m/z* $C_{14}H_{15}NOS_2$ found: 278.0673 $[M+H]^+$, calculated 278.0664 $[M+H]^+$.

3.7.1.10 2-((Z)-5-(4-*tert*-Butylbenzylidene)-4-oxo-2-thioxothiazolidin-3-yl) acetic acid (MJ5B)

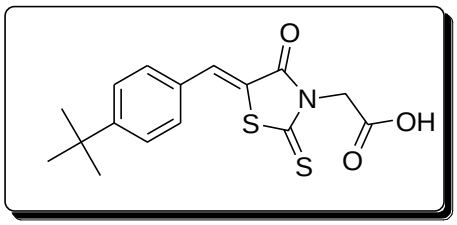

Bright yellow crystal (1.34 g, 95%); R_f 0.4 (EtOAc/Pet ether, 3: 7). M.p 201 – 202 °C, υ_{max} (KBr)/cm^{-1} 1727s υ (C=O), 1208s υ (C=S) ^{1}H NMR (300 MHz, DMSO-d_6): δ 9.98 (s, 1H, O*H*), 7.60 (s, 1H, H-7), 7.56 (m, 2H, H-2, H-6), 7.52 (m, 2H, H-3, H-5), 4.75 (s, 2H, C*H*$_2$), 1.31 (s, 9H, (C*H*$_3$)3. ^{13}C NMR (101 MHz, DMSO-d_6): δ 193.71, 167.70, 154.98, 134.37, 131.24 (2C), 130.63, 129.89, 126.93(2C), 126.44, 45.51, 35.34, 31.22

(3C). HRMS (ESI): *m/z* $C_{16}H_{17}NO_3S_2$ found: 336.0744 $[M+H]^+$, calculated 336.0728 $[M+H]^+$.

3.7.1.11 (Z)-5-(5-chloro-2-hydroxybenzylidene)-2-thioxothiazolidin-4-one (MJ6A)

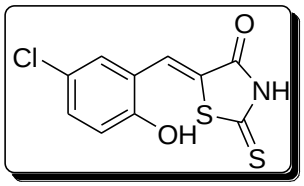

Bright yellow crystal (1.30 g, 97%); R_f 0.4 (EtOAc/Pet ether, 3: 7). M.p. 220 – 223 °C; ^{1}H NMR (400 MHz, DMSO-d_6): δ 7.73 (s, 1H), 7.12 – 6.68 (m, 3H, H-3, H-4, H-6). ^{13}C NMR (101 MHz, DMSO-d_6): δ 194.40, 173.42, 167.54, 154.61, 143.32, 130.02, 129.01, 128.36, 127.21, 126.43. HRMS (ESI): *m/z* $C_{10}H_6ClNO_2S_2$ found: 270.9521 $[M-H]^+$, calculated 270.9528 $[M-H]^+$.

3.7.1.12 2-((Z)-5-(5-chloro-2-hydroxybenzylidene)-4-oxo-2-thioxothiazolidin-3-yl)acetic acid (MJ6B)

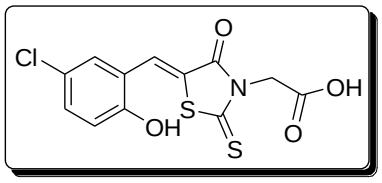

Bright yellow crystal (1.34 g, 98%); R_f 0.4 (EtOAc/Pet ether, 3: 7). M.p. 252 – 254 °C; ^{1}H NMR (400 MHz, DMSO-d_6): δ 7.94 (s, 1H, H-7), 6.92 – 6.49 (m, 3H, Ph), 4.30 (s, 2H, CH_2). ^{13}C NMR (101 MHz, DMSO-d_6): δ 192.73, 174.20, 166,74, 155.43, 137.90, 130.01, 128.91, 127.68, 119.20, 119.18, 116.30, 46.27. HRMS (ESI): *m/z* $C_{12}H_8ClNO_4S_2$ found: 328.9583 $[M-H]^+$, calculated 328.9583 $[M-H]^+$.

3.7.1.13 (Z)-5-(4-Hydroxy-3-methoxybenzylidene)-2-thioxothiazolidin-4-one (MJ7A)

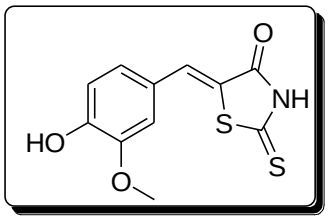

Bright yellow crystal (1.43 g, 89%); R_f 0.4 (EtOAc/Pet ether, 3: 7). M.p. 223 – 224 °C (lit. 230 – 231 °C); υ_{max}

(KBr)/cm^{-1} 3348s υ (NH), 3260s υ (OH); 1715s υ (C=O), 1155s υ (C=s) ^{1}H NMR (300 MHz, DMSO-d$_6$): δ 9.93 (s, 1H, N*H*), 7.56 (s, 1H, H-7), 7.14 (d, *J* = 2.1 Hz, 1H, H-5), 7.08 (m, 1H, H-6), 6.94 (d, *J* = 8.2 Hz, 1H, H-2), 3.84 (s, 3H, OC*H*$_3$).^{13}C NMR (75 MHz, DMSO-d$_6$): δ 195.26, 169.23, 149.84, 148.03, 132.49, 124.91, 124.31, 121.14, 116.26, 114.36, 55.61. HRMS (ESI): *m/z* $C_{11}H_9NO_3S_2$ found: 268.0108 $[M+H]^+$, calculated 268.0102 $[M+H]^+$.

3.7.1.14 2-((Z)-5-(4-Hydroxy-3-methoxybenzylidene)-4-oxo-2-thioxothiazolidin-3-yl) acetic acid (MJ7B)

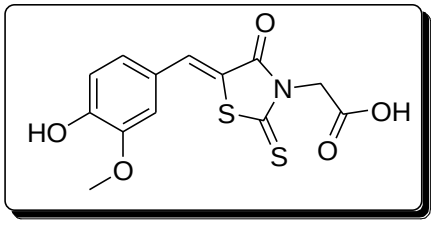

Bright yellow crystal (1.31 g, 96%); R$_f$ 0.4 (EtOAc/Pet ether, 3: 7). M.p. 255 – 256 °C; υ$_{max}$ (KBr)/cm^{-1} 3351s υ (OH), 1737s υ (C=O),1698s υ (C=O), 1182s υ (C=S) ^{1}H NMR (400 MHz, DMSO-d$_6$): δ 10.19 (s, 1H, O*H*), 9.78 (s, 1H), 7.81 (s, 1H, H-7), 7.44 – 7.39 (m, 2H), 7.24 – 7.16 (m, 2H), 6.99 – 6.93 (m, 2H), 4.75 (s, 2H, C*H*$_2$), 3.86 (s, 3H, OC*H*$_3$).^{13}C NMR (101 MHz, DMSO-d$_6$): δ 191.41, 167.76, 151.02, 135.42, 126.46, 125.98, 124.81, 116.95, 115.88, 115.26, 111.29, 56.15, 45.45. HRMS (ESI): *m/z* $C_{13}H_{11}NO_5S_2$ found: 326.0184 $[M+H]^+$, calculated 326.0157 $[M+H]^+$.

3.7.1.15 (Z)-5-(2-Hydroxy-3-methoxybenzylidene)-2-thioxothiazolidin-4-one (MJ8A)

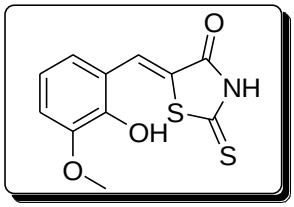

Bright yellow crystal (1.45 g, 90%); R$_f$ 0.4 (EtOAc/Pet ether, 3: 7). M.p. 249 – 251 °C; υ$_{max}$ (KBr)/cm^{-1} 3312s υ (NH), 3145s υ (OH), 3054s υ (CH), 2851s υ (C=C),1707s υ (C=O), 1210s υ (C=S); ^{1}H NMR (300 MHz, DMSO-d$_6$): δ 9.72 (s, 1H, N*H*), 7.87 (s, 1H, H-7), 7.10 (m, 1H, H-6), 6.94 – 6.88 (m, 2H, H-4, H-5), 3.85 (s, 3H, OC*H*$_3$).^{13}C

NMR (75 MHz, DMSO-d_6): δ 195.85, 169.23, 148.01, 146.83, 127.11, 124.22, 120.23, 120.16, 119.61, 114.33, 55.96. HRMS (ESI): $C_{11}H_9NO_3S_2$ found: *m/z* 268.0102 $[M+H]^+$, calculated 268.0185 $[M+H]^+$.

3.7.1.16 2-((Z)-5-(2-Hydroxy-3-methoxybenzylidene)-4-oxo-2-thioxothiazolidin-3-yl) acetic acid (MJ8B)

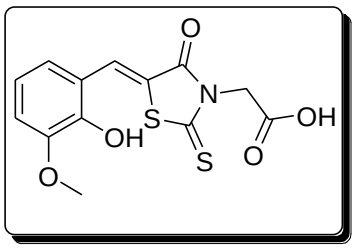

Bright yellow crystal (1.34 g, 98%); R_f 0.4 (EtOAc/Pet ether, 3: 7). M.p. 249 – 251 °C; υ_{max} (KBr)/cm^{-1}1725s υ (C=O), 1219s υ (C=S) ^{1}H NMR (400 MHz, DMSO-d_6): δ 8.07 (s, 1H, H-7), 7.15 (dd, *J* = 7.7, 1.7 Hz, 1H, H-4), 7.02 – 6.91 (m, 2H, H-5, H-6), 4.74 (s, 2H, C*H*$_2$), 3.86 (s, 3H, OC*H*$_3$).^{13}C NMR (101 MHz, DMSO-d_6): δ 194.23, 167.76, 167.00, 148.64, 147.65, 130.11, 121.27, 121.18, 120.55, 120.41, 115.36, 56.57, 45.46. HRMS (ESI): *m/z* $C_{13}H_{11}NO_5S_2$ found: 326.0293 $[M+H]^+$, calculated 326.0157 $[M+H]^+$.

3.7.1.17 (Z)-5-(3-*tert*-Butyl-2-hydroxybenzylidene)-2-thioxothiazolidin-4-one (MJ9A)

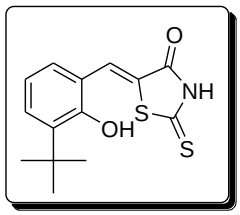

Bright yellow crystal (1.59 g, 90%); R_f 0.4 (EtOAc/Pet ether, 3: 7). M.p. 148 – 150 °C; υ_{max} (KBr)/cm^{-1} 3172s υ (NH), 3087s υ (OH), 2865s υ (C=C), 1712s υ (C=O), 1191s υ (C=S) ^{1}H NMR (400 MHz, DMSO-d_6): δ 13.12 (s, 1H, N*H*), 11.83 (s, 1H, O*H*), 9.97 (s, 1H, H-7), 7.65 (dd, *J* = 7.6, 1.7 Hz, 1H, H-4), 7.57 (dd, *J* = 7.7, 1.6 Hz, 1H, H-6), 7.08 – 6.98 (m, 1H, H-5), 1.38 (s, 9H, (C*H*$_3$)3. ^{13}C NMR (101 MHz, DMSO-d_6): δ 205.72, 199.18, 177.10, 160.41, 137.55, 134.42, 132.96, 124.71 121.18, 120.01, 34.87, 29.80 (3C). HRMS (ESI): *m/z* $C_{14}H_{15}NO_2S_2$ found: 293.0548$[M+H]^+$, calculated 293.0544.

3.7.1.18 2-((Z)-5-(3-*tert*-Butyl-2-hydroxybenzylidene)-4-oxo-2-thioxothiazolidin-3-yl)acetic acid (MJ9B)

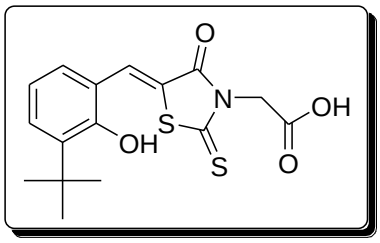

Bright yellow crystal (1.29 g, 94%); R_f 0.4 (EtOAc/Pet ether, 3: 7). M.p. 231 – 233 °C; ^{1}H NMR (400 MHz, DMSO-d$_6$): δ 11.84 (s, 1H, O*H*), 7.74 (s, 1H, H-7), 7.67 (dd, *J* = 7.6, 1.7 Hz, H-4), 7.58 (dd, *J* = 7.7, 1.6 Hz, H-6), 7.12 – 6.92 (m, 1H, H-5), 4.70 (s, 2H, C*H*$_2$), 1.38 (s, 9H, C*H*$_3$)3. ^{13}C NMR (101 MHz, DMSO-d$_6$): δ 193.44, 167.73, 166.90, 162.24, 134.56, 133.55, 132.96, 125,71, 121.18, 120.01, 118.92, 115.70, 34.89, 29.83 (3C). HRMS (ESI): *m/z* $C_{16}H_{17}NO_4S_2$ found: 351.0589 $[M+H]^+$, calculated 351.0599.

3.7.1.19 (Z)-5-(4-hydroxybenzylidene)-2-thioxothiazolidin-4-one (MJ10A)

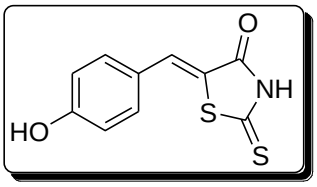

Bright yellow crystal (1.50 g, 90%); R_f 0.4 (EtOAc/Pet ether, 3: 7). M.p. 184-185 °C; ^{1}H NMR (300 MHz, DMSO-d$_6$): δ = 7.57 (s, 1H, H-7), 7.53 (d, *J* = 8.7 Hz, 2H, H-2 and H-6), 7.03 (d, *J* = 8.7 Hz, 2H, H-3 and H-5). ^{13}C NMR (75 MHz, DMSO-d$_6$): δ = 195.67, 169.72, 160.28, 132.90, 132.26, 123.92 (2C), 121.14, 116.44 (2C). HRMS (ESI): *m/z* $C_{10}H_7NO_2S_2$ found: 236.9910 $[M-H]^+$, calculated 236.9918.

3.7.1.20 2-((Z-5-(4-hydoxybenzylidene)-4-oxo-2-thioxothiazolidin-3-yl)acetic acid (MJ10B)

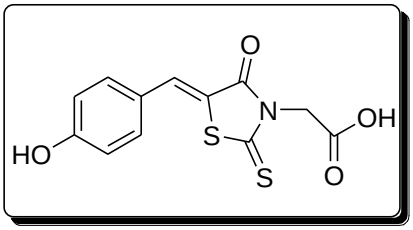

Bright yellow crystal (1.50 g, 90%); R_f 0.4 (EtOAc/Pet ether, 3: 7). M.p. >300 °C; ^{1}H NMR (300 MHz, DMSO-d$_6$): δ = 7.57 (s, 1H, H-7), 7.53 (d, *J* = 8.7 Hz, 2H, H-2 and H-6), 7.03 (d, *J* = 8.7 Hz, 2H, H-3 and H-5), 4.72 (s, 2H, C*H*$_2$). ^{13}C NMR (75 MHz, DMSO-d$_6$): δ = 192.67,

173.72, 166.28, 156.90, 142.26, 123.92, 121.14, 116.44, 45.62. HRMS (ESI): *m/z* $C_{12}H_9NO_4S_2$ found: 294.9973 $[M]^+$, calculated 294.9973.

3.7.1.21 (Z)-5-(4-Methoxybenzylidene)-2-thioxothiazolidin-4-one (MJ11A)

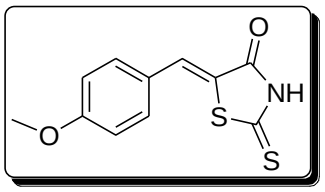

Bright yellow crystal (1.38 g, 91%); R_f 0.4 (EtOAc/Pet ether, 3: 7). M.p. 254 – 255 °C (lit.[16b] 260-261 °C); υ_{max} (KBr)/cm^{-1} 3014s υ (NH), 1683s υ (C=O), 1165s υ (C=S);.^{1}H NMR (400 MHz, DMSO-d_6): δ 7.60 (s, 1H, H-7), 7.59 – 7.54 (m, 2H, H-3, H-5), 7.14 – 7.08 (m, 2H, H-2, H-6), 3.84 (s, 3H, OC*H*$_3$).^{13}C NMR (101 MHz, DMSO-d_6): δ 195.97, 169.90, 161.83, 133.12 (2C), 132.32, 125.98, 122.77, 115.57 (2C), 56.03. HRMS (ESI): *m/z* $C_{11}H_9NO_2S_2$ found: 252.0134 $[M+H]^+$, calculated 252.0153 $[M+H]^+$.

3.7.1.22 2-((Z)-5-(4-Methoxybenzylidene)-4-oxo-2-thioxothiazolidin-3-yl) acetic acid (MJ11B)

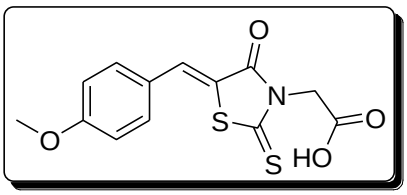

Bright yellow crystal (1.26 g, 97%); R_f 0.4 (EtOAc/Pet ether, 3: 7). M.p. 136 – 138 °C (lit. 250 – 253 °C); υ_{max} (KBr)/cm^{-1} 1742s υ (C=O), 1732s υ (C=O), 1976s υ (C=S); ^{1}H NMR (400 MHz, DMSO-d_6): δ 7.82 (s, 1H, H-7), 7.61 (m, 2H, H-3, H-5), 7.10 (m, 2H, H-2, H-6), 4.70 (s, 2H, C*H*$_2$), 3.82 (s, 3H, OC*H*$_3$).^{13}C NMR (101 MHz, DMSO-d_6): δ 203.27, 174.19, 167.74, 134.62, 133.56 (2C), 119.85, 115.72 (2C), 45.28, 36.42. HRMS (ESI): *m/z* $C_{13}H_{11}NO_4S_2$ found: 310.0201 $[M+H]^+$, calculated 310.0208 $[M+H]^+$.

3.7.1.23 (Z)-5-(2,4,6-tryhydroxybenzylidene)-2-thioxothiazolidin-one (MJ12A)

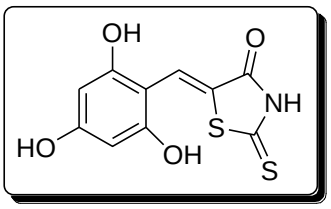

Bright yellow crystal (1.10 g, 96%); R_f 0.4 (EtOAc/Pet ether, 3: 7). M.p. 159 - 161 °C; ^{1}H NMR (400 MHz, DMSO-d_6): δ = 7.73 (s, 1H, H-7), 5.91 (s, 2H, H-3, H-5). ^{13}C NMR (101 MHz, DMSO-d_6): δ 194.37, 168.10, 167.77, 161.12, 133.25, 130.47, 118.19, 117.92. HRMS (ESI): *m/z* $C_{10}H_7NO_4S_2$ found: 326.9862 $[M+H]^+$, calculated 326.9871 $[M+H]^+$.

3.7.1.24 2-((Z)-5-(2,4,6-tryhydroxybenzylidene)-4-oxo-2-thioxothiazolidin-3-yl)acetic acid (MJ12B)

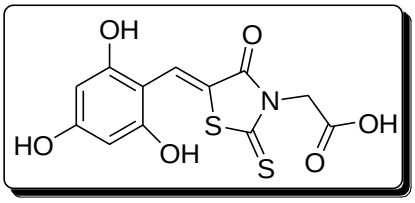

Bright yellow crystal (1.12 g, 95%); R_f 0.4 (EtOAc/Pet ether, 3: 7). M.p. 228 - 231 °C; ^{1}H NMR (400 MHz, DMSO-d_6): δ = 7.74 (s, 1H, H-7), 5.90 (s, 2H, H-3, H-5), 4.72 (s, 2H, C*H*$_2$). ^{13}C NMR (101 MHz, DMSO-d_6): δ 194.40, 168.08, 167.75, 161.10, 160.06, 133.25, 130.47, 118.19, 117.92, 48.47. HRMS (ESI): *m/z* $C_{12}H_9NO_6S_2$ found: 268.9809 $[M+H]^+$, calculated 268.9816 $[M+H]^+$.

3.7.2 General procedure for the synthesis of propargylated thiazolidinethiones (MJ029 series)

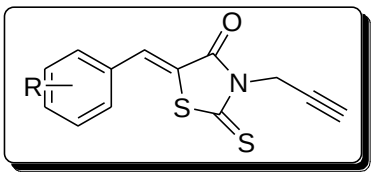

To a solution of 2-thioxothiazolidin-4-one (100 mg) in DMF (2 mL) was added 1.5 equivalents of K_2CO_3 and propargyl bromide respectively. The reaction mixture was allowed to stir at room temperature overnight. The reaction progress was monitored on TLC (EtOAc/Pet ether, 3: 7) and upon completion the DMF was co-evaporated with toluene several times. The remaining residue was purified by

chromatography using a silica-gel column (EtOAc/Pet Ether, 3: 7) giving bright yellow compounds in low yields.

3.7.2.1 (Z)-5-Benzylidene-3-(prop-2-ynyl)-2-thioxothiazolidin-4-one (MJ029-1)

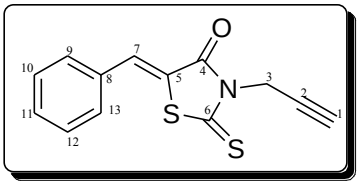

Bright yellow powder (0.0404 g, 23%). M.p (115-117 °C) ^{1}H NMR (300 MHz, $CDCl_3$): δ 8.06 (s, 1H, H-7), 7.63 – 7.18 (m, 5H, Ph), 4.78 (d, *J* = 2.5 Hz, 2H, H-3$_a$, H-3$_b$), 2.53 (t, *J* = 2.5 Hz, 1H, H-1).^{13}C NMR (75 MHz, $CDCl_3$): δ 191.96, 166.38, 165.10, 137.30, 137.00, 130.61, 130.18, 129.87, 128.61, 127.90, 125.92, 53.38, 44.62.

3.7.2.2 (Z)-5-(2-Hydroxybenzylidene)-3-(prop-2-ynyl)-2-thioxothiazolidin-4-one (MJ029-2)

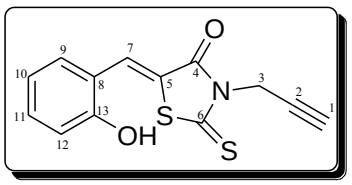

Bright yellow powder (0.0323 g, 25%). M.p (133-134 °C) ^{1}H NMR (300 MHz, $CDCl_3$): δ 8.10 (s, 1H, H-7), 7.70 (d, *J* = 8.0 Hz, 1H, Ph), 7.53 – 7.39 (m, 2H, Ph), 7.34 – 7.23 (m, 1H, Ph), 4.78 (d, *J* = 2.5 Hz, 2H, H-3$_a$, H-3$_b$), 2.53 (t, *J* = 2.4 Hz, 1H, H-1), 1.56 (s, 1H, O*H*).^{13}C NMR (75 MHz, $CDCl_3$): δ 192.64, 166.36, 165.16, 133.95, 133.39, 132.67, 131.83, 129.36, 128.03, 126.65, 125.67, 53.35, 44.58.

3.7.2.3 (Z)-5-(2,4-Dichlorobenzylidene)-3-(prop-2-ynyl)-2-thioxothiazolidin-4-one (MJ029-3)

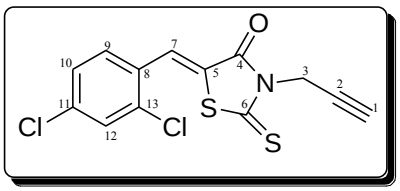

Bright yellow powder (0.0650 g, 38%). M.p (86-87 °C) ^{1}H NMR (300 MHz, $CDCl_3$): δ 7.78 (s, 1H, H-7), 7.56 – 7.42 (m, 3H, Ph), 4.78 (d, *J* = 2.5 Hz, 2H, H-3$_a$, H-3$_b$), 2.52 (t, *J* = 2.5 Hz, 1H, H-1).^{13}C NMR (101 MHz, $CDCl_3$): δ 192.98, 167.08, 165.29, 155.04, 134.28, 130.74, 130.42, 126.46, 121.45, 75.78, 53.27, 44.58, 31.11.

3.7.2.4 (Z)-5-(4-*tert*-Butyl-2-chlorobenzylidene)-3-(prop-2-ynyl)-2-thioxothiazolidin-4-one (MJ029-5)

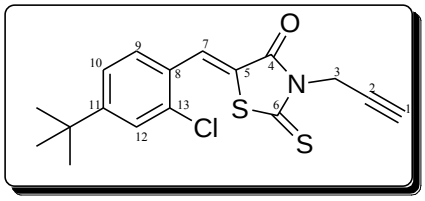

Bright yellow powder (0.0556 g, 33%). M.p (105-107 °C) ^{1}H NMR (300 MHz, $CDCl_3$): δ 7.74 (s, 1H, H-7), 7.26 (s, 1H, Ph), 7.15 – 7.13 (m, 2H, Ph), 3.95 (d, *J* = 2.5 Hz, 2H, H-3$_a$, H-3$_b$), 2.54 (t, *J* = 2.4 Hz, 1H, H-1), 1.26 (s, 9H, 3 x C*H*$_3$). ^{13}C NMR (101 MHz, CDCl3): δ 193.03, 167.02, 151.09, 139.48, 130.11, 130.13, 128.34, 124.39, 122.98, 117.03, 76.12, 53.88, 31.49, 31.37 (3 x C).

3.7.2.5 (Z)-5-(4-Methoxybenzylidene)-3-(prop-2-ynyl)-2-thioxothiazolidin-4-one (MJ029-11)

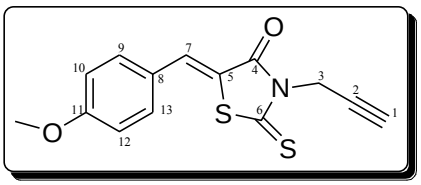

Bright yellow powder (0.0501 g, 29%). M.p (130-132 °C) ^{1}H NMR (300 MHz, $CDCl_3$): δ 7.79 (s, 1H, H-7), 7.53 – 7.46 (m, 4H, Ph), 4.92 (s, 3H, C*H*$_3$), 4.78 (d, *J* = 2.5 Hz, 2H, H-3$_a$, H-3$_b$), 2.52 (t, *J* = 2.5 Hz, 1H, H-1).^{13}C NMR (101 MHz, $CDCl_3$): δ 192.84, 166.98, 165.23, 134.17, 133.19, 131.00, 130.69 (2C), 129.40 (2C), 122.64, 75.81, 53.30, 44.58.

3.7.3 General procedure for the synthesis of sulfonated thiazolidinethiones (MJ081 series)

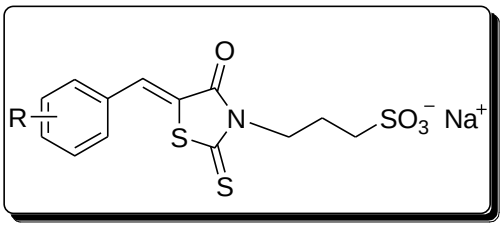

To a solution of 2-thioxothiazolidin-4-one (100 mg) in DMF (2 mL) was added NaH (60%, 30 mg, 0.75 mmol) at low temperature (0 °C). The reaction mixture was allowed to stir for 30 minutes at low temperature (0 °C) before 1,3-propanesultone (1.5 equiv) was added. The reaction mixture was allowed to continue

to stir for an additional 30 minutes at low temperature before the reaction mixture was allowed to attain room temperature overnight. The reaction progress was monitored through TLC (EtOAc/Pet ether, 7:3) and upon the completion the DMF was co-evaporated with toluene. The residue was dissolved in water (5 mL) and was washed in EtOAc (50 mL) several times to remove the unreacted material. The aqueous layer was lyophilized and the product was isolated as yellow crystals in high yields.

3.7.3.1 Sodium 3-((Z)-5-benzylidene-4-oxo-2-thioxothiazolidin-3-yl)propane-1-sulfonate (MJ 081-1)

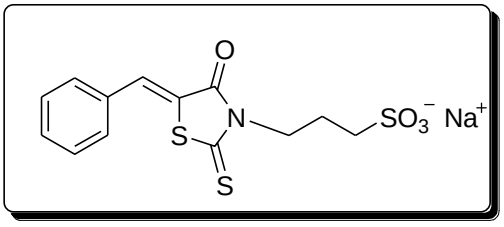

Yellow crystals (0.132 g, 80%). M.p (158-161 °C)^{1}H NMR (400 MHz, D_2O): δ 8.40 (s, 1H, H-7), 7.59 (d, *J* = 7.5 Hz, 2H, H-2, H-6), 7.42 (d, *J* = 7.5 Hz, 2H, H-3, H-5), 7.35 (d, *J* = 8.3 Hz, 1H, H-4), 3.65 (t, *J* = 6.4 Hz, 2H, H-10), 2.66 (t, *J* = 7.2 Hz, 1H, H-8). 1.98 - 1.88 (m, 2H, H-9). ^{13}C NMR (101 MHz, DMSO-d_6): δ 192.19, 166.24, 141.39, 135.21, 128.69, 128.02, 126.39, 114.95, 49.38, 41.76, 23.04.

3.7.3.2 Sodium 3-((Z)-5-(4-tert-butylbenzylidene)-4-oxo-2-thioxothiazolidin-3-yl)propane-1-sulfonate (MJ081-5)

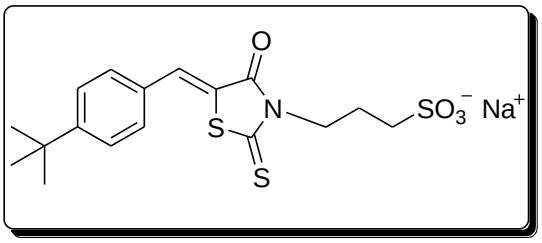

Yellow crystals (0.123 g, 81%). M.p (114-118 °C) ^{1}H NMR (400 MHz, DMSO-d_6): δ 7.69 (s, 1H, H-7), 7.56 (m, 2H, H-2, H-6), 6.96 (m, 2H, H-3, H-5), 4.08 (t, *J* = 7.3 Hz, 2H, H-10), 3.44 (t, *J* = 6.4 Hz, 2H, H-8), 2.03 – 1.92 (m, 2H, H-9), 1.30 (s, 9H, (C*H*$_3$)3. ^{13}C NMR (101 MHz, DMSO-d_6): δ ^{13}C NMR (101 MHz,

$CDCl_3$): δ 192.21, 166.32, 149.18, 142.03, 132.14, 126.04, 124.90, 116.06, 49.43, 41.73, 40.69, 31.39, 21.96.

3.7.3.3 Sodium 3-((Z)-5-(2-hydroxy-3-methoxybenzylidene)-4-oxo-2-thioxothiazolidin-3-yl)propane-1-sulfonate (MJ 081-8)

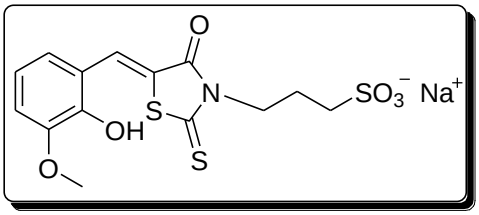

Yellow crystals (0.128 g, 83%). M.p (269-272 °C) ^{1}H NMR (400 MHz, DMSO-d_6): δ 7.79 (s, 1H, H-7), 7.63 (d, *J* = 8.8 Hz, 2H), 7.13 (d, *J* = 8.8 Hz, 2H), 4.10 (t, *J* = 7.3 Hz, 2H, H-10), 3.85 (s, 3H, OC*H*$_3$), 2.51 – 2.50 (t, *J* = 7.3, 2H, H-8), 2.08 – 1.87 (m, 2H, H-9). ^{13}C NMR (101 MHz, DMSO-d_6): δ 192.34, 166.29, 151.28, 147.28, 142.20, 122.32, 119.96, 117.92, 115.88, 114.94, 56.21, 49.45, 42.33, 21.65.

3.7.3.4 Sodium 3-((Z)-5-(4-methoxybenzylidene)-4-oxo-2-thioxothiazolidin-3-yl)propane-1-sulfonate (MJ081-11)

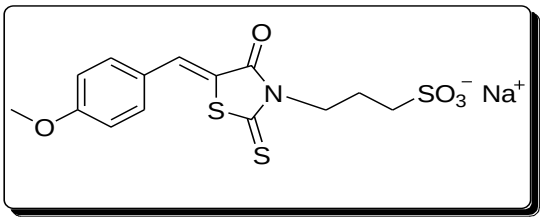

Yellow crystals (0.134 g, 85%). M.p (324-327 °C) ^{1}H NMR (400 MHz, DMSO-d_6): δ 7.81 (s, 1H, H-7), 7.60 (m, 2H, H-3, H-5), 7.64 – 7.47 (m, 2H, H-2, H-6), 4.10 (t, *J* = 7.3 Hz, 2H, H-10), 3.83 (s, 3H, OC*H*$_3$), 2.50 (t, *J* = 7.0 Hz, 2H, H-8), 1.98 (m, 2H, H-9). ^{13}C NMR (101 MHz, DMSO-d_6): δ 192.21, 166.22, 160.01, 142.78, 127.54, 127.45, 116.11, 114.17, 56.02, 49.43, 42.60, 21.02.

3.8 References:

1. **B-Rao, C., Subramanian, J. and Sharma, S. D. 2009.** Managing protein flexibility in docking and its applications. *Drug Discovery Today*. **14**: 394-400.
2. **Krovat, E. M., Steindl, T. and Langer, T. 2005.** Recent advances in docking and scoring. *Current Computer Aided-drug Design*. **1**(1): 93-102.
3. **Joseph-McCarthy, D., Baber, J. C., Feyfant, E., Thompson, D. C. and Humblet, C. 2007.** Lead optimization via high-throughput molecular docking. *Current Opinion in Drug Discovery and Development*. **10**(3): 264-274.
4. **Orry, A. J. W., Abagyan, R. A. and Cavasotto, C. N. 2006.** Structure-based development of target-specific compound libraries. *Drug Discovery Today*. **11**: 261-266.
5. **Khan, F., Yadav, D. K., Maurya, A. and Srivastava, S. K. 2012.** Modern methods and web resources in drug design and discovery. *Letters in Drug Design and Discovery*. **8**(5): 469-490.
6. **Helm, J. S., Hu, Y., Chen, L., Gross, B. and Walker, S. 2003.** Identification of active-site inhibitors of MurG using a generalizable, high-throughput glycosyltransferase screen. *Journal of the American Chemical Society*. **125**: 11168-11169.
7. (a). **Vetting, M. W., Frantom, P. A. and Blanchard, J. S. 2008.** Structural and enzymatic analyses of MshA from *Corynebacterium glutamicum*: Substrate-assisted catalysis. *Journal of Biochemistry and Molecular Biology*. **283**(23): 15834-15844. (b). **Vilchèze, C., Av-Gay, Y., Attarian, R., Liu, Z., Hazbón, M. H., Colangeli, R., Chen, B., Liu, W., Alland, D., Sacchettini, J. C. and Jacobs Jr. R. W. 2008.** Mycothiol biosynthesis is essential for

ethionamide susceptibility in *Mycobacterium tuberculosis*. *Molecluar Microbiology*. **69**(5): 1316-1329. (c). **Newton, G. L., Koledin, T., Gorovitz, B., Rawat, M., Fahey, R. C. and Av-Gay, Y. 2003.** The glycosyltransferase gene encoding the enzyme catalyzing the first step of mycothiol biosynthesis (*mshA*). *Journal of Bacteriology*. **185**: 3476-3479.

8. **Hu, Y., Helm, J. S., Chen, L., Ginsberg, C., Gross, B., Kraybill, B., Tiyanont, K., Fang, X., Wu, T. and Walker, S. 2004.** Identification of selective inhibitors for the glycosyltransferase MurG *via* high-throughput screening. *Chemistry and Biology*. **11**: 703–711.
9. **Carlson, E. E., May, J. F. and Kiessling, L. L. 2006.** Chemical probes of UDP-Galactopyranose Mutase. *Chemistry and Biology*. **13**: 825–837.
10. **Soltero-Higgin, M., Carlson, E. E., Phillips, J. H. and Kiessling, L. L. 2004.** Identification of Inhibitors for UDP-Galactopyranose Mutase. *Journal of the American Chemical Society*. **126:** 10532-10533.
11. **Singh, G. S. and Mmolotsi, B. J. 2005.** Synthesis of 2-azetidinones from 2-diazo-1, 2-diaryl ethanones and *N*-(2-thienylidene) imines as possible antimicrobial agents. *Farmaco*. **60**(9): 727-730.
12. **Rahman, V. P. M., Mukhtar, S., Ansari, W. H. and Lemiere, G. 2005.** Synthesis, stereochemistry and biological activity of some novel long alkyl chain substituted thiazolidin-4-ones and thiazan-4-one from 10-undecenoic acid hydrazide. *European Journal of Medicinal Chemistry*. **40**: 173-184.
13. **Jain, A. K., Vaidya, A., Ravichandran, V., Kashaw, S. K. and Agrawal, R. K. 2012.** Recent developments and biological activities of thiazolidinone derivatives. *Bioorganic and Medicinal Chemistry*. **20**: 3378-3395.

14. **Sim, M. M., Ng, S. B., Buss, A. D., Crasta, S. C., Goh, K. L. and Lee, S. K. 2002.** Benzylidene rhodanines as novel inhibitors of UDP-*N*-acetylmurate/L-alanine ligase. *Bioorganic and Medicinal Chemistry Letters*. **12**(4): 697-699.

15. **Andres, C. J., Bronson, J. J., D'Andrea, S. V., Deshpande, M. S., Falk, P. J., Grant-Young, K. A., Harte, W. E., Ho, H. T., Misco, P. F., Robertson, J. G., Stock, D., Sun, Y. and Walsh, A. W. 2000.** 4-Thiazolidinones: Novel inhibitors of the bacterial enzyme MurB. *Bioorganic and Medicinal Chemistry Letters.* **10**(4): 715-717.

16. **Tomasic, T. and Masic, L.P. 2009.** Rhodanine as a privileged scaffold in drug discovery. *Current Medicinal Chemistry.* **16**(13): 1596–1629.

17. **Metwally, N. H., Rateb, N. M. and Zohdi, H. F. 2011.** A simple and green procedure for the synthesis of 5-arylidene-4-thiazolidinones by grinding. *Green Chemistry Letters and Reviews.* **4**(3): 225-228.

18. **Abhinit, M., Ghodke, M. and Pratima, N. A. 2009.** Exploring potential of 4-thiazolidinone: A brief review. *International Journal of Pharmacy and Pharmaceutical Sciences*. **1**(1): 47-64.

19. **Alizadeh, A., Rostamnia, S., Zohreh, N. and Hosseinpour, R. 2009.** A simple and effective approach to the synthesis of rhodanine derivatives *via* three-component reactions in water. *Tetrahedron Letters*. **50**: 1533-1535.

20. **El'tsov, O. S. and Mokrushin, V. S. 2003.** Reaction of 4,5-dinitro-imidazole with ethylenediamine and some transformations of the obtained 5-(2-aminoethylamino)-4-nitro-1H-imidazole (III). *Cheminfo*. **34**: 1-1.

21. **Pratap, U. R., Jawale, D. V., Bhosle, M. R. and Mane, R. A. 2011**. *Saccharomyces cerevisiae* catalyzed one-pot three component synthesis of 2,3-diaryl-4-thiazolidinones. *Tetrahedron Letters*. **52**: 1689-1691.

22. **Bolognese, A., Correale, G., Manfra, M., Lavecchia, A., Novellino, E. and Barone, V. 2004.** Thiazolidin-4-one formation. Mechanistic and synthetic aspects of the reaction of imines and mercaptoacetic acid under microwave and conventional heating. *Organic and Biomolecula Chemistry*. **2**: 2809-2813.

23. **Gouveia, F. L., de Oliveira, R. M. B., de Oliveira, T. B., da Silva, I. M., do Nascimento, S. C., de Sena, K. X. F. R. and de Albuquerque, J. F. C. 2009.** Synthesis, antimicrobial and cytotoxic activities of some 5-arylidene-4-thioxo-thiazolidine-2-ones. *European Journal of Medicinal Chemistry*. **44**(5): 2038-2043.

24. **Khodair, A. I. and Gesson, J. 2011.** A new approach for the N- and S-galactosylation of 5-arylidene-2-thioxo-4-thiazolidinones. *Carbohydrate Research*. **346**: 2831–2837.

25. **Opletalova, V., Dolezel, J., Kralova, K., Pesko, M., Kunes, J. and Jampilek, J. 2011.** Synthesis and characterization of (*Z*)-5-arylmethylidenerhodanines with photosynthesis-inhibiting properties. *Molecules*. **16**: 5207-5227.

26. **Dolezel, J., Hirsova, P., Opletalova, V., Dohnal, J., Marcela, V., Kunes, J. and Jampilek, J. 2009.** Rhodanineacetic acid derivatives as potential drugs: Preparation, hydrophobic properties and antifungal activity of (5-arylalkylidene-4-oxo-2-thioxo-1,3-thiazolidin-3-yl)acetic acids. *Molecules*. **14**: 4197-4212.

27. **Efe, C., Lykakis, L. N. and Stratakis, M. 2011.** Gold nanoparticles supported on TiO_2 catalyze the cycloisomerisation/oxidative dimerisation of aryl propargyl ethers. *Chemical Communications*. **47**: 803-805.

28. **Radi, M., Botta, L., Casaluce, G., Bernardini, M. and Botta, M. 2010.** Practical one-pot two-step protocol for the microwave-assisted synthesis of highly functionalized rhodanine derivatives. *Journal of Combinatorial Chemistry*. **12**: 200–205.

CHAPTER 4

Synthesis of substrate mimics as potential inhibitors of MshA

4.1 Introduction

Glycosyltransferase inhibitors attracted considerable attention in recent years, not only for their involvement as a tool for fundamental studies of complex carbohydrate-mediated biological processes but also as a foundation for the development of new drugs against many diseases.[1-4] This include natural product sugar nucleotide mimic inhibitors such as nikkomycins, tunicamycin as well as a variety of synthetic inhibitors (Fig. 4-1).[5,6] Sugar nucleotides play an essential role in carbohydrate metabolism and glycoconjugate biosynthesis.

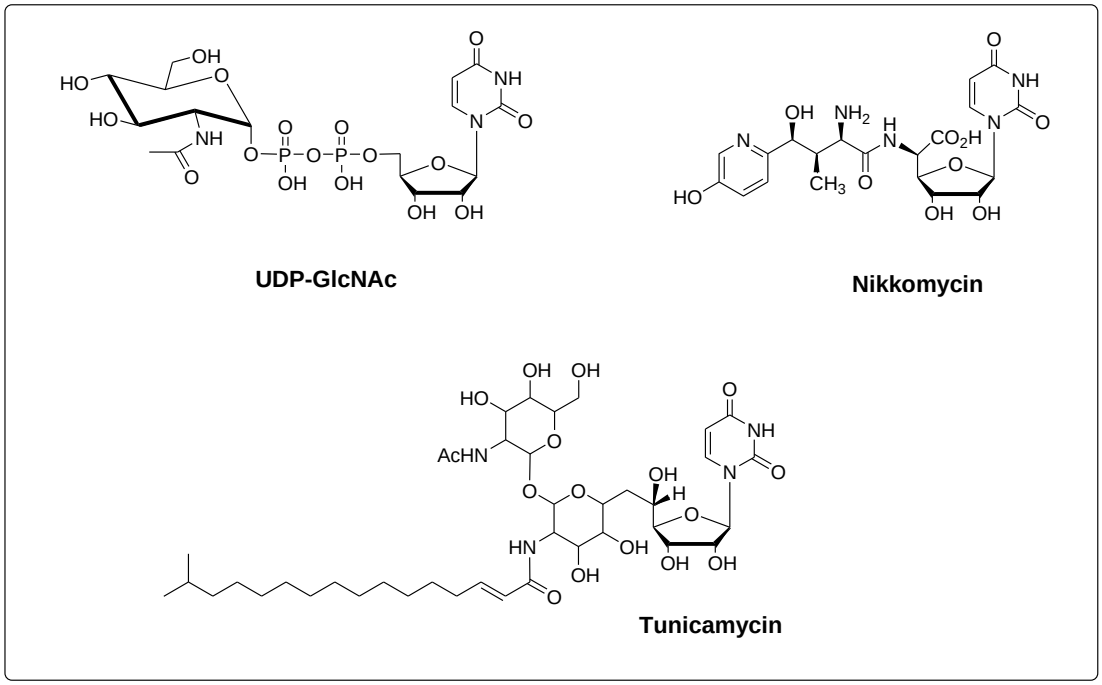

Figure 4-1: Examples of sugar nucleotide mimic inhibitors.

In an attempt to find a replacement for the polar pyrophosphate link in sugar nucleotides, Wang *et al.*[6] investigated malonic and tartaric moieties. However, all the compounds tested showed poor inhibition towards the glycosyltransferases. Kimura

and Bugg, proposed that tunicamycin utilized a L-rhamnose sugar moiety to mimic the pyrophosphate-Mn^{2+} complex of UDP-GlcNAc and subsequently inhibits the transfer of GlcNAc-1-P from UDP-GlcNAc to polyprenyl monophosphates in a variety of organisms.[7] Tunicamycin is a non-selective inhibitor of glycosyltransferases and hence, relatively toxic.

However, the rational drug design of inhibitors requires information about the three-dimensional structure of the enzyme.[8,9] As this would ensure the donor and acceptor portions of the substrate mimic are placed in correct orientation that allow their binding into their respective binding sites. Vetting *et al*.[10] reported the three-dimensional structure and basic kinetic properties of the retaining glycosyltransferase MshA from *Corynebacterium glutamicum* (cgMshA) and subsequently Framton *et al.*[11] reported UDP-(5F)-GlcNAc as the first competitive inhibitor of UDP-GlcNAc, the natural substrate of the MshA. The study further revealed that cgMshA undergoes large conformational change upon the binding of the UDP-(5F)-GlcNAc and subsequently assume the oxocarbenium transitional-state proposed for retaining glycosyltransferase enzymes. Although, the kinetic data revealed that UDP-(5F)-GlcNAc is a slow inhibitor of MshA, the study has provided invaluable information in the design of MshA inhibitors. Since the appearance of the three-dimensional structure of MshA, enormous effort has been made to identify and design potential inhibitors of MshA.

The main focus in this chapter is to report the design and synthesis of the substrate mimics for glycosyltransferase, MshA. The substrate mimics were designed in such a way that they mimic the naturally occurring substrate UDP-GlcNAc (Fig. 4-1) of

MshA by retaining the sugar moiety and nucleoside fragments of the natural substrate, which are both involved in binding inside the MshA active site.

The rationale behind the design of the substrate mimic derivatives was the desire to find a potential substitute for the pyrophosphate moiety of UDP-GlcNAc. Studies have revealed that all three parts of UDP-GlcNAc (uridine, the pyrophosphate and the sugar moiety) are involved to some extent in binding to the glycosyltransferase active site. The pyrophosphate moiety bind strongly to a divalent metal cation usually Mn^{2+} in the glycosyltransferase active site. Therefore finding the replacement of the pyrophosphate moiety of sugar-nucleoside diphosphate donors with an isosteric group like 1,2,3 triazole or phosphonate is desirable.

The synthetic strategy to produce substrate mimic analogs centered on the incorporation of a stable 1,2,3-triazole or phosphonate to replace the pyrophosphate moiety or anomeric oxygen of the natural substrate of MshA respectively. The incorporation of sulphur on the anomeric position of the sugar donor will result in the formation of a more stable thioglycosylated molecule.

The use of thioglycosides towards the synthesis of inhibitors has received widespread attention due to their versatility in the biological field.[12] The advantage of thioglycosides is that they are well tolerated by most biological systems[13,14], more resistant to enzymatic or chemical degradation[14] and more likely to reach their target. In this chapter, molecular dynamic docking experiments were performed in the mshA enzyme active site to aid further substrate mimics design.

4.2 Docking of the substrate mimics in the MshA substrate binding pocket

Following a computational simulation procedure described (Chapter 3, Section 3.2), molecular docking simulations were performed on the substrate mimics (**4-25** and **4-34**) prior to their synthesis. The docking results showed that all the substrate mimics assumed the same orientation as natural substrate (UDP-GlcNAc) within the MshA binding pocket, with 1,2,3-triazole (**4-25**) occupying same position as pyrophosphate moiety of the natural substrate.

Furthermore, docking analysis showed a strong interaction between the substrate mimic (**4-25**) and specific amino acid residues (ARG231, GLU316, LYS236 and GLU324 (x2) in the binding pocket of MshA, thus forming five new hydrogen bonds. The newly formed hydrogen bonds are indicated by dashed yellow lines (Fig. 4-2). From the estimated free energy of ligand binding (ΔG), the inhibition constant (Ki) for each ligand was calculated. K_i is calculated by the equation: $K_i = \exp [(\Delta G^* 1000)/ (R^*T)]$ where ΔG is the docking energy, R (gas constant) is 1.98719 kcal/Kmol and T (Temperature) is 298.15 K. Only the best pose with the lowest binding energy and K_i was considered. The binding energy for the docked substrate mimic (**4-25**) was found to be -73.62 kcal/Kmol**.**

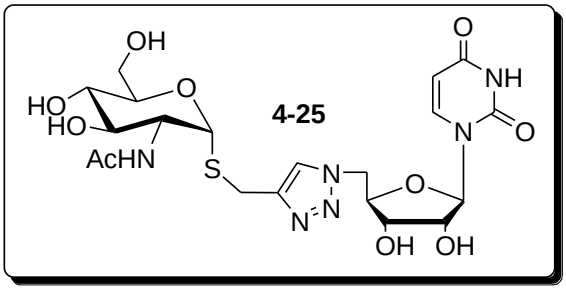

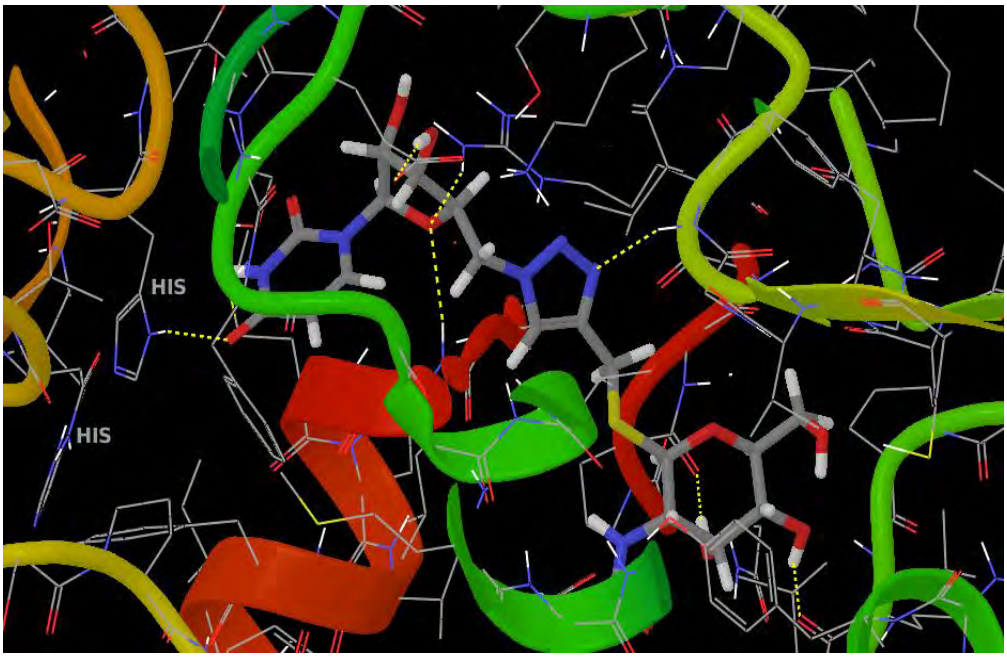

Figure 4-2: Docked structures of substrate mimic (**4-25**) in the active site of MshA. Newly formed hydrogen bonds are indicated by dotted yellow lines.

Similar observations were made with substrate mimic (**4-34**)**.** The molecular docking studies revealed key amino acid residues (THR134, LYS236 (x2), ARG231, VAL321, GLY23, CYS262, ARG294 and GLU324 (x2) interact with substrate mimic (**4-34**) in the binding pocket of MshA, thus forming ten new hydrogen bonds (Fig. 4-3). The binding energy for the docked substrate mimic (**4-34**) was found to be -94.40 kcal/Kmol, thus making it the best potential inhibitor for MshA. This observation was in agreement with the previous studies on the glycosyltransferase MurG.[31]

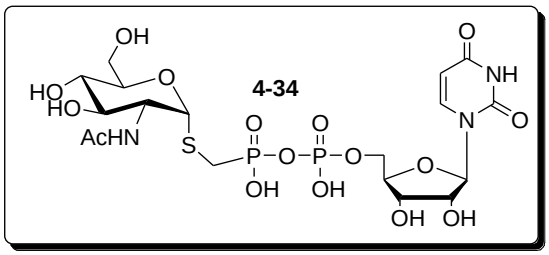

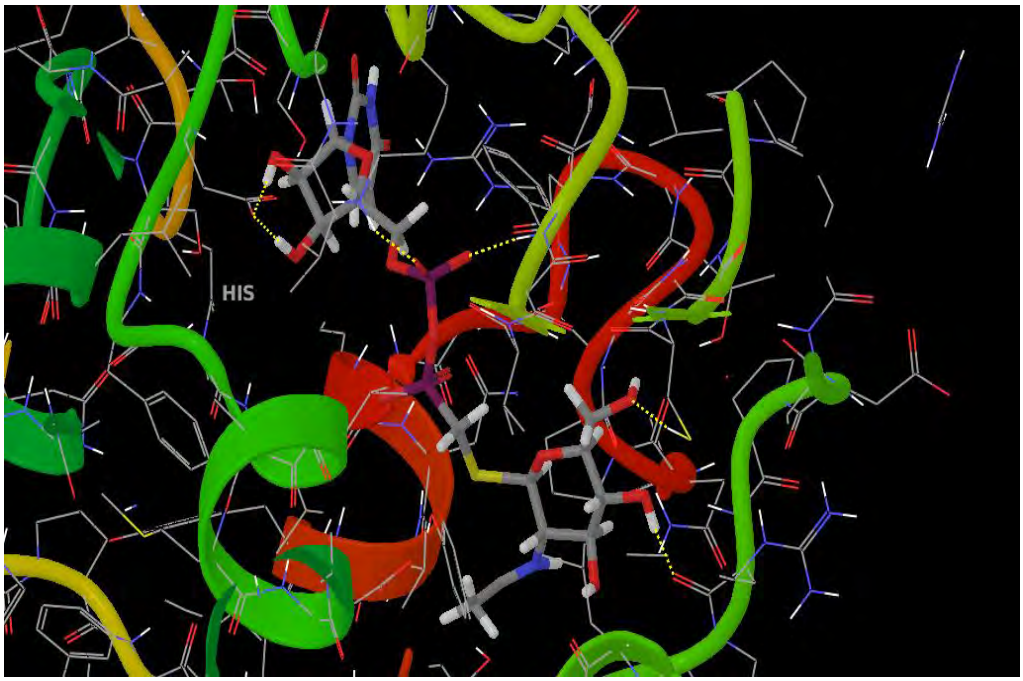

Figure 4-3: Docked structures of substrate mimic (**4-34**) in the active site of MshA. Newly formed hydrogen bonds are indicated by dotted yellow lines.

Following the successful docking of the substrate mimics in the MshA binding pocket, several attempts were made to dock tunicamycin, a natural inhibitor of glycosyltransferases in the MshA binding pocket. However, the docking results returned poor binding energies and inhibition constants (Data not shown). This could be attributable to the large size or long aliphatic side chain of tunicamycin that renders the molecule too flexible. However, despite the setback with docking of tunicamycin in the active site of MshA, the synthesis of substrate mimics (**4-25, 4-29** and **4-34**) was conceptualized following successful docking experiments of these target substrate mimics.

4.3 A Retrosynthetic analysis of substrate mimics (4-25, 4-29 and 4-34)

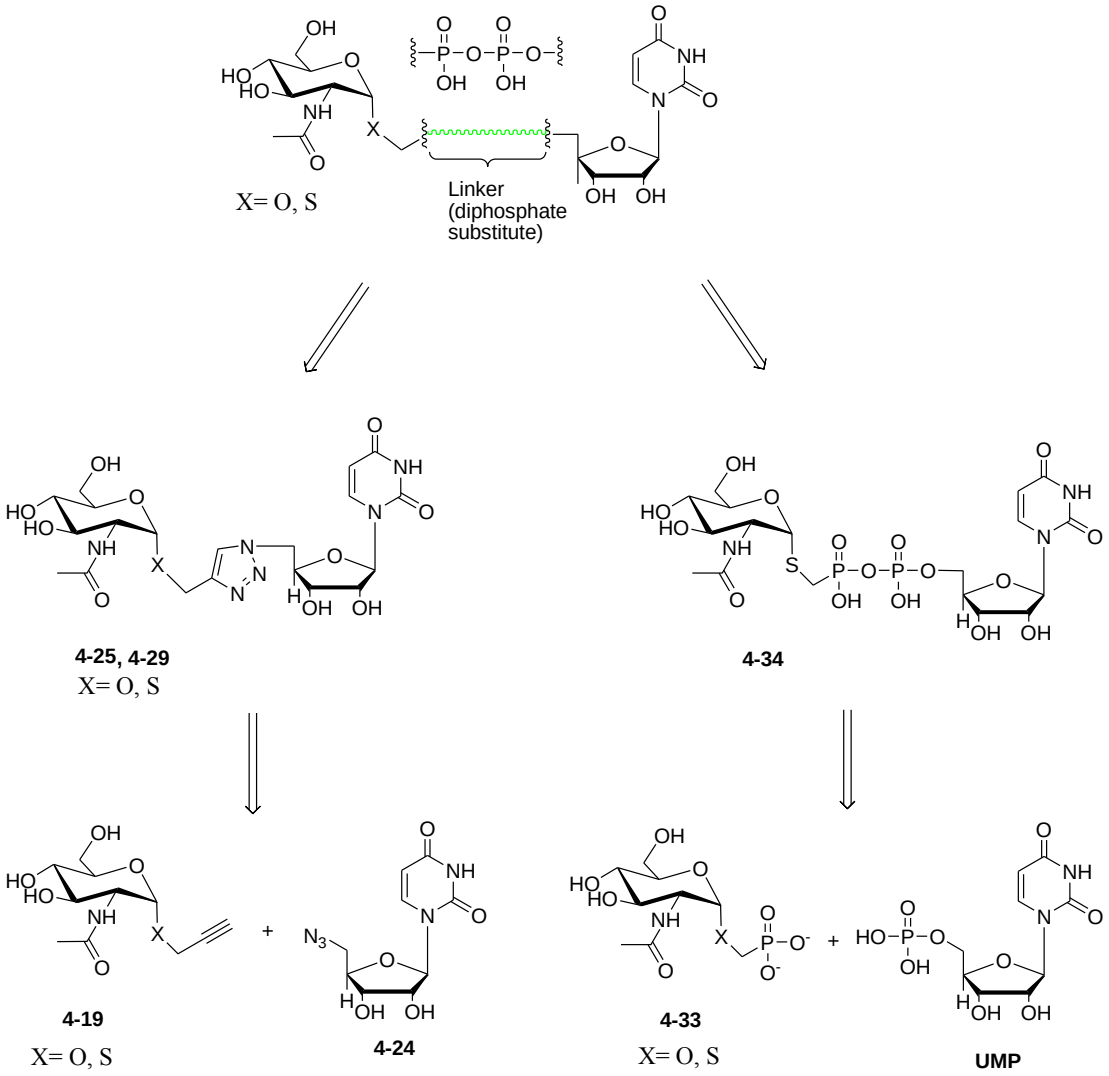

Figure 4-4: A retrosynthetic approach towards the synthesis of the target molecules.

As indicated by the retrosynthetic analysis (Fig. 4-4), the total synthesis of the target substrate mimics (**4-25** and **4-29**) was conceived as achievable *via* a convergent strategy involving the coupling of terminal alkyne moiety (**4-19**) and 5'-deoxy-5'-azido-uridine (**4-24**). Huisgen coupling of the two intermediates (**4-19** and **4-24**) will result in the formation of a substrate mimic with the desired 1,2,3-triazole as a substitute for pyrophosphate. 5'-Deoxy-5'-azido-uridine (**4-24**) can be achieved in 4 steps from commercially available uridine. Terminal alkyne moiety (**4-19**) can be

achieved in a series of steps from glucosamine. Likewise, the total synthesis of the target substrate mimic (**4-34**) can be achieved *via* the coupling of the target intermediate (**4-33**) and uridine monophosphate (UMP).

4.3.1 Synthesis of thioglycosides

Since the appearance of the first report of glycosyl thiol synthesis by Fischer and Delbruck in 1909, various methods for the synthesis of glycosyl thiols (**4-1**) have been reported. The most frequently used method involves the treatment of glycosyl halides (**4-2**) (Scheme 4-1) with thiourea in acetone followed by mild hydrolysis with alkali metal disulfide. Other methods include the use of anomeric thioacetates under slighty basic conditions.

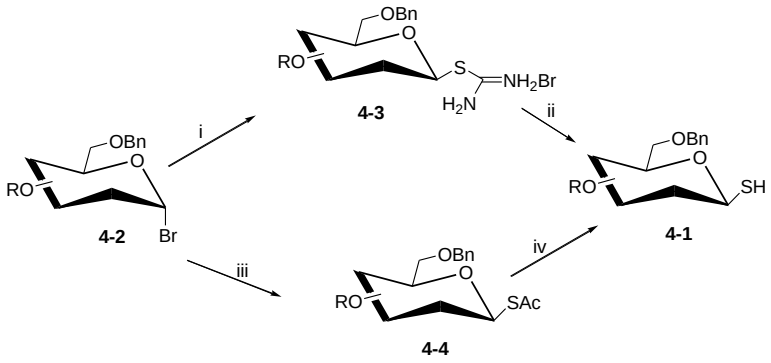

Scheme 4-1: Reaction conditions: (i) Thiourea, (ii) $Na_2S_2O_5$, DCM/water, (iii) KSAc (iv) NaSMe, MeOH/$CHCl_3$.

Generally the synthesis of α-glycoside intermediates by the direct glycosylation of the anomeric carbon has been a challenge for numerous reasons. Stereoselectivity at the anomeric carbon is governed by a number of factors such as the type of solvent used, reaction conditions e.g. temperature, anomeric effect and the possible involvement of the participating group on the carbon adjacent to the anomeric carbon.[15,16] The formation of β-glycosides is favored *via* anchimeric participation of the acetamide

carbonyl oxygen with anomeric carbon. Furthermore, complexation with the glycoside donors, activating reagents and other Lewis acids.[17]

β-anomers are generally prepared by equatorial addition of the nucleophiles to the anomeric carbon whereas α-anomers are prepared by axial addition. However, the interaction of these groups with anomeric centres affords the formation β-anomers since the nucleophile can only approach from the top. The substituent on the anomeric carbon would prefer the more stable equatorial position with minimised unfavoured interactions.

However, Bernades *et al.*[18] have described a direct procedure for the synthesis of anomeric α-glycosyl thiols in one synthetic step from their anomeric alcohols using Lawesson's reagent which serves as a sulphur donor (Scheme 4-2).

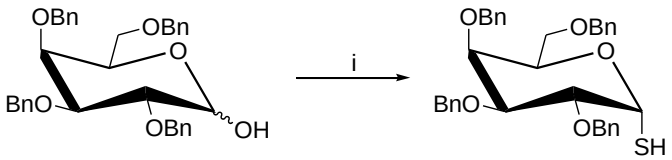

4-5 **4-6**

Scheme 4-2: Reaction conditions: (i) Lawesson's reagent, dioxane/toluene.

Similar studies were reported by Davis and co-workers using Lawesson's reagent which was found to be able to directly convert the reducing sugars or unprotected sugars into their corresponding α-glycosyl thiols. However, this procedure was found to have some setbacks because of the tendency to form numerous by-products making it difficult to purify and resulting in lower yields. Thus, a procedure for the synthesis of *α*-glycosyl thiols was lacking. Such a procedure would facilitate the synthesis of *α*-*S*-linked saccharides and glycoconjugates.

Knapp and Myers[19] reported a procedure for the synthesis of glycosyl thiol (**4-1**) whereby 2-acetamido-2-deoxy-1,3,4,6-tetra-*O*-acetyl-β-D-galactopyranose (**4-7**) (Scheme 4-3) was treated with Lawesson's reagent in hot toluene to form the GalNAc-thiazolidine ring (**4-8**). Following the successful formation of the thiazoline ring and subsequent hydrolysis of the ring through the cleavage of the C-S bond led to the desired α-GalNAc mercaptan (**4-9**). This procedure was found to be very efficient and the product was isolated as the α-anomer in quantitative yields.

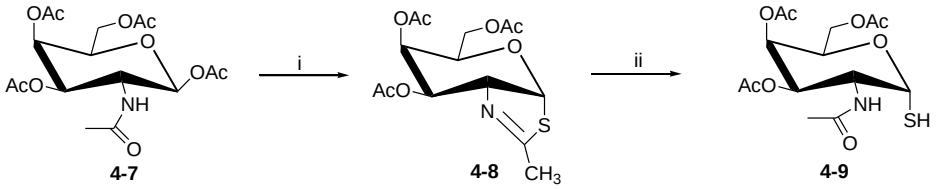

Scheme 4-3: Reaction conditions: (i) Lawesson's reagent, toluene, 80 °C; (ii) TFA, wet MeOH.

The deprotection of (**4-8**) to the α-mercaptan (**4-10**) has been achieved under Zemplén conditions (Scheme 4-4). The successful preparation of glycosyl thiol (**4-1**), presented a valuable intermediate toward the synthesis of GalNAc thioconjugates.

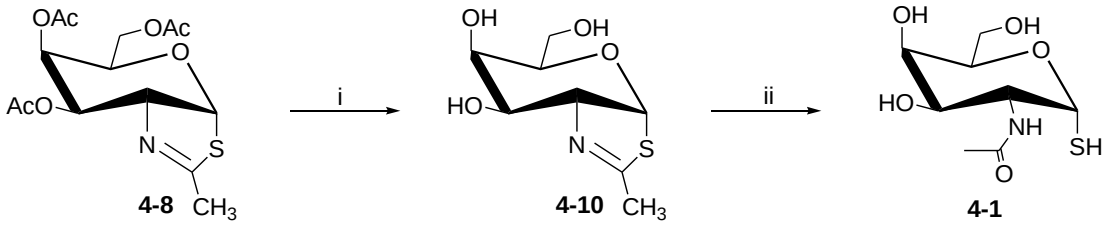

Scheme 4-4: Reaction conditions: (i) NaOMe, MeOH; (ii) TFA, wet MeOH.

The substrate mimics have been designed to compete with UDP-GlcNAc for binding to the active site of MshA. It is for this reason that it was decided to pursuit the synthesis and evaluation of these substrate mimics as part of identifying selective inhibitors targeting MshA. Our synthetic strategy for the assembly of substrate

mimics began with the synthesis of the key substrate intermediate α-GlcNAc mercaptan (**4-17**).

4.3.2 Synthesis of α-GlcNAc mercaptan

The synthesis of 2-acetamido-2-deoxy-3,4,6-tri-*O*-acetyl-1-α-thio-D-glucopyranose (α-GlcNAc mercaptan) (**4-17**) (Scheme 4-5) has been successfully achieved in a series of steps following the modified protocols of Knapp and Myers[19,20] and Myszka *et al.*[21] respectively. 2-Deoxy-2-[*p*-methoxybenzylidene(amino)]-D-glucopyranose (**4-12**) was prepared from commercially available D-glucosamine hydrochloride (**4-11**) in a procedure that utilizes *p*-anisaldehyde to protect the amine (NH_2) as a Schiff base followed by the global acetylation of the remaining hydroxyl groups in the presence of pyridine and acetic anhydride to give 1,3,4,6-tetra-*O*-acetyl-2-deoxy-2-[*p*-methoxybenzylidene(amino)]-*β*-D-glucopyranose (**4-13**). The 4-methoxybenzylidene protecting group was hydrolyzed by the treatment of compound (**4-13**) with 5 M HCl in acetone to afford 1,3,4,6-tetra-*O*-acetyl-β-D-glucosamine hydrochloride (**4-14**), which was subsequently acetylated to afford 2-acetamido-2-deoxy-1,3,4,6-tetra-*O*-acetyl-β-D-glucopyranose (**4-15**) in excellent yields. The structure of (**4-15**) was confirmed by the ^{1}H and ^{13}C NMR spectra with the presence of the strong resonance of the OAc (s, 12 protons) at δ_H 1.97 ppm and another resonance at δ_H 2.04 ppm (s, 3 protons) which correspond to N*H*Ac.

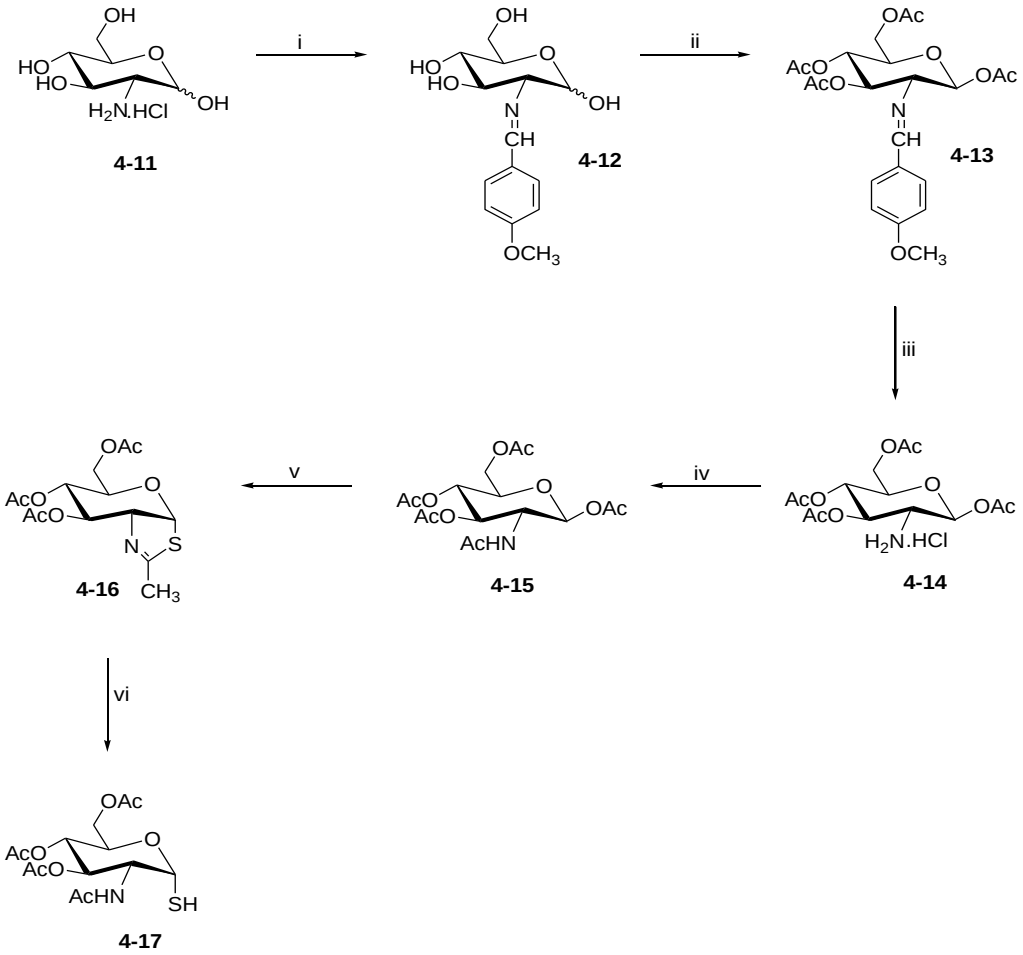

Scheme 4-5: Reaction conditions: (i) aq 1M NaOH, *p*-CH_3O-C_6H_4-CHO; (ii) Py, Ac_2O; (iii) Acetone, 5M HCl; 99% (iv) Py, Ac_2O; 97% (v) Lawesson's reagent, toluene, 80 °C; 100 (vi) TFA, wet MeOH, H_2O, 0 °C; 2 hr; 95%..

Following the successful synthesis of compound (**4-15**), the next step was to treat compound (**4-15**) with Lawesson's reagent in the presence of toluene to convert the amide into the GlcNAc-thiazoline (**4-16**). The structure of the latter was confirmed by ^1H and ^{13}C NMR spectroscopy, which showed key diagnostic signals at δ_H 2.28 ppm (^1H NMR) and δ_C 20.7 ppm (^{13}C NMR) corresponding to methyl (CH_3) attached to the thiazoline ring. Another diagnostic feature was the presence of the downfield doublet for H-1 (J = 7.1 Hz) confirming the alpha anomeric stereochemistry at C-1 position.

The GlcNAc-thiazoline ring was hydrolyzed by the cleavage of the imine carbon-sulphur bond rather than the anomeric carbon-sulphur bond and the opening of the thiazoline ring to give 2-acetamido-2-deoxy-3,4,6-tri-*O*-acetyl-1-thio-α-D-glucopyranose (**4-17**)[22] as a golden brown syrup in 100% yield. The structure of (**4-17**) was confirmed using the ^{1}H NMR and ^{13}C NMR spectroscopic data.

The disappearance of the methyl singlet of the thiazoline ring resonating at δ_H 2.28 ppm in the spectrum of (**4-16**) was diagnostic in (**4-17**). The ^{13}C NMR spectrum of (**4-17**) also confirmed the absence of the methyl and imine carbon resonance and the appearance of the NHAc methyl resonance at δ_C 22.79 ppm.

4.3.3 Synthesis of thioglycoside analogues

The successful synthesis of α-mercaptan (**4-17**) (Scheme 4-5) enabled subsequent synthesis of the desired substrate mimics. The *S*-alkylation of α-mercaptan (**4-17**) in a mixture of 1:1 propargyl bromide and triethylamine produced propargyl thioglycoside (**4-18**) which was subsequently deacetylated under standard Zemplén deacetylation conditions (sodium methoxide in methanol) to furnish *N*-((2*R*,3*R*,5*S*)-tetrahydro-4,5-dihydroxy-6-(hydroxymethyl)-2-(prop-2-ynylthio)-2*H*-pyran-3-yl)acetamide (**4-19**) in a 100% yield (Scheme 4-6).

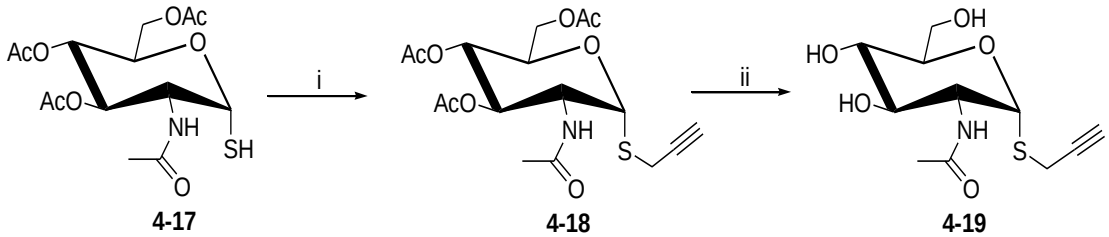

4-17 **4-18** **4-19**

Scheme 4-6: Reactions conditions: (i) Et_3N, C_3H_3Br, 77%; (ii) MeOH, NaOMe, 52%.

The ^{1}H NMR spectroscopic data of compound (**4-18**) showed the presence of the propargyl group. Thus, resonating at δ_H 5.05 ppm and integrating for two methylene protons as well as δ_H 2.21 ppm for the alkyne proton respectively. This was further supported by the notable absence of the thiol group observed in the ^{1}H NMR spectrum of (**4-18**). Finally, ESI HRMS evaluation gave a *m/z* 402.1222 $[M+H]^+$ ($C_{17}H_{24}NO_8S$) which required *m/z* 402.1223 $[M+H]^+$, thus supporting the proposed structure of compound (**4-18**).

The structure of compound (**4-19**) was also confirmed by the ^{1}H NMR spectrum showing the complete disappearance of *O*-acetyl associated signals which resonated at δ_H 2.02, 2.01, and 1.90 ppm and the appearance of new hydroxyl group signals resonating at δ_H 5.11, 4.85 and 4.58 ppm, respectively. Finally, ESI HRMS evaluation gave a *m/z* 275.0826 $[M+H]^+$ ($C_{11}H_{17}NO_5S$) which required *m/z* 275.0827 $[M+H]^+$, thus supporting the proposed structure of compound (**4-19**).

With pure (**4-19**) in hand, the next objective was to synthesize the 1,2,3-triazole as a linking component between α-glycoside and nucleotide (5'-deoxy-5'-azido-uridine).

4.3.4 Synthesis of 5'-deoxy-5'-azido-uridine derivatives (4-21 – 4-24)

In order to secure a complete synthesis of the desired substrate mimic, the 5'-deoxy-5'-azido-uridine (**4-24**) had to be synthesized. The synthesis of this nucleotide has been achieved in a four step synthesis from relatively cheap and commercially available uridine. Thus, the synthesis of 5'-deoxy-5'-azido-uridine derivatives (**4-24**) (Scheme 4-7) has been achieved following the modified procedure of Winans and Bertozzi.[23] The synthesis of 2',3'-*O*-isopropylidene (**4-21**) has been synthesized using the commercially available uridine (**4-20**).

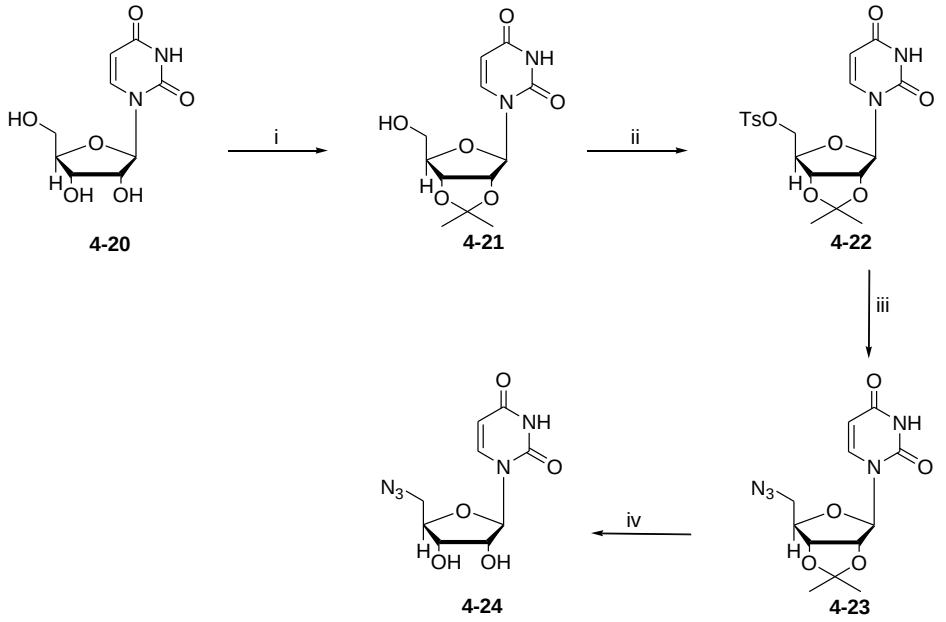

Scheme 4-7: Reactions conditions: Reagents and conditions: (i) TsOH, 2.2-dimethoxypropane, DMF, 65 °C, 100%; (ii) TsCl, Pyridine, DMF, 65 °C, 93%; (iii) NaN_3, DMF, 65 °C, 98%; (iv) 90% TFA/H_2O, 95%.

The uridine moiety was selectively protected at position 2' and 3' using 2,2-dimethoxypropane to furnish compound (**4-21**) as a white solid in 100% yield after silica gel column chromatography. The ^{1}H NMR spectroscopic data showed the presence of two strong methyl peaks resonating at δ_H 1.58 and δ_H 1.36 ppm, respectively. These signals indicated successful protection of the two hydroxyl groups in compound (**4-20**). The tosylation of compound (**4-21**) at position five using *p*-toluenesulfonyl chloride (TsCl) and in the presence of pyridine in DMF provided the tosylated product (**4-22**) in good yield (100%).

The diagnostic features in the ^{1}H NMR spectrum of (**4-22**) were the tosyl methyl resonance at δ_H 2.45 and the aromatic resonances at δ_H 7.78 and δ_H 7.34 ppm respectively. Furthermore, the infrared (IR) spectrum showed two strong absorbances at 1173 and 1374 cm^{-1}, which are a characteristic of sulfonyl (S=O) stretches. The

absence of the hydroxyl group resonance in ^{1}H NMR spectrum was further evidence that the tosylation had taken place.

The tosyl group was subsequently substituted with a azide moiety in the presence of sodium azide (NaN_3) in DMF to produce 5'-deoxy-5'-azido-2',3'-*O*-isopropylidene uridine (**4-23**) (Scheme 4-7) in quantitative yield. The ^{1}H NMR spectrum of (**4-23**) showed the disappearance of the two aromatic protons resonating at δ_H 7.78 and δ 7.34 ppm, and the absence of the tosyl methyl resonance at δ_H 2.45 ppm, respectively.

Deprotection of compound (**4-23**) ultimately gave 5'-deoxy-5'-azido-uridine (**4-24**) in 90% yield. The ^{1}H NMR spectrum of (**4-24**) showed the disappearance of the two methyl resonances at δ_H δ 1.58 and δ_H 1.36 ppm respectively and the appearance of a broad singlet resonating at δ_H 5.30 ppm, integrating for two protons. Another significant feature in the ^{1}H NMR spectrum of compound (**4-24**) is the protons resonating at δ_H 3.70 ppm assigned to 5'-deoxy-5'-azido-uridine.

The coupling of the terminal alkyne moiety of (**4-19**) and 5'-deoxy-5'-azido-uridine (**4-24**) in the presence Cu(II) sulphate pentahydrate and sodium ascorbate as a reducing agent led to formation of triazole thioglycoside (**4-25**) (Scheme 4-8), which is one of the target molecules in this study. This substrate mimic has been tailored in such a way that it retains the carbohydrate and nucleoside fragments of the natural substrate UDP-GlcNAc, which are both involved in binding of MshA active site while the pyrophosphate of the natural substrate is substituted by the 1,2,3-triazole.

However, prior to the synthesis of thioglycosides (**4-25**) using the Cu(II) catalyzed reaction, several attempts were made using Cu(I) mediated reaction as a catalyst in a mixture of water and *t*-BuOH (1:1) at room temperature resulted in a mixture of

products as witnessed by TLC, which proved difficult to separate. Other challenges encountered with this synthetic procedure ranged from the lengthy reaction times and poor isolated yields. The reaction took more than seven days for significant product formation and this is despite the increase in temperature and reagents. The slow reaction using just Cu(I) in the mixture of *t*-BuOH and water could be due to Cu(I) being oxidized to Cu(II). Cu(I) is the active species needed to facilitate this triazole-forming reaction.

Surprisingly the use of a combination of Cu(II) and sodium ascorbate tremendously improved product formation and a slightly improved yield of 30% was obtained at room temperature within 24 hr. Unlike in the Cu(I) catalysed reaction, the Cu(II) catalysed reaction gave much better chemoselectivity with the desired product being identified. The persistently low yields of the copper assisted cycloaddition reactions could be attributed to inability to consume all the starting material during the reaction and this phenomenon has been noted in both Cu(I) and Cu(II) reactions, respectively.

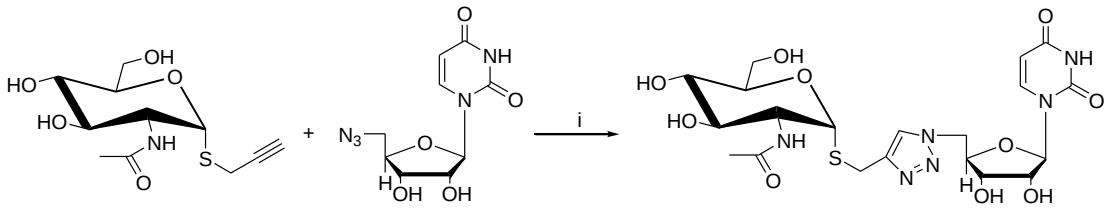

4-19 **4-24** **4-25**

Scheme 4-8: Reactions conditions: (i) $CuSO_4.5H_2O$ and sodium ascorbate; 33%.

The structure of thioglycoside (**4-25**) was confirmed by the ^1H NMR spectrum and the key diagnostic feature in the spectrum of this compound was the presence of a deshielded triazole singlet proton resonating at δ_H 8.01 ppm which was consistent with that reported in the literature.[25,26] Further evidence of formation of this compound (**4-25**) was the disappearance of the alkyne proton in compound (**4-19**). ^{13}C

NMR spectrum analysis supported the formation of the triazole further with the presence of a carbon signal resonating at δ_C 143.25 which was consistent with the triazole. Finally, ESI HRMS evaluation gave a *m/z* 545.1663 $[M+H]^+$, $C_{20}H_{29}N_6O_{10}S$ which required *m/z* 545.1666 $[M+H]^+$), thus supporting the proposed structure of the triazole linked substrate mimic, compound (**4-25**) (Fig. 4-5).

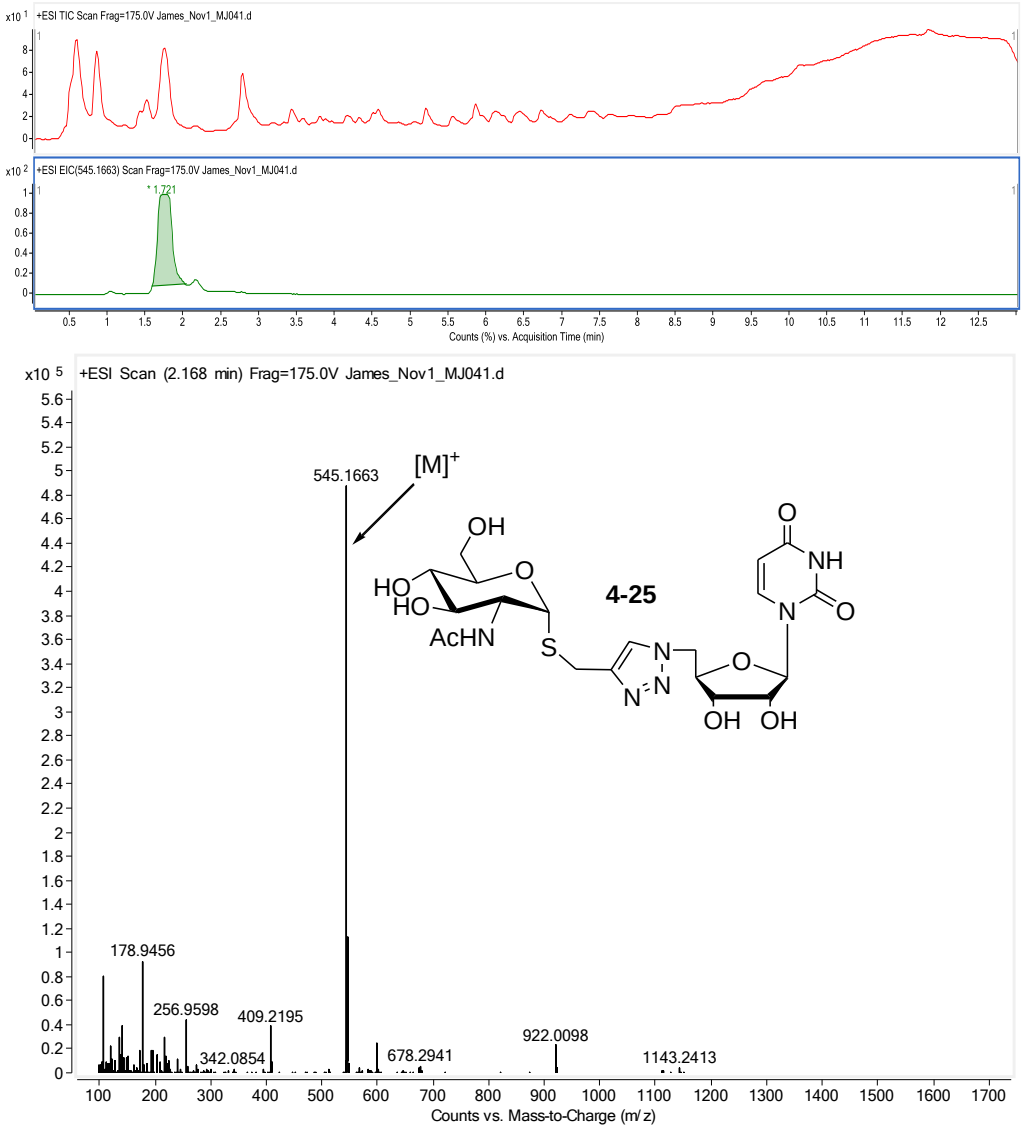

Figure 4-5: The HRMS spectrum showing the molecular ion peak of compound **4-25**.

4.3.5 Synthesis of [1'-(5''-deoxyuridin)-1'*H*-1',2',3'-triazol-4'-yl] methyl 2-acetamido-2-deoxy-α-D-glucopyranoside (**4-29**).

Having successfully synthesized the α-propargyl thioglycoside (**4-19**), the α-propargyl glycoside was attempted for utilization in the Huisgen coupling. *N*-Acetyl glucosamine (**4-27**) (Scheme 4-9) has been successfully synthesised from relatively cheap and commercially available glucosamine hydrochloride (**4-26**) in a procedure described by Babic and Pecar.[27] In this procedure, glucosamine hydrochloride (**4-26**) was allowed to stir in the solution of NaOMe/MeOH for 1 hr at room temperature before acetic anhydride was added, subsequently the mixture was allowed to stir overnight.[27] The structure of (**4-27**) was confirmed by the spectroscopic data with ^{1}H NMR spectrum showing the presence of the methyl resonance (NHAc) as a singlet resonating at δ_H 2.01 ppm integrating for three protons. The alkylation of (**4-27**) in the presence of propargyl alcohol and excess H_2SO_4 immobilized on silica gel gave the propargyl glycoside (**4-28**) as a racemic mixture. The activated silica gel was prepared as reported recently by Roy and Mukhopadhyay using concentrated H_2SO_4 on silica gel.[28]

The desired α-propargyl glycoside (**4-28**) was obtained through the recrystallization of the anomeric mixture. The ^{1}H NMR spectrum of compound (**4-28**) has confirmed that the alkylation had taken place, with the presence of two methylene protons on the propargyl moiety resonating at δ_H 3.30 ppm and triplet resonating δ_H 2.83 ppm for the alkyne proton. By using the same conditions used to access [1'-(5''-deoxyuridin)-1'*H*-1',2',3'-triazol-4'-yl] methyl 1-thio-2-acetamido-2-deoxy-α-D-glucopyranoside (**4-25**) (Scheme 4-7), [1'-(5''-deoxyuridin)-1'*H*-1',2',3'-triazol-4'-yl] methyl 2-acetamido-2-deoxy-α-D-glucopyranoside (**4-29**) was successfully synthesized in 33% yield (Scheme 4-9).

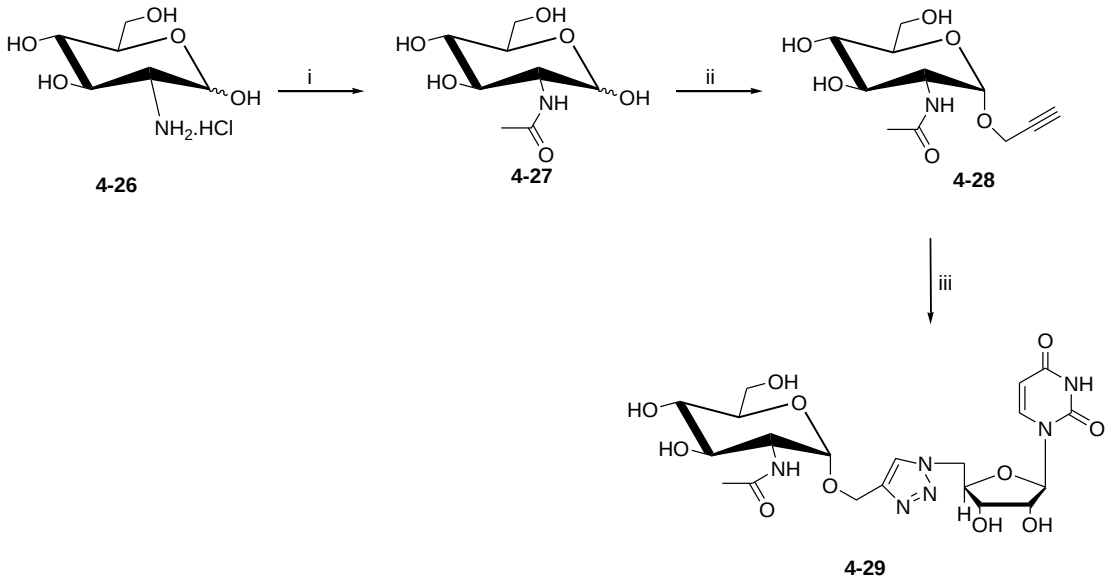

Scheme 4-9: Reactions conditions: (i)MeOH, NaOMe solution, Ac_2O, RT; (ii) Propargyl alcohol, H_2SO_4-silica, 65 °C; (iii) $CuSO_4.5H_2O$, Ascorbic acid, 1:1 H_2O/TBA, 33%.

4.3.6 Synthesis of bis-triethylammonium uridin-5'-yl (2-acetamido-2-deoxy-α-D-glucopyranosylthiomethylphosphono) phosphate (4-34).

As indicated by the retrosynthetic analysis (Fig. 4-4), the total synthesis of the target substrate mimic (**4-34**), requires the coupling of deacetylated glycosylthiomethyl phosphonate (**4-33**) and uridine monophosphate (UMP). The synthesis of deacetylated glycosylthiomethyl phosphonate (**4-33**) involves a series of activation steps from 2-acetamido-2-deoxy-3,4,6-tri-*O*-acetyl-1-thio-α-D-glucopyranose (**4-17**) (Scheme 4-10).

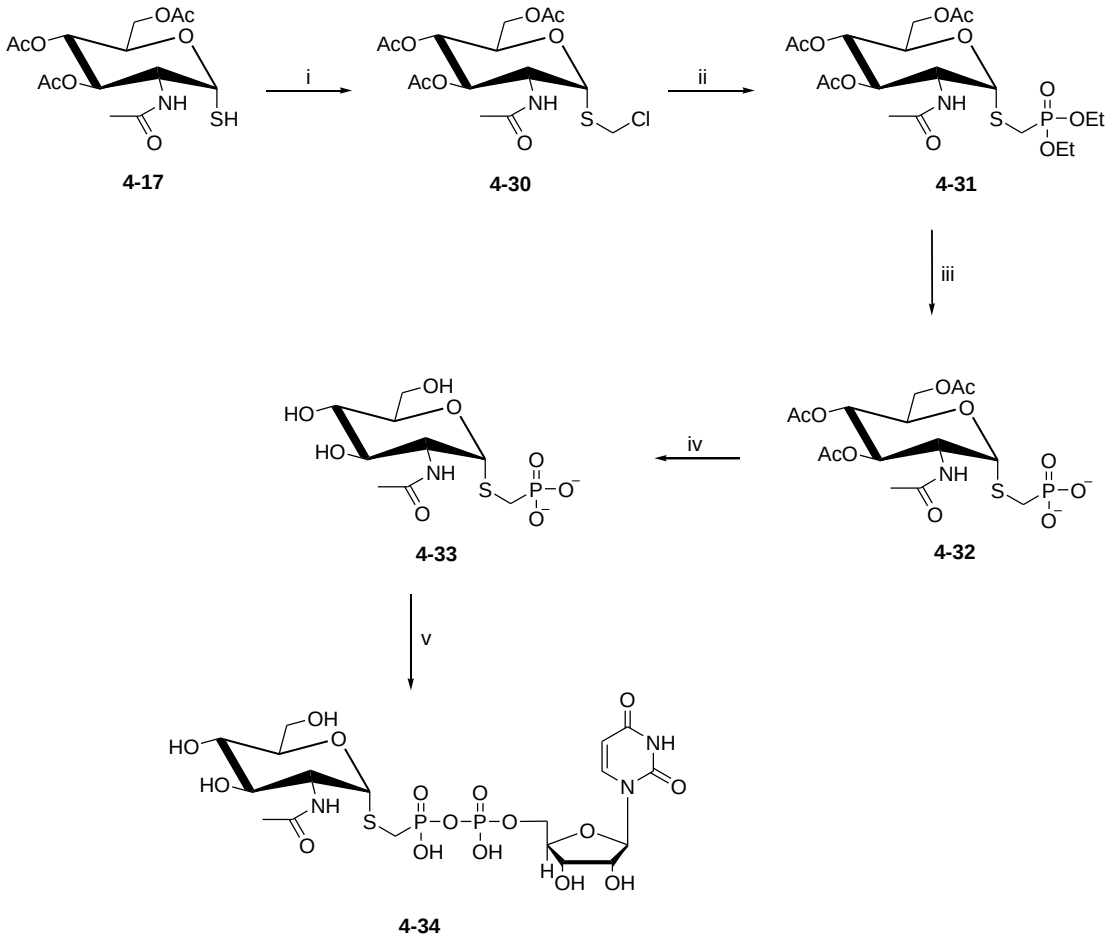

Scheme 4-10: Reactions conditions: (i) DBU, DCM; 46% (ii) Et_3PO_4; 65% (iii) TMSBr, 2,6-lutidine, CAN; 95% (iv) MeOH, NaOMe; (v) Py, 1*H*-tetrazole, UMP-morpholidate, 37%.

By using a procedure described by Zhu and Schmidt,[29,30] 2-acetamido-2-deoxy-3,4,6-tri-*O*-acetyl-1-thio-α-D-glucopyranose (**4-17**) was treated with dichloromethane (DCM) and 1,8-diazabicyclo[5.4.0]undec-7-ene (DBU) to furnish glycosylthiomethyl chloride (**4-30**) in 46% yield. The Arbuzov reaction of methylene chloride (**4-30**) with triethyl phosphite gave rise to the desired glycosylthiomethyl phosphonate (**4-31**) as an amorphous salt in quantitative yield.

The structure of (**4-31**) was confirmed by the analysis of NMR spectroscopic data which was in agreement with the literature.[30] The ^{1}H NMR spectrum showed a triplet integrating for ten ethoxy protons (2 × OEt) resonating at δ_H 1.25 ppm. Glycosylthiomethyl phosphonate (**4-31**) was subsequently treated with the

bromotrimethylsilane (TMSBr) in the presence of excess 2,6-lutidine to deprotect the phosphate ester, thus, giving rise to phosphonic acid compound (**4-32**) as a lutidinium salt in quantitative yield.

The ^{1}H NMR spectrum of (**4-32**) confirmed the deprotection of the molecule by virtue of the complete disappearance of OEt protons from the ^{1}H NMR spectrum. Subsequently, the deacetylation of phosphonic acid compound (**4-32**) to glycosylthiomethyl phosphonate (**4-32**) was achieved under standard Zemplén deacetylation conditions. Toward the synthesis of target substrate mimic (**4-34**), glycosylthiomethyl phosphonate (**4-33**) was coupled with UMP-morpholidate in the presence of anhydrous 1*H*-tetrazole to produce the desired bis-triethylammonium uridin-5'-yl (2-acetamido-2-deoxy-α-D-glucopyranosylthiomethylphosphono) phosphate (**4-34**) in low yield (37%) with recovery of starting material (Scheme 4-10).

4.4 Conclusion

In summary, substrate mimics (**4-25, 4-29** and **4-34**) were successfully prepared as inspired by molecular docking simulations. The phosphate bridge of UDP-GlcNAc was modified by substitution of the scissile phosphate oxygen with a methylene or complete substitution of the phosphate bridge with triazole. Furthermore, the docking studies have revealed that substrate mimics assume the same orientation as the UDP-GlcNAc in the MshA binding site, thus forming interactions with the key vicinal amino acid residues. In addition, the prepared substrate mimics and their intermediates were characterized using a variety of complementary techniques including LC-MS, IR, ^{13}C and ^{1}H NMR. Finally, the screening of the prepared

substrate mimics as the potential inhibitors of glycosyltransferase MshA will be reported in the subsequent Chapters (Chapter 5 and Chapter 6 respectively).

4.5 Experimental:

4.5.1 Synthesis of 1,3,4,6-tetra-*O*-acetyl-β-D-glucosamine hydrochloride (4-14)[20]

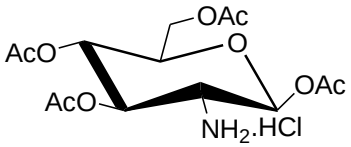

An aqueous solution of NaOH (1M, 120 mL) was added to D-glucosamine hydrochloride (**4-11**) (25g, 116 mmol) and the mixture was allowed to dissolve while stirring. *p*-Anisaldehyde (17 ml, 0.14mol) was added in small aliquots after which product crystallization started. The solution was allowed to stir for 6 hr and refrigerated for overnight. The precipitated product was filtered and washed with cold water followed by a mixture of ethanol and diethyl ether to give 2-deoxy-2-[*p*-methoxybenzylidene (amino)]-D-glucopyranose (**4-12**). This intermediate compound was completely dried before being added to an ice cooled mixture of pyridine (135 mL, 113 mmol) and Ac_2O (75 mL, 0.9 mmol). The mixture was allowed to stir in an ice-bath for 1 hr and then overnight at room temperature. The solution was poured into approximately 500 mL of ice-water after which a precipitate formed. The precipitated white product was filtered, washed with cold water and dried under vacuum to give (2*S*,3*R*,4*R*,5*S*,6*R*)-6-(acetoxymetoxymethyl)-3-((*E*)-4-methoxybenzylideneamino)tetrahydro-2*H*-pyran-2,4,5-triyl triacetate (**4-13**) as a white solid (54.0 g, 100%). The Schiff base product (50 g, 108 mmol) was dissolved in warm acetone (300 mL) followed by the addition of HCl (5 M; 15 mL) which immediately formed of a white precipitate. The mixture was allowed to cool, after which diethyl ether (300 mL) was added and the precipitate refrigerated overnight. The precipitated product was filtered and washed with diethyl ether (100 mL) and dried to give 1,3,4,6-tetra-*O*-acetyl-β-D-glucosamine hydrochloride (**4-14**) as a white

solid (41.0 g, 99%). The product was used in the next reaction without any further purification.

4.5.2 Synthesis of 2-acetamido-2-deoxy-1,3,4,6-tetra-*O*-acetyl-β-D-glucopyranose (4-15)[32]

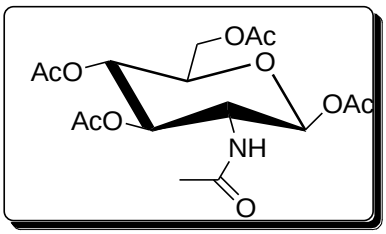

To a solution of 1,3,4,6-tetra-*O*-acetyl-β-D-glucosamine hydrochloride (**4-14**) (22.5 g, 58.7 mmol) in DCM (150 mL) at 0 °C was added acetic anhydride (18 mL) followed by pyridine (18 mL). The solution was allowed to stir for 30 min followed by the addition to ice-water. After organic extraction (DCM 150 mL) and drying with $MgSO_4$ the solution was filtered through celite and the filtrate was concentrated under reduced pressure to give 2-acetamido-2-deoxy-1,3,4,6-tetra-*O*-acetyl-β-D-glucopyranose (**4-15**) as a white solid (22.2 g, 97%). M.p (184-185 °C) ^{1}H NMR (400 MHz, $CDCl_3$): δ 5.95 (d, *J* = 9.5 Hz, 1H, N*H*), 5.65 (d, *J* = 8.8 Hz, 1H, H-1), 5.13 (dd, *J* = 10.4, 9.4 Hz, 1H, H-3), 5.04 (dd, *J* = 9.7, 9.5 Hz, 1H, H-4), 4.24 (m, 1H, H-2), 4.19 (m,1H, H-6_a), 4.07 (dd, *J* = 2.3, 12.4 Hz, H-6_b), 3.57 (m, 1H, H-5), 2.04 (s, 3H, NHAc), 1.97 (s, 12H, 4 x OAc). ^{13}C NMR (101 MHz, $CDCl_3$): δ 171.14, 170.61, 170.16, 169.48, 169.27, 92.55, 72.74 (2C), 68.05, 61.77, 52.91, 23.05, 20.81, 20.57 (3C).

4.5.3 Synthesis of (3aR,5R,6R,7R,7aR)-5-(acetoxymethyl-6,7-diacetoxy-2-methyl-5,6,7,7a-tetra-hydro-3aH-pyrano[3,2-*d*]thiazole (4-16)[20]

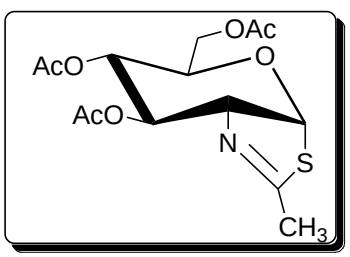

To a solution of 2-acetamido-2-deoxy-1,3,4,6-tetra-*O*-acetyl-β-D-glucopyranose (**4-15**) (3.2 g, 8.22 mmol) in toluene (30 mL) was added Lawesson's reagent (2.1 g, 5.4 mmol). The reaction mixture was heated at 80 °C for

1.5 hr, after which the pH of the reaction was adjusted by the addition of sodium bicarbonate (3.0 g, 35.7 mmol). The reaction mixture was concentrated under reduced pressure. Purification by chromatography using a silica-gel column (320 g, EtOAc:DCM, 4:6, R_f 0.2) gave (3aR,5R,6R,7R,7aR)-5-(acetoxymethyl-6,7-diacetoxy-2-methyl-5,6,7,7a-tetra-hydro-3aH-pyrano[3,2-*d*]thiazole (**4-16**) as a golden yellow syrup (2.84 g, 100%). ^{1}H NMR (300 MHz, $CDCl_3$): δ 6.22 (d, *J* = 7.1 Hz, 1H, H-1), δ 5.55 (dd, *J* = 3.4, 1.9 Hz, 1H, H-3), 4.97 (ddd, *J* = 9.5, 1.7, 1.3 Hz, 1H, H-4), 4.45 (m, 1H, H-2), 4.06 (m, 2H, H-6), 3.52 (m, 1H, H-5) 2.28 (s, 3H, C*H*$_3$), 2.11 (s, 3H, OAc) 2.06 (s, 3H, OAc) 2.05 (s, 3H, OAc).^{13}C NMR (101 MHz, $CDCl_3$): δ 170.31, 169.30, 169.03, 167.85, 88.63, 76.53, 70.56, 69.15, 68.28, 63.09, 20.71, 20.63, 20.49, 20.44.

4.5.4 Synthesis of 2-acetamido-2-deoxy-3,4,6-tri-*O*-acetyl-1-thio-α-D-glucopyranose (4-17)[20]

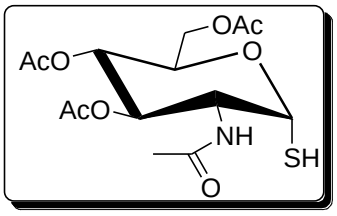

A solution of (3aR,5R,6R,7R,7aR)-5-(acetoxymethyl-6,7-diacetoxy-2-methyl-5,6,7,7a-tetra-hydro-3aH-pyrano[3,2-*d*]thiazole (**4-16**) (1 g, 2.9 mmol) in MeOH (10 mL) was cooled to 0 °C, before addition of TFA (300 μL) and H_2O (300 μL). The reaction mixture was allowed to warm to room temperature over a period of 2 hr. The reaction mixture was concentrated under reduced pressure. Purification by chromatography using a silica-gel column (100 g, EtOAc:DCM; 1:1; R_f 0.4) gave 2-acetamido-2-deoxy-3,4,6-tri-*O*-acetyl-1-thio-α-D-glucopyranose (**4-17**) as an oil (0.988 g, 95%). ^{1}H NMR (400 MHz, $CDCl_3$): δ 7.17 (s, 1H, N-*H*), 5.87 (d, *J* = 8.1 Hz, 1H, H-1), 5.68 (dd, *J* = 7.0, 5.3 Hz, 1H, H-3), 5.02 (m, 2H, H-6), 4.39 (m, 1H, H-5), 4.17 (dd, *J* = 12.3, 4.2 Hz, 1H, H-4), 4.03 (dd, *J* = 12.2, 2.0 Hz, 1H, H-2), 2.01 (s, 3H, 1 x N*H*Ac), 1.94 (s, 9H, 3 x OAc).^{13}C NMR (101 MHz, $CDCl_3$): δ

171.38, 170.74, 170.61, 169.23, 78.68, 70.44, 68.87, 68.20, 61.80, 52.40, 22.79, 20.56, 20.55, 20.44.

4.5.5 Synthesis of (2*R*,3*S*,4*R*,5*R*,6*R*l)-5-acetamido-2-(acetoxymethyl)-6-(prop-2-ynylthio)tetrahydro-2*H*-pyran-3,4-diyl diacetate (4-18)

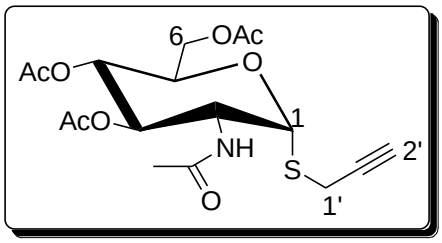

2-Acetamido-2-deoxy-3,4,6-tri-*O*-acetyl-1-thio-α-D-glucopyranose (**4-17**) **(**0.220 g, 0.606 mmol) was dissolved in 4 mL of DCM and 1.1 mol equivalents of triethylamine and propargyl bromide were added to yield (2*R*,3*S*,4*R*,5*R*,6*R*)-5-acetamido-2-(acetoxymethyl)-6-(prop-2-ynylthio)tetrahydro-2*H*-pyran-3,4-diyl diacetate (**4-18**) as cream white crystals (0.187 g, 77%). M.p (175 - 178 °C). ^{1}H NMR (300 MHz, $CDCl_3$) δ 5.94 (d, *J* = 8.6 Hz, 1H, H-1), 5.62 (d, *J* = 5.4 Hz, 1H, H-3), 5.05 (d, *J* = 9.3 Hz, 2H, H-1'), 4.52 (ddd, *J* = 10.6, 8.8, 5.4 Hz, 1H, H-5), 4.25 (m, 2H, H-6), 4.04 (dd, *J* = 12.0, 2.0 Hz, 1H, H-4), 3.44 (m, 1H, H-2), 2.21 (m, 1H, H-2'), 2.10 (s, 3H, NHAc) 2.02 (s, 3H, OAc), 2.01 (s, 3H, OAc), 1.90 (s, 3H, OAc). ^{13}C NMR (75 MHz, $CDCl_3$): δ 171.30, 170.45, 169.99, 169.09, 83.45, 78.66, 76.99, 71.86, 71.00, 68.71, 68.11, 61.68, 52.00, 22.89, 20.47, 19.11, 17.95. HRMS (ESI): *m/z* $C_{17}H_{24}NO_8S$ found: 402.1222 $[M-H]^+$, calculated 402.1223.

4.5.6 Synthesis of *N*-((2*R*,3*R*,5*S*)-tetrahydro-4,5-dihydroxy-6-(hydroxymethyl)-2-(prop-2-ynylthio)-2*H*-pyran-3-yl)acetamide (4-19)

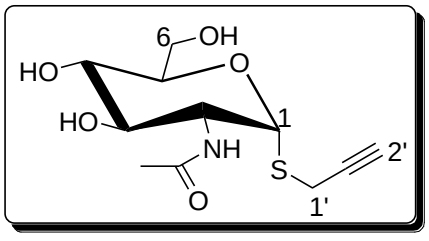

(2*R*,3*S*,4*R*,5*R*,6*R*l)-5-Acetamido-2-(acetoxymethyl)-6-(prop-2-ynylthio)tetrahydro-2*H*-pyran-3,4-diyl diacetate (**4-18**) (0.4 g, 0.997 mmol) was dissolved in 4 mL of methanol,

followed by the addition of NaOMe (0.080 g, 1.448 mmol). The reaction was allowed to stir at room temperature overnight. Subsequently, the reaction was quenched by the addition of amberlyst® A-21 iron-exchange resin (0.5 g). The amberlyst® A-21 iron-exchange resin were filtered at the end of the reaction and the filtrate was concentrated under reduced pressure. Purification by chromatography using a silica-gel column (40 g, MeOH:DCM, 1:9, R_f 0.1) to give *N*-((2*R*,3*R*,5*S*)-tetrahydro-4,5-dihydroxy-6-(hydroxymethyl)-2-(prop-2-ynylthio)-2*H*-pyran-3-yl)acetamide (**4-19**) as a solid (0.20 g, 52%). M.p (176 - 178 °C). ^{1}H NMR (400 MHz, DMSO-d_6): δ 7.87 (s, 1H, N*H*), 5.54 (d, *J* = 5.2 Hz, 1H, H-1), 5.11 (s, 1H, O*H*), 4.85 (s, 1H, O*H*), 4.58 (s, 1H, O*H*), 3.95 – 3.83 (m, 1H, H-2), 3.69 (dd, *J* = 9.2, 4.2 Hz, 2H, H-6), 3.58 – 3.48 (m, 1H, H-5), 3.48 – 3.39 (m, 1H, H-4), 3.30 (dd, *J* = 4.8, 2.4 Hz, 2H, H-1'), 3.10 (s, 1H, H-2'), 1.86 (s, 3H, N*H*Ac).^{13}C NMR (75 MHz, DMSO-d_6): δ 169.40, 81.94, 80.20, 73.53, 73.03, 70.73, 70.67, 60.46, 53.81, 22.32, 15.93. HRMS (ESI): *m/z* $C_{11}H_{17}NO_5S$ found: 275.0826 $[M+H]^+$, calculated 275.0827.

4.5.7 Synthesis of 2,3-*O*-isopropylidine uridine (4-21)[23]

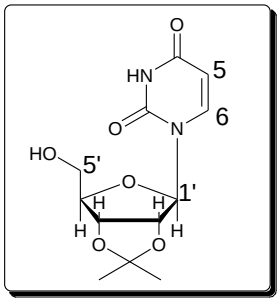

Uridine (**4-20**) (5.0 g, 21.0 mmol) and *p*-toluenesulfonic acid (0.6 g, 3.48 mmol) were added to a flask followed by DMF (68 mL). The reaction was allowed to stir until a complete solution was obtained. 2,2-Dimethoxypropane (10 mL, 82 mmol) was then added to the reaction followed by heating at 65 °C. The reaction was monitored by TLC and was judged to be complete after 2 hr. Approximately 1 g Amberlyst® A-21 ion-exchange resin was added to neutralize the reaction. The reaction mixture was stirred briefly before it was filtered through celite. Subsequently, the filtrate was concentrated under reduced pressure. Purification by chromatography using a silica-gel column (500 g; DCM/MeOH, 10:1) gave 2,3-*O*-

isopropylidine uridine (**4-21**) as a white solid (6 g, 100%). M.p (169 – 161 °C) ^{1}H NMR (300 MHz, $CDCl_3$) δ 7.82 (d, *J* = 8.1 Hz, 1H, H-6), 5.87 (d, *J* = 8.1 Hz, 1H, H-1'), 5.57 (d, *J* = 3.0 Hz, 1H, H-5), 5.04 (dd, *J* = 3.0, 6.6 Hz, 1H, H-2'), 4.98 (dd, *J* = 3.0, 6.6 Hz, 1H, 3'), 4.29 (m, 1H, H- 4'), 3.93 (dd, *J* = 2.4, 12.0 Hz, 1H, H-5'$_{\alpha}$), 3.81 (dd, *J* = 3.5, 12.0 Hz, 1H, H-5'$_{\beta}$), 2.17 (s, 1H, O*H*), 1.58 (s, 3H, C*H*$_3$), 1.36 (s, 3H, C*H*$_3$). ^{13}C NMR (101 MHz, $CDCl_3$) δ 166.19, 152.05, 143.88, 114.90, 102.39, 94.15, 88.34, 85.79, 82.19, 63.03, 27.58, 25.54.

4.5.8 Synthesis of 2,3-*O*-isopropylidine-5-*O*-toluenesulfonyluridine (4-22)[23]

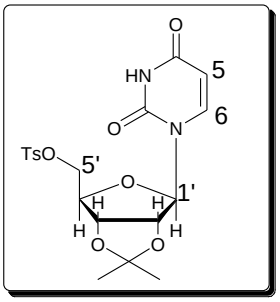

2,3-*O*-Isopropylidine uridine (**4-21**) (4.1 g, 14.4 mmol) was suspended in DCM (58 mL) and subsequently pyridine (11.7 mL, 114 mmol) was added resulting in complete dissolution. *p*-Toluenesulfonyl chloride (TsCl) (7.5 g, 39.3 mmol) was added to the reaction and the solution turned yellowish and slightly warm. The reaction was heated by the reflux for approximately 2 hr, at which point it was judged to be complete by TLC (DCM: MeOH 10:1). The reaction was diluted with 250 mL of DCM and washed with 0.5 M HCl (5 x 100 mL) and saturated $NaHCO_3$ (2 x 100 mL) followed by the drying of the organic layer over Na_2SO_4. The solvent was concentrated under reduced pressure. Purification by chromatography using a silica-gel column (400 g; MeOH:DCM, 1–5% gradient) gave 2,3-*O*-isopropylidine-5-*O*-toluenesulfonyluridine (**4-22**) as a white solid (5.87 g, 93 %). M.p (145 – 147 °C) ^{1}H NMR (400 MHz, $CDCl_3$) δ 9.06 (s, 1H, NH), 7.78 (d, *J* = 8.3 Hz, 2H, Ts), 7.34 (d, *J* = 8.0 Hz, 2H, Ts), 7.25 (m, 1H, H-6), 5.71 (d, *J* = 8.0 Hz, 1H, H-1'), 5.66 (d, *J* = 2.1 Hz, 1H, H-5), 4.93 (dd, *J* = 2.4, 6.4 Hz, 1H, H-2'), 4.79 (dd, *J* = 3.6, 6.4 Hz, 1H, H-3'), 4.35 (m, 1H, H-4'), 3.74 (m, 1H, H-5'$_{\alpha}$), 3.55 (m, 1H, H-5'$_{\beta}$), 2.45 (s, 3H, OTs), 1.55 (s, 3H, C*H*$_3$), 1.34 (s, 3H, C*H*$_3$). ^{13}C NMR (101 MHz, $CDCl_3$)

163.82, 150.17, 145.30, 142.73, 132.66, 129.91, 127.96, 115.01, 103.11, 95.27, 84.89, 84.31, 80.81, 69.18, 27.03, 25.20, 21.71.

4.5.9 Synthesis of 5-azido-deoxy-2,3-*O*-isopropylidene uridine (4-23)[23]

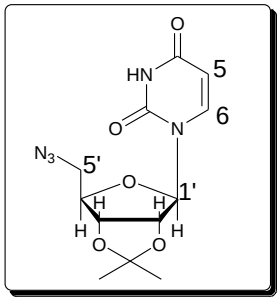

2,3-*O*-Isopropylidine-5-*O*-toluenesulfonyluridine (**4-22**) (6.0 g, 14 mmol) was dissolved in DMF (34 mL) followed by the addition of NaN_3 (3.4 g, 68 mmol). The suspension was allowed to stir overnight at 65 °C. Upon the completion of the reaction water was added to the reaction mixture and the aqueous solution was extracted with ethyl acetate (3 x). The organic layers were combined and dried over $MgSO_4$. Subsequently the organic solvent was concentrated under reduced pressure. Purification by chromatography using a silica-gel column (600 g; MeOH:DCM, 1 – 5%) gave 5-azido-deoxy-2,3-*O*-isopropylidene uridine (**4-23**) as a white solid (4.2 g, 98%). M.p (108-110 °C) ^{1}H NMR (400 MHz, $CDCl_3$) δ 10.03 (s, 1H, N-*H*), 7.31 (d, *J* = 8.0, 1H, H-6), 5.76 (d, *J* = 8.0 Hz, 1H, H-1'), 5.67 (d, *J* = 2.4 Hz, 1H, H-5), 5.01 (dd, *J* = 4.0, 6.4 Hz, 1H, H-2'), 4.82 (dd, *J* = 4.0, 6.4 Hz, 1H, H-3'), 4.24 (m, 1H, H-4'), 3.66 (d, *J* = 5.6, 2H, H-5'), 1.56 (s, 3H, C*H*$_3$), δ 1.34 (s, 3H, C*H*$_3$).^{13}C NMR (101 MHz, $CDCl_3$) δ 163.21, 150.03, 142.31, 114.82, 102.89, 94.72, 85.75, 84.31, 81.49, 52.36, 27.10, 25.25.

4.5.10 Synthesis of 5-azido-5-deoxy uridine (4-24)[23]

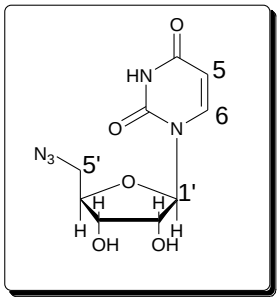

5-Azido-deoxy-2,3-*O*-isopropylidene uridine (**4-23**) (2.6 g, 8.41 mmol) was added to 90 % TFA/water (50 mL). The reaction mixture was monitored by TLC (DCM:MeOH, 6:1) and judged to be complete within 20 minutes. The reaction mixture was concentrated under reduced pressure. Purification

by chromatography using a silica-gel column (250 g;.MeOH/DCM, 1–5% gradient) gave 5-azido-5-deoxy uridine (**4-24**) as a white glasslike product (2.14 g, 95 %). M.p (150-151 °C, Lit[33] 150-150.5 °C) ^{1}H NMR (300 MHz, DMSO) δ 11.29 (s, 1H, N-*H*), 7.70 (d, *J* = 9.0 Hz, 1H, H-6), 5.82 (d, *J* = 5.4 Hz, 1H, H-1'), 5.71 (dd, *J* = 2.4, 8.1 Hz, 1H, H-5), 5.30 (s, 2H, O*H*), 4.22 (m, 1H, H-2'), 4.10 (m, 1H, H-3'), 4.00 (m, 1H, H-4'), 3.70 (dd, *J* = 3.2, 13.4 Hz, H-5').^{13}C NMR (101 MHz, $CDCl_3$) δ 166.05, 142.61, 125.23, 101.62, 91.70, 83.71, 74.77, 71.68, 53.01.

4.5.11 Synthesis of [1'-(5''-deoxyuridin)-1'*H*-1',2',3'-triazol-4'-yl] methyl 1-thio-2-acetamido-2-deoxy-α-D-glucopyranoside (4-25)

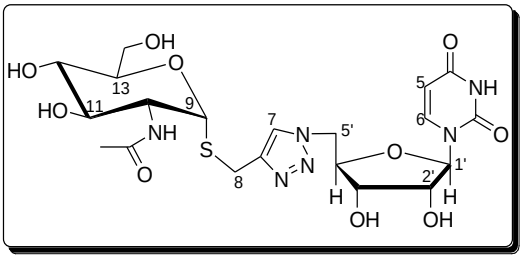

To a solution of product *N*-((2*R*,3*R*,5*S*)-tetrahydro-4,5-dihydroxy-6-(hydroxymethyl)-2-(prop-2-ynylthio)-2*H*-pyran-3-yl)acetamide (**4-19**) (0.0325 g, 0.5 mmol) and 5'-adizo-5'-deoxyuridine (**4-24**) (0.0337 g, 0.5 mmol) in a 1:1 mixture of water and *tert*-butyl alcohol (1 mL) at room temperature was added sodium ascorbate (300 µL of freshly prepared 1 M solution in water, 0.1 mmol) and copper (II) sulphate pentahydrate (300 µL of freshly prepared 0.1 M solution in water, 0.1 mmol). After 72 hr, the product was formed and the reaction mixture was concentrated under reduced pressure. Purification by chromatography using a silica-gel column (3 g;.MeOH/DCM, 1: 6) to give [1'-(5''-deoxyuridin)-1'*H*-1',2',3'-triazol-4'-yl] methyl 1-thio-2-acetamido-2-deoxy-α-D-glucopyranoside (**4-25**) as an oil (0.090 g, 33%). ^{1}H NMR (400 MHz, D_2O) δ 7.90 (s, 1H, H-7), 7.27 (d, *J* = 8.2 Hz, 1H, H-6), 5.79 (d, *J* = 7.9 Hz, 1H, H-1'), 5.71 (d, *J* = 3.4 Hz, 1H, H-5), 5.26 (d, *J* = 5.5 Hz, 1H, H-9), 4.25 (m, 1H, H-2'), 4.08 (m, 1H, H-11), 4.05 (m, 1H, H-10), 3.96 (m, 1H, H-5'), 3.82 (dd,

1H, H-14$_{a'}$), 3.76 (m, 1H, H-13), 3.74 (m, 1H, H-5'), 3.72 (s, 2H, H-8), 3.65 (m, 1H, H-3'), 3.54 (dd, 1H, H-14$_{b'}$), 36 (m, 1H, 12), 1.89 (s, 3H, NHAc). ^{13}C NMR (75 MHz, D_2O): δ 174.15, 166.21, 151.53, 142.36, 142.12, 125.41, 102.61, 91.47, 90.12, 80.88, 77.56, 76.63, 72.59, 71.92, 70.34, 58.64, 53.87, 51.50, 50.75, 21.83. HRMS (ESI): *m/z* $C_{20}H_{29}N_6O_{10}S$ found: 545.1663 $[M+H]^+$, calculated 545.1666.

4.5.12 Synthesis of N-(tetrahydro-2,4,5-trihydroxy-6-(hydroxymethyl)-2H-pyran-3-yl)acetamide (4-27)

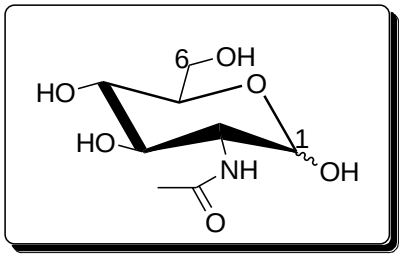

Glucosamine hydrochloride (**4-26**) (5 g, 23.2 mmol) was dissolved in NaOMe which was further diluted to a 0.5 M solution using methanol (50 mL). The mixture was allowed to stir for 1 hr at room temperature before acetic anhydride (1.5 equiv) was added. The mixture was allowed to shake gently overnight, after which a milky solution was produced, filtration and storage of the filtrate at -41 °C resulted in the crystallization of the desired product *N*-acetyl-D-glucosamine (**4-27**). R_f 0.2 (MeOH/DCM, 1:4).

4.5.13 Synthesis of *N*-((2S,3R,5S)-tetrahydro-4,5-dihydroxy-6-(hydroxymethyl)-2-(prop-2-ynyloxy)-2H-pyran-3-yl)acetamide (4-28)[25]

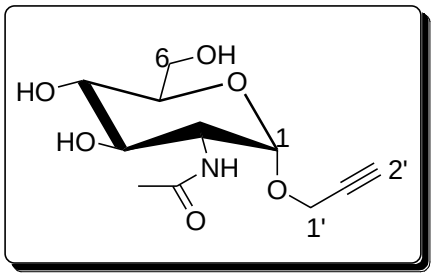

H_2SO_4-silica[28] (6 g) was added to a stirred suspension of *N*-acetyl-D-glucosamine (**4-27**) (1 g, 4.52 mmol) in propargyl alcohol (4 mL). The reaction mixture was allowed to stir at 65 °C overnight. The reaction was monitored using TLC (MeOH/DCM, 1:4) and the reaction mixture was concentrated in vacuo upon the completion. The residue was purified using the silica gel column chromatography (100g; MeoH/DCM, 1:4) followed by

recrystallization in methanol to give the desired product *N*-((2S,3R,5S)-tetrahydro-4,5-dihydroxy-6-(hydroxymethyl)-2-(prop-2-ynyloxy)-2H-pyran-3-yl)acetamide (**4-28**) as a white solid (0.260 g, 22%). M.p (173 – 175 °C, Lit 172 – 173 °C). ^{1}H NMR (300 MHz, MeOH) δ 4.98 (d, *J* = 3.8 Hz, 1H, H-1), 4.25 (1H, dd, *J* = 2.3 Hz, J = 16.1 Hz, H-1'$_a$), 4.24 (1H, dd, *J* = 2.3 Hz, J = 16.1 Hz, H-1'$_b$), 3.94 (1H, dd, *J* = 3.8 Hz, *J* = 10.7 Hz, H-2), 3.85 (1H, dd, *J* = 2.2 Hz, *J* = 12.3 Hz, H-6), 3.77 (1H,dd, *J* = 5.0 Hz, *J* = 12.3, H-6), 3.69–3.72 (2H, m, H-3, H-5), 3.47 (t, *J* = 9.5 Hz, 1H, H-4), 2.83 (t, *J* = 2.3 Hz, 1H, H-2'), 2.01 (s, 3H, N*HAc*). ^{13}C NMR (125 MHz, MeOH): δ 174.53, 95.93, 79.04, 75.77, 72.28, 70.88, 69.79, 60.32, 55.10, 53.39, 21.83.

4.5.14 Synthesis of [1'-(5''-deoxyuridin)-1'*H*-1',2',3'-triazol-4'-yl] methyl 2-acetamido-2-deoxy-α-D-glucopyranoside (4-29)[25]

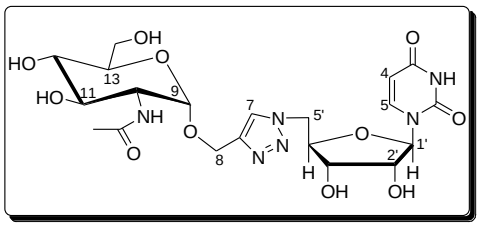

To a solution of product *N*-((2S,3R,5S)-tetrahydro-4,5-dihydroxy-6-(hydroxymethyl)-2-(prop-2-ynyloxy)-2H-pyran-3-yl)acetamide (**4-28**) (0.0325 g, 0.5 mmol) and 5'-adizo-5'-deoxyuridine (**24**) (0.0337 g, 0.5 mmol) in a 1:1 mixture of water and *tert*-butyl alcohol (1 mL) at room temperature was added sodium ascorbate (300 μL freshly prepared 1 M solution in water, 0.1 mmol) and copper (II) sulphate pentahydrate (300 μL freshly prepared 0.1 M solution in water, 0.1 mmol). After 72 hr, the product was formed and the reaction mixture was concentrated under reduced pressure. Purification by chromatography using a silica-gel column (3 g; MeOH/DCM, 1: 6) to give [1'-(5''-deoxyuridin)-1'*H*-1',2',3'-triazol-4'-yl] methyl 2-acetamido-2-deoxy-α-D-glucopyranoside (**4-29**) as an oil (33%). ^{1}H NMR (400 MHz, DMSO-d$_6$) δ 8.01 (s, 1H), 7.32 (d, *J* = 8.2 Hz, 1H), 5.77 (d, *J* = 8.2 Hz, 1H), 5.69 (d, *J* = 3.6 Hz, 1H), 4.87 (d, *J* = 3.8 Hz, 1H), 4.68 (1H, d, *J* = 12.9 Hz), 4.78–4.74 (m, 2H), 4.86 (1H, dd, J = 3.3 Hz, J = 15.0 Hz,), 4.36–4.31 (m, 1H), 4.30

(dd, *J* = 3.6 Hz, *J* = 5.7 Hz, 1H), 4.12 (t, *J* = 6.3 Hz, 1H), 3.85 (1H, dd, *J* = 3.8 Hz, *J* = 10.7 Hz), 3.65–3.76 (m, 3H), 3.55–3.59 (1H, ddd, *J* = 10 Hz, *J* = 4.4 Hz, *J* = 2.8 Hz), 3.42 (t, *J* =10 Hz, 1H), 1.89 (s, 3H). ^{13}C NMR (125 MHz, D_2O): δ 174.18, 166.09, 151.19, 143.78, 142.53, 126.08, 102.18, 96.21, 91.53, 80.69, 72.47, 72.11, 70.79, 69.88, 69.77, 60.38, 60.01, 53.47, 50.81, 21.69.

4.5.15 Synthesis of chloromethyl 3,4,6-tri-*O*-acetyl-2-acetamido-2-deoxy-1-thio-α-D–glucopyranoside (4-30)[25,26]

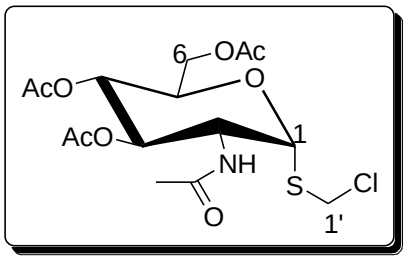

To a solution of 2-acetamido-2-deoxy-3,4,6-tri-*O*-acetyl-1-α-thio-D-glucopyranose (**4-17**) (1 g, 2.75 mmol) in anhydrous DCM (46 mL) was added DBU (0.5 mL, 3.3 mmol). The reaction mixture was allowed to stir overnight at room temperature, after which the TLC indicated the disappearance of the starting material. The reaction mixture was concentrated under reduced pressure. Purification by chromatography using a silica-gel column (100 g; EtOAc/Pet ether, 2:1) gave the desired product chloromethyl 3,4,6-tri-*O*-acetyl-2-acetamido-2-deoxy-1-thio-α-D–glucopyranoside (**4-30**) as a off-white foam, (0.486 g, 43%). ^{1}H NMR (300 MHz, $CDCl_3$): δ 5.87 (d, *J* = 8.2 Hz, 1H, H-1), 5.67 (d, *J* = 5.5 Hz, 1H, H-3), 5.04 (d, 9.3 Hz, 2H, H-1'), 4.48 (ddd, *J* = 10.6, 8.3, 5.6 Hz, 1H, H-2), 4.23 (ddd, *J* = 13.6, 6.5, 3.5 Hz, 2H, H-6), 4.04 (dd, *J* = 13.0, 3.2 Hz, 1H, H-5), 3.70 (m, 1H, H-4), 2.03 (s, 3H, NHAc), (s, 9H, 3 x 3 OAc). ^{13}C NMR (75 MHz, $CDCl_3$): δ 171.40, 170.39, 170.17, 169.13, 81.84, 71.18, 68.66, 61.80, 51.91, 29.99, 22.84, 20.53, 20.52. 20.41.

4.5.16 Synthesis of diethyl (3,4,6-tri-*O*-acetyl-2-acetamido-2-deoxy-α-D-glucopyranosylthiomethyl) phosphonate (4-31)[26]

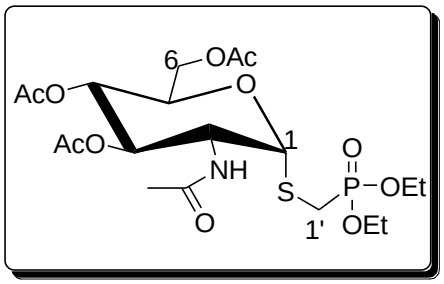

Chloromethyl 3,4,6-tri-*O*-acetyl-2-acetamido-2-deoxy-1-thio-α-D–glucopyranoside (**4-30**) (0.381 g, 0.930 mmol) was refluxed in $P(OEt)_3$ (7.3 mL) at 160 °C for 48 hr. The reaction mixture was concentrated under reduced pressure. Purification by chromatography using a silica-gel column (40 g; toluene:acetone, 5:1) to give diethyl (3,4,6-tri-*O*-acetyl-2-acetamido-2-deoxy-α-D-glucopyranosylthiomethyl) phosphonate (**4-31**) as a white amorphous solid (0.309 g, 65%). ^{1}H NMR (400MHz, $CDCl_3$) δ 6.24 (d, J = 7.1 Hz, 1H), 5.76 (d, J = 5.1 Hz, 1H), 5.17 (m, 2H), 4.47 (m, 1H), 4.30 (m, 1H), 4.24 (m, 1H), 4.11 (m, 5H), 3.55 (m, 1H), 3.48 (m, 1H), 2.10, 2.05, 2.04, 1.96 (4s, 12H), 1.25 (t, J = 7.1 Hz, 6H). ^{13}C NMR (101 MHz, $CDCl_3$): δ 170.08, 169.88, 169.79, 168.83, 82.71, 75.12, 73.14, 68.18, 62.68, 62.12, 61.68, 52.23, 21.11, 20.03, 19.97, 15.83, 15.67.

4.5.17 Synthesis of bis-2,6-lutidinium (3,4,6-tri-*O*-acetyl-2-acetamido-2-deoxy-α-D-glucopyranosylthiomethyl) phosphonate (4-32)[26]

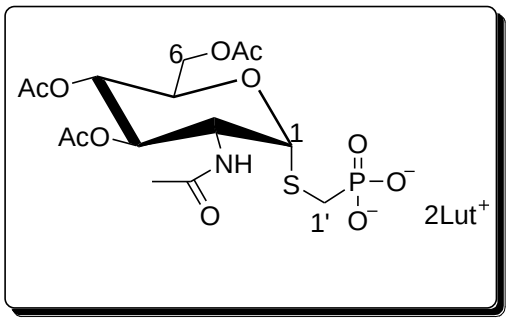

To a stirred solution of diethyl (3,4,6-tri-*O*-acetyl-2-acetamido-2-deoxy-α-D-glucopyranosylthiomethyl) phosphonate (**4-31**) (7.7 g, 15.0 mmol) in dry CH_3CN (8.6 mL) was added 2,6-lutidine (2.58 mL, 2.4 mmol) under N_2 gas. After cooling at 0 °C, TMSBr (2.37 mL, 1.9 mmol) was added dropwise to the mixture. The cooling bath was removed after 30 min, and the reaction mixture was allowed to stir at room temperature for 24 hr. The solvent was removed under reduced pressure and the residue was azeotroped several times with dry CH_3CN

to give bis-2,6-lutidinium (3,4,6-tri-*O*-acetyl-2-acetamido-2-deoxy-α-D-glucopyranosylthiomethyl) phosphonate (**4-32**) as a white solid (6.6 g, 97%). The litidium salt was used in the next reaction without any further purification.

4.5.18 Synthesis of (2-acetamido-2-deoxy-α-d-glucopyranosylthiomethyl) phosphonate (4-33)

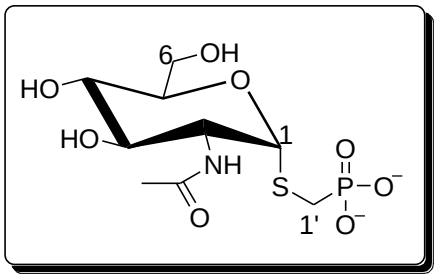

To a stirred solution of bis-2,6-lutidinium (3,4,6-tri-*O*-acetyl-2-acetamido-2-deoxy-α-D-glucopyranosylthiomethyl) phosphonate (**4-32**) (2.0 g, 6.08 mmol) in methanol (4 mL) was added NaOMe (0.149 g, 2.8 mmol). The reaction mixture was allowed to stir at room temperature for overnight. The following day the reaction mixture was neutralized by the addition of Dowex iron exchange resins and equivalent volume of water. The solution was filtered and lyopholized to give 2-acetamido-2-deoxy-α-d-glucopyranosylthiomethyl phosphonate (**4-33**). ^{1}H NMR (400MHz, D_2O): δ 5.08 (d, *J* = 5.7 Hz, 1H, H-1), 3.86 (d, *J* = 9.9 Hz, 2H, H-2, H-3), 3.63 (m, 1H), 3.56 (m, 2H), 3.16 (t, *J* = 9.5 Hz, 1H, H-4), 2.25 (m, 2H, H-1') 1.78 (s, 3 H, NHAc).

4.5.19 Synthesis of bis-triethylammonium uridin-5'-yl (2-acetamido-2-deoxy-α-D-glucopyranosylthiomethylphosphono) phosphate (4-34)[26]

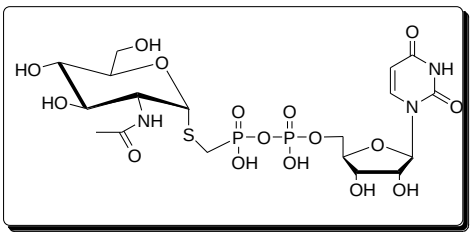

The crude lutidium salt (**4-33**) (148 mg, 0.22 mmol) was coevaporated several times with dry pyridine. After addition of 4-morpholine-*N,N*-dicyclohexylcarboxamidinium uridine 5'-monophosphomorpholidate (0.165 g, 0.24 mmol), the mixture was again coevaporated twice with dry pyridine, then dried under high vacuum for several

hours. Subsequently, the solid was taken up in dry pyridine (6 mL) under nitrogen gas and to this solution pre-dried 1*H*-tetrazole (0.031 g, 0.44 mmol) was added. After the solution was allowed to stir at room temperature for three days, Hünigs base (0.17 mL, 0.99 mmol) and water (6 mL) were added, and then the solution was concentrated under reduced pressure. The residue was coevaporated again with the same amount of Hünigs base-water and dried under vacuum. ^{1}H NMR (400 MHz, D_2O): δ 7.50 (d, *J* = 8.1 Hz, 1H), 5.53 (d, *J* = 7.1 Hz, 2H), 5.23 (d, *J* = 5.4 Hz, 1H), 4.85 (t, *J* = 10.3 Hz, 1H), 4.73 (t, *J* = 9.7 Hz, 1H), 4.36 (dd, *J* = 10.7, 4.3 Hz, 2H), 4.23 (dd, *J* = 12.7, 3.3 Hz, 1H), 4.12 (m, 4H), 3.89 (m, 1H), 3.90 (d, *J* = 12.3 Hz, 1H), 2.74 (t, *J* = 14.3 Hz, 1H), 2.64 (t, *J* = 14.2 Hz, 1H). ^{13}C NMR (101 MHz, D_2O): δ 174.41, 166.49, 151.09, 141.01, 102.01, 87.79, 83.20, 81.89, 73.22, 71.79, 70.31, 69.69, 69.09, 63.90, 59.90, 53.11, 24.89, 21.29.

4.6 References:

1. **Compain, P. and Martin, O. R. 2003.** Design, synthesis and biological evaluation of iminosugar-based glycosyltransferase inhibitors. *Current Topics in Medicinal Chemistry*. **3**: 541-560.
2. **Qian, X. and Palcic, M. M. 2000.** Glycosyltransferase inhibitors. In *Carbohydrates in Chemistry and* Biology. Wiley-VCH: Weinheim, **3**: 293-312.
3. **Zou, W. 2005.** *C*-glycosides and aza-*C*-glycosides as potential glycosidase and glycosyltransferase inhibitors. *Current Topics in Medicinal Chemistry*. **5**: 1363-1391.
4. **Sears, P. and Wong, C. H. 1999.** Carbohydrate mimetics: A new strategy for tackling the problem of carbohydrate-mediated biological recognition. *Angewandte Chemie International Edition*. **38**: 2301-2324.
5. **Qiao, L., Murray, B. W., Shimazaki, M., Schultz, J. and Wong, C-H. 1996.** Synergistic inhibition of human α-1,3-fucosyltransferase V. *Journal of the American Chemical Society*. **118:** 7653-7662.
6. **Wang, R., Steensma, D. H., Takaoka, Y., Yun, J. W., Kajimoto, T and Wong, C-H. 1997.** A search for pyrophosphate mimics for the development of substrates and inhibitors of glycosyltransferases. *Bioorganic and Medicinal Chemistry*. **4:** 661-672.
7. **Kimura, K. and Bugg, T. D. H. 2003.** Recent advances in antimicrobial nucleoside antibiotics targeting cell wall biosynthesis. *Nature Products Reports*. **20**: 252–273.
8. **Ünligil, U. M. and Rini, J. M. 2000.** Glycosyltransferase structure and mechanism. *Current Opinion in Structural Biology*. **10**: 510-517.

9. **Compain, P. and Martin, O. R. 2001.** Carbohydrate mimetics-based glycosyltransferase inhibitors. *Bioorganic and Medicinal Chemistry*. **9**: 3077-3092.

10. **Vetting, M. W., Frantom, P. A. and Blanchard, J. S. 2008.** Structural and enzymatic analyses of MshA from *Corynebacterium glutamicum*: Substrate-assisted catalysis. *Journal of Biochemistry and Molecular Biology*. **283**(23): 15834-15844.

11. **Frantom, P. A., Coward, J. K. and Blanchard, J. S. 2010.** UDP-(5F)-GlcNAc acts as a slow-binding inhibitor of MshA, a retaining glycosyltransferase. *Journal of the American Chemical Society*. **132**: 6626–6627.

12. **El Ashry, E. S. H., Awad, L. F., Abdel Hamid, H. M. and Atta. A. I. 2006.** Microwave irradiation for accelerating the synthesis of thioglycosides. *Synthetic Communications*. **36**: 2769–2785.

13. **Cohen, S. B. and Halcomb, R. L. 2000.** Synthesis and characterization of an anomeric sulfur analogue of CMP-sialic acid. *The Journal of Organic Chemistry*. **65**(19): 6145–6152.

14. **Driquez, H. 2001.** Thiooligosaccharides as tools for structural biology. *ChemBioChem*. **2**(5): 311-318.

15. **Fugedi, R. and Levy, D. E. 2006.** The organic Chemistry of sugars. *CRC Press*, New York, pp. 90-93, 102-104.

16. **Juaristi, E. and Cuevas, G. 1995.** The anomeric effect. *CRC Press*, USA, pp. 4, 8.

17. **Castro-Palomino, J. C. and Schmidt, R. R. 2000.** *N*-Thiodiglycoloyl derivatives of glucosamine as glycosyl donors. *Tetrahedron Letters*. **4**: 629–632.

18. **Bernardes, G. J. L., Gamblin, D. P. and Davis, B. G. 2006.** The direct formation of glycosyl thiols from reducing sugars allows one-pot protein glycoconjugation. *Angewandte Chemie International Edition*. **45**: 4007–4011.

19. **Knapp, S. and Myers, D. S. 2002.** Synthesis of α-GalNAc thioconjugates from an α-GalNAc mercaptan. *Journal of Organic Chemistry*. **67**: 2992-2999.

20. **Knapp, S. and Myers, D. S. 2001.** α-GlcNAc thioconjugates. *Journal of Organic Chemistry*. **66**: 3636-3638.

21. **Myszka, H., Bednarczky, D., Najder, M. and Kaca, W. 2003.** Synthesis and induction of apoptosis in B cell chronic leukemia by diosgenyl 2-amino-2-deoxy-β-D-glucopyranoside hydrochloride and its derivatives. *Carbohydrates Research*. **338**: 133-141.

22. **Knapp, S., Gonzalez, S., Myers, D. S., Eckman, L. L. and Bewley, C. A. 2002.** Shortcut to mycothiol analogues. *Organic Letters*. **4**: 4337-4339.

23. **Winans, K. A. and Bertozzi, C. R. 2002.** An inhibitor of the human UDP-GlcNAc 4-epimerase identified from uridine-based library: A strategy to inhibit *O*-linked glycosylation. *Chemistry and Biology*. **9**: 113-129.

24. **Horton, D. and Wander, J. D. 1980.** The carbohydrates: Chemistry and Biochemistry. *Academic press*: New York, IB. 727-728.

25. **Yeoh, K. K., Butters, T. D., Wilkinson, B. L. and Fairbanks, A. J. 2009.** Probing replacement of pyrophosphate *via* click chemistry; synthesis of UDP-sugar analogues as potential glycosyl transferase inhibitors. *Carbohydrate Research*. **344**: 586–591.

26. **Rowan, A. S., Nicely, N. I., Cochrane, N., Wlassoff, W. A., Claiborne, A. and Hamilton, C. J. 2009.** Nucleoside triphosphate mimicry: a sugar triazolyl nucleoside as an ATP-competitive inhibitor of *B. anthracis* pantothenate kinase. *Organic and Biomolecular Chemistry*. **7**: 4029–4036.

27. **Babic, A. and Pecar, S. 2007.** An improved total synthesis of UDP-*N*-acetyl-muramic acid. *Tetrahedron Letters*. **48**: 4403-4405.

28. **Roy, B. and Mukhopadhyay, B. 2007.** Sulfuric acid immobilized on silica: An excellent catalyst for Fischer type glycosylation. *Tetrahedron Letters*. **48**(22): 3783-3787.

29. **Zhu, X. and Schmidt, R. R. 2004.** Glycosylthiomethyl chloride: A new species for *S*-neoglycoconjugate synthesis. Synthesis of 1-*N*-glycosylthiomethyl-1,2,3-triazoles. *The Journal of Organic Chemistry*. **69**: 1081-1085.

30. **Zhu, X., Stolz, F. and Schmidt, R. R. 2004.** Synthesis of thioglycoside-based UDP-sugar analogues. *The Journal of Organic Chemistry*. **69**: 7367-7370.

31. **Trunkfield, A. E., Gurcha, S. S., Besra, G. S. and Bugg, T. D. H. 2010.** Inhibition of *Escherichia coli* glycosyltransferase MurG and *Mycobacterium tuberculosis* Gal transferase by uridine-linked transition state mimics. *Bioorganic and Medicinal Chemistry*. **18**: 2651–2663.

32. **Kaushal, G. P. and Elbein, A. D. 1986.** Properties of solubilized UDP-GlcNAc: dolichyl phosphate-GlcNAc-1-P-transferase from soybean cultured cells. *Plant Physiology*. **82**: 748-752.

33. **Yamamoto, I., Sekine, M. and Hata, T. 1980.** One-step synthesis of 5'-azido-nucleosides. *Journal of the Chemical Society*. **1**: 306-310.

CHAPTER 5

MshA inhibition studies

5.1 Introduction

In this chapter designed inhibitors reported in Chapters 3 and 4 respectively, are evaluated for their inhibitory effects against MshA. Pure enzyme (MshA) used in conducting enzyme assay inhibition studies was isolated from *Corynebacterium glutamicum* (cgMshA) in a procedure described by Vetting *et al.*[1]

Vetting *et al*.[1] reported the crystal structure coordinates of MshA and subsequent enzymatic studies defined the kinetic parameters of UDP-GlcNAc and 1-L-Ins-1-P substrates for cgMshA. The results corroborated with the previous studies of Newton and co-workers[2] on MshA from a crude extract of *Mycobacterium smegmatis*. The EXPRESSO alignment of cgMshA and tbMshA protein sequence shows that there is 99% sequence similarity (alignment of similar amino acid residues) between the two enzymes. However, for these studies cgMshA was preferred over tbMshA because cgMshA can be obtained in high purity (>95%), thereby reducing any chances that inhibition observed could be due to other contaminants. For the enzyme activity UDP-GlcNAc and 1-L-Ins-1-P were obtained commercially.

5.2 Screening and detection methods for MshA inhibitors

A structure-based, *in silico* search approach to find selective inhibitors for glycosyltransferase MurG was attempted by Walker and co-workers.[3] MurG is a member of the nucleotide-sugar glycosyltransferases (NDP-Gtases) family and this group of enzymes catalyze the transfer of sugars from nucleotides to a wide range of glycosyl acceptors.[4] Walker *et al*. screened a 50 000 component library of compounds to find selective glycosyltransferase MurG inhibitors using a high throughput (HTP)

screening method based on a fluorescent donor displacement assay. In addition, the study showed that the compounds identified in the donor displacement screen on MurG were selective for MurG relative to other enzymes that utilize similar or identical substrates, including the structurally related enzymes.

Considering the success of Walker *et al*. on the structure-based search for selective inhibitors for glycosyltransferase MurG, we envisaged the design of selective inhibitors specific to glycosyltransferase MshA using computer simulated molecular docking (Chapters 3 and 4 respectively). MshA is involved in the formation of 3-phospho-1-D-*myo*-inosityl-2-acetamido-2-deoxy-α-D-glucopyranoside by transferring *N*-acetylglucosamine from UDP-*N*-acetylglucosamine (UDP-GlcNAc) to 1-L-Ins-1-P (Fig. 5-1).

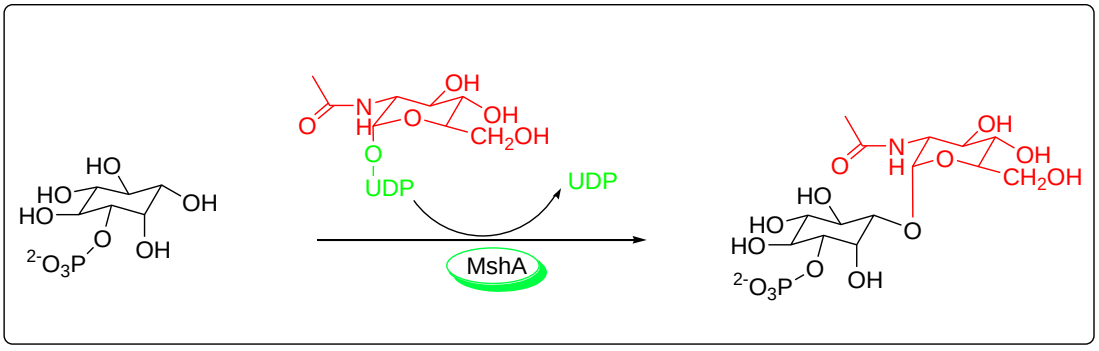

Figure 5-1: MshA catalyzed reaction.

5.2.1 Pyruvate kinase/Lactate dehydrogenase coupled enzyme assay

The pyruvate kinase/lactate dehydrogenase (PK/LDH) coupled enzyme assay is normally used to assay the enzymes that use ATP during the course of the reaction. Vetting *et al.*[1] used PK/LDH coupled enzyme assay to assay the activity of the MshA. The PK/LDH coupled enzyme assay method is based on the measurement of UDP as a byproduct generated during the transglycosylation reaction. During the assay, UDP is coupled to the conversion of NADH into NAD^+ through pyruvate kinase (PK) and

lactate dehydrogenase (LDH); therefore NAD^+ is photometrically measured at 340 nm. The PK/LDH coupled enzyme assay is summarized in Figure 5-2 below.

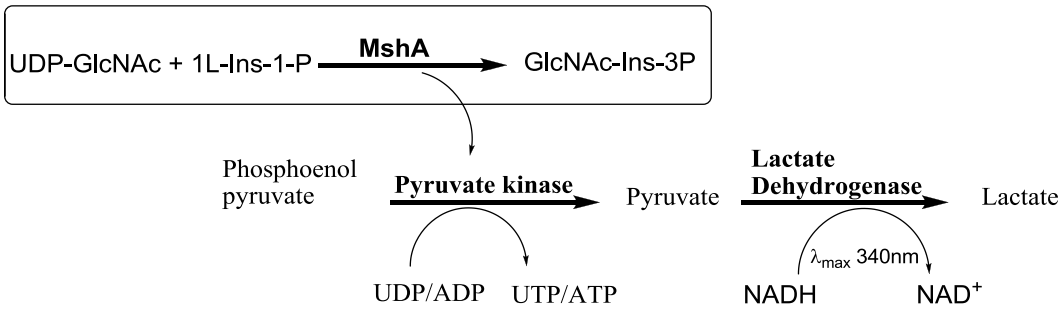

Figure 5-2: Example of coupled enzyme assay.

The rationale to perform PK/LDH coupled enzyme assays was to screen small focused libraries of the structure-based designed compounds for the inhibitory effects against cgMshA. Therefore the library that shows any significant inhibitory effects against cgMshA in PK/LDH coupled enzyme assays would be screened further in a whole cell assay. In other words, the PK/LDH coupled enzyme assay would serve as a platform for the pre-selection of hit compounds for further development and screening.

5.2.1.1 Inhibition studies of cgMshA using the PK/LDH coupled enzyme assay

The PK/LDH coupled enzyme assay was used to determine the inhibition of cgMshA reaction by series of structure based designed inhibitors reported in Chapters 3 and 4 respectively. This was done by measuring the initial rates of the reactions to which inhibitors at a set concentration 100 μM were added and comparing these to the uninhibited cgMshA reaction initial rate. However, the results obtained following the published PK/LDH coupled enzyme assay protocol by Vetting *et al.*[1] exhibited large standard error bars thus making it difficult to reach a logical conclusion.

In an attempt to resolve the assay instability, the method published by Vetting *et al.*[1] was modified by increasing the amount of pyruvate kinase (PK) and phosphoenolpyruvate (PEP) in the reaction mixture. These modifications made the first step of the PK/LDH coupled enzyme assay proceed faster and significantly reduced the standard error bars (Fig. 5-3).

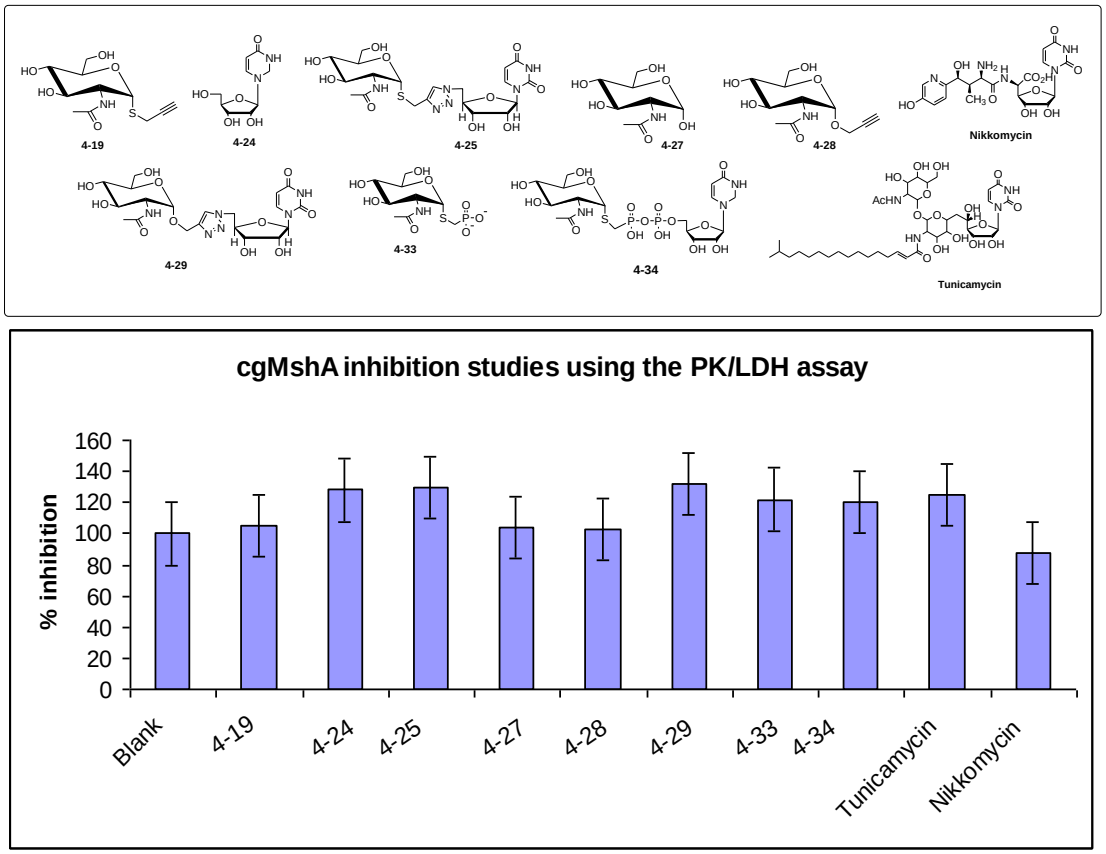

Figure 5-3: Inhibition of cgMshA reaction as determined by the PK/LDH coupled enzyme assay. Inhibition studies perfomed in triplicate, with the uninhibited cgMshA reaction used as a blank. A blank reaction contained cgMshA, UDP-GlcNAc, 1-L-Ins-1-P, TEA enzyme buffer and no inhibitor whereas the reaction mixtures contained cgMshA, UDP-GlcNAc (100 μM), 1-L-Ins-1-P (100 μM), inhibitor. The synthesized inhibitors were tested at 100 μM each whereas the commercially obtained inhibitors (tunicamycin and nikkomycin) were tested at 12 μM and 20 μM respectively.

Apart from large standard error bars, it was also observed that not all the inhibitors reported could be analyzed using the PK/LDH coupled enzyme assay. For example, all the thiazolidinethione derivatives were found to be bright yellow in color (even

when diluted to a lower concentration 100 μM), thus interfering with the change in absorbance occurring during the oxidation of NADH to NAD^+. To confirm the interference of thiazolidinethione derivatives with the oxidation NADH to NAD^+, the ultra violet (UV) spectra of the prepared thiazolidinethione derivatives were studied. The representative compounds from each thiazolidinethione series displayed two absorption bands with maxima at 230 – 270 and 290 - 340 nm (Data not shown). It was against this background that it was concluded that thiazolidinethione absorbance interfere with the absorbance frequency indicative of oxidation of NADH to NAD^+.

Although it was possible to measure the inhibition of the colourless compounds using the PK/LDH coupled enzyme assay method, it has been observed that no statistically significant data differences exist between the inhibitors (substrate mimics) tested and a blank. In some instances, the inhibition levels exceeded the 100% threshold (Fig. 5-3). As a result the PK/LDH coupled enzyme assay method was abandoned and an alternative screening method for cgMshA was required.

5.2.2 Transcreener® ADP^2 FI assay Kit

The Bellbrook Laboratory Transcreener® ADP^2 FI assay kit was identified as an alternative assay method for cgMshA. This assay kit uses an increase in the fluorescent intensity to measure the amount of ADP produced during the enzyme reaction. This is done through ADP displacing the ADP-tracer from a complex in which it is bound to an ADP monoclonal antibody-quencher conjugate leading to an increase in fluorescent intensity. Therefore, the amount of ADP produced is directly proportional to the increase in fluorescent intensity (Fig. 5-4). This assay method was considered ideal due to its reliance on the fluorescent intensity and as such it would allow the assay of the synthesized inhibitors.

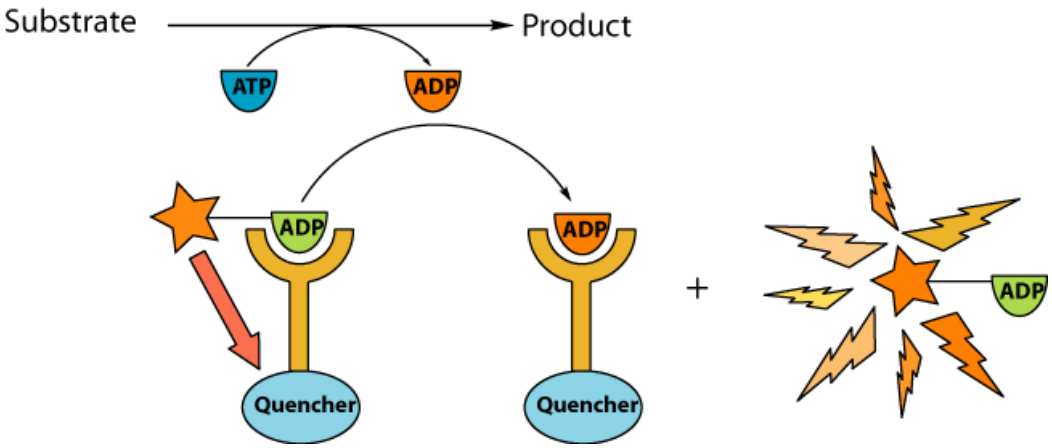

Figure 5-4: Transcreener® ADP² FI assay kit mode of action.

5.2.2.1 UDP standard curve and assay development

The sensitivity of the Transcreener® kit reagent towards UDP had to be tested since UDP is produced during the MshA reaction instead of ADP. Two standard curves were generated to simulate the conversion of ATP to ADP and the conversion of UDP-GlcNAc to UDP respectively. This was done by adding different volumes of 50 µM ATP and ADP together, and 50 µM UDP-GlcNAc and UDP. These different volumes simulate the percentage conversion of 50 µM ATP to 50 µM ADP and 50 µM UDP-GlcNAc to 50 µM UDP respectively. From the percentage conversion standard curve it can be seen that although the conversion of UDP-GlcNAc and UDP could be tracked with the Transcreener® kit, the sensitivity towards UDP was about have half of what it is towards ADP (Fig. 5-5).

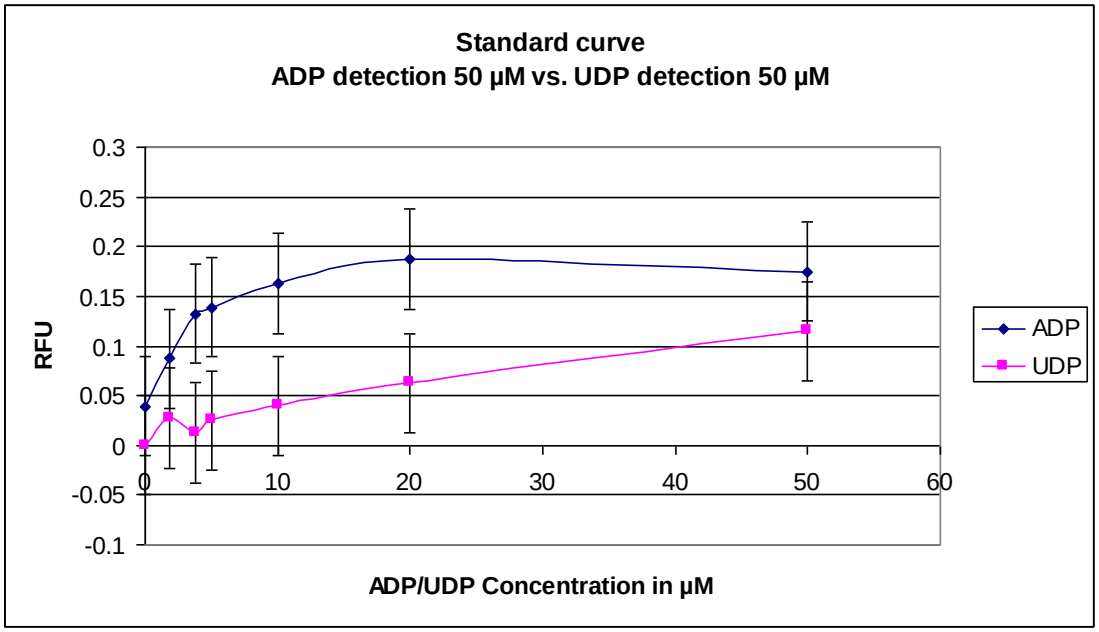

Figure 5-5: Standard curve of the simulated conversion of 100 µM UDP-GlcNAc to 100 µM UDP, compared to simulated conversion of 50 µM ATP to 50 µM ADP.

The results obtained suggest that the Transcreener® kit could not be used for the continuous assay of MshA due to its relatively small increase in fluorescence that corresponded to the increase in UDP concentration from 0 to 50 µM. Hence it was further attempted to improve the sensitivity of the Transcreener® kit towards UDP so that the kit could be used in a non-continuous assay of MshA. Another standard curve was subsequently prepared to simulate the conversion of 100 µM UDP-GlcNAc to 100 µM UDP, i.e. by using double the amount of substrate prescribed by the manufacturer. The simulated conversion of 100 µM UDP-GlcNAc to 100 µM UDP was compared to the simulated conversion of 50 µM ATP to 50 µM ADP (Fig. 5-6). This change has significantly increased the sensitivity of the Transcreener® kit towards UDP.

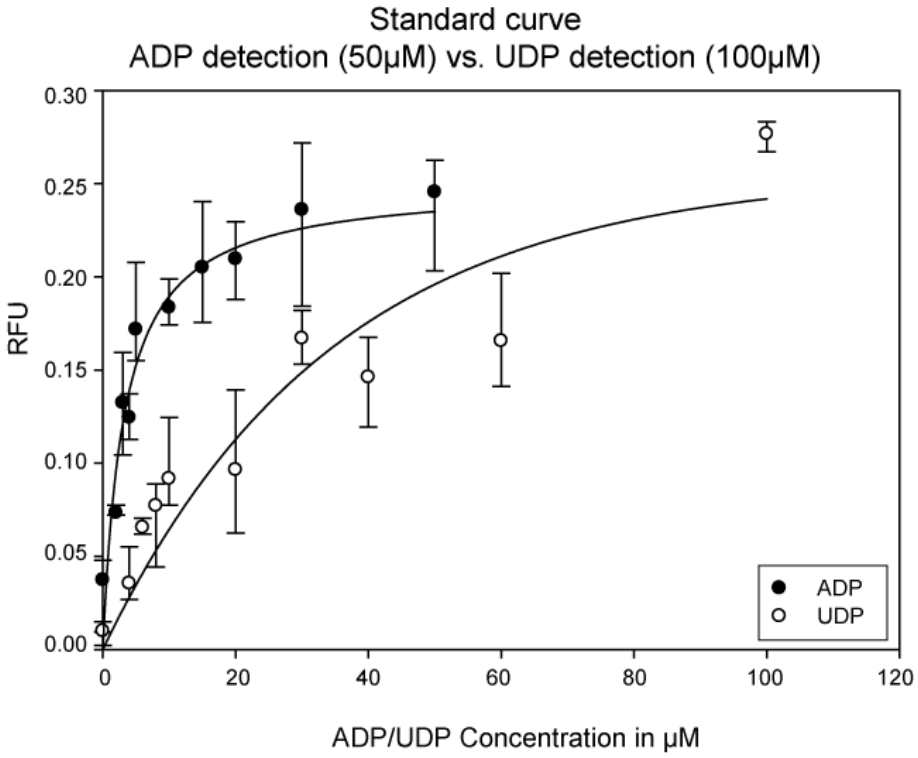

Figure 5-6: Standard curve of the simulated conversion of 100 µM UDP-GlcNAc to 100 µM UDP, compared to simulated conversion of 50 µM ATP to 50 µM ADP.

However, although the sensitivity of the assay was improved, big standard error bars were obtained when the Transcreener® assay was performed in a non-continuous manner. In an attempt to improve the standard error bars of the non-continuous assay, double the amount of antibody-quencher conjugate compared to that prescribed by the manufacturer was used in the detection mixture. Although this has tremendously improved the standard error bars of the non-continuous assay, the sensitivity of the kit towards UDP has slightly dropped (Fig. 5-7). However, the increase in fluorescence due to the increase in UDP was fortunately still large enough to investigate the Transcreener-based non-continuous assay of MshA.

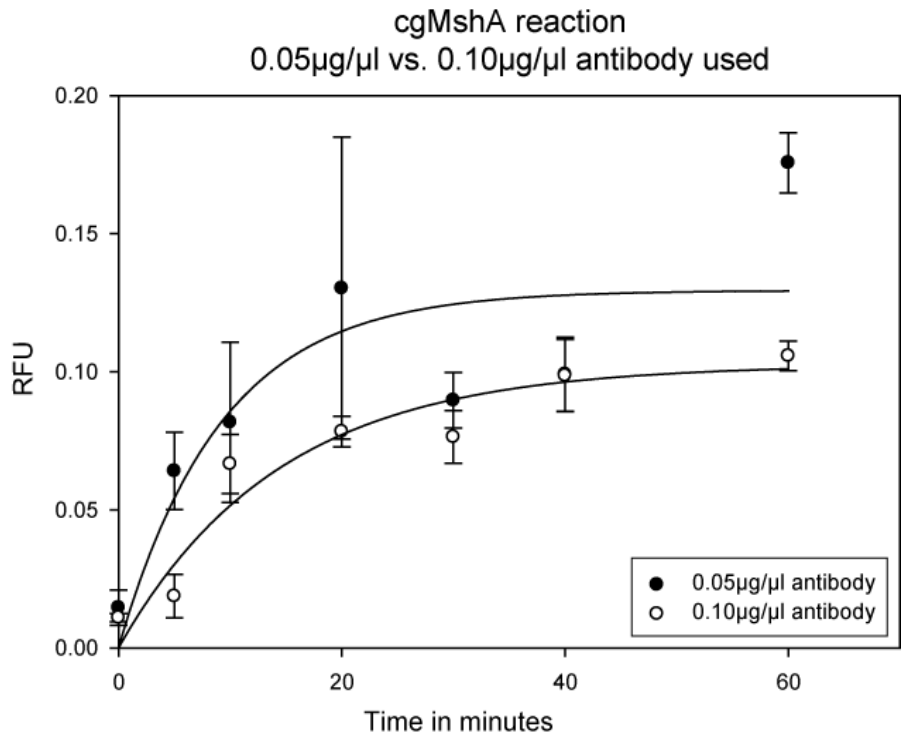

Figure 5-7: cgMshA reaction analyzed with Transcreener® kit. The cgMshA reaction mixtures contained 180 nM cgMshA, 100 µM UDP-GlcNAc, 100 µM 1-L-Ins-1-P and cgMshA assay buffer.

5.2.2.2 Inhibition studies

Having established the optimal conditions for the Transcreener® kit in the non-continuous assay of cgMshA, the next objective was to determine the inhibition of cgMshA by substrate mimics (both commercially obtained and synthesized). The trial inhibition study was done with synthetic substrate mimics (**4-25, 4-34**) and naturally occurring substrate mimics such as tunicamycin and nikkomycin. However, no statistically significant data differences existed between the tested compounds in comparison with the blank, except for substrate mimic (**4-34**). Figure 5-8 shows the trial inhibition studies results obtained using the Transcreener® kit assay.

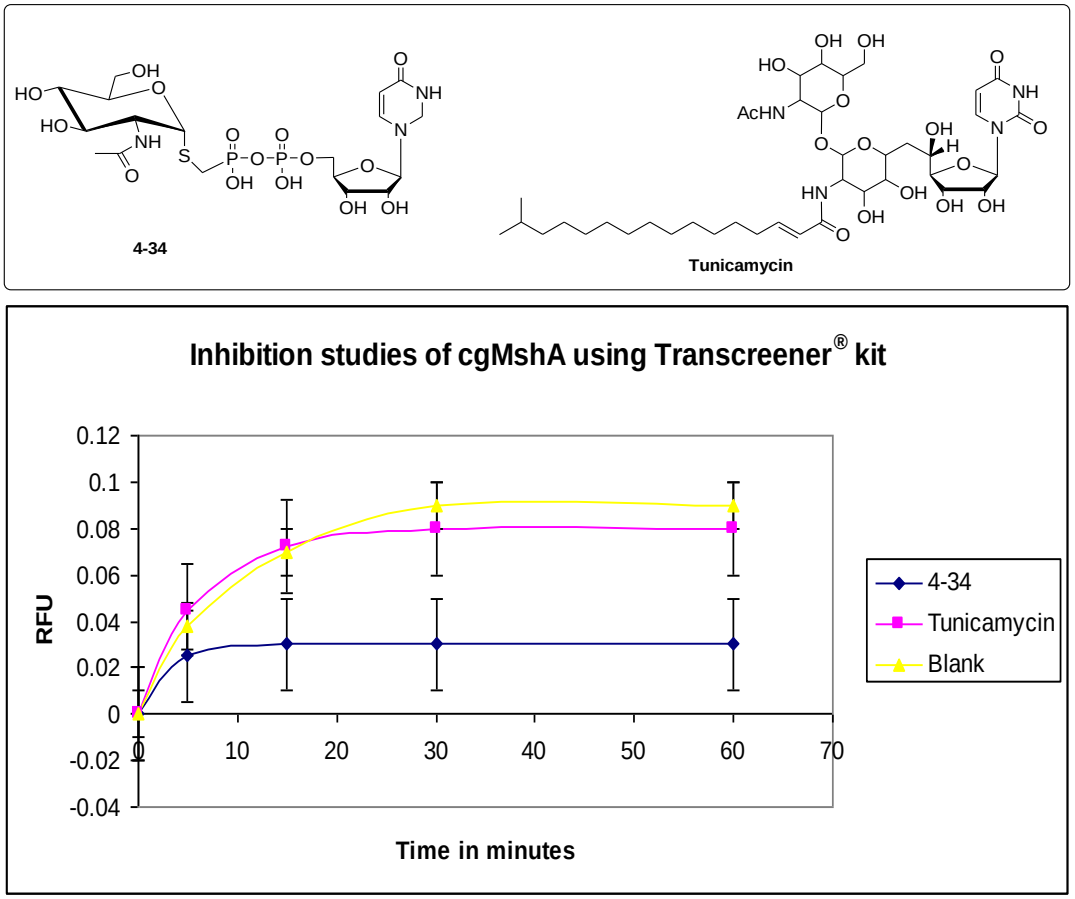

Figure 5-8: Inhibition studies of cgMshA using the Transcreener® kit. A blank reaction contained cgMshA, UDP-GlcNAc, 1-L-Ins-1-P, TEA enzyme buffer and no inhibitor. The reaction mixtures contained cgMshA, UDP-GlcNAc (100 µM), 1-L-Ins-1-P (100 µM), inhibitor and TEA enzyme buffer, all incubated at 37 °C. At specific time intervals 25 µL aliquots were removed, the reaction stopped by heat inactivation of cgMshA and 25 µL Transcreener® kit detection buffer was added. The sample/detection buffer mixture was incubated for 1 hr at room temperature before the fluorescent intensity was measured at λ_{ex} 590nm and λ_{em} 617nm.

Based on the enzyme assay displayed in Figure 5-8, compound **4-34** has strong inhibitory effects against cgMshA whereas tunicamycin demonstrated insignificant inhibitory effects against cgMshA. Furthermore, this assay method could be adopted for screening other libraries of compounds.

Since the trial reaction Transcreener® assay kit in Figure 5-8 has shown that the bulk of enzyme activity occurs in the first 10 minutes, it was decided to reduce the time of the reaction to 5 minutes and to take the 25 μL aliquots at 0, 2 and 5 minute intervals, to ensure that the increase in fluorescence is linear over the measurement interval. Furthermore, a diverse library of compounds has been included in the assay including chromogenic compounds such thiazolidinethione derivatives. The results obtained with substrate mimic **4-34** in both trial and detailed inhibition experiments were consistent and reproducible (Fig. 5-8 and 5-9 respectively).

Tunicamycin was not included in further cgMshA inhibition studies because there was little difference between tunicamycin and the blank in the trial experiment (Fig. 5-8). Thus suggesting that tunicamycin does not bind to MshA and corroborates with the computational study. Full cgMshA inhibition studies results of Transcreener® assay kit are displayed in Figure 5-9. The initial rates for the reactions to which inhibitors were added were compared to the initial rate of an uninhibited reaction and were reported as a percentage inhibition. The percentage inhibition bar charts were drawn using Microsoft® Office Excel® 2007.

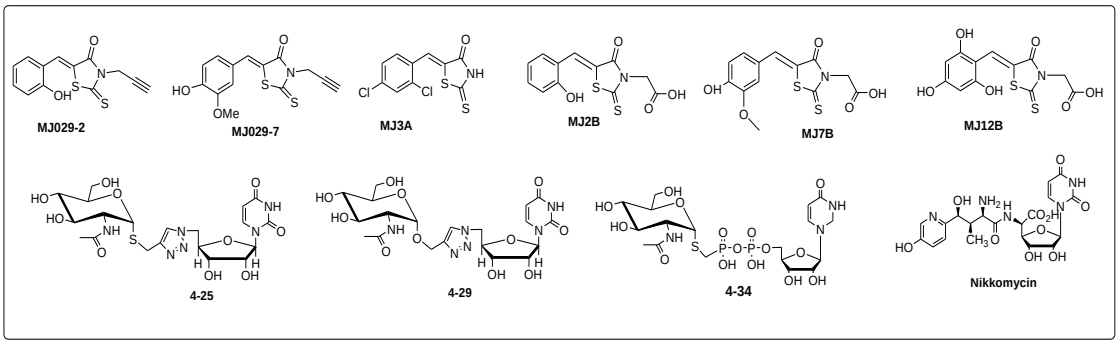

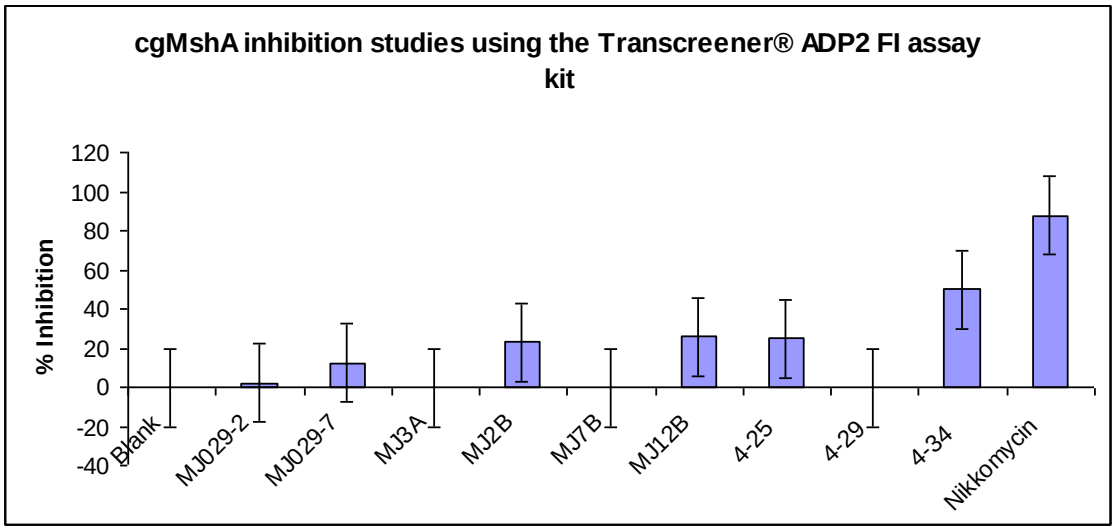

Figure 5-9: Full inhibition studies of cgMshA using Transcreener® kit. A blank reaction contained cgMshA, UDP-GlcNAc, 1-L-Ins-1-P, TEA enzyme buffer and no inhibitor. The reaction mixtures contained cgMshA, UDP-GlcNAc (100 µM), 1-L-Ins-1-P (100 µM), inhibitor and TEA enzyme buffer, all incubated at 37 °C.

Although the Transcreener® kit has enabled the effective analysis of inhibitory effects of a wide range of compounds, large standard error bars remained a problem. Numerous attempts were made to improve the Transcreener® kit without any success. As a result, further screening with the Transcreener® kit was discontinued.

5.3 Conclusion

In this study an attempt was made to screen a series of structure-based designed inhibitors against cgMshA using the PK/LDH coupled enzyme assay and Transcreener® assay kit based enzyme assay approaches respectively. The PK/LDH

coupled enzyme assay method could not be used to assay all the compounds synthesized whereas Transcreener® assay kit also resulted in large standard error bars thus making it difficult to extract reliable SAR for the thiazolidinethione derivatives. However, substrate mimic (**4-34**) have displayed promising inhibitory properties against MshA in the enzyme assay and the results were consistent with the molecular docking dynamics observed (as reported in chapter 4). Based on the kinetic data (data not shown) obtained, this substrate mimic (**4-34**) to have lost a significant amount of activity owing to the presence of the competitive inhibitor. However, the information obtained will lay a solid foundation in the design of future inhibitors for the large family of MshA enzyme. Since the study focused on a relatively small library of compounds, the complete library was considered for whole cell screening.

5.4 Experimental

5.4.1 Coupled enzyme assays conditions

The coupled enzyme assay conditions were as follows; 180 nM cgMshA, 100 μM UDP-GlcNAc, 100 μM 1-L-Ins-1-P, 200 μM NADH, 500 μM PEP (phosphoenolpyruvate), 0.01 M $MgCl_2$, 6 units pyruvate kinase and 16 units lactate dehydrogenase in a final volume of 100 μL made up with assay buffer (50 mM TEA (triethylamine buffer, pH: 7.8)), at 25 °C. Inhibitors were added at a final concentration of 100 μl (0.4% $^{v}/_{v}$ DMSO). The decrease in absorbance at 340 nm was measured with the Thermo VarioSkan™ spectrophotometer. The synthetic inhibitors were tested at 100 μM each whereas the commercially obtained inhibitors tunicamycin and nikkomycin were tested at 12 μM and 20 μM respectively.

5.4.2 Transcreener® ADP² FI assay kit

The amount of ADP² Antibody-IRDye® QC-1 quencher used in the ADP detection mixture was determined according to an equation provided by the manufacturer and determined to be 0.05 µg/µL. Each 25 µl ADP detection mixture contained 0.25 µL 800 nM ADP Alexa594 Tracer, 2.5 µL 10x stop and detect buffer B, 0.90 µl ADP² Antibody-IRDye® QC-1 quencher and 21.35 µL cgMshA assay buffer (50 mM TEA, 10 mM $MgCl_2$ at pH 7.8). Later the amount of ADP² Antibody-IRDye® QC-1 quencher added was doubled to 1.80 µL per 25 µL ADP detection mixture. The standard curves were prepared by adding concentrations of ATP and ADP together corresponding to 0%, 4%, 6%, 8%, 10%, 20%, 30%, 40%, 60%, 100% conversion of ATP. The same was done for UDP-GlcNAc and UDP. The final volume of the standard curve samples were 25 µL to which 25 µL ADP detection mixtures was added. After incubation for 1 hr at RT the fluorescent signal was measured on a Thermo VarioSkan™ spectrophotometer, set at λ_{ex} 590 nm and λ_{em} 617 nm.

The cgMshA reaction mixtures contained 180 nM cgMshA, 100 µM UDP-GlcNAc, 100 µM 1-L-Ins-1-P and cgMshA assay buffer. The reaction mixtures were incubated at 37 °C and 25 µL aliquots were taken at 0, 5, 10, 15, 30 and 60 mins, after which the reaction was stopped by incubating the aliquot at 95 °C for 5 min. After all the aliquots were processed 25 µL ADP detection mixture was added, the mixture incubated for 1 hr and the fluorescent signal measured. The reactions were performed in triplicate. The inhibition studies were performed similarly except for the addition of the specific inhibitor and the aliquots were taken at 0, 2 and 5 mins, respectively. Similarily, the synthesized inhibitors were tested at 100 µM whereas tunicamycin and nikkomycin were tested at 12 µM and 20 µM respectively.

5.5 References:

1. **Vetting, M. W., Frantom, P. A. and Blanchard, J. S. 2008.** Structural and enzymatic analyses of MshA from *Corynebacterium glutamicum*: Substrate-assisted catalysis. *Journal of Biochemistry and Molecular Biology*. **283**(23): 15834-15844.
2. **Newton, G. L., Ta, P., Bzymek, K. P. and Fahey, R. C. 2006.** Biochemistry of the initial steps of mycothiol biosynthesis. *Journal of Biological Chemistry*. **201**(45): 33910-33920.
3. **Helm, J. S., Hu, Y., Chen, L., Gross, B. and Walker, S. 2004.** Identification of selective inhibitors for the glycosyltransferase MurG *via* high-throughput screening. *Chemistry and Biology*. **11**: 703-711.
4. **Hu, Y. and Walker, S. 2002.** Remarkable structural similarities between diverse glycosyltransferases. *Chemistry and Biology*. **9**: 1287-1296.

CHAPTER 6

Whole cell inhibition studies

6.1 Introduction

The purpose of this study was to evaluate the inhibitory effects of the structure-based designed inhibitors reported in Chapters 3 and 4 respectively against the non pathogenic *M.tb* H37Rv whole cells. Unlike the *in vitro* enzyme assay screen, whole cell based assays have the advantage of selecting compounds that are able to penetrate cells and reach the intracellular targets. Despite this advantage, the whole cell screen is incapable of indicating target selectivity. However, in this study the results of the whole cell screen assays of the structure-based designed inhibitors are presented.

The rational to pursue the whole cell screen assay was based on the molecular dynamic docking study, which was used to design the structure-based designed inhibitors for the MshA enzyme active site. The molecular dynamics docking study revealed some excellent binding affinity data of the structure-based designed inhibitors in the MshA binding pocket. Additionally, excellent interaction between inhibitors and certain amino acids in the binding pocket of MshA were observed. Furthermore, lower binding energies and good inhibition constants were also observed during the molecular dynamic docking.

6.2 Biological evaluation of substrate mimics

The substrate mimics (synthesized and commercially obtained) were screened for inhibitory effects against *M.tb* H37Rv whole cells at an initial concentration of 100 μM. The level of inhibition was compared with the uninhibited cells which served as a positive control. DMSO was included in the blank test since all the stock solutions of the inhibitors were prepared in DMSO.

Almost all the substrate mimics analyzed exhibited poor activity against *M.tb* H37Rv whole cells with the exception of tunicamycin (Fig. 6-1). Tunicamycin is natural nucleotide antibiotic produced by several *Streptomyces* species[1a] and mimics the activity of natural sugar-nucleotide substrates. The structure of tunicamycin was reported by Takatsuki *et al.*[1b] and shares common structural features with UDP-GlcNAc (Fig. 6-2). The general poor activity of the substrate mimics could be attributed to poor membrane permeability.[2] Being relatively large polar molecules, substrate mimics could find it difficult to cross the cell membrane due to its hydrophilic nature. As a result, the substrate mimics are unable to penetrate the cells and eventually unable to reach their intended targets. However, tunicamycin contains a long chain lipophilic fatty acid amide group which allows it to be more flexible, thereby allowing it to change its conformation and thus increasing its chances to cross through the lipid bilayer into the cell.

As shown in Figure 6-1, tunicamycin displayed the highest potency against *M.tb* H37Rv whole cells by inhibiting the cell growth by up to 95% even when tested at a concentration <10 μM. The level of inhibition obtained is comparable with the level of inhibition obtained with isoniazid (INH, 0.365 μM), the current first line TB drug. The results obtained with tunicamycin corroborated with previous studies on the enzymes that utilize UDP-GlcNAc as substrate.[3] Kaushal and Elbein have demonstrated that enzymes involved in the transfer of GlcNAc-1-P from UDP-GlcNAc to dolichyl-PP-GlcNAc were very sensitive to tunicamycin.[3] Furthermore, various studies have demonstrated that tunicamycin specifically inhibits transfer of GlcNAc-1-P and not other reactions involving the transfer of GlcNAc.[4,5] However, the inhibition observed in the whole cell screening (Fig. 6-1) could be due to the non-selective glycosyltransferase binding ability of tunicamycin.

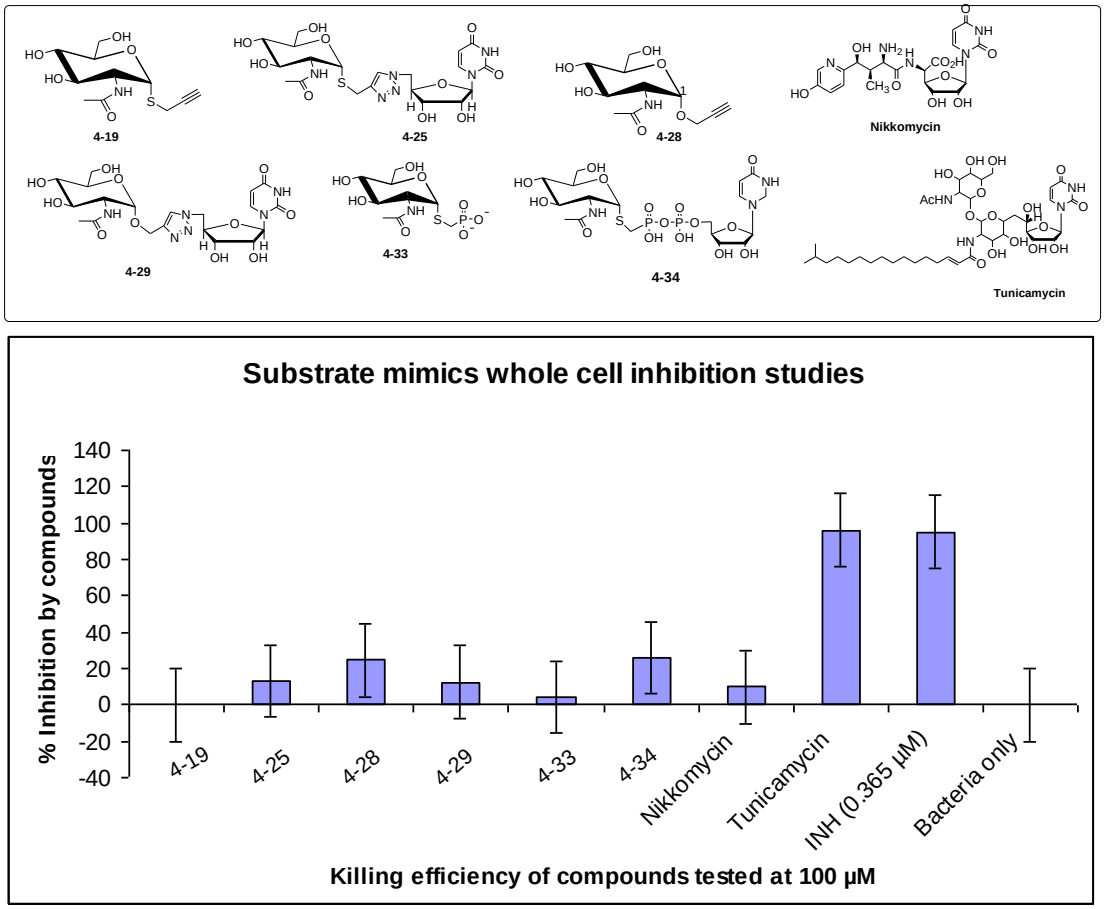

Figure 6-1: Effects of substrate mimics on *M.tb* H37Rv whole cells.

Substrate mimic (**4-34**) did not display the desired activity in *M.tb* (Fig. 6-1). However, this substrate was evaluated against *M. smegmatis* using microplate alamarBlue® assay (MABA) in a procedure described by Franzblau *et al*.[11] The substrate displayed moderate anti-mycobacterial activity by inhibiting *M. smegmatis* between 25 and 50 µM (MABA assay results Appendix I). However, no inhibition was observed when the substrate was tested at lower concentration between 12.5 and 25 µM. The whole cell inhibition results of substrate mimic (**4-34**) corroborated with the enzyme assay results (Chapter 5, Fig. 5-8), which have showed that substrate mimic (**4-34**) have inhibitory effects against MshA. The results were further in agreement with the earlier observation made with the molecular dynamic docking which indicated that substrate mimic (**4-34**) has a strong binding affinity towards MshA (Chapter 4, Fig. 4-3).

Different classes of naturally occurring antibiotics such as campuramycin (Fig. 6-3) could be considered for future lead molecule development for TB drugs. Like tunicamycin, these substrate mimics share some common structural similarities with the natural substrate of MshA, UDP-GlcNAc. The structures of these naturally occurring substrate mimics mainly consist of a uridine nucleoside which plays an important role in binding to MshA binding pocket.

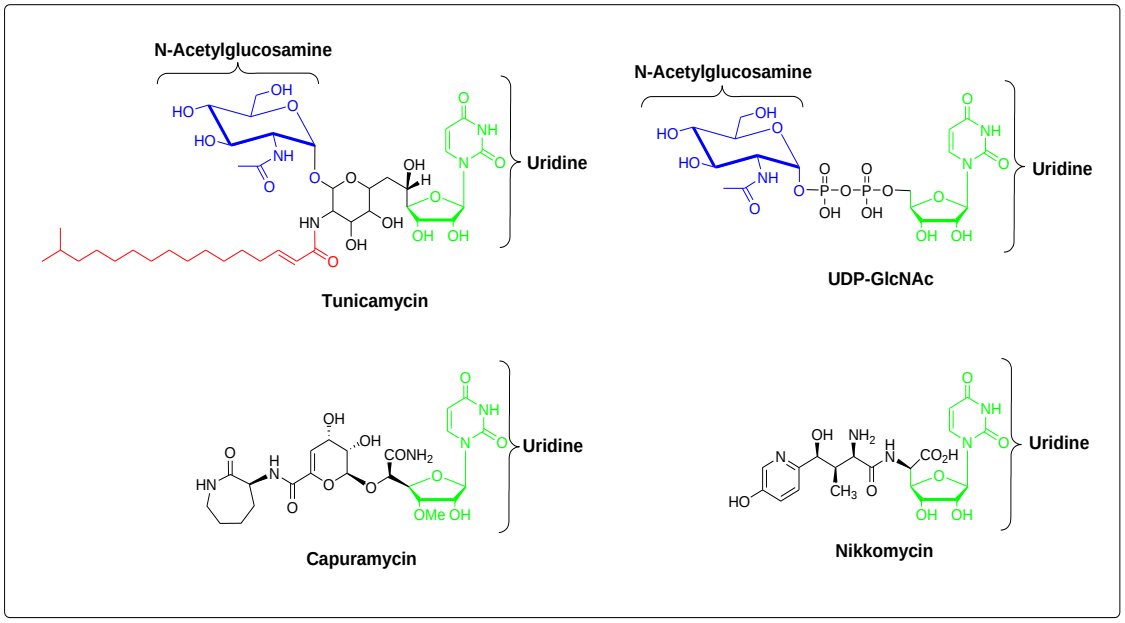

Figure 6-3: Comparison of structural features of various natural occurring substrate mimics with the natural substrate (UDP-GlcNAc) of glycosyltransferase.

The studies by Koga *et al.*[6] have shown that capuramycin derivatives had significant inhibitory effects against mycobacterial species both *in vivo* and *in vitro* by killing more than 90% of the bacilli within 48 hr. Furthermore, the substrate had shown lower toxicity levels when administered in mice. The study by Reddy *et al.*[7] demonstrated that capuramycin analogues kill over 90% of the bacilli within 48 hr of treatment at low concentrations and this has the potential to reduce the duration for TB treatment. However, thorough investigation on SARs studies of capuramycin

analogues are required in order to improve the pharmacokinetic properties of this substrate mimic.

6.3 Biological evaluation of thiazolidinethione-based compounds as MshA inhibitors

A study by Kucukguzel *et al.*[8] reported excellent anti-tubercular activity of thiazolidinone derivatives with inhibition levels as high as 90 and 98% and IC_{50} value of about 6.25 µg/mL. Andres *et al.*[9] also reported good inhibition of the MurB enzyme using thiazolidinone derivatives. Similarily, Helm *et al.*[10] synthesized and screened a focused library of diverse small molecules bearing the 2-thioxothiazolidin-4-one (rhodanine) core as the potential inhibitors of glycosyltransferase (Fig. 6-4). The 2-thioxothiazolidin-4-one derivatives reported were rationally designed to inhibit the glycosyltransferase and hence we targeted 2-thioxothiazolidin-4-one derivatives as potential inhibitors of the glycosyltransferase MshA in this study.

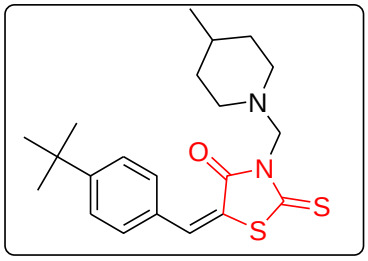

Figure 6-4: Representative of the compound from the family of glycosyltransferase MurG inhibitors with the common core highlighted.[10]

6.3.1 Biological evaluation of thiazolidinethione derivatives (MJ1A - MJ12A and MJ1B - MJ12B) against *M.tb*

The success of the reported studies on the 2-thioxothiazolidin-4-one derivatives against glycosyltransferase MurG was encouraging.[10] Therefore in this study a series of thiazolidinethione derivatives from two different libraries (**MJ1A - MJ12A** and

MJ1B - MJ12B) were screened for activity against *M.tb* (Table 6-1). A fair number of these molecules were found to inhibit the growth *M.tb* in moderate to good levels in whole cell assays.

However, the data obtained from the whole cell screening, shows that only four compounds (**MJ3A, MJ2B, MJ7B** and **MJ12B**) sourced from the two libraries displayed an $IC_{50} \geq 20$ μM. The results of the compounds with high potency are shown (in red) in Table 6-1. Amongst the tested compounds (*Z*)-5-(2,4-dichlorobenzylidene)-2-thioxothiazolidin-4-one (**MJ3A**) and 2-((*Z*)-5-(4-hydroxy-3-methoxybenzylidene)-4-oxo-2-thioxothiazolidin-3-yl)acetic acid (**MJ7B**) were found to be the most potent compounds with inhibition levels of 88 and 86%, respectively.

The inhibition data complemented the molecular docking studies on thiazolidinethione-based derivatives which indicated these set of compounds could be potential inhibitors for MshA based on their binding energy and good inhibition constants. As discussed in Chapter 3 and Chapter 4 respectively, molecular dynamics docking studies was performed in the MshA enzyme active site to aid further drug design.

In addition, the lipophilicities of the thiazolidinethione derivatives were calculated using ChemDraw Ultra 8.0. These derivatives have shown reasonable propabilities of being well absorbed, with calculated partition coefficient (clog P) below 5.0 (Table 6-1). cLog P serves as one of the most fundamental principle for prediction of ADMET properties of drug candidates. Thus, building accurate predictive ADMET models for early decision making in drug discovery would be a challenge without accurate prediction of log P.

Table 6-1: Antimycobacterial activities of thiazolidinethione derivatives (**MJ1A - MJ12A** and **MJ1B - MJ12B**). Compounds were tested at initial concentration of 100 µM using BACTEC 460^{TM} system.

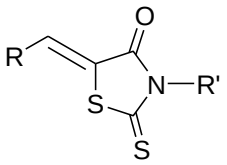

Entry	Code	R	R'	Mw	cLog P	% Inhibition (100 µM)
1	**MJ1A**		H	220.9	2.04	26
2	**MJ2A**	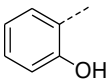	H	236.9	1.65	38
3	**MJ3A**	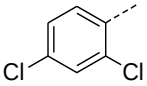	H	288.9	3.15	88
4	**MJ4A**	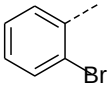	H	298.9	2.86	22
5	**MJ5A**	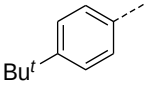	H	277.0	3.74	32
6	**MJ6A**	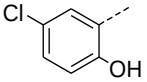	H	270.9	2.20	34
7	**MJ7A**	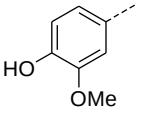	H	267.0	1.52	44
8	**MJ8A**	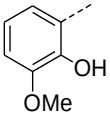	H	267.0	1.52	39
9	**MJ9A**	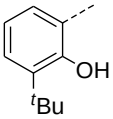	H	293.0	3.35	20
10	**MJ10A**	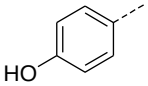	H	236.9	3.74	28
11	**MJ11A**	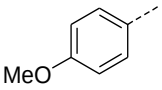	H	251.0	1.91	39
12	**MJ12A**	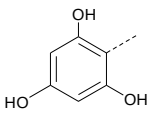	H	268.9	0.87	41
13	**MJ1B**		-C*H*$_2$COOH	279.0	1.54	42

Entry	Code	R	R'	Mw	cLog P	% Inhibition (100 µM)
14	**MJ2B**	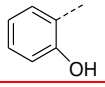	-C*H*$_2$COOH	294.9	1.15	75
15	**MJ3B**	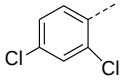	-C*H*$_2$COOH	346.9	2.65	33
16	**MJ4B**		-C*H*$_2$COOH	356.9	2.37	26
17	**MJ5B**	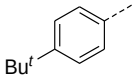	-C*H*$_2$COOH	335.0	3.24	45
18	**MJ6B**	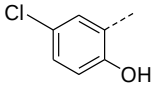	-C*H*$_2$COOH	328.9	1.71	43
19	**MJ7B**	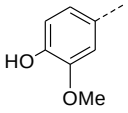	-C*H*$_2$COOH	325.0	1.02	86
20	**MJ8B**	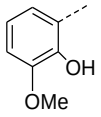	-C*H*$_2$COOH	325.0	1.02	37
21	**MJ9B**	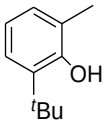	-C*H*$_2$COOH	351.0	2.85	40
22	**MJ10B**	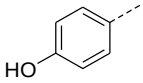	-C*H*$_2$COOH	294.9	1.15	28
23	**MJ11B**	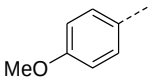	-C*H*$_2$COOH	309.0	1.41	32
24	**MJ12B**	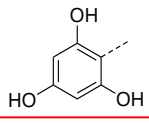	-C*H*$_2$COOH	326.9	0.37	68

The results obtained with the *N*-alkylated 2-thioxothiazolidin-4-one derivatives corroborated with the findings of the inhibition studies of other glycosyltransferase MurG,[10] whereby seven out of eleven compounds screened against MurG were constituted by a five member ring, nitrogen containing heterocyclic aryl or alkyl substituent at *N*-1 and arylidene substituent at position 3 (Fig. 6-5).

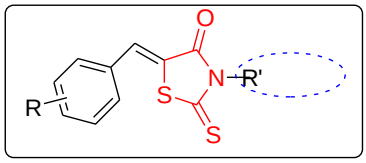

Figure 6-5: Representative of the compound from the family of glycosyltransferase inhibitors screened in this study with the common core and possible *N*-1 extension highlighted.

The most potent thiazolidinethione derivatives were selected and subjected to further testing at lower concentrations (10, 1 and 0.1 µg/mL). The results are summarized in Table 6-2. At 10 µg/mL, the compounds displayed moderate inhibition. However the activity was not significant when they were tested at concentrations below 1 µg/mL.

Table 6-2: Effects of thiazolidinethione derivatives on the *M.tb* H37Rv growth. cLog P of the compounds was predicted using ChemDraw Ultra 8.0.

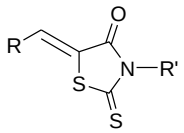

Entry	Code	R	R'	Mw	clog P	% Inhibition (µg/mL) 10	1	0.1
1	**MJ3A**	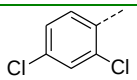	H	288.9	3.15	48	11	-
2	**MJ2B**	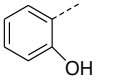	-C*H*$_2$COOH	294.9	1.15	12	11	-
3	**MJ7B**	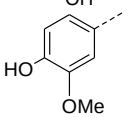	-C*H*$_2$COOH	325.0	1.02	35	15	-
4	**MJ12B**	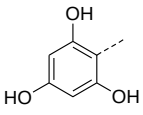	-C*H*$_2$COOH	326.9	0.37	22	7	-

- = No Inhibition

6.3.2 Biological evaluation of *N*-propargylated thiazolidinethione derivatives (MJ029 series) against *M.tb.*

As a first step towards the expansion of SARs, the thiazolidinethiones library (**MJ1A - MJ12A**) was *N*-alkylated using propargyl bromide to generate a series of new compounds (**MJ029**). This series of compounds (**MJ029**) was screened *in vitro* for their anti-tuberculosis activity and the results are displayed in Figure 6-6. Preliminary screening was conducted at a concentration of 100 µg/mL and this class of compounds showed significant anti-tubercular activity. *N*-alkylation of thiazolidinethione derivatives with the propargyl moiety led to compounds that exhibited significant inhibition. This suggested that the introduction of the propargyl moiety to the thiazolidinethione moiety leads to a significant improvement in *M.tb* inhibitions as compared to non-*N*-substituted thiazolidinethione derivatives.

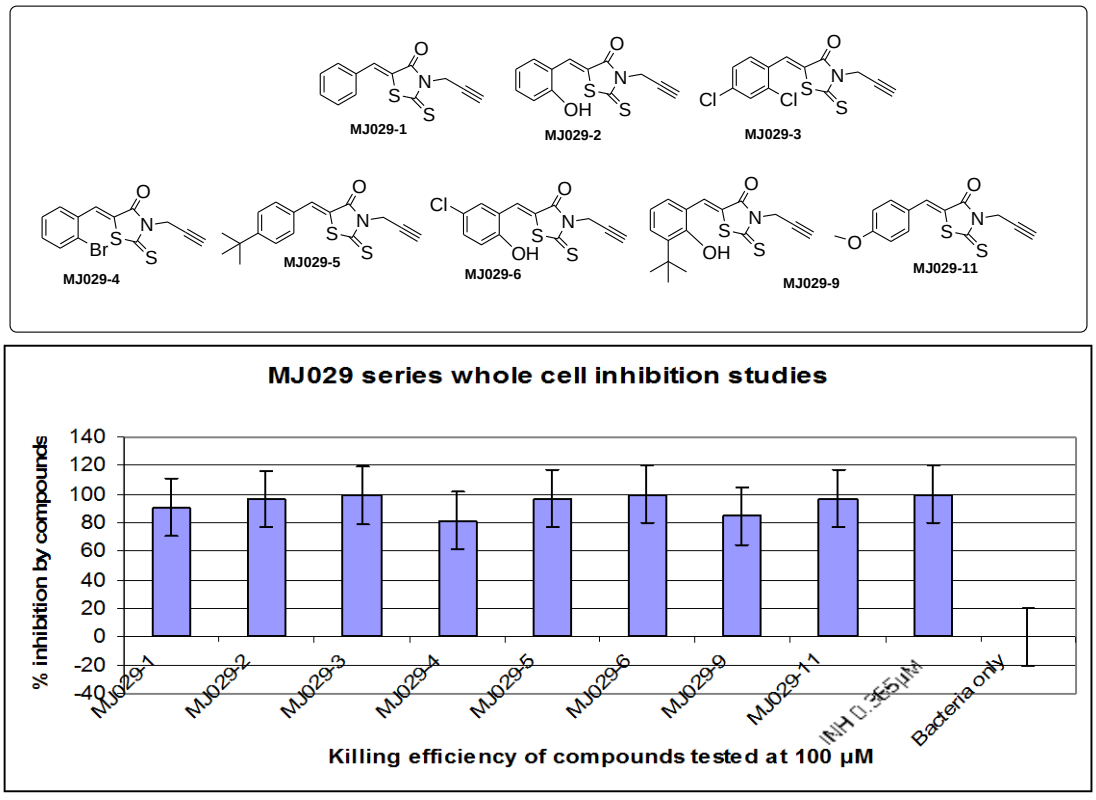

Figure 6-6: Effects of propargylated thiazolidinethione derivatives on the *M.tb* growth. Compounds were tested at initial concentration of 100 µM using BACTEC 460^{TM} system.

6.3.3 The Biological evaluation of sulfonated thiazolidinethione derivatives (MJ081 series) against *M. smegmatis*

The addition of *N*-propylsulfonate moiety to thiazolidinethione derivatives (**MJ1A - MJ12A**) led to the formation of a new series of compounds (**MJ081**). This series of compounds was screened *in vitro* for anti-mycobacterial activity against *M. smegmatis* using microplate alamarBlue® assay (MABA, (Appendix I)) in a procedure described by Franzblau *et al*.[11]

In addition, several compounds drawn from different libraries (**MJ1A-MJ12A**, **MJ1B-MJ12B**, **MJ029** series and substrate mimic **4-34**) were screened for anti-mycobacterial activities against *M. smegmatis*. This included the compounds that had previously displayed excellent activity against *M.tb* in the BACTEC 460™ system. The purpose of including the previously screened compounds was to establish if there is any correlation between the results obtained using the two assay methods.

The compounds were screened at different concentrations (100 μM, 50 μM, 25 μM and 12.5 μM) for anti-mycobacterial activity (Table 6-3). All the compounds analyzed have displayed excellent anti-mycobacterial activity at the concentration of 50-100 μM.

However, moderate inhibition was observed when compounds were screened at a concentration of 25-50 μM, with the exception of **MJ081-6** which displayed strong inhibitory effects at this concentration range. Finally no anti-mycobacterial activity was observed when compounds were screened at the concentration below 25 μM (Appendix I). Thus, the additions of *N*-propylsulfonate moiety to thiazolidinethione derivatives have not been able to substantially enhance the activity of these

derivatives in the current study. However, the data obtained here is encouraging and deserve further investigation.

Table 6-3: Effects of thiazolidinethione derivatives on the *M. smegmatis* growth. cLog P of the compounds was predicted using ChemDraw Ultra 8.0.

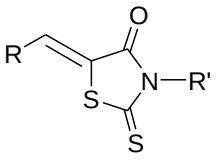

Entry	Code	R	R'	Mw	clogP	Concentration ranges 100<>50	50<>25	25<>12.5
1	**MJ081-1**		-(CH_2)$_3$$SO_3$H	365.4	1.31	++	+	-
2	**MJ081-2**	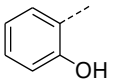	-(CH_2)$_3$$SO_3$H	381.4	0.92	++	+	-
3	**MJ081-3**	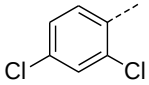	-(CH_2)$_3$$SO_3$H	434.3	2.43	++	+	-
4	**MJ081-6**	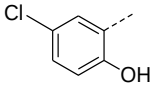	-(CH_2)$_3$$SO_3$H	415.8	1.48	++	+	-
5	**MJ081-8**	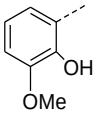	-(CH_2)$_3$$SO_3$H	411.4	0.80	++	+	-
6	**MJ081-11**	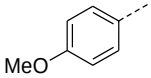	-(CH_2)$_3$$SO_3$H	395.4	1.19	++	+	-
7	**MJ3A**	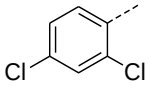	H	288.9	3.15	++	+	-
8	**MJ7B**	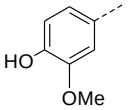	-CH_2CO_2H	325.0	1.02	++	+	-
9	**MJ029-2**	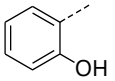	-CH_2C≡CH	275.3	2.1	++	+	-
10	**MJ029-3**	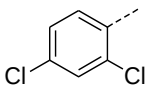	-CH_2C≡CH	326.2	3.6	++	+	-
11	**MJ029-11**	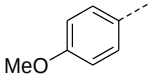	-CH_2C≡CH	289.3	2.36	++	+	-

++ = Strong Inhibition (100<>50), + = Moderate Inhibition (50<>25), - = No Inhibition (25<>12.5)

6.4 Intracellular drug testing

The purpose of this part of the study was to further explore the inhibitory effects of the most potent extra-cellular inhibitors of *M.tb*, by comparing the fate of *M.tb* in infected macrophages. The inhibitors that have demonstrated the ability to inhibit the growth of *M.tb in vitro* at 10 μM*,* were selected and tested further for their ability to inhibit the growth within the host macrophages.

However, based on the criteria used for the selection of the inhibitors for intracellular screening, only tunicamycin met out the set standard (higly potent at 10 μM). However, other inhibitors sourced from the prepared library of compounds were nevertheless selected and included in the intracellular screening. BACTEC 460^{TM} measurements were used to analyze bacterial survival within the macrophages.

6.4.1 Drug testing in the macrophages

After extra-cellular screening of the most active compounds, intracellular testing was performed on a THP1 cell line. Human macrophage-like cell line THP1 (ATCC TIB-202) was chosen for drug screening because the cells are easily accessible. The THP-1 macrophages were infected with *M.tb* at a multiplicity of infection (MOI) 5:1 for up to 2 days. On day 3 post-infection, the *M.tb* infected macrophages were treated with inhibitors and incubated for different time intervals (4, 8, 12 and 24 hr) post-drug exposure.

As shown in Figure 6-7 below, tunicamycin has been able to inhibit the growth of intracellular *M.tb* by up to 95% at low concentration (10 μM). The results suggest that it could be possible that tunicamycin binds to other glycosyltransferases other than MshA, thereby resulting in the inhibition of the growth of intracellular *M.tb.* The results obtained with the intracellular inhibition studies are in contrast with the earlier

findings in the study (molecular docking studies and enzyme (cgMshA) assay) whereby it demonstrated that tunicamycin does not bind to MshA.

However, these results suggest that tunicamycin could be used as a potential lead compound. Further investigation on SARs studies of tunicamycin derivatives are required in order to improve the drug like properties of this natural substrate mimic.

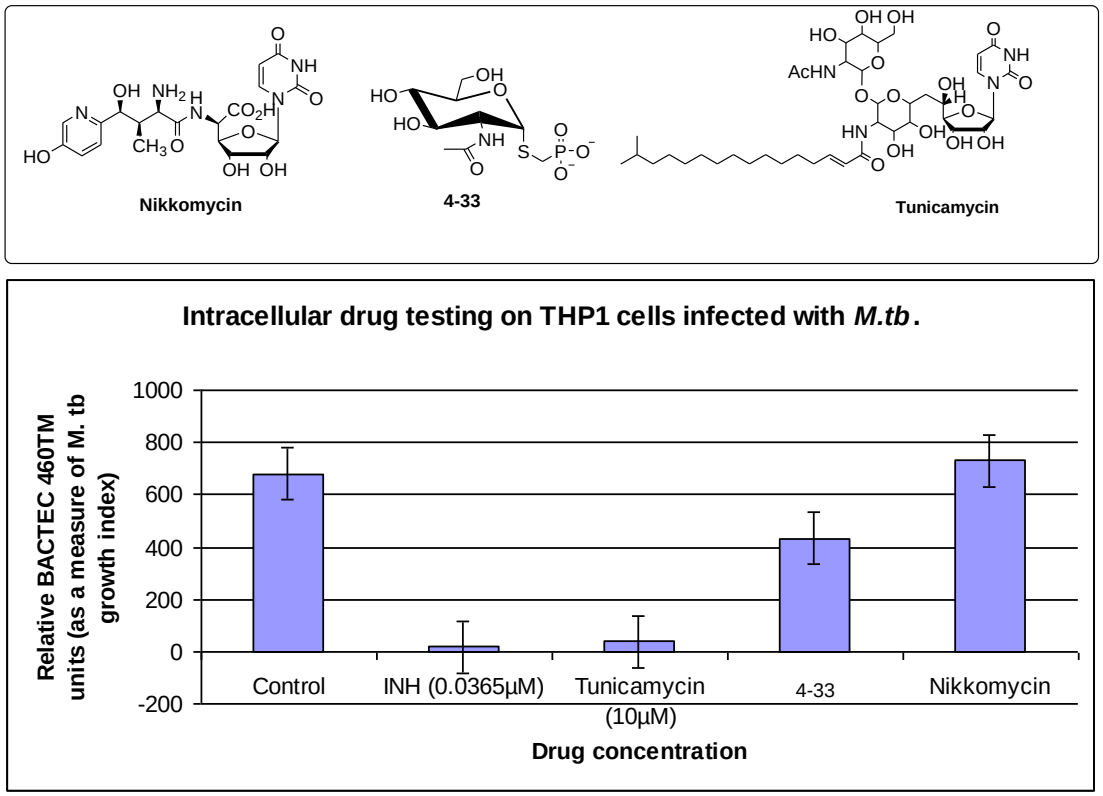

Figure 6-7: Intracellular drug testing on THP1 cells infected with *M.tb* at MOI 5:1. *M.tb* was inoculated into BACTEC 460™ vial containing Middlebrook 7H12 medium. INH was used as a positive control at 0.0365 µM concentration, while the negative control *M.tb*-infected macrophages without any drug added.

6.5 Conclusion

In summary, this study allowed the screening of numerous structure-based designed inhibitors. Several hit compounds that were capable of inhibiting MshA were identified. Due to its hydrophilic property, it was not completely suprising that none of the substrate mimics synthesized displayed satisfactory inhibitory activity in the

whole cell assay against MshA even at a concentration as high as 100 μM with the exception of **4-34**. Tunicamycin appears to be the most potent inhibitor and has inhibited the growth of *M.tb* H37Rv up to 95% even when tested at concentrations below 10 μM. However, the inhibition could be due to non-selective binding of this inhibitor to other glycosyltransferases within the mycobacterial species.

On the other hand, thiazolidinethione derivatives **MJ3A, MJ2B, MJ7B, and MJ12B** have displayed an $IC_{50} \geq 20$ μM during the preliminary screening. *N*-alkylated thiazolidinethione derivatives (**MJ029** series) proven to be excellent inhibitors of *M.tb* H37Rv and had tremendously improved (displayed an $IC_{50} < 20$ μM) the activity of thiazolidinethiones (**MJ1A – MJ12A**) after the *N*-alkylation. The results obtained from *M.tb* H37Rv screening have laid a foundation for future development of hit compounds for optimization. The hit compounds can now be optimized further to attain lead status.

6.6 Experimental

6.6.1 Monitoring *M.tb* growth in the presence of inhibitors using the BACTEC 460™ system

The *M.tb* H37Rv (1 mL aliquots) were thawed and grown directly in BACTEC 460™ vials with various concentrations of inhibitors (between 0 and 100 μg/mL). *M.tb* was cultured for 7 days before the addition of inhibitors. Untreated *M.tb* was grown under the same conditions (as the treated *M.tb* with no inhibitor added) to serve as a control. Mycobacterial growth was monitored by the BACTEC 460™ instrument which measures of the uptake of radioactively labelled ^{14}C triacylglycerides.[12] The minimal inhibitory concentrations for the drugs were calculated based on BACTEC 460™ growth index readings.

6.6.2 Culture conditions for the THP1 cell line

The THP-1 human macrophage cell line were grown at 37 °C in 5% CO_2 in Roswell Park Memorial Institute (RPMI) 1640 (Sigma, USA) supplemented with 10% heat-inactivated FCS (Gibco^{TM}, Invitrogen, Germany) with penicillin-streptomycin, 1% final concentration (Invitrogen). Cells were placed in a 50 mL tube + 8 mL (+/-10 mL) medium and pelleted by spinning at 13 000 rpm for 5 minutes at 21 °C. The supernatant was removed and the tube was dragged over round-bottom 96 well plate to re-suspend the pellet. A 10 mL aliquot of complete RPMI 1640 medium was added to the tube to re-suspend cells. All of the liquid was aliquoted into a flask (small filter cap TC flask), and incubated at 37 °C for three days. Cells were checked everyday and fresh medium added every 2nd or 3rd day. Cells were harvested at 1 week, pelleted and re-suspend in fresh complete RPMI, lacking antibiotics and counted using a haemocytometer.

THP-1 cells were differentiated into macrophages by using phorbol myristic acetate (PMA, Sigma, USA). Once differentiated THP1 cells become adherent monolayers and stop dividing and to acquire typical characteristics of macrophages such as the capacity to phagocytize bacteria and to express bactericidal activities.[13] PMA was added to a final concentration of 100 nM and 1 mL of cells added per well in 24 well plates at a concentration of 5 x 10^5 cells/mL (all experiments were done in triplicate). Cells were incubated overnight, and non-adherent cells were removed by washing 3 times with 1 mL ice-cold phosphate buffered saline. At selected time points after infection with *M.tb*, infected macrophages were exposed to inhibitors and intracellular survival was assessed.

6.6.3 Macrophage infection

1 mL aliquots of *M.tb* were removed from the -80 °C freezer and thawed. Mycobacteria were passaged 30 times through a with 1 mL insulin syringe to remove clumps. The required amount of mycobacteria was centrifuged at 13 000 rpm for 20 minutes. The supernatant was removed and bacilli were re-suspended in 1 mL medium (RPMI, 10% FCS). The required amount was centrifuged at 13 000 rpm for 20 minutes, and the supernatant removed. A 1 mL aliquot of medium (RPMI, 10% FBS) was added and passed 10 times through a 1 mL insulin syringe. Macrophages were infected at an MOI of 5:1 and incubated for 4 hours at 37 °C, in the presence of 5% CO_2. Non-ingested *M.tb* was then washed off with RPMI containing 10% FCS. Infected macrophages were incubated at 37 °C in fresh medium that was renewed every 2 days thereafter.

6.6.4 Evaluating inhibitory effects of novel compounds designed against MshA

At day 1 or day 2 post infection, *M.tb*-infected macrophages were treated with candidate inhibitors to determine the optimal concentrations and treatment time for inhibitory effect on mycobacterial growth. At selected time-points during the drug treatments, infected macrophages were lysed with 0.1% Triton X-100 (Sigma-Aldrich, USA) to isolate *M.tb*. Mycobacteria were pelleted at 13 000 rpm for 20 minutes, and re-suspended in 1 mL 7H12 Middlebrook medium. The samples were analysed for *M.tb* growth in a BACTEC 460^{TM} instrument. Inhibitory effects of each test compound were evaluated in relation to infected treated controls.

6.7 References:

1. (a). **Price, N. P. J. and Tsvetanova, B. 2007.** Biosynthesis of the tunicamycins: A review. *Journal of Antibiotics*. **60**(8): 485–491. (b). **Takatsuki, A., Kawamura, K., Okina, M., Kodama, Y., Ito, T. and Tamura, G. 1977.** *Agricultural and Biological Chemistry.* **4**: 2307-2309.
2. **Hu, Y., Helm, J. S., Chen, L., Ginsberg, C., Gross, B., Kraybill, B. Tiyanont, K., Fang, X., Wu, T. and Walker, S. 2004.** Identification of selective inhibitors for the glycosyltransferase MurG via High-Throughput Screening. *Chemistry and Biology*. **11**: 703–711.
3. **Kaushal, G. P. and Elbein, A. D. 1986**. Properties of solubilized UDP-GlcNAc: dolichyl phosphate-GlcNAc-1-P-transferase from soybean cultured cells. *Plant Physiology*. **82**: 748-752.
4. **Tkacz, J. S. and Lampen, J. O. 1975.** Tunicamycin inhibition of polyisoprenyl *N*-acetylglucosaminyl pyrophosphate formation in calf-liver microsomes. *Biochemical Biophysical Research Communications.* **65:** 248-257.
5. **Struck, D. L. and Lennarz, W. J. 1977.** Evidence for the participation of saccharide-lipids in the synthesis of the oligosaccharide chain of ovalbumin. *Journal of Biological Chemistry.* **252:** 1007-1013.
6. **Koga, T., Fukuoka, T., Doi, N., Harasaki, T., Inoue, H., Hotoda, H., Kakuta, M., Muramatsu, Y., Yamamura, N., Hoshi, M. and Hirota, T. 2004.** Activity of capuramycin analogues against *Mycobacterium tuberculosis*, *Mycobacterium avium* and *Mycobacterium intracellulare in vitro* and *in vivo*. *Journal Antimicrobial chemotherapy*. **54**(4): 755-760.

7. **Reddy, V. M., Einck, L. and Nacy, C. A. 2008.** *In vitro* antimycobacterial activities of capuramycin analogues. *Antimicrobial Agents and Chemotherapy*. **52**(2): 719-721.

8. **Kucukguzel, S. G., Oruc, E. E., Rollas, S., Sahin, F. and Ozbek, A. 2002.** Synthesis, characterization and biological activity of novel 4-thiazolidinones, 1,3,4-oxadiazoles and some related compounds. *European Journal of Medicinal Chemistry*. **37**:197-206.

9. **Andres, C. J., Bronson, J. J., Andrea, S. V. D., Deshpande, M. S., Falk, P. J., Grant-Young, K. A., Harte, W. E., Ho, H. T., Misco, P. F., Robertson, J. G., Stock, D., Sun, Y. and Walsh, A. W. 2000.** 4-Thiazolidinones: Novel inhibitors of the bacterial enzyme MurB. *Bioorganic and Medicinal Chemistry Letters*. **10**: 715-717.

10. **Helm, J. S., Hu, Y., Chen, L., Gross, B. and Walker, S. 2004**. Identification of selective inhibitors for the glycosyltransferase MurG *via* high-throughput screening. *Chemistry and Biology*. **11**: 703-711.

11. **Franzblau, S.G., Witzig, R. S, Mclaughlin, J. C., Torres, P., Madico, G., Hernandez, A., Degnan, M. T., Cook, M. B., Quenzer, V. K., Ferguson, R. M. and Gilman, R. H. 1998.** Rapid, low-technology MIC determination with clinical *Mycobacterium tuberculosis* isolates by using the microplate Alamar Blue assay. *Journal of Clinical Microbiology*. **36**(2): 362-366.

12. **Roberts, G. D., Goodman, N. L., Heifets, L., Larsh, H. W., Lindner, T. H., McClatchy, M. R., McGinnis, J. K., Siddiqi, S. H. and Wright, P. 1983.** Evaluation of the BACTEC radiometric method for recovery of mycobacteria and drug susceptibility testing of *Mycobacterium tuberculosis* from acid-fast smear positive specimens. *Journal of Clinical Microbiology*. **18**: 689–696.

13. **Tsuchiya, S., Kobayashi, Y., Goto, Y., Okumura, H., Nakae, S., Konno, T. and Tada, K. 1982.** Induction of maturation in cultured human monocytic leukemia cells by a phorbol diester. *Cancer Research.* **42**:1530–1536.

CHAPTER 7

7.1 Overall summary and conclusion

The main aim of this research project was to synthesize and evaluate glycosyltransferase (MshA) inhibitors. The enzyme (MshA) plays a crucial role in the biosynthesis of mycothiol, which is implicated in the redox maintenance of the mycobacteria. The enzymes involved in the redox maintenance of the bacteria have not been fully explored and considered to be possible drug targets. The current anti-tuberculosis drugs and the anti-tuberculosis drug candidates in clinical stages mainly target the enzymes that are involved in the biosynthesis of the bacterial cell wall. Nevertheless, none of the anti-tuberculosis drug candidates target the enzymes involved in the redox maintenance of mycobacteria.

A specific focus of this research project included the synthesis of mimics of the sugar-nucleotide of the natural substrate (UDP-GlcNAc) of MshA. MshA catalyzes the first essential step leading towards the biosynthesis of mycothiol and requires both UDP-GlcNAc and 1-L-Ins-1-P as substrates. Successful inhibition of this enzyme could lead to novel leads in an unexplored pathway targeting tuberculosis.

In an attempt to design substrate mimics and thiazolidinethione derivatives, *in silico* active site docking studies of MshA, using computer simulations (Autodock 4.2 software) was attempted. Subsequently, a series of thiazolidinethione derivatives (**MJ1A – MJ12A** and **MJ1B – MJ12B**) was synthesized and screened for anti-tuberculosis activity. Of these thiazolidinethione derivatives screened, four compounds (**MJ3A, MJ2B, MJ7B** and **MJ12B**) were identified as potential drug-like inhibitors of MshA by inhibiting *M. tuberculosis* growth (≥ 70%).

Further development of thiazolidinethione derivatives (**MJ1A - MJ12A**), steered by biological activity in conjunction with docking studies culminated in a synthesis of potent propargylated thiazolidinethione derivatives (**MJ029** series). Biological results have showed that the propargylated thiazolidinethione derivatives (**MJ029** series) have excellent antituberculosis activity by inhibiting *M. tuberculosis* growth by >80% at 100 μg/mL.

While the exact target could not conclusively be determined to be MshA, the mechanism of action of these compounds is yet unknown, the enhanced activity of this series of compounds is attributable to the addition of the propargyl moiety. The discovery that thiazolidinethione derivatives inhibit the growth of *M. tuberculosis* provides a starting point for future investigations of these scaffolds, which may yield more potent MshA inhibitors and provide additional structure–activity relationships.

In addition, substrate mimics were synthesized and screened for anti-tuberculosis activity. As suspected, substrate mimics synthesized displayed moderate activity, except for substrate mimic (**4-34**) which turned out to be an interesting candidate for MshA inhibition by displaying the highest potency. Based on these biological results, it was concluded that the replacement of the pyrophosphate moiety of the naturally occurring substrate, UDP-GlcNAc, with a 1,2,3-triazole mimic led to non-isosteric analogs (**4-25** and **4-29**) displaying weak inhibitory activities.

These results were in agreement with the previous study of Vidal *et al.*[1] Vidal *et al.* investigated the *in vitro* inhibitory activities of non-isosteric analogues of natural nucleotide diphosphate sugars (UDP-Gal, UDP-Fuc and UDP-GlcNAc) as glycosyltransferases (β-1,4-GalT, FUT3 and *LgtA*) inhibitors. However, none of the

non-isosteric analogues screened displayed significant inhibitory activity at a concentration of up to 3.5 mM in fluorescence assay against glycosyltransferases.[1]

In addition, tunicamycin, a naturally occurring substrate mimic, have been evaluated for anti-tuberculosis activity against MshA. The biological results indicated that this substrate mimic is highly potent against mycobacteria species at very low concentration. Although, tunicamycin had inhibited the growth of *M.tb*, the Transcreener® assay results have indicated that this substrate mimic is not a good inhibitor of MshA, which was also corroborated by docking studies. Thus, it could be possible that tunicamycin binds to other glycosyltransferases within the mycobacterial species with the exception of MshA.

The study describes in detail the total synthesis of 1-L-Ins-1-P which is an important co-substrate required for enzyme (MshA) assays. Although this substrate is commercially available, the cost involved in the procurement of the substrate (400$/mg) were high and unsustainable considering the amount of the assays planned. Therefore it was decided to pursue the synthesis of this substrate in relatively large scale in our laboratory. The substrate was synthesized in a total of 9 steps from *myo*-inositol, using a combination of protocols. Analytical techniques such as ^{1}H NMR, ^{13}C NMR, ^{31}P NMR spectroscopy as well as mass spectrometry were employed to fully characterize the substrate. The challenges involved with the synthesis of this substrate were highlighted. The synthetic route described in this thesis led to an improved large scale synthesis of 1-L-Ins-1-P.

In conclusion, the thiazolidinethione scaffolds and substrate mimic (**4-34**) can be developed further into lead compounds considering their selective binding towards MshA. Although tunicamycin appears to be inhibiting the growth of the

mycobacterial species, the specificity of this inhibitor towards MshA needs to be modulated. Further *in silico* ADMET predictive models could be explored in synthesizing the modified tunicamycin derivatives that could be specific to MshA binding.

References:

1. **Vidal, S., Bruyere, I., Malleron, A., Auge, C. and Praly, J. P. 2006.** Non-isosteric *C*-glycosyl analogues of natural nucleotide diphosphate sugars as glycosyltransferase inhibitors. *Bioorganic and Medicinal Chemistry*. **14**: 7293–7301.

Appendix I

Microplate alamarBlue® assay (MABA)

Slightly modified MABA assay was carried out as described by Franzblau *et al.*[1] Briefly, *M. smegmatis* culture were allowed to grow till the optical density (OD) of 0.6 was reached before the cells were treated with different drug concentrations. Subsequently the treated cells were incubated for 24 hr at 37 °C before resazurin was added and the cells were allowed to grow further for another 24 hr before the color development was monitored. A blue color in the wells was interpreted as no growth, purple color was interpreted as moderate inhibition, whereas a pink color was scored as growth. The outer perimeter wells of the sterile 96 well plates were filled with sterile Milli-Q water to minimize the evaporation during the incubation.

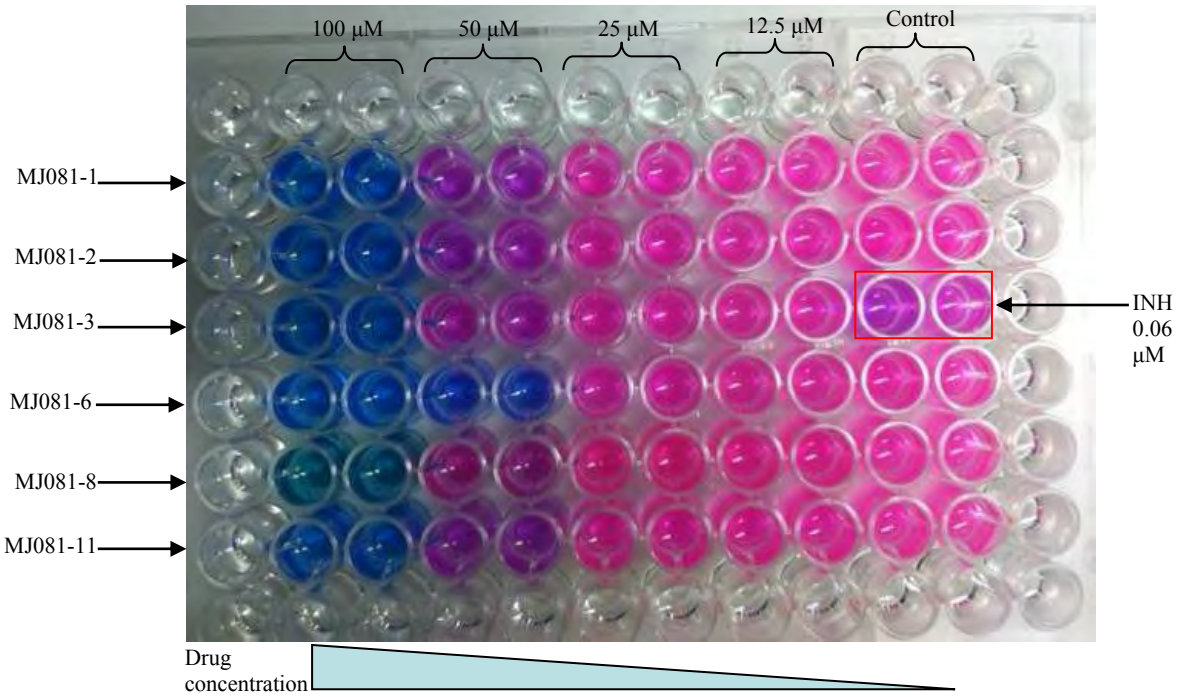

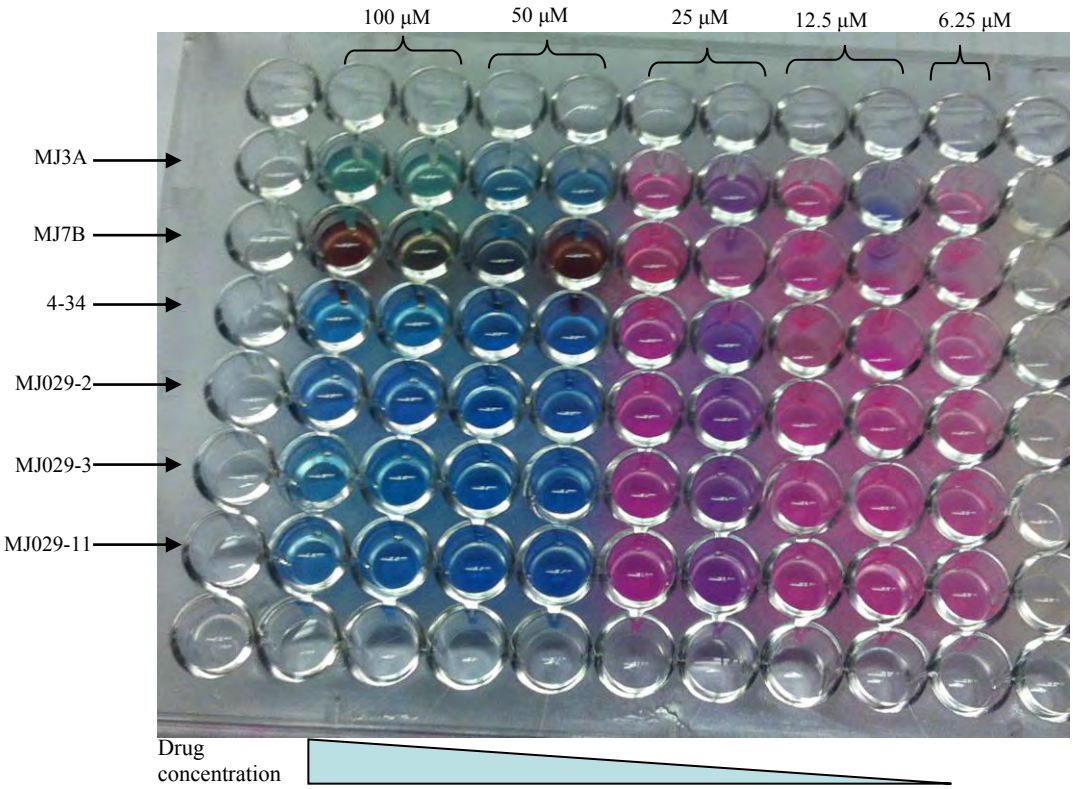
100 µM
50 µM
25 µM
12.5 µM
6.25 µM
MJ3A
MJ7B
4-34
MJ029-2
MJ029-3
MJ029-11
Drug concentration

References:

1. **Franzblau, S.G., Witzig, R. S, Mclaughlin, J. C., Torres, P., Madico, G., Hernandez, A., Degnan, M. T., Cook, M. B., Quenzer, V. K., Ferguson, R. M. and Gilman, R. H. 1998.** Rapid, low-technology MIC determination with clinical *Mycobacterium tuberculosis* isolates by using the microplate Alamar Blue assay. *Journal of Clinical Microbiology*. **36**(2): 362-366.